[redacted]

(NASA-CR-101600) EXTENDED APOLLO SYSTEMS UTILIZATION STUDY PROLONGED MISSIONS. VOLUME 3 SUBSYSTEMS FINAL REPORT (North American Aviation, Inc.) 338 p

ff No. 602(D)

(PAGES)

Cr-101600

(NASA CR OR TMX OR AD NUMBER) (C

AVA [redacted]

AND CONTRACTORS ONLY

LIBRARY COPY

APR 8 1969

N79-76145

00/12 Unclas 11106

NORTH AMERICAN AVIATION, INC.
SPACE and INFORMATION SYSTEMS DIVISION

[redacted]

[redacted]

C69-1114

Contract No. NAS9-3140

Accession No. 07667-65

29

SID 65-968-3A

EXTENDED APOLLO SYSTEMS UTILIZATION STUDY
PROLONGED MISSIONS [U]

Final Report

Volume 3. Subsystems

2 August 1965

Prepared by

Apollo Extension Systems Division

L.M. Tinnan
Program Development Manager

H. P. Burns
Assistant Chief Engineer

~~This document contains information affecting the national defense of the United States within the meaning of the Espionage Laws, Title 18 U.S.C. Section 793 and 794. Its transmission or revelation of its contents in any manner to an unauthorized person is prohibited by law.~~

NORTH AMERICAN AVIATION, INC.
SPACE and INFORMATION SYSTEMS DIVISION

Downgraded at 3-year intervals: declassified after 12 years; DOD DIR 5200.10.

[redacted]

FOREWORD

This volume constitutes a portion of the Prolonged Missions Final Report (SID 65-968). It was prepared as a part of the Extended Apollo Systems Utilization Study conducted by the Space and Information Systems Division of North American Aviation, Inc., for the National Aeronautics and Space Administration's Manned Spacecraft Center under Contract NAS9-3140, dated 6 July 1964. Previously documented as a part of the same contract were the Apollo X studies under report number SID 64-1860.

This final report consists of four volumes:

Volume 1. Configuration 90

Volume 2. Configuration and Performance Analysis

Volume 3. Subsystems

Volume 4. Space Operations and Systems Analysis

TECHNICAL REPORT INDEX/ABSTRACT

ACCESSION NUMBER 07667-65

DOCUMENT SECURITY CLASSIFICATION [redacted]L

TITLE OF DOCUMENT EXTENDED APOLLO SYSTEMS UTILIZATION STUDY, PROLONGED MISSIONS, VOLUME 3: SUBSYSTEMS

LIBRARY USE ONLY

AUTHOR(S) C. GOULD, B. WENDROW, P. LEONARD, J. BATES, P. ANDREWS, A. CORMACK

CODE

ORIGINATING AGENCY AND OTHER SOURCES NAA-S&ID

DOCUMENT NUMBER SID 65-968-3A

PUBLICATION DATE 7/30/65

CONTRACT NUMBER NAS9-3140

DESCRIPTIVE TERMS

SUBSYSTEM LIFE EXTENSION: COMMUNICATIONS/DATA, ELECTRICAL POWER, PROPULSION, ENVIRONMENTAL CONTROL, STABILITY AND CONTROL, EARTH LANDING SYSTEM. MISSION DURATIONS FROM 90 TO 600 DAYS. THREE AND SIX-MAN CREWS.

ABSTRACT

Subsystems parametric data derived during the Prolonged Missions portion of the Extended Apollo Systems Utilization Study is presented for earth orbital durations of 90, 120, 360, and 600 days. Characteristics of subsystems as a function of mission duration are presented in terms of weight, volume, power requirements, and reliability. Block II Apollo subsystems were used as a starting point; considerations for extending operating life include spares and redundancy, and expendables required for the four durations were sized. When Apollo Block II subsystem weights and volumes became very large, alternative concepts were considered. The methodology by which subsystems were chosen for a given mission is treated in Volume 4 of this report.

FORM 131-V REV 11-64
PUBLICATIONS USE ONLY

PREFACE

For the past several years the NASA Manned Spacecraft Center has been examining the application of the Apollo spacecraft to missions alternate to the basic lunar landing mission for which it is currently designed. The overall objective of these studies is an assessment of the advantages and disadvantages associated with the application of developed hardware to these other potential missions.

The initial Extended Mission Apollo study, initiated in August 1963 under contract to NASA/MSC, examined the suitability of Apollo as an earth-orbital biomedical/behavioral experimental laboratory. These experiments were to provide a basic from which man's suitability for protracted space missions could be determined. Three basic configuration concepts (see frontispiece) were investigated throughout the study. Configuration Concept I utilizes only the Apollo command and service modules (CSM), with experimental in-orbit work space made available in the command module by the elimination of one crewman from the current crew size of three. The Apollo CSM subsystems were modified to sustain orbital operations for periods of up to 120 days without resupply. Configuration Concept II consists of the Apollo CSM plus a 5600-cubic-foot laboratory module built within the geometric limits of the LEM adapter. In this concept, the CSM subsystems support the laboratory module functions for the 120-day resupply period. Consequently, Concept II has a laboratory which is dependent on the CSM subsystems. The third configuration (Concept III) is similar to Concept II with respect to the addition of the separate laboratory module within the LEM adapter section. However, the Concept III laboratory was designdd to carry its own subsystems; therefore, it is considered to be independent of the CSM subsystems. The subsystems in the CSM-independent laboratory module were designed for a one-year continuous operation with resupply of expendables by the Apollo CSM as required.

Results of the initial Extended-Mission Apollo studies revealed several additional factors that warranted further investigation. The required 120-day resupply cycle dictated the use of advanced subsystem concepts in several areas. For example, the existing fuel cell electrical power system in Apollo was replaced with a solar cell-battery power system to eliminate the excessive weight and volume penalties attributable to the fuel cells and associated expendables. Additionally, a molecular

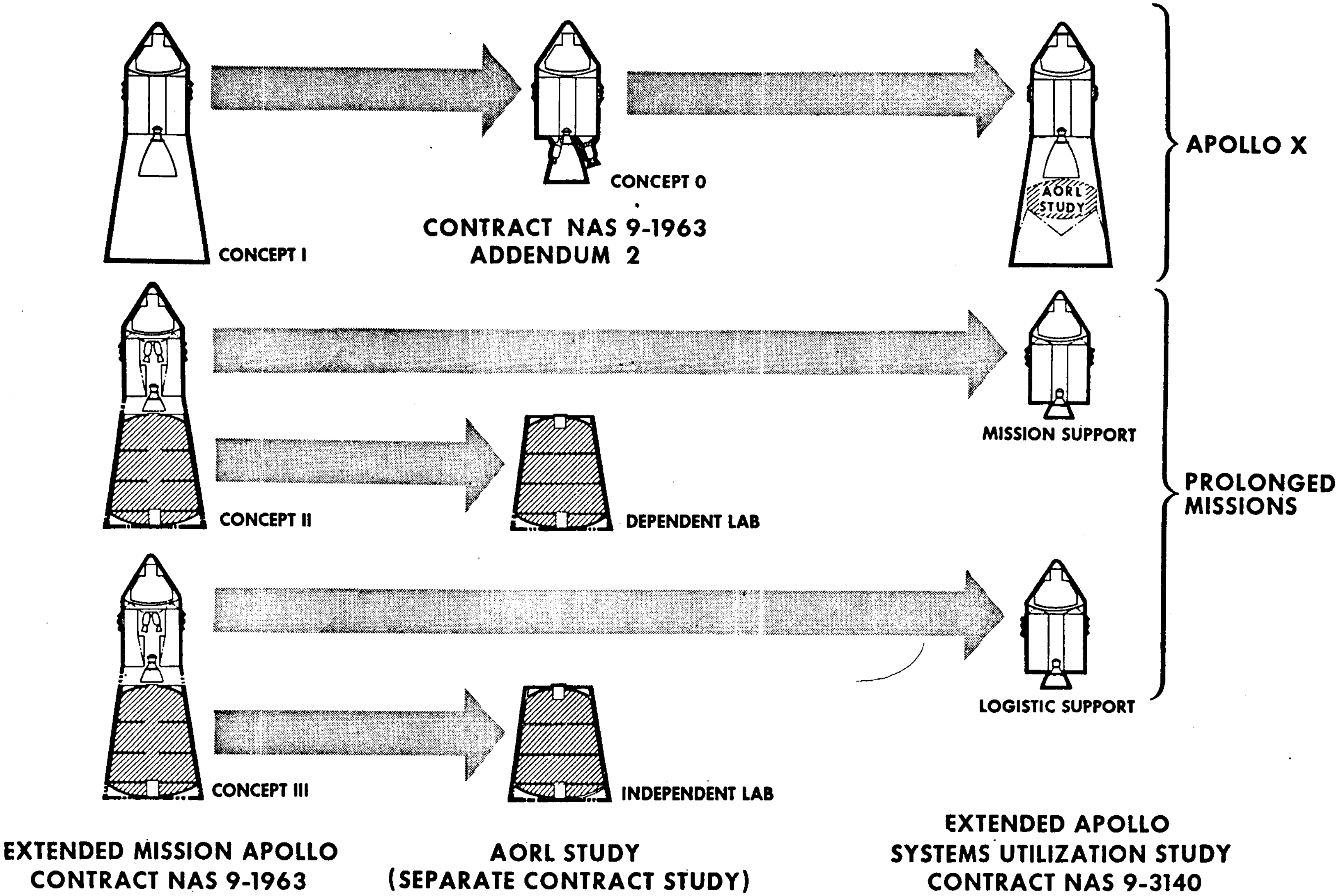
APOLLO X
CONCEPT I
CONCEPT 0
CONTRACT NAS 9-1963
ADDENDUM 2
AORL STUDY
PROLONGED MISSIONS
MISSION SUPPORT
CONCEPT II
DEPENDENT LAB
LOGISTIC SUPPORT
CONCEPT III
INDEPENDENT LAB
EXTENDED MISSION APOLLO
CONTRACT NAS 9-1963
AORL STUDY
(SEPARATE CONTRACT STUDY)
EXTENDED APOLLO
SYSTEMS UTILIZATION STUDY
CONTRACT NAS 9-3140

SYSTEM EVOLUTION

sieve was employed in the environmental control system to eliminate the large weight and volume attendant with using the existing Apollo lithium hydroxide CO_2 removal system for 120 days. Consequently, the limiting mission duration which might result from using only current Apollo subsystem concepts was not known. Also, although the feasibility of extending the life of the current Apollo subsystems had been established in the initial study, specific techniques for accomplishing this life extension had yet to be determined.

For these reasons, further studies were initiated as an addendum to the Extended-Mission Apollo contract. Their purpose was to define the design characteristics and the maximum earth orbital mission duration of the Apollo CSM, assuming restriction to use of existing Apollo subsystem concepts. This configuration was identified as Concept 0. Included in this study was examination of each subsystem to determine the life extensions possible through the addition of spares and redundancies. The study concluded that the earth-orbital duration capability of Concept 0 was approximately 90 days (based on Saturn IB payload limits).

After review of these findings, NASA initiated the current Extended Apollo Systems Utilization Study, one part of which was to define in depth the design and operational characteristics of a vehicle based on the identical subsystems approach employed in Concept 0, but limited arbitrarily to a 45-day maximum mission duration. This vehicle, identified as Apollo X, is one of the configuration approaches included in the current AES Preliminary Definition Phase program.

The remainder of the Extended Apollo Systems Utilization Study, part of which is reported in this volume, has been devoted to the examination of CSM characteristics for potential earth orbital durations up to 600 days. The external laboratories associated with these potential configurations have been examined by NASA under a separate contract study. The primary objective of these was to provide subsystem and vehicle characteristics parametrically and independent of missions in "handbook" form such that configurations for specific durations could be parametrically assembled by NASA for projected earth orbital missions of their choice. Both mission and logistics support functions were examined to allow for potential dependent or independent laboratory operations.

Particular emphasis is placed upon a 90-day CSM configuration (Configuration 90). This particular design represents a potential AES follow-on phase, since the current AES program includes mission durations of up to only 45 days. Within the Configuration 90 studies, emphasis is placed upon a range of possible configurations that could be used to support either an independent or dependent laboratory module under varying resupply requirements.

Configuration 90-1 permits the employment of only extensions to the current Apollo subsystem concepts and, although not technically desirable from the standpoint of weight and volume margins, represents the minimum development cost approach for support of laboratories of this duration. Configuration 90-2 employs advanced subsystem changes in two areas; namely, the power system and ECS, where a nuclear isotopic power source replaces the fuel cells and cryogenic portion of the power system and a molecular sieve replaces the lithium hydroxide method for CO_2 removal, respectively. Configuration 90-3 is based upon Configuration 90-2 with the exception that crew size is increased to six men. This dictates changes in the earth landing system which are incorporated in the form of external attenuation to reduce landing impact loads. Configuration 90-4 is based upon a logistics support requirement where all subsystems are assumed to be in a quiescent orbital state, but a requirement for six crewmen is retained as in Configuration 90-3.

CONTENTS

Page

INTRODUCTION 1

COMMUNICATIONS/DATA SYSTEMS 2

ENVIRONMENTAL CONTROL SYSTEMS 15
  SUBSYSTEMS TRADEOFF DATA 15
    Carbon Dioxide Removal Systems 16
      Lithium Hydroxide 16
      Molecular Sieve 17
      Electrodialysis 18
      CO_2 Freeze Out 20
    CO_2 Reduction - O_2 Recovery Systems 21
      Sabatier Reaction - Without Methane Decomposition 21
      Sabatier Reaction - With Methane Decomposition 23
      Bosch Reaction 23
      Molten Electrolyte 25
    Water Electrolysis Units 25
      Double Membrane Cell (H_2SO_4) 25
      Phosphorous Pentoxide Cell 26
      KOH with Platinum-Asbestos-Nylon Wick 27
    Water Recovery Systems 28
      Electrodialysis 28
      Air Evaporation - Waste Heat 30
      Vapor Compression 31
      Vacuum Distillation-Pyrolysis 32
      Atmospheric Condensate Purification System 34
  DESIGN CALCULATIONS. 37
    CO_2 Removal Systems 37
      LiOH 37
      Molecular Sieve 38
    Total Weight Penalty - Scheme 1 39
      Molecular Sieve 39
    Total Weight Penalty - Scheme 2 40
      Molecular Sieve 40
    Total Weight Penalty - Scheme 2 41
      Molecular Sieve Summary 41
      Electrodialysis System 41
      Comparison of CO_2 Removal Systems 44
    CO_2 Reduction - O_2 Recovery 48
      Sabatier Reaction - Without Methane Decomposition 48
      Sabatier With Methane Decomposition 49
      Bosch Reaction 49
      Comparison of CO_2 Reduction - O_2 Recovery Systems . . . 50

Page

- Water Electrolysis . . . 50
  - Double Membrane Cell (H_2SO_4) . . . 50
  - Phosphorous Pentoxide Cell . . . 53
  - KOH with Platinum-Asbestos-Nylon-Wick Unit . . . 54
  - Comparison of Water Electrolysis . . . 55
- Atmospheric Constituents Storage - Oxygen and Nitrogen . . . 55
  - Storage Requirements . . . 55
- Storage Requirements . . . 56

PROLONGED MISSIONS ECS RECOMMENDATIONS . . . 59
- 90-Day Mission . . . 59
- Mission Longer than 90 Days . . . 63
- 120-Day Mission . . . 67
- 180-Day Mission . . . 67
- 360- and 600-Day Missions . . . 67

EARTH LANDING SYSTEM . . . 69

BLOCK II RECOVERY SYSTEM LIFE EXTENSION ANALYSIS . . . 69
- Radiation Effects Analysis . . . 69
- Temperature Effects . . . 71
- Ultrahigh Vacuum Effects . . . 73
- Effect of Prolonged Parachute Packing Stresses . . . 74
- Combined Environmental Effects . . . 76
- Controlled Compartment Pressure . . . 77

SYSTEM TEST REQUIREMENTS . . . 79
- Test Requirements . . . 79
  - Laboratory Test Parameters . . . 80
  - Laboratory Development Tests . . . 80

SIX-MAN VEHICLE ELS ANALYSIS . . . 83
- Spacecraft Recovery Rationale . . . 84
- Recovery System Parametric Analysis . . . 87
  - Paraglider . . . 87
  - Rotor Recovery System . . . 88
  - Balloon System . . . 88
  - Parachutes . . . 90
- Recovery System Selection . . . 91
  - Landing Characteristics . . . 91
  - Crew Safety and System Reliability . . . 93
  - System Weight and Volume . . . 94
  - Development Risk . . . 95
  - Selected Systems . . . 95

IMPACT ATTENUATION SYSTEMS . . . 97
- Attenuator Concepts . . . 97
  - Velocity Attenuators . . . 99
  - Ballistic Reel . . . 99
  - Ballistic Pulley . . . 99
  - Pressure Increase in Canopy . . . 99
  - Energy Absorbing Systems . . . 102
  - Landing Attitudes . . . 103
  - Landing Dynamic Analysis . . . 103
  - Attenuation System Selection . . . 104

Page

GUIDANCE AND NAVIGATION SYSTEMS . . . 113
- DESIGN FACTORS . . . 115
- APOLLO BLOCK II G&N SYSTEM . . . 119
  - Reliability Analyses . . . 120
  - Performance . . . 127
- N35-S G&N SYSTEM . . . 131
  - Reliability . . . 131
  - Performance . . . 134
- STRAPDOWN SYSTEMS . . . 137
  - System Description . . . 138
- CONCLUSIONS. . . . 143

POWER SYSTEMS . . . 145
- SOLAR CELL POWER SYSTEM . . . 147
  - Solar Cell Array Evaluation . . . 147
    - Solar Cell Array Types . . . 147
    - Cell-Associated Cost Trends . . . 154
    - Weight, Area and Cost Comparisons of 4 KW Arrays . . . 155
  - Solar Array - Spacecraft Mechanical Interfaces . . . 156
    - Stowage of the Solar Array for Launch . . . 157
    - Solar Array Configuration . . . 169
    - Solar Array Structure . . . 170
    - Orientation of the Solar Array . . . 171
  - Secondary Energy Storage . . . 171
    - Battery Characterization . . . 171
    - Estimated Cyclic Life . . . 172
    - Charge Rate . . . 174
    - Battery Pack Weight and Volume . . . 174
    - Power Required to Recharge Battery . . . 176
    - Battery Selection . . . 176
  - Solar Cell Power System Design . . . 178
- ISOTOPE POWER SYSTEM . . . 183
- POWER CONDITIONING, DISTRIBUTION, AND CONTROL . . . 185
  - Reliability of the Power Conversion and Distribution System . . . 185
  - Power Conversion . . . 186
  - D-C Systems . . . 191
    - Electric Motors . . . 192
    - DC Communications Systems . . . 195
- CONCLUSIONS . . . 197

PROPULSION AND REACTION CONTROL SYSTEMS . . . 199
- MAIN PROPULSION SYSTEMS . . . 201
  - Main Propulsion Engines . . . 201
  - Propellant Feed Systems and Tanks . . . 208
- REACTION CONTROL SYSTEM . . . 213
  - RCS Engines . . . 213
  - RCS Tanks . . . 222
    - Tanks with Plastic Bladders . . . 222
    - Tanks with Metal Bellows . . . 224
    - Conclusions . . . 228

Page

STABILIZATION AND CONTROL SYSTEMS 231
APOLLO BLOCK II SYSTEM 233
Reaction Jet Sizing 233
Maneuver Requirements 233
Attitude Hold 237
Local Vertical Attitude Hold 240
Inertial Attitude Hold 243
Solar Panel Considerations 243
System Requirements Summary 253
Reliability Analysis 259
Manual Maneuver Mode 260
Local Vertical Modes 261
Drift Mode 262
Damping Mode 264
Inertial Hold Mode 264
Orbit Maintenance Mode 266
TVC Mode 267
De-energized Failures 268
ALTERNATE CONTROL SYSTEMS 271
Rotational Maneuvers - Reaction Wheel 271
Attitude Hold 274
Solar Panel Considerations 275
Momentum Storage Requirements 276
Sizing Reaction Wheels 278
Windage Losses 279
Momentum Requirements for Twin Gyros 280
Twin Gyro Sizing 282
Desaturation Considerations 284
POWER SYSTEM CONSTRAINTS 287
Fuel Cells 287
Isotope 287
Solar Panels 287

APPENDIX A. INVERTERS 291
PARAMETER RELATIONSHIPS FOR AN EXTENDED-TIME-PERIOD MISSION . . . 293
SELECTION OF 1, 2, OR 3 PHASES 301
LIMITATIONS OF 28-VOLT D-C SUPPLY 311
MODULAR-REPLACEMENT CONCEPT OF REDUNDANCY 313
THREE LEVELS OF RELIABILITY IMPROVEMENT 321

ILLUSTRATIONS

Figure Page

1 Communications/Data Subsystem Initial Relations vs Orbital Duration Utilizing Apollo X Equipment Only 4
2 Reliability of VHF Voice Function 5
3 Reliability of Command Function 5
4 Reliability of Common Function (Premodulation Processor) . . . 6
5 Reliability of Telemetry Function 7
6 Reliability of Television Function 8
7 Reliability of S. Band Voice Function 8
8 Reliability of Tracking Function 9
9 Carbon Dioxide Freeze-out Subsystem Diagram 9
10 CO_2 Removal Techniques. 44
11 CO_2 Removal - Electrodialysis vs. Molecular Sieve Total Weight Penalties 3 Men 45
12 CO_2 Removal Electrodialysis vs. Molecular Sieve Total Weight Penalties 3 Men 45
13 Weight Penalty Breakdown Molecular Sieve No CO_2 Reduction (Scheme #2) 46
14 Weight Penalty Breakdown Molecular Sieve CO_2 Reduction Incorporated in ECS 46
15 Electrodialysis Weight Penalty Breakdown No CO_2 Reduction . 47
16 Electrodialysis Weight Penalty Breakdown With CO_2 Reduction in ECS 47
17 Weight Penalty BOSCH - CO_2 Reduction System 51
18 Weight Penalty Sabatier CO_2 Reduction System 51
19 CO_2 Reduction System Weight Comparison 52
20 Electrolysis Unit Double Membrane Cell 56
21 Electrolysis Unit Phosphorous Pentoxide Cell 57
22 Electrolysis Unit KOH With Plat-ASB-Nylon Wick 57
23 Electrolysis Unit Comparison 58
24 Hardware Plus Expendables Weight Versus Mission Duration . . 60
25 Mission Duration Days 66
26 ELS Compartment Inside Wall Temperature vs Orbital Period for 200 nm Earth Orbit 72
27 Orbital Storage Duration (Days) Vaporizing Substance Weight as Function of Storage Time 78
28 Apollo Impact Attenuation System Schematic 83
29 Paraglider Deployment and Landing Sequence 88
30 Rotary Wing Deployment And Landing Sequence 89
31 Special Purpose Balloon Deployment Sequence 89
32 Lift-to-Drag Ratio Versus Landing Velocity for Cloverleaf and Parasail Parachutes 92
33 Vertical Velocity Versus Horizontal Velocity for Steerable Parachute 92
34 Earth Landing System Weight Comparison 94

Figure Page

35 Earth Landing System Configuration - Three-Legged Gear and Retrorockets . . . 105
36 Earth Landing System Configuration - Extended Heat Shield and Retrorockets . . . 107
37 Landing Stability Envelope of Three-Legged Landing Configuration . . . 109
38 Landing Stability Envelope for Heat Shield Down Configuration . 109
39 Summary Comparison of Candidate Attenuation Concepts . . . 110
40 Apollo G&N Boost Reliability . . . 121
41 Apollo G&N Parametric Reliability . . . 122
42 Probability of Success for Box Level Sparing . . . 122
43 Apollo G&N Parametric Reliability (Expanded) . . . 123
44 Electronic Coupling Unit - Subassembly Sparing . . . 125
45 Apollo Guidance Computer-Module Level Sparing . . . 126
46 Velocity Errors for Short Term Maneuvers . . . 128
47 Local Vertical Uncertainty (1σ) versus Orbit Position Accuracy. . . . 129
48 N35-S Boost Reliability . . . 133
49 N35-S G&N System Parametric Reliability . . . 135
50 Local Vertical Uncertainty (1σ) versus Orbit Position Accuracy. . . . 135
51 Velocity Increment vs. Perigee Altitude . . . 139
52 Gyro Drift Rate Versus Attitude Error Allocation . . . 139
53 Strapdown Configuration Block Diagram . . . 142
54 Power System Flow Diagram . . . 146
55 Basic Solar Array Module . . . 167
56 Solar Array Module Cross Sections . . . 167
57 Plan View of Laboratory and Extended Solar Array . . . 169
58 Skeletal Structure of Solar Array . . . 170
59 Change Rate as Function of Terminal Voltage . . . 173
60 Cycle Life of Hermetically Sealed Nickel and Silver-Cadmium Cells as a Function of Varying Percent Depths of Discharge 9 (25°C) . . . 173
61 Cycle Life of Hermetically Sealed Nickel and Silver-Cadmium Cells as a Function of Charge Rate - (25°C) . . . 175
62 Cycle Life of Hermetically Sealed Nickel and Silver-Cadmium Cells as a Function of Total Battery Pack Weight - (25°C) . 175
63 Cycle Life of Hermetically Sealed Nickel and Silver-Cadmium Cells as a Function of Total Battery Pack Volume - (25°C) . 177
64 Typical Charge Acceptance Curves for Nickel and Silver-Cadmium Secondary Batteries . . . 177
65 Solar Cell System Area . . . 179
66 Solar Cell Power System Weight . . . 179
67 Solar Cell Power System Cost . . . 180
68 Relationship Between Orbital Altitude and Aerodynamic Drag . 181
69 Power Distribution Reliability Diagram . . . 187
70 PDS Reliability for Prolonged Mission Apollo . . . 191
71 Two Phase Inverter - Motor Schematic . . . 193
72 Propellant Fraction - Liquid Propellant Propulsion Systems . 207
73 Propellant Fraction - Solid Propellant Motors . . . 207

Figure Page

74 Initial Vehicle Weight - 1000 Lb. 211
75 Pressurization System Wt. Vs. Propellant Weight 212
76 Short-Pulse Reaction-Control-System Engine, Performance Schematic 217
77 Limit-Cycle Theory for Reaction-Control Engines, Schematics . 218
78 Propellant Requirements a Function of Thrust Level for Reaction-Control-System Limit-Cycle Operation 221
79 Reaction Control System Tank with Plastic Bladder 223
80 Effect of Nuclear Radiation on Physical Characteristics . . 224
81 Bellows Tank Configuration 225
82 Weight of Bellows Tank Assembly vs. Tank Radius & Bellows Span for Volume of 7.1 Ft^3 226
83 Weight of Bellows Tanks Vs. Loadable Volume 227
84 Reaction Control System Total Impulse Vs. Total Weight . . 229
85 Minimum Impulse Bit vs. Pulse Width 234
86 Rotational Maneuver Propellant Requirements 235
87 Variation of Effective Specific Impulse 238
88 Theoretical Propellant Flow Rate for Limit Cycle Operation . 238
89 Theoretical Jet Starts for Limit Cycle Operation 240
90 Biased Limit Cycle Propellant Factor 241
91 Fixed and Movable Solar Panel Configuration 245
92 Yearly Average of the Sun Line Angle (ζ) 246
93 Vehicle Orientations for Movable Solar Panels 247
94 Roll, Yaw Control Law for Local Vertical and Local Horizontal Vehicle Control 247
95 Solar Panel Pointing Requirements 249
96 Aerodynamic Disturbance Torques in Local Vertical Mode Configuration #1 250
97 Aerodynamic Disturbance Torques in Local Vertical Mode Configuration #2 251
98 Aerodynamic Disturbance Torques in Local Horizontal Mode . . 251
99 Reaction Control System Total Weight 254
100 Reaction Jet Reliability as a Function of Actuations and Operating Time 254
101 Orbit Mode Success Diagrams 256
102 Manual Maneuver Mode Reliability 261
103 Local Vertical Mode Reliability 263
104 Drift Mode Reliability 263
105 Damping Mode Reliability 265
106 Inertial Hold Mode Reliability. 266
107 Orbit Maintenance Mode Reliability 267
108 TVC Mode Reliability 268
109 Typical Effect of De-Energized Failures 269
110 Maneuver-Torque Requirements for Reaction Wheels 272
111 Vehicle Maneuver-Momentum Requirements 273
112 Maneuver-Torque Requirements for Reaction Wheels 273
113 Maximum Stored Momentum to Counter Disturbance Torques - Y Axis 277
114 Maximum Stored Momentum to Counter Disturbance Torques - Z Axis 277

Figure Page

115 Reaction Wheel Design Criteria 279
116 Gyro Angular Momentum Requirements 282
117 Effect of Rotor Radium on System Weight 283
118 Rotor Radius for Minimum Weight 284
119 Isotope or Fuel Cell Peak Power Penalties 288
120 Solar Panel Peak Power Penalties 289
121 Block Diagram of a Phase-Shift Regulated Static Inverter . . 298
122 Output Voltage Vector Diagram for Phase-Shift Regulated Inverter 299
123 Definitions of Flux Distribution and Core Dimensions of Output Transformer 304
124 Voltage Applied to the Primary Coils and the Flux Distribution in Each Core Leg 305
125 Actual Output Transformer Long Lamination Dimensions . . . 306
126 Actual Output Transformer Short Lamination Dimensions . . . 307
127 Single-Phase Inverter Plan 308
128 Identical Power-Stage-Transformer 2-Phase Inverter Plan . . 309

TABLES

Table		Page
1	Initial Reliability Predictions for Communications/Data Subsystem Utilizing Only Apollo X Equipment (No Spares)	4
2	Number of Spares Required for Communications/Data System To Achieve Allocated Goals	10
3	Number and Types Spares	11
4	Regenerative Systems Weight and Power Breakdown	65
5	Functional Thresholds of Sequence Controller Components	71
6	Recovery Concepts Comparison	96
7	Impact Attenuation System Conditions (No Double Emergencies Assumed).	98
8	Apollo G&N Failure Rates	120
9	Apollo Block II G&N Equipment Weights	124
10	AGC Variations	126
11	Apollo Block II G&N Error Sources	129
12	N35-S Physical Characteristics	132
13	D62A Computer Variations	134
14	N35-S Error Sources	134
15	Cost vs. Solar Cell Efficiency for Conventional and Concentrator Arrays	152
16	Cost Comparison, Conventional Versus Concentrator Arrays with Solar Cell Efficiency	152
17	Comparison of 4 KW Conventional and Concentrator Arrays	156
18	PDS Reliability Analysis for Prolonged Mission Apollo	189
19	Performance and Design Characteristics of Aerojet-General AJ10-137 Apollo S/M Engine	202
20	LEM Descent Engine Performance and Design Characteristics	203
21	SPS Propellant Load	209
22	Engine Propellant Inlet Requirements	211
23	Assumed Characteristics of Configurations	231
24	Rotational Maneuver Jet Starts (per jet, per maneuver)	235
25	Procedure for Determination of Jet System Maneuver Requirements	236
26	Procedure for Determination of Jet Requirements During Local Vertical Hold	242
27	Procedure for Determination of Jet System Requirements During Inertial Attitude Hold	244
28	RMS Disturbance Torque Summary for Vehicles With Fixed Solar Panels (ft-lb)	245
29	Reaction Propellant for Vehicle Pointing (lb/day) - Movable Solar Panels	249
30	Procedure for Analysis of Reaction System Requirements on a Vehicle Utilizing Solar Panels	252

Table		Page
31	System Component Summary (Block II SCS)	255
32	Inertial Attitude Hold Momentum Requirements (ft-lb-sec/orbit)	275
33	Maximum Integrated Torque Value per Orbit for Vehicle with Fixed Panels (ft-lb-sec).	276
34	Summary of Power System Penalties	290

INTRODUCTION

This volume presents the subsystems parametric data generated for the Prolonged Missions portion of the Extended Apollo Systems Utilization Study. The parametric data is presented in a form so that the characteristics of a subsystem for four earth orbital durations (90 days, 120 days, 360 days, and 600 days) can be easily ascertained.

The overall objective of the study was to identify the characteristics of subsystems as a function of mission duration. These characteristics were defined in terms of weight, volume, power requirements, and reliability. These subsystems studies used Apollo Block II subsystems as a starting point and considered extensions required for longer life (such as spares and redundancy) and also sized expendables. Since some Apollo subsystems weights and volumes become very large for extended missions, alternative subsystems were investigated. The methodology by which each subsystem is chosen for a given mission is treated in Volume 4. A subsystem cannot be selected independent of other subsystems or the mission profile; what is required is an evaluation of its interaction with other systems and the total integrated system. An application of the methodology is treated in the volume dealing with Configuration 90 (Volume 1).

The basic philosophy of the subsystems study was to treat certain parameters as variables and determine the effect of the variation on other parameters. For example, for electronic subsystems such as G&CS or Communications/Data, the operating hours per day was varied and its affect on system reliability and weight/volume determined as a function of mission duration. The environmental control systems operate continuously; their reliability is an explicit function of mission duration. However, the size of the crew affects the design in that weight is a function of the expendables required. Therefore, this study established the weight and volume versus mission duration of various ECS functions with crew size as a parameter - three or six men.

The design of the earth landing system is almost independent of mission duration (except for storage thermal and pressure problems); however, it is dependent on crew size and water versus land landing. The crew size was varied between three and six men. From an earth landing system viewpoint any size crew greater than three and less than six dictates a design which could be used for land landings due to the impact attenuation problem; a crew size of three or less can be accommodated by the Apollo Block II system.

The power system is a continuously operating system and therefore its reliability is a direct function of mission duration. Its design weight and volume is dictated by the required average power level and the vehicle design (placement of system components).

The main propulsion system size is dictated by total vehicle weight and the required maneuvers. Its reliability is a direct function of the mission duration and environment. The reaction control system sizing is related to the number of attitude maneuvers (and their slewing rate), the amount of time within a deadband, vehicle weight, etc The reliability of the system is a function of the number of operations per mission. The reaction control system is intimately related to the G&CS; the calculation of propellant requirements is, therefore, treated in the stabilization and control system section; the problems associated with hardware design are treated in the Propulsion and Reaction Control System section.

Since the selection of any subsystem is affected by the mission profile (as described above), three missions/configurations of particular interest were a logistics support vehicle, a mission support vehicle and a combined mission/logistics support vehicle. These three configurations are treated in each individual section. As a general rule, the logistics support vehicle subsystems are those treated in SID 65-179; the mission support vehicle subsystems will vary depending on mission profile and duration. The combined mission/logistics support vehicle subsystems are the same as those for a mission support vehicle, but with the added capability to withstand extended periods of space storage.

The succeeding sections of this volume treat the subsystems in alphabetical order.

COMMUNICATIONS/DATA SYSTEMS

An analysis of the communications/data subsystem including the TV and Command Decoder was performed for a total of four different orbital durations of 90, 120, 360, and 600 days, each with orbital operational periods of 2, 4, and 6 hours per day.

Initially, reliability predictions based on Apollo X hardware only and utilizing Apollo X failure rates were determined for each of the 12 different missions. These results are shown in Table 1 and illustrated in Figure 1. From Table 1, it can be seen that none of the initial reliability estimates for any of the missions achieve the assigned goals for those missions.

Next, the minimum number of spares which would be required to enable the reliability of each mission to achieve its allocated goal was determined. In determining the items which should be spared, the minimum risk criteria was employed in the following manner. The initial reliabilities of each unit were examined until the lowest reliability item was found. This item would be spared and the new system reliability computed. The reliabilities were then re-examined until the next lowest reliability was found. This item was then spared and the new system reliability computed. This procedure was repeated until the allocated reliability goal was achieved.

The reliability of the communications/data system is composed of the reliability of the individual portions of the system. The reliability of the various communication/data system functions for 90, 120, 360, and 600 days durations is illustrated in Figures 2 to 8. Figure 2 illustrates the VHF voice function. It is seen that this function requires spares only for high usage rates.

Figure 3 illustrates the command functions; spares are required again for high usage rates. Figures 4 through 8 illustrate the reliability of the other functions including the use of spares.

Tables 2 and 3 show the number of spares required to achieve the required reliability.

From the table it can be seen that at least 2 spares would be required for both the 90 day mission and 120 day missions of 2 hours per day operation. At least 11 spares would be required for the 600 day mission of 6 hours per day operation.

[redacted]

TABLE 1
Initial Reliability Predictions for Communications/Data Subsystem Utilizing Only Apollo X Equipment (No Spares)

ORBITAL OPS	90 DAY MISSION	120 DAY MISSION	360 DAY MISSION	600 DAY MISSION
2 hrs/day	0.98801	0.98448	0.95087	0.91589
4 hrs/day	0.97595	0.96773	0.89785	0.82351
6 hrs/day	0.96355	0.95087	0.84233	0.72686

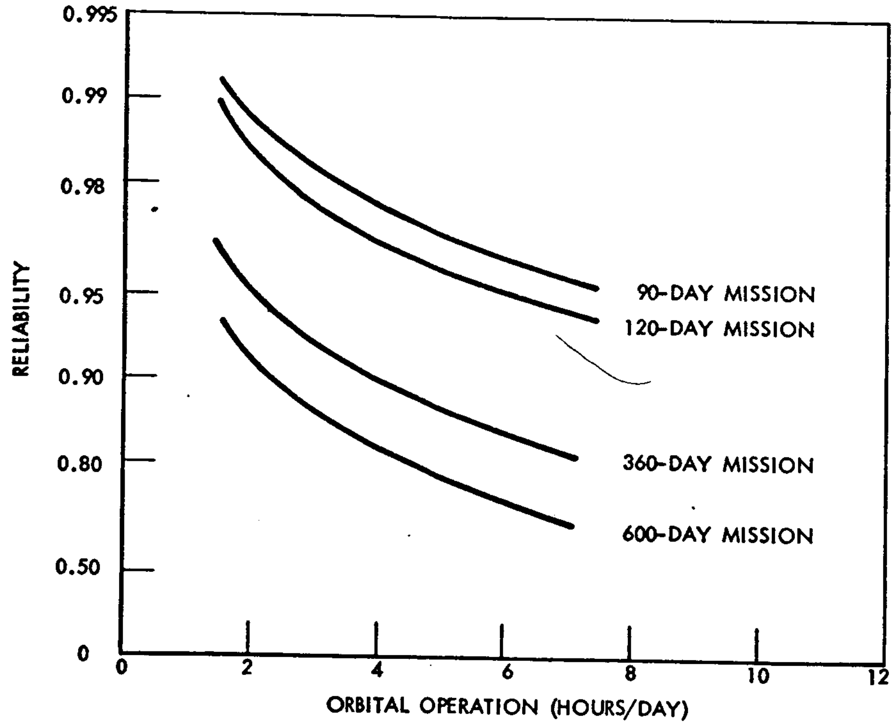

Figure 1. Communications/Data Subsystem Initial Relations vs Orbital Duration Utilizing Apollo X Equipment Only

[redacted]

CO[redacted]

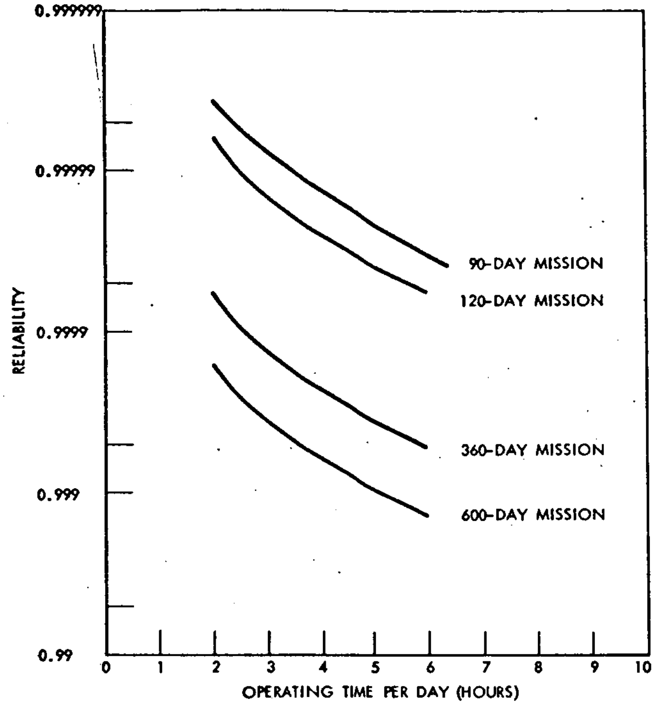

Figure 2. Reliability of VHF Voice Function

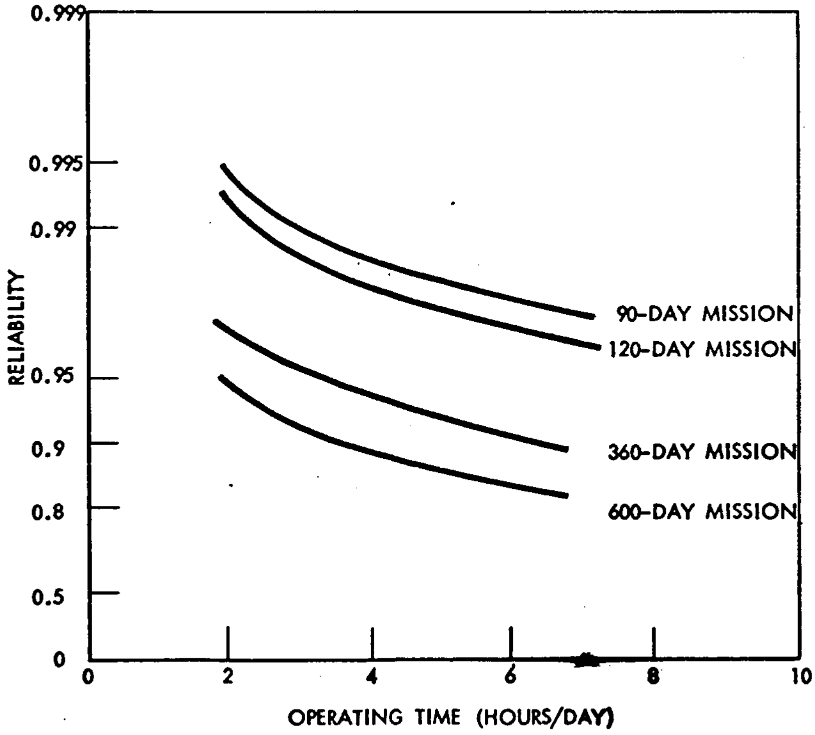

Figure 3. Reliability of Command Function

[redacted]

[redacted]

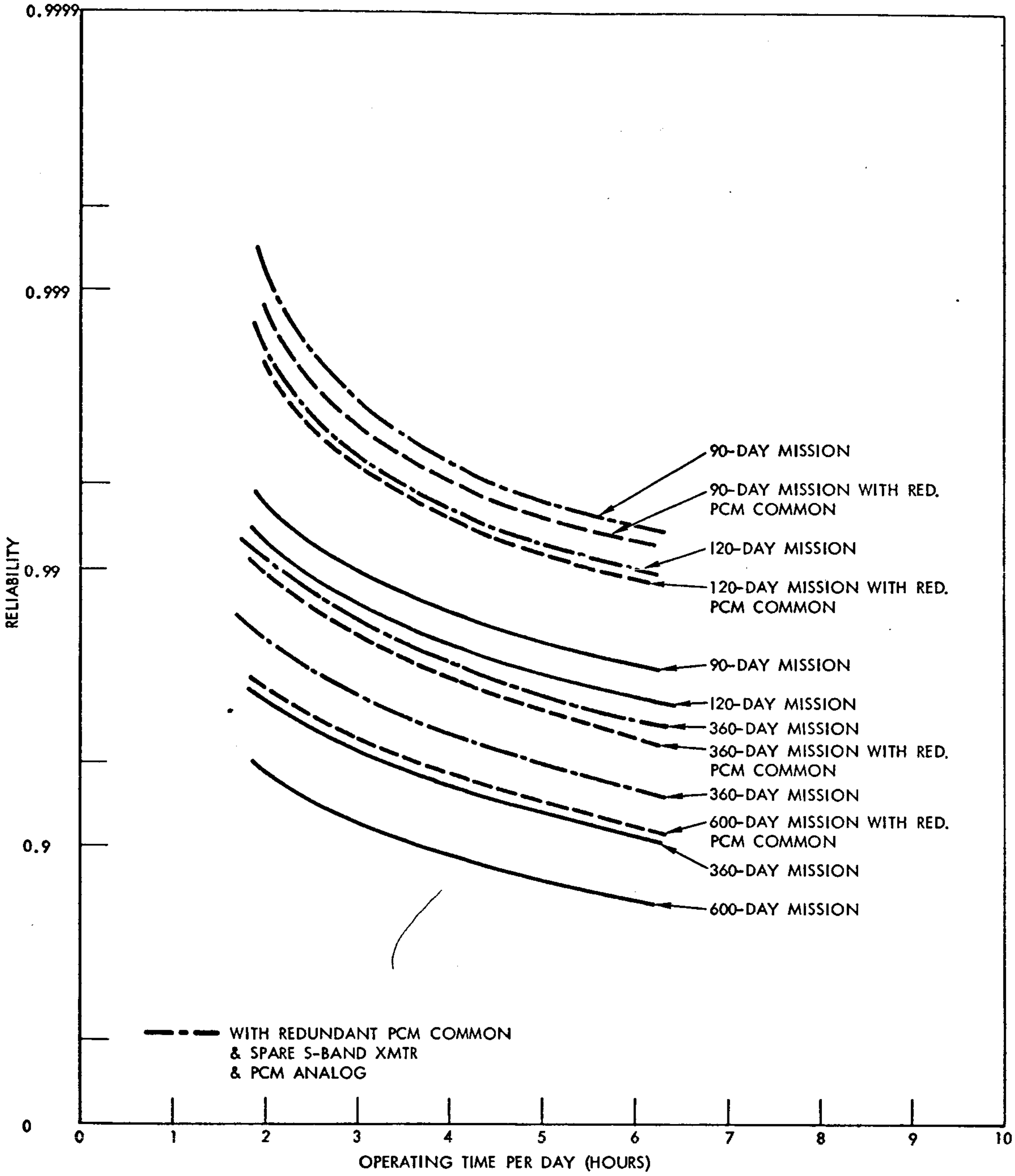

Figure 4. Reliability of Common Function (Premodulation Processor)

[redacted]

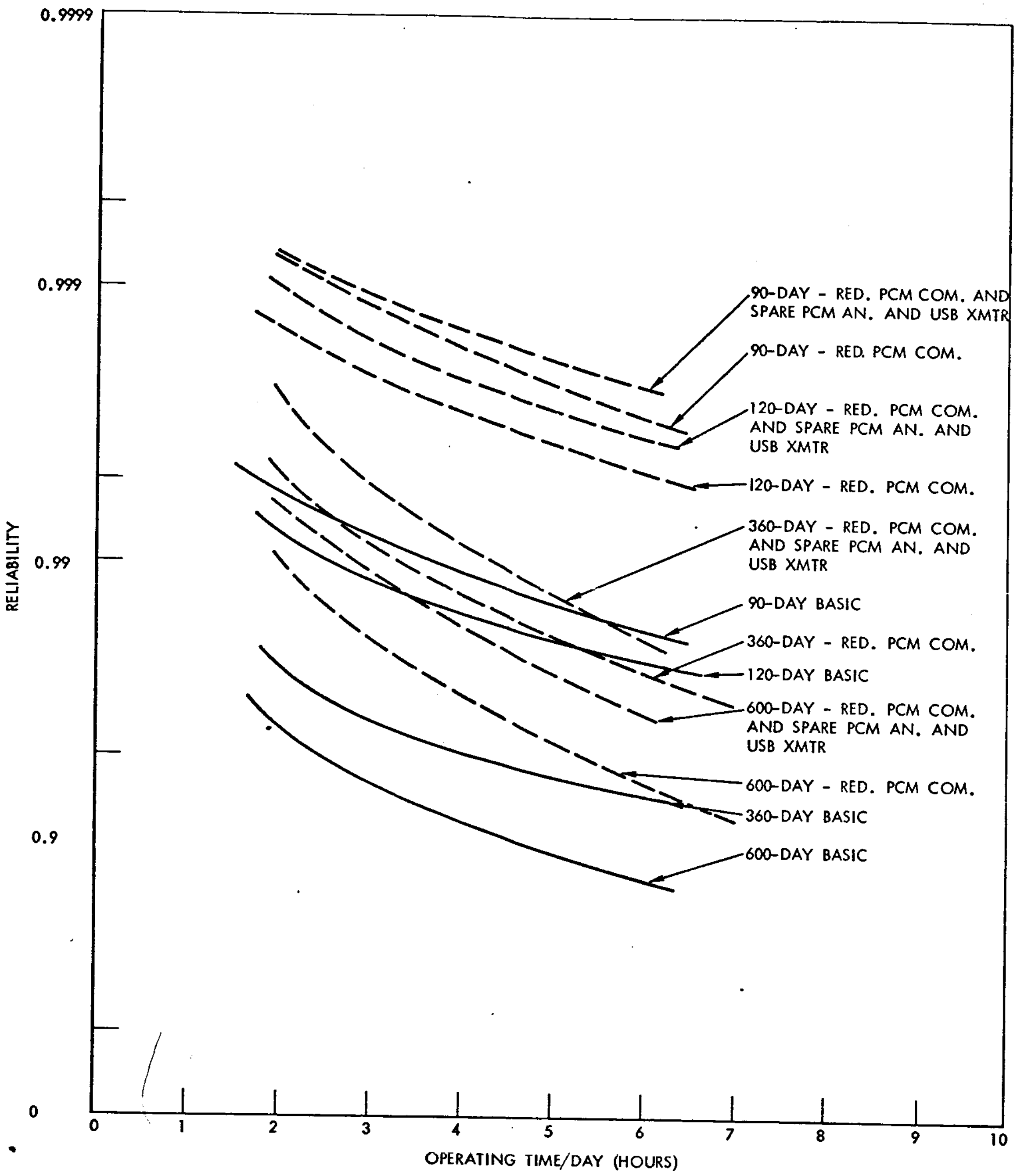

Figure 5. Reliability of Telemetry Function

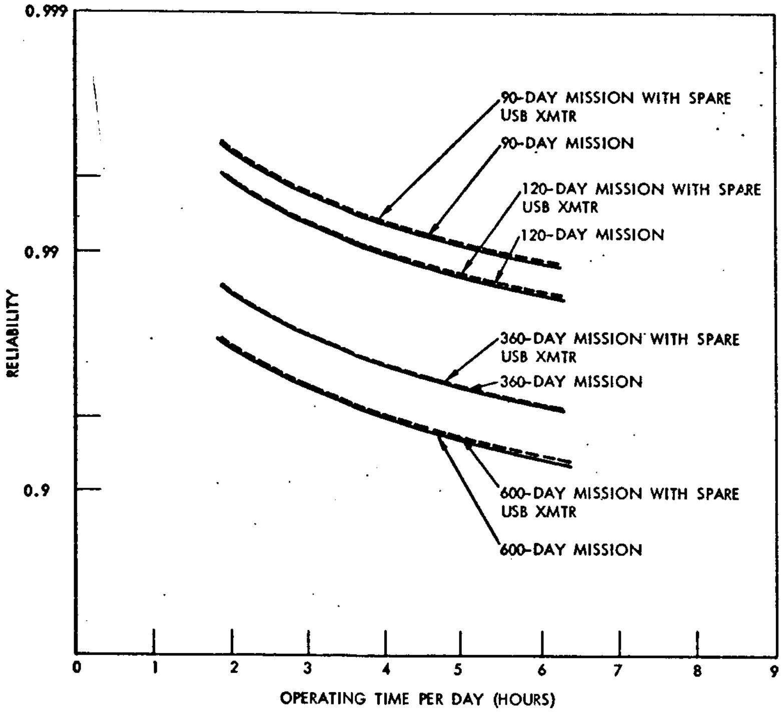

Figure 6. Reliability of Television Function

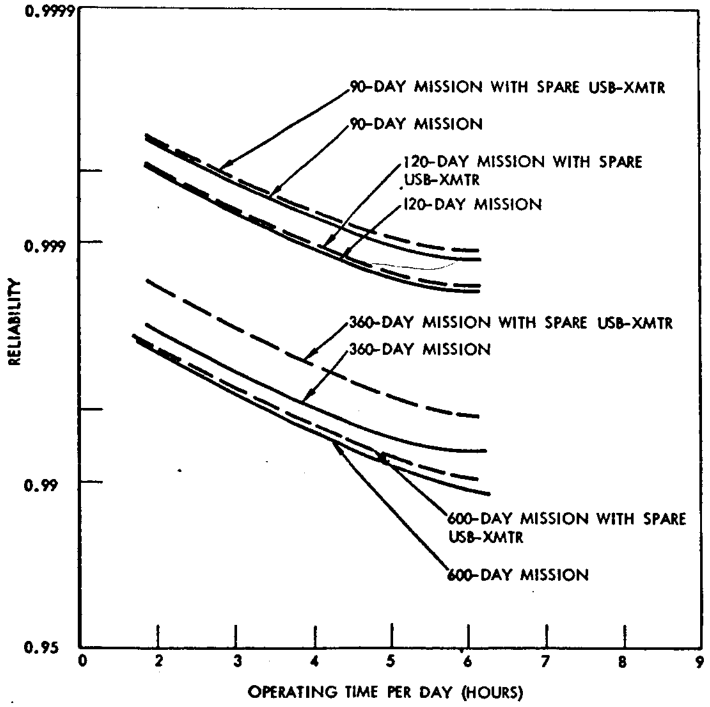

Figure 7. Reliability of S Band Voice Function

CON[redacted]

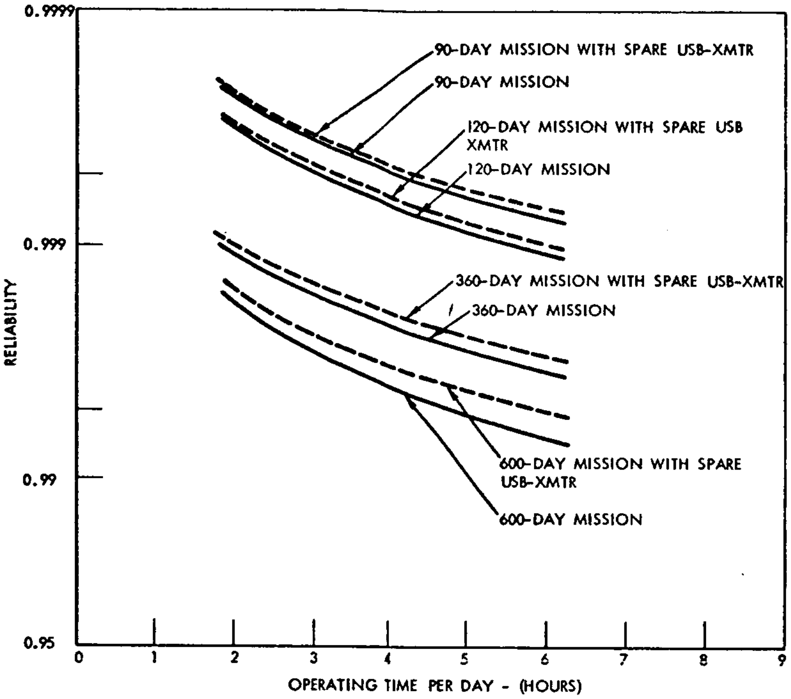

Figure 8. Reliability of Tracking Function

[redacted]

TABLE 2
Number of Spares Required for Communications/Data System to Achieve Allocated Goals

MISSIONS	HR/DAY OPN.	INITIAL RELIABILITY	SPARES REQ'D	FINAL RELIABILITY
90 day	2	0.98801	2	0.99610
120 day	2	0.98488	2	0.99523
360 day	2	0.95087	5	0.99555
600 day	2	0.91589	6	0.99459
90 day	4	0.97595	3	0.00482
120 day	4	0.96773	4	0.99555
360 day	4	0.89785	7	0.99707
600 day	4	0.82351	9	0.99478
90 day	6	0.96355	4	0.99460
120 day	6	0.95087	5	0.99555
360 day	6	0.84233	8	0.99483
600 day	6	0.72886	11	0.99369

TABLE 3
Number and Types Spares

ORBITAL OPERATIONS - 2 Hours/Day

1. 90 Day Mission Initial Reliability = 0.98801 Goal = 0.99350

2 Spares Required

1 DSE
1 TV

Final R = 0.99610

2. 120 Day Mission Initial Reliability = 0.98488 Goal = 0.99352

2 Spares Required

1 DSE
1 TV

Final R = 0.99523

3. 360 Day Mission Initial Reliability = 0.95087 Goal = 0.99357

5 Spares Required

1 DSE
1 TV
1 CMM'D Decoder
1 PMP
1 HF Xceiver

Final R = 0.99555

4. 600 Day Mission Initial Reliability = 0.91589 Goal = 0.99359

6 Spares Required

1 DSE
1 TV
1 CMM'D Decoder
1 PMP
1 HF Xceiver
1 PCM

Final R = 0.99459

ORBITAL OPERATIONS - 4 Hour/Day

1. 90 Day Mission Initial Reliability = 0.97595 Goal = 0.99350

3 Spares Required

1 DSE
1 TV
1 CMM'D Decoder

Final R = 0.99482

[redacted]

2. 120 Day Mission Initial Reliability = 0.96773 Goal = 0.99352

4 Spares Required

1 DSE
1 TV
1 CMM'D Decoder
1 PMP

Final R = 0.99555

3. 360 Day Mission Initial Reliability = 0.89785 Goal = 0.99357

7 Spares Required

1 DSE
1 TV
1 CMM'D Decoder
1 PMP
1 PCM
1 HF Xceiver
1 "C" Band Xponder

Final R = 0.99707

4. 600 Day Mission Initial Reliability = 0.82351 Goal = 0.99359

9 Spares Required

2 DSE
1 TV
1 CMM'D Decoder
1 PMP
1 PCM
1 HF Xceiver
1 "C" Band Xponder
1 USB Xceiver

Final R = 0.99478

ORBITAL OPERATIONS - 6 Hour/Day

1. 90 Day Mission Initial Reliability = 0.96355 Goal = 0.99350

4 Spares Required

1 DSE
1 TV
1 CMM'S Decoder
1 PMP

Final R = 0.99460

2. 120 Day Mission Initial Reliability = 0.95087 Goal = 0.99352

5 Spares Required

1 DSE
1 TV
1 CMM'D Decoder
1 PMP
1 HF Xceiver

Final R = 0.99555

[redacted]

3. 360 Day Mission Initial Reliability = 0.84233 Goal = 0.99357

8 Spares Required

2 DSE
1 TV
1 CMM'D Decod
1 PCM
1 PMP
1 HF Xceiver
1 "C" Band Xponder

Final R = 0.99483

4. 600 Day Mission Initial Reliability = 0.72886 Goal = 99359

11 Spares Required

2 DSE
2 PCM
2 "C" Band Xponder
1 TV
1 CMM'D Decoder
1 PMP
1 HF Xceiver
1 USB Xceiver

Final R = 0.99369

ENVIRONMENTAL CONTROL SYSTEMS

ENVIRONMENTAL CONTROL SYSTEM

ENVIRONMENTAL CONTROL SYSTEMS

ECS systems requirements were examined for missions ranging up to 600 days in duration. The results are presented in this section in three categories: subsystem tradeoffs, recommended systems for discrete mission durations, and recommended systems for a group of 90 day missions.

SUBSYSTEMS TRADEOFF DATA

The purpose of this section of the study is to collect and compare data on the subsystems which make up the ECS system. The following subsystems were considered:

1. CO_2 removal
2. CO_2 reduction and oxygen recovery
3. Oxygen recovery by water electrolysis
4. Water recovery
5. Condensate purification

Much has been written in the past few years on the above subsystems, with the intent of developing regenerative ECS systems for long duration space flight. Some of the work is substantiated by laboratory experiments, and shows promise of ultimate practical development. However, a great deal of the literature is based on what might be theoretically possible, with little or no experimental backing. In this present study, only those subsystems which are realistic have been included.

The data for each subsystem are presented in a format which includes the subsystem characteristics, process factors, state-of-the-art, and comments. Comparisons of the subsystems are presented graphically, in the form of weight versus mission duration.

CO_2 Output	2.25 lb/man-day
O_2 Uptake	2.00 lb/man-day
H_2O Metabolically Produced	.99 lb/man-day
H_2O Input (food & drink)	6.00 lb/man-day
Wash Water Required	5.00 lb/man-day
Urine Output (H_2O only)	3.32 lb/man-day

Humidity Condensate (res. & pers.)	3.32 lb/man-day
Cabin Temperature	72 ± 3°F
Total Cabin Pressure	7.0 psia
Oxygen Partial Pressure	3.1 psia
CO_2 Partial Pressure	5 mm Hg
H_2O Partial Pressure (40-60% R.H.)	10 mm Hg
Leak Rate C/M	5 lb/day
Leak Rate L/M	5 lb/day
Power Supply	Solar Cell + Battery or Isotope
Volume C/M	210 ft^3
Volume L/M	1360 ft^3

CARBON DIOXIDE REMOVAL SYSTEMS

Lithium Hydroxide

Characteristics - The system consists of two parallel canisters packed with lithium hydroxide. Air from the main conditioning loop is passed through one canister; the CO_2 is chemically absorbed, forming Li_2CO_3 and H_2O, and releasing heat to the air stream. The LiOH must be replaced periodically. The equipment is generally connected in the pressure suit loop, or the main cabin air loop. No direct power input is required, although a part of the main air loop blower pressure drop can be assessed to the LiOH system. The heat of the chemical reaction also imposes a penalty, since it must be removed by the thermal control loop liquid in the main heat exchanger.

Process Factors

	3 Men	6 Men
Fixed Hardware (lb)	16.4	23.4
LiOH Required (lb)		
90 Days	719.0	1438
360 Days	2875	5750
600 Days	4800	9600
Heat Produced, BTU/hour	364	728

	3 Men	6 Men
System ΔP, inches H_2O	2.44	3.21
Power Equivalent to ΔP, watts	26	68
H_2O produced (credit) pounds/day	2.76	5.52

State-of-the-Art - This system may be considered to be fully developed and available immediately. It has been used on the Mercury, and is planned for use on both Gemini and Apollo.

Comments - The system is simple, proven in operation, and has no moving parts. The only disadvantage is its severe weight penalty for mission durations greater than 3 weeks.

Molecular Sieve

Characteristics - Molecular sieve is the trade name for the most commonly used synthetic zeolite (metal-ion alumino-silicates). The name molecular sieve is commonly used for the entire CO_2 adsorption system which normally contains a water adsorbent, heaters, control valves, etc., as well as the zeolite beds. In general the units being developed utilize a water adsorbent such as silica gel to remove the water from the cabin "air" prior to CO_2 absorption in the zeolite bed. This is necessary since the zeolites have a greater affinity for water than for CO_2. Most of the systems being developed consist of two silica gel beds and two "molecular sieve" beds. One set is being desorbed, or regenerated, while the other set is adsorbing water and CO_2. A CO_2 saturated molecular sieve bed and a water saturated silica gel bed can be desorbed by exposing the beds to a vacuum, raising the bed temperature or a combination of both. Exposing the "loaded" beds to the vacuum of space is a very effective method of regeneration. The adsorbent is lost however, and this introduces a weight penalty for water make-up. If CO_2 reduction - O_2 regeneration is included, the CO_2 must be collected for reduction. Three schemes are therefore generally considered:

1. Both CO_2 and water are vacuum desorbed overboard to the space vacuum. (Non-conservation system)

2. Water is desorbed by heat and returned to the cabin. CO_2 is vacuum desorbed overboard to the space vacuum. (Water conservation system)

3. Water is desorbed by heat and returned to the cabin. CO_2 is desorbed by heat and retained for reduction to O_2. (CO_2 concentrator system)

Scheme 1 requires power to operate a timer, valves and a small blower. This amounts to about 8-15 watts per man. Scheme 2 requires the same power as Scheme 1 plus a heater in the silica gel bed which adds approximately 70 to 100 watts per man, or a total of 78 to 115 watts per man. Scheme 3 requires the same power as Scheme 2 plus a heater in the CO_2

adsorber bed which adds an additional 80 to 100 watts per man, or a total of 158 to 215 watts per man. If a waste heat liquid coolant source is available, it might be used to supply the heat for desorption in either Scheme 2 or 3. The heat of water desorption is rejected back to the cabin since the process "air" stream is used to desorb the water and carry it back to the cabin atmosphere.

Process Factors

	3 Men	6 Men
Fixed Hardware Weight (Scheme 2 or 3)	55 lb	75 lb
Power Required (total)		
Scheme 1	35 watts	60 watts
Scheme 2	285 watts	500 watts
Scheme 3	560 watts	950 watts
Spare Parts Weight (or redundancy added)	0.10 lb/day	0.13 lb/day
Process Flow Rate (5 mmHg CO_2, 50% eff. mole. sieve ads)^2	27 lb/hour	54 lb/hour
Volume (Scheme 2)	1.5 ft^3	2.2 ft^3

State-of-the-Art - This system is in the flight hardware development stage. Flight type units have been delivered which are being evaluated by the NASA agency at present. This system may therefore be considered as presently available.

Comments - This system, while more complex than the non-regenerable CO_2 adsorbent LiOH, is a fairly simple, straight-forward system. The main reliability disadvantage is the valves which are cycled frequently and the high pressure rise blower(s) which must operate for the duration of the mission. For missions longer than several weeks a regenerable system offers a weight saving over a non-regenerable system.

Electrodialysis

Characteristics - The electrodialysis CO_2 "scrubber" consists of 4-cell modules plus accessories. A number of such modules may be stacked in series electrically but with like gas and liquid streams manifolded in parallel. The four cells of each module have coordinated functions and are compartments containing a packing of very small spheres of ion exchange resins. The compartment dividers are anion or cation selective membranes. Current flow is through the packings and the membranes.

In operation, moist air containing CO_2 is forced through the absorber cell where the CO_2 reacts with hydroxyl ions to form carbonate and bicarbonate ions as follows:

$$2.8\ CO_2 + 4OH^- = 1.6\ HCO_3^- + 1.2\ CO_3^= + 1.2\ H_2O$$

The carbonate and bicarbonate ions are driven electrically through the cation selective membrane into the concentrator cell where they react with hydrogen ions to form CO_2 as follows:

$$1.6\ HCO_3^{-} + 1.2\ CO_3^{=} + 4H^{+} = 2.8\ CO_2 + 2.8\ H_2O$$

Separation of the CO_2 from the H_2O completes the scrubbing process. It is necessary to provide a hydroxyl ion supply for the absorber cell and a hydrogen ion supply for the concentrator cell. In the anode cell, electrolysis of H_2O generates the hydrogen ions which are transported electrolytically through an anion selective membrane into the concentrator cell. In a similar manner, hydroxyl ions are generated in the cathode cell and pass through a cation selective membrane into the absorber cell. The reactions are

Anode: $2H_2O = O_2 + 4H^{+} + 4\bar{e}$

Cathode: $4\ H_2O + 4\ \bar{e} = 2H_2 + 4\ OH^{-}$

The primary mode of heat rejection is by an excess flow of H_2O throughout the anode and cathode cells. The rate is about 40 lb/hr (for 3 men) for each stream. Circulation of this water through an external heat exchanger is necessary.

All four of the streams leaving each module contain water plus a gas - one is cabin "air" plus a slight amount of H_2O, the second is H_2 plus H_2O, the last is CO_2 plus H_2O. Therefore, three different water-gas separation cycles must be included in the system, as well as the water supply system. In addition to separating CO_2 from cabin air at an efficiency of about 50%, this system electrolyzes enough water to provide about 35% of the metabolic oxygen requirement. If CO_2 reduction and electrolysis are incorporated, this would decrease the size and power of the electrolysis unit.

Process Factors

	3 Men	6 Men
Fixed Hardware Weight, Unit only	40 lb	65 lb
Blower Weight	12 lb	16 lb
Aux. 3 Pumps & 3 Separators Weight	10 lb	16 lb
Aux. Water Tanks (3) Weight	18 lb	24 lb
Power, Basic Unit (2100 watt-hr/lb of CO_2 removed)	600 watts	1200 watts
Power, Blower (20 in P)	120 watts	180 watts
Power, Pumps (3)	20 watts	30 watts

[redacted]

Spare Parts Weight	0.10 lb/day	0.13 lb/day
Electrolysis Credit (Electrolysis Penalty = 5.35 lb/lb O_2/day and 123 watts/lb O_2)	2.1 lb of O_2/ day	4.2 lb of O_2/ day

State-of-the-Art - This system is in the "flight type" development stage, IONICS, Inc., have delivered units similar to flight hardware to potential contractors for evaluation.

Comments - Some of the control problems associated with this system which are not discussed in detail by the developer are: (1) Humidification of the "air" + CO_2 entering the unit. This is necessary to avoid drying out of the membranes. (2) Gas-liquid separation. Since there are three H_2O streams each with a different gas (O_2, CO_2, and H_2) leaving the unit, each requires a liquid-gas separator. Because the separation is not 100% effective, the H_2O streams should be kept separate, so it requires three water accumulator tanks plus three water metering devices. The system control becomes fairly complicated. (3) The water-gas separators proposed are microporous membranes, which have not been shown to operate at zero g. (4) Complex manifolding presents difficult redundancy addition. However, this system appears to be fairly simple in operation. Cycling, for instance, is not required.

The reliability of the unit depends mainly on the reliability of the membranes and packing. Since the packing must be very dense, (the ion exchange resin spheres have to touch each other for electrical conduction) the pressure drop is very high. This could cause the resin spheres to become relocated or could cause puncture of the membranes.

The electrodialysis system is considered less reliable than the molecular sieve.

CO_2 Freeze Out

Characteristics - This system is of interest in a vehicle where a cryogenic heat sink is available or where the power penalty is very low. This heat sink may, in some cases, be provided by the cryogenic oxygen or nitrogen used in atmosphere supply. The "air" plus CO_2 mixture is cooled to a temperature below the CO_2 freezing point (-109°F) but above the air liquification point (-317°F). The water is removed from the "air" prior to introduction into the CO_2 freeze out section. This is accomplished in several ways; one, by first freezing out the water, then freezing out the CO_2. The main disadvantage is the large heat sink required. An average of 1200 BTU/hr per man is required. This requirement would rapidly "boil-off" the available cryogenic oxygen and/or nitrogen. For this reason, a regenerative cooling system such as a Brayton, Sterling, or Rankine cycle would be preferable. The power requirement is on the order of 440 watts/man assuming an efficiency of 80 percent for the cooling cycle. Thus, for a three man system the power requirement alone would be a minimum of 1300 watts. Equipment weight is estimated to be slightly higher than the molecular sieve system.

Since the power requirement is much higher than the other systems and the equipment weighs more, this system will not be considered further for incorporation in the subject vehicle.

The use of CO_2 freeze-out systems is dependent on the existence and availability of a cryogenic heat sink. This heat sink may be provided by cryogenic oxygen used for breathing or nitrogen supplied for pressurization. In some applications, cryogenic hydrogen used for power generation can be employed with only a slight system weight penalty. Figure 9 shows the differences between freeze-out and absorption CO_2 removal systems and freeze out system integration with the cryogenic heat sink.

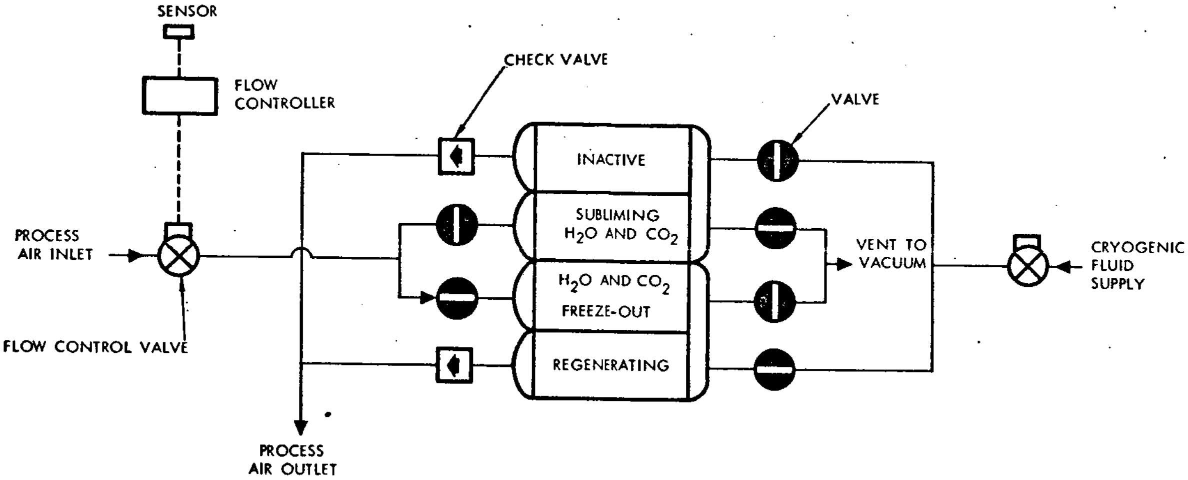
SENSOR
FLOW CONTROLLER
CHECK VALVE
VALVE
INACTIVE
SUBLIMING H_2O AND CO_2
H_2O AND CO_2 FREEZE-OUT
REGENERATING
PROCESS AIR INLET
FLOW CONTROL VALVE
VENT TO VACUUM
CRYOGENIC FLUID SUPPLY
PROCESS AIR OUTLET

Figure 9. Carbon Dioxide Freeze-Out Subsystem Diagram

CO_2 REDUCTION - O_2 RECOVERY SYSTEMS

Sabatier Reaction - Without Methane Decomposition

Characteristics - The Sabatier systems are based on a reaction which produces methane, and hence the systems do not require any carbon removal. The reaction is

$$CO_2 + 2H_2 = CH_4 + 2H_2O$$

The reaction requires suitable catalysis for low temperature operation and avoidance of side reactions such as

$$CO_2 + 2H_2 = C + 2H_2$$

which takes place at about 1000 F. The system operates as follows:

CO_2 and H_2 are fed to the Sabatier reactor which is at about 600 F (the reaction is exothermic). The product gases CH_4 and H_2O vapor with some traces of CO_2, H_2, CO, and N_2 are then passed to a cooler. The H_2O is condensed and the gas-water mixture is passed to a separator. The water is removed from the gas stream which is jettisoned overboard. The water now is electrolyzed (which is not an integral part of the Sabatier system) into H_2 and O_2. The O_2 is fed to the cabin and the H_2 passes to the reactor along with make-up H_2 from storage to complete the cycle. The result of jettisoning is the loss of both carbon and hydrogen from the vehicle. The carbon is expendable and its loss is not important. Hydrogen dumped overboard in the form of methane, however, requires hydrogen make-up so that reaction can continue. Approximately 1/2 the required hydrogen input is not regained and must be made up. The storage of this hydrogen for prolonged periods is a major problem and introduces large weight and volume penalties. In addition to the methane dumped overboard, some unreacted H_2 and CO_2 will be dumped, as well as some unseparated or uncondensed water. These losses constitute another important weight trade-off consideration and depend on the reactor conversion efficiency and water condenser separator efficiency. Achievable conversion (reaction) efficiencies of from 90 to 97 percent have been reported. The water removal efficiency is 95 to 98 percent. Therefore, the overall efficiency is from 87 to 95 percent. Catalyst consumption is reported to be very low. Cabin gas is normally used to cool the reactor so the temperature remains about 600 F. Coolant is required to condense the water in the cooler.

Process Factors

	3 Men	6 Men
Fixed Hardware Weight	48 lb	84 lb
Power		
Reactor (for start up only)	45 watts	60 watts
Water Separator (cont.)	15 watts	25 watts
Expendables		
Spares	0.10 lb/day	0.14 lb/day
Hydrogen Inc. Storage	1.2 lb/day	2.4 lb/day
Heat Produced (1640 BTU/lb)	460 BTU/hr	920 BTU/hr
To be Removed by Air Loop (40%)	185 BTU/hr	370 BTU/hr

State-of-the-Art - The Sabatier CO_2 reactor is in the advanced laboratory test model stage. Flight type hardware has supposedly been built but no data has been found to verify this.

Comments - The system is very simple. The main method of control is the metering of H_2 and CO_2 to the reactor. The system is run slightly H_2 rich. The storage and handling of H_2 appears to be the major problem area. The hydrogen make-up imposes a weight disadvantage on long missions.

Sabatier Reaction - With Methane Decomposition

Characteristics - To eliminate the hydrogen make-up requirements in the Sabatier system, various techniques for methane decomposition have been proposed. One scheme forms acetylene (C_2H_2) and hydrogen in an electric arc furnace. The H_2 is separated by a palladium filter and is recycled to the Sabatier reactor. Carbon is also formed in the arc process which not only presents a handling problem but tends to short out the arc. The main drawback is the high power requirement of about 500 watts for a three man system. Also, the development is in the preliminary stage.

Another technique utilizes the net reaction

$$CO_2 + CH_4 = 2H_2O + 2\ C$$

Here the method is actually a Bosch reaction being accomplished in two steps. The pyrolysis of CH_4 directly to C and H_2 was also considered, but this requies a temperature of about 2000 F and the carbon formed is very hard and difficult to remove from the pyrolyzer. None of the discussed systems appear to offer any advantage over the Bosch reaction, therefore, the system will not be compared with the other CO_2 reduction techniques.

Bosch Reaction

Characteristics - The Bosch reaction systems are based on the net reaction given by

$$CO_2 + 2H_2 \overset{CAT}{\underset{1100\ F}{}} 2H_2O + C = 921\ BTU/lb\ CO_2$$

This reaction requires an iron catalyst, operating at temperature of 900 to 1200 F. The equilibrium conversion of CO_2 to steam is not complete and depends upon the temperature, and upon the products of the primary and secondary reactions taking place. Secondary reactions which may occur are

$$CO_2 + 4H_2 = CH_4 + 2H_2O$$

$$CO_2 + H_2 = CO + H_2O$$

$$CO + 3H_2 = CH_4 + H_2O$$

Ideally the system operates as follows. The Bosch reactor is fed pure CO_2 along with recycle gases. (CO, H_2, CH_4, etc.) The resultant reaction with an iron catalyst at about 1100 F produces carbon and water vapor. The conversion efficiency is about 30 to 50 percent. The water vapor along with non-reacted gases passes to a heat exchanger which heats the non-condensable gases passing back to the reactor. The water vapor is then condensed and carried by the non-condensable (non-reacted) gases to the liquid-gas separator. The water is removed from the gas stream and passed to an electrolysis unit (not part of the system) for "breaking down" into H_2 and O_2. The non-condensable gases are recycled back to the reactor via the heat exchanger.

[redacted]

Carbon removal can present a problem as it is sooty and somewhat difficult to collect and remove from the system. One manufacturer has developed a scraper which continually scrapes the carbon loose and transports it via the recycle gas to a regenerable stainless steel filter.

Total conversion efficiencies of 95 to 98 percent are stated and a carbon-to-catalyst consumption ratio of from 20 to 200 have been quoted. A value of 100 is assumed, or 1 pound of catalyst consumed per 100 pounds of carbon formed.

An electrical heater is incorporated in the reactor to maintain the temperature at the required 1000 to 1200 F.

Process Factors	3 Men	6 Men
Fixed Hardware Weight	55 lbs.	96 lbs.
Power		
Reactor	150 watts	260 watts
Blower	50 watts	80 watts
Instr. & Controls	20 watts	20 watts
	220 watts	360 watts
Expendables		
Spares	0.10 lb/day	0.14 lb/day
Catalyst (0.0027 lb/lb treated)	0.018 lb/day	0.036 lb/day
Carbon Filter	0.15 lb/day	0.25 lb/day
Heat Produced (921 Btu/lb)	258 Btu/hr	516 Btu/hr.
To Be Removed by Air Loop (20%)	52 Btu/hr	104 Btu/hr.

State-of-the-Art - The Bosch reactor is in the flight-type hardware state. A flight-type system has been built and is being evaluated presently.

Comments - One advantage of this system is that hydrogen make-up is not required. In fact, a slight amount of H_2 is dumped to space as H_2O is electrolyzed to make up the cabin O_2. Another advantage of this system is that if necessary the Bosch reactor can be operated as a Sabatier reaction by turning off reactor power and allowing the temperature to decrease to about 600 F. This, however, would require additional H_2 to be available. The system is fairly simple and is similar to the Sabatier system in maintainability, reliability, and operation.

Molten Electrolyte

Characteristics - The best developed molten electrolyte system to-date is based on the electrolysis of lithium carbonate as given by

$$\mathrm{Li_2CO_3} \xrightarrow{\text{Electrolysis}} \mathrm{Li_2O + C + O_2}$$

The lithium oxide is reacted with CO_2 to reform the carbonate and thus close the cycle. The major problem with this system is the removal of the hard carbon from the cathode which is normally immersed in the (100 F) molten electrolyte. Theoretically no H_2O or CO are formed, but the bases could be formed if water vapor enters the cell, or if CO_2 feed and the power are not controlled accurately. These gases could therefore be found in the resultant O_2 stream. The most severe draw back to this system is the high power requirement. It is calculated to require approximately 11.7 kw-hr per pound of oxygen. This is compared with about 3.0 kw-hr per pound of oxygen for the Bosch or Sabatier systems plus water electrolysis. The system is also not well enough developed to be considered for a project in the near future. For these reasons this system will not be considered for the subject vehicle.

WATER ELECTROLYSIS UNITS

Double Membrane Cell (H_2SO_4)

Characteristics - This system consists of two ion-exchange membranes with a thin screen catalyst/electrode bonded to the outer face of each membrane where gaseous products are evolved. Water with 32 percent (by weight) of H_2SO_4, added to make it conducting, is fed into the narrow space between the two ion-exchange membranes. The membranes are current conductors and provide a liquid-gas separation which is inherently independent of gravity. The three-phase contact of liquid electrolyte with gaseous products across the ion-exchange membrane is reported to stable.

Process Factors		3 Men	6 Men
Fixed Hardware Weight			
Current Density	Voltage	Wt. (lb)	Wt. (lb)
20	1.75	56.5	85
40	1.90	33	50
60	1.95	25	38

Process Factors (continued)	3 Men	6 Men
Power (2950 watt-hr/lb O_2 produced)	732 watts	1464 watts
Pump (Electrolyte Circulation)	30 watts	46 watts
Volume	1.4 ft^3	2.0 ft^3
Expendables or Spares	0.07 lb/day	0.1 lb/day
Heat Rejection (sensible)	880 Btu/hr.	1760 Btu/hr.

State-of-the-Art - A flight-type hardware unit has been delivered to NASA for evaluation. The membrane and electrodes are practically identical to those used in the Gemini fuel cell.

Comments - This system is very simple and one of the lightest of the cells investigated. Its design specification calls for a life of 8000 to 10,000 hours.

Phosphorous Pentoxide Cell

Description - Air with water vapor flows into a cell where the water vapor is absorbed into a matrix of P_2O_5 with a binder which forms an acid. Electrolysis of the acid releases O_2 and H_2 gases and reforms the P_2O_5. One advantage of this system is that it dehumidifies cabin air, so that this function might be eliminated from the thermal control and atmospheric control loop. This saves only approximately 8 to 15 pounds, however credit is given for that amount.

The gas-liquid separation is achieved by the semi-solid barrier of P_2O_5 between the electrodes. The system operation should be independent of gravity. One of the major disadvantages of this system is that phosphorous pentoxide is an inherently poor conductor of electricity. If the membrane is made very thin to overcome the low electrical conductivity, it will be difficult to prevent the diffusion of hydrogen into the oxygen or "air" stream. The low electrical conductivity of the membrane requires high power consumption even at low current densities. The low current densities require large electrode areas of very expensive platinum. This too is a disadvantage as the estimated 65 square feet of platinum would cost on the order of $70,000 for the anodes and cathodes.

Process Factors	3 Men	6 Men
Weight (for 28 volts)	100 lbs	160 lbs
Power	1270 watts	2540 watts
Volume	1.2 ft^3	2.0 ft^3
Expendables or Spares	0.12 lbs/day	0.16 lbs/day
Heat Rejection (sensible)	2600 Btu/hr	5200 Btu/hr

State-of-the-Art - This system is in the laboratory development stage and the problem areas cited above may be eliminated in the future.

Comments - The high power requirement and higher than normal equipment weight indicates that this system is not competitive with other techniques. If the conductivity problem is solved, the system will become more competitive. It is a simple system with a good reliability rating.

KOH with Platinum-Asbestos-Nylon Wick

Characteristics - This cell relies on capillary and surface tension forces for zero-g operations. An electrolyte of H_2O with 30 percent KOH is fed from a reservoir into the cell by a nylon wick. The wick is in direct contact with the hydrogen electrode on one side. The other side of the wick is pressed against a layer of asbestos paper which holds electrolyte against the oxygen electrode. Both electrodes are of platinum black on a platinum screen and are pressed against a monel screen. These screens serve as current collectors and provide gas passages.

One area which could be a problem is that of maintaining a gas-liquid interface by electrolyte surface tension along. Tests show gas has been formed without visible bubbling and without any electrolyte spray detected. The possibility remains of pressure disturbances between electrolyte and gaseous products which could either force electrolyte away from the electrodes or cause flooding of electrolyte into the gases.

Cooling is another area of concern. The heat rejection rate is about the same as other types of cells, however, circulation of the electrolyte is essentially blocked by the wick and asbestos paper. Cooling tubes can be incorporated, or a forced air convection system supplied.

Process Factors	3 Men	6 Men
Unit Weight (1.9 volts-100 amps/ft^2)	20 lbs	35 lbs
Power - Unit Only	750 watts	1500 watts
Accessories (Coolant Pump)	30 watts	45 watts
Heat Rejection (sensible)	920 Btu/hr	1840 Btu/hr.
Volume	0.1 ft^3	0.15 ft^3
Spare Parts (or redundant items)	0.01 lb/day	0.10 lb/day

State-of-the-Art - This system is considered to be in the flight type hardware state and is available.

Comments - This system is very simple with a minimum of moving parts. The main objection is its pressure sensitivity as to liquid-gas interface. This, however, is stated to be no problem by the manufacturer. Reliability is reported to be high.

WATER RECOVERY SYSTEMS

Electrodialysis

Characteristics - This system involves three basic steps. These are: (1) treatment with a complexing agent (urine only), (2) absorption for removal of additional organic constituents, and (3) demineralization which is accomplished by electrodialysis.

Urine Water Recovery - The first step is to add the complexing agent to the urine. This is normally added to the "batch" of urine in the collection or feed tank. The urine, now containing a urea precipitate, is pumped to the reservoir through a series of expendable charcoal filters, which removes the precipitate and other organic compounds. A millipore filter in the feed line serves to prevent any bacteria from getting into the system. When the reservoir is full, a level sensor automatically shuts off the feed pump and starts the circulating pump. This commences the demineralization step whereby electrolytes are removed in the electrodialysis stack. The liquid is continuously recycled past an ultra-violet lamp (which assures water sterility), a conductivity probe (which measures the concentration of inorganic salts), into the electrodialysis stack and back to the reservoir. Electrolyte removal is accomplished in the stack by the migration of ions through alternate anion and cation membranes (in parallel) into the concentrate stream. An imposed d.c. voltage provides the driving force for migration (anions toward the anode and cations toward the cathode). Some water passes through the membrane with the ions (endomatic water) amounting to about 5 percent of the total liquid feed. About 1.6 percent of this water is recovered in the membrane permeation unit. The residue from the membrane permeation is a thick homogeneous liquid which is collected in collapsible plastic containers. These containers are then sealed and placed in a waste storage unit. Static liquid-gas separators remove any H_2 and O_2 that is produced in the electrodialysis stack. After passing through the electrodialysis stack, the dilute stream passes back into the reservoir. Cycling of the liquid is continued until the conductivity probe detects an acceptable low concentration of electrolytes. When this point is reached, a micro-switch automatically actuates a three-way solenoid valve which allows the liquid to pass through a charcoal filter for final filtering and into a recovered water holding tank.

Wash Water Recovery - Purification of used wash water is accomplished in basically the same manner as urine water recovery. The main difference is that the complexing agent is not required and the amount of charcoal required for pretreatment is drastically reduced.

The weight of expendables (charcoal, millipore filters, and pretreatment chemical) is the major factor in this system. The charcoal requirement is very high for urine water recovery.

Process Factors -(Assuming 3.32 lb urine per man-day and 5.00 lb wash water per man-day)

	Urine System	Wash Water System
Fixed Unit Weight	19.7 lbs	9.8 lbs
Expendable Weights		
Charcoal	0.535 lb/day	0.0117 lb/day
Millipore Filters	0.00427 lb/day	0.0078 lb/day
Pretreatment Chemical	0.056 lb/day	0
Total	0.595 lb/day	0.0195 lb/day
Power Requirement	20 watts	10 watts
Volume		
Unit (fixed)	1.65 ft^3	0.55 ft^3
Expendables	.0213 ft^3/day	0.0078 ft^3/day
Recovery Efficiency	91.6%	96.2%

State-of-the-Art - Large non-flight weight commercial electrodialysis units have been operating for a number of years. A small scale flight type unit has been operated in the laboratory and several units have been tested by the NASA and the Air Force. The state of system development can be classed between "prototype" and "flight-type" hardware.

Comments - The system is fairly simple and straightforward. The main objection is to the large expendables requirement. The unit is very competitive for wash water reclamation, but for urine water recovery it becomes very heavy for missions over one month. If an effective method can be devised for charcoal regeneration, the system will be very competitive.

Air Evaporation - Waste Heat

Characteristics - A sealed, closed loop in which "air" is circulated by a fan through a heater, evaporator, condenser, and a water separator makes up the main part of this system. The "air" is at cabin pressure and of the same composition as cabin "air" to minimize leakage. The urine and/or wash water is pretreated with a complexing agent then metered to wicks located within the evaporator. The "air" which is at 130-140 F is passed through the wicks. Water in the fluid is evaporated to the "air" stream, precipitating solids, impurities, and non-volatiles within the wicks. The "air", saturated at the evaporator outlet temperature of 80 to 85 F then enters the condenser. The condenser cools the air below the dew point and the resultant condensed water vapor is entrained in the air stream. The "air" then passes the entrained water droplets to the separator where they are collected from the "air"stream and pumped to the post treatment canister. This canister contains activated charcoal and is the final purification step. The water then passes to a collection or storage tank. The "air" now at 65-70 F (out of the condenser) passes to the heater where it will be heated to 130-140 F and passed over the wicks continuing the process.

If waste heat is available at 135-150 F, the system power is very low or about 15 to 30 watts for a fan. If an electrical heater is required, it will take approximately 400 to 500 watts for a urine and wash water system. Collant is required to supply the condenser with a heat sink.

Process Factors (Three Men)

	Urine System	Wash Water System
Fixed Unit Weight	8.6 lbs	11.6 lbs

	Urine System	Wash Water System
Expendable Weight		
Pretreatment Chemical	0.099 lb/day	Not Required
Wicks	0.107 lb/day	0.03 lb/day
Charcoal Filters	0.082 lb/day	0.03 lb/day
Total	0.288 lb/day	0.06 lb/day
Power Requirement		
Fan	15 watts	20 watts
Heater (if waste heat source is not available)	180 watts	270 watts
Volume		
Unit	0.6 ft^3	0.8 ft^3
Expendables	0.029 ft^3/day	0.006 ft^3/day
Recovery Efficiency	95-97%	98%

State of the Art - A flight-type unit has been built and delivered to the NASA for evaluation.

Comments - This system has a high reliability since it requires very little control and has a minimum of moving parts. The system is very light and has no corrosion or scaling problems. There is some possibility of odor problems, however, this is minimal. Maintenance is minimal and part replacement is simple.

Vapor Compression

Characteristics - This system consists essentially of an evaporator, compressor, and a condenser. The evaporator is actually a cylinder inside the cylindrical condenser. The compressor is enclosed in the evaporator shell. The whole unit rotates to compensate for zero-g gas-liquid separation problems.

The process is as follows. Wash water or urine containing a chemical disinfectant is fed into the evaporator section of the unit. The heat from the condenser vaporizes the liquid at about 0.35 psia. The compressor motor gives up heat which is utilized as make-up heat for vaporization since some of the heat given up by the condensing vapor is lost to the surrounding atmosphere. Vapor from the evaporating surface is compressed to about 0.7 psia and delivered to the condenser side of the drum where it condenses. The liquid is then passed to the post treatment system. All residue is collected in a plastic bag type liner which lines the evaporator shell. The liner is changed frequently. A vacuum is used to remove non-condensable gases from the condenser chamber so a pressure build-up is prevented.

Process Factors (Three Men)

	Urine Processing	Wash Water Processing
Fixed Unit Weight	27 lbs	33 lbs
Expendable Weights		
Liners	0.041 lbs/day	0.011 lbs/day
Charcoal	0.090 lbs/day	0.020 lbs/day
Ion Exchange, Etc.	0.010 lbs/day	0.002
Total	0.141 lbs/day	0.033 lbs/day
Power Requirements	17 watts	26 watts
Volume		
Unit	.5 ft^3	1.0 ft^3
Expendables	0.0065 ft^3/day	0.0017 ft^3/day
Recovery Efficiency	93%	96%

State-of-the-Art - A flight-type system has been delivered to the NASA for evaluation. An improved version has also been delivered to the Air Force.

Comments - Some of the Advantages of this unit are low power, volume, and overall weight. The process while being fairly simple requires complex mechanical equipment. The rotating unit could leak as it is below cabin pressure and has rotating seals. Also replacement of the liner is difficult and done almost daily. The system, however, is definitely competitive.

Vacuum Distillation-Pyrolysis

Characteristics - Vacuum distillation involves low temperature, low pressure vaporization of water. The vapor, which contains some volatile organics carried over in the distillation (and possibly some ammonia), is then passed through a pyrolysis chamber which oxidizes these products.

The process is as follows: urine and/or wash water is metered into the evaporator. The evaporator operating pressure is from 0.8 to 1.2 psia. The evaporater is capable of operation at zero-g due to the non-wettable membrane at the discharge end of the evaporator. Only vapor will pass through the membrane. Heat from a warm glycol source as well as from the hot vapor is used for vaporization. The vapor then passes to the regenerative heat exchanger where it is heated to about 1350 F. A small amount of air is mixed with this hot water as it leaves the heat exchanger. The mixture is then passed to the pyrolysis chamber where ammonia (if present) and volatile organics are oxidized. The catalyst is heated electrically and in turn heats the vapor to about 1500 F. Vapor leaving the pyrolysis chamber passes to the regenerative heat exchanger where it gives up most of its sensible heat to the vapor passing to the pyrolysis chamber from the evaporator. The vapor then enters the evaporator where additional heat is lost to the liquid feed. The relatively cool vapor then enters the condenser where it is condensed. Cool glycol is normally used to remove heat from the condenser. Condensate and non-condesnable gases are forced out of the condenser by a piston periodically actuated by compressed air or nitrogen. The liquid-gas separator is used to collect the non-condensable gases. These gases are then vented to space.

Process Factors (Three Men)

	Urine Processing	Wash Water Processing
Fixed Unit Weight	9.5 lbs.	14 lbs.
Expendables Weight		
Air (oxidation)	0.032 lb/day	0.018 lb/day
Power Requirements		
Pyrolysis Heater	45 watts	80 watts
Instrumentation	5 watts	5 watts
Volume		
Unit	.75 ft^3	1.4 ft^3
Expended (air)	0.0011 ft^3/day	0.00063 ft^3/day
Recovery Efficiency	95%	95%

State of the Art - A system has been built under NASA contract. This system has been operated successfully at one g.

Comments - This system is simpler in that it requires no pre or post treatment and has a minimum of moving parts. The only expendable is air or oxygen which is easily supplied. The overall weight and volume is very low, especially for long missions. The quality of water is excellent and the recovery rate is high. One area of concern is the very high temperature of the pyrolysis chamber and its effect as to material degradation in time. Also, the non-wettable membrane has a questionable reliability. Since the system operates below cabin pressure leakage problems could occur. This system with all things considered is a very promising one for incorporation in the subject vehicle.

Atmospheric Condensate Purification System

Characteristics - The water recovery systems previously discussed are all capable of cabin atmospheric condensate (humidity) purification. However, since the impurity level of atmospheric condensation is much lower than either urine or wash water, a simple filtration system can be used. Several sources state that the atmospheric condensate is in fact potable when collected except for the possible presence of pathogenic micro-organisms and a slight odor. The filtration system is as follows: The water is passed through an activated carbon bed then through a bacteria filter. This has been found to be adequate for the processed water to meet the purity standards. No change of state is required. This system can be used to purify wash water, however, the expendables weight is greatly increased.

Process Factors (Three Men)

	Atmospheric Condensate System	Wash Water System
Fixed Weight	1.6 lbs	3.5 lbs
Expendable Weight		
Carbon and Canisters	0.029 lb/day	0.30 lb/day
Bacteria Filters	0.003 lb/day	0.05 lb/day
Total	0.032 lb/day	0.035 lb/day
Volume	0.001 ft^3/day	0.01 ft^3/day
Power	0	0
Recovery Efficiency	99.5%	99%

State-of-the-Art - A system for atmospheric condensate purification of the flight-type hardware configuration has been delivered to the NASA and is being evaluated at present.

Comments - This system is by far the most simple and lightest for atmospheric condensate purification. For wash water the system is competitive with the other systems. Reliability is very high.

DESIGN CALCULATIONS

The following assumptions are used in assessing weight penalties:

1. Power Penalty (P.P.)
    - a. Solar cells + batteries = 700 lb/kw (0.7 lb/watt)
    - b. Isotope: Negligible - since excess power is available ECS is assumed to receive free power.

    All items will be calculated assuming solar cells and batteries used for power source.

2. Heat Rejection Penalty (H.R.P.)
    - a. Sensible Heat = 0.01 lb/Btu per hr
    - b. Latent Heat - 28 lb/lb H_2O per hr cond.

CO_2 REMOVAL SYSTEMS

LiOH

Based on 2.25 lb/man-day of CO_2 output, the LiOH requirement is 2.66 lb/man-per day or 8.0 lb/day for three men, 16.0 lb/day for six men. Therefore the requirement versus mission duration is:

Mission Duration	Man-Days (Three Men)	LiOH Reqd (lb) (Three Men)	LiOH Reqd (lb) (Six Men)
0 days	0	16	32
90 days	270	720	1440
180 days	540	1440	2880
360 days	1080	2880	5760
600 days	1800	4800	9600

Therefore (0.0409)(2.25) (3) = 2.76 lb H_2O produced per day. This water will not be required if water recovery is utilized so no credit can be made to the LiOH system for water production.

NOTE: 0.0409 lb H_2O is formed per lb CO_2 absorbed.

Heat Rejection Penalty

For three men, the sensible heat produced is 246 Btu/lb, and the latent heat is 118 Btu/hr. The penalty is therefore (0.01 lb) (246) = 2.5 lb and (28) (2.76/24) = 3.2 lb. The total heat rejection penalty (for three men) is therefore 2.5 + 3.2 = 5.7 lb, which is negligible.

Since the volume of the LiOH is significant, the penalties are shown below for various mission durations.

Mission Lt.	Man-Days		Volume (ft^3) (Three Men)	Volume (ft^3) (Six Men)
0 days	0	(fixed vol.)	.5	1.0
90 days	270		31.5	63
180 days	540		63.0	126
360 days	1080		126.0	252
600 days	1800		210.0	410

Power Requirement - Negligible

Molecular Sieve

Scheme 1 (both CO_2 and H_2O desorbed to space vacuum) Nonconservation systems)

Fixed Unit Weight

Mission Duration (Days)	Basic Wt. & Spares	Fixed Unit Wt. (lb) 3 Men	6 Men
0	40 lb + 0	40	
	57 lb + 0		57
90	40 lb + (90)(.10)	49	
	57 lb + (90)(.13)		69
180	40 lb + (180)(.10)	58	
	57 lb + (180)(.13)		80
360	40 lb + (360)(.10)	76	
	57 lb + (360)(.13)		104
600	40 lb + (600)(.10)	100	
	57 lb + (600)(.13)		135

Power Penalty - Three Men (35 watts)(0.7 lb/watt) = 24.5 lb

Power Penalty - Six Men (60 watts)(0.7 lb/watt) = 42 lb

Heat Rejection Penalty - Three Men (35 watts)(3.4.4)(0.01) = 1.2 lb

Heat Rejection Penalty - Six Men (60 watts)(3.4.4)(0.01) = 2.0 lb

TOTAL WEIGHT PENALTY - SCHEME 1

Mission Duration (Days)	Fixed Unit + P.P. + H.R.P.	Total Wt. Penalty Three Men	Six Men
0	40 + 24.5 + 1.2	65.7 lb	
	57 + 42 + 2		101 lb
90	49 + 24.5 + 1.2	74.7 lb	
	69 + 42 + 2		113 lb
180	58 + 24.5 + 1.2	83.7 lb	
	80 + 42 + 2		124 lb
360	76 + 24.5 + 1.2	101.7 lb	
	104 + 24.5 + 1.2		148 lb
600	100 + 24.5 + 1.2	125.7 lb	
	135 + 42 + 2		179 lb

Molecular Sieve

Scheme 2 (water desorbed by heat and returned to cabin. CO_2 vacuum desorbed to space vacuum.) Water conservation system.)

Fixed Unit Weight

Mission Duration (Days)	Basic Wt. & Spares	Fixed Unit Wt. (lb) 3 Men	6 Men
0	55 lb + 0	55	
	75 lb + 0		75
90	55 lb + (90)(.10)	64	
	75 lb + (90)(.13)		87
180	55 lb + (180)(.10)	73	
	75 lb + (180)(.13)		99
360	55 lb + (360)(.10)	91	
	75 lb + (360)(.13)		122
600	55 lb + (600)(.10)	155	
	75 lb + (600)(.13)		153

Power Penalty - 3 Men (285 watts)(.7 lb/watt) = 200 lb

Power Penalty - 6 Men (500 watts)(.7 lb/watt) = 350 lb

Heat Rejection Penalty - 3 Men (285 watts)(3.414)(.01) = 9.8 lb

Heat Rejection Penalty - 6 Men (500 watts)(3.414)(.01) = 17 lb

TOTAL WEIGHT PENALTY - SCHEME 2

Mission Duration (Days)	Fixed Wt. + P.P. + H.R.P.	Total Weight Penalty (lb) Three Men	Six Men
0	55 lb + 200 + 10	265	
	75 lb + 350 + 17		442
90	64 lb + 200 + 10	274	
	87 lb + 350 + 17		454
180	73 lb + 200 + 10	283	
	99 lb + 350 + 17		466
360	91 lb + 200 + 10	301	
	122 lb + 350 + 17		489
600	115 lb + 200 + 10	325	
	153 lb + 350 + 17		520

Molecular Sieve

Scheme 3 (water desorbed by heat and returned to cabin. CO_2 is desorbed by heat and retained for reduction to O_2 - CO_2 concentrator system.)

Fixed Unit Weight

Mission Duration (Days)	Basic Wt. & Spares	Fixed Unit Wt. (lb) 3 Men	6 Men
0	55 lb + 0	55	
	75 lb + 0		75
90	55 lb + (90)(.10)	64	
	75 lb + (90)(.13)		87
180	55 lb + (180)(.10)	73	
	75 lb + (180)(.13)		99
360	55 lb + (360)(.10)	91	
	75 lb + (360)(.13)		122
600	55 lb + (600)(.10)	115	
	75 lb + (600)(.13)		153

Power Penalty - 3 Men (560 watts)(0.7 lb/watt) = 390 lb

Power Penalty - 6 Men (950 watts)(0.7 lb/watt) = 665 lb

Heat Rejection Penalty - 3 Men (560 watts)(3.414)(0.01) - 19 lb

Heat Rejection Penalty - 6 Men (950 watts)(3.414)(0.01) - 32 lb

TOTAL WEIGHT PENALTY - SCHEME 2

		Total Weight Penalty (lbs)	
Mission Duration (Days)	Fixed Wt. + P.P. + H.R.P.	Three Men	Six Men
0	55 lb + 390 + 19	464	
	75 lb + 665 + 32		772
90	64 lb + 390 + 19	473	
	87 lb + 665 + 32		784
180	73 lb + 390 + 19	482	
	99 lb + 665 + 32		796
360	91 lb + 390 + 19	500	
	122 lb + 665 + 32		819
600	115 lb + 390 + 19	524	
	153 lb + 665 + 32		850

Molecular Sieve Summary

If CO_2 reduction is not used, Scheme 1 or 2 can be used since CO_2 is not retained. If CO_2 reduction is incorporated, Scheme 3 must be incorporated into the system. If waste heat can be utilized for desorption, the power penalty of Scheme 2 and 3 will be the same as Scheme 1. System weight will increase about 20 percent.

Electrodialysis System

Fixed Unit Weight

		Fixed Unit Weight (lb)	
Mission Duration (Days)	Basic Wt. & Spares	Three Men	Six Men
0	90 lb + 0	90	
	121 lb + 0		121
90	90 lb + (90)(.10)	99	
	121 lb + (90)(.13)		133
180	90 lb + (180)(.10)	108	
	121 lb + (180)(.13)		144
360	90 lb + (360)(.10)	126	
	121 lb + (360)(.13)		168
600	90 lb + (600)(.10)	150	
	121 lb + (600)(.13)		199

Power Penalty - 3 Men (740)(.7 lb/watt) = 518 lb

Power Penalty - 6 Men (1410)(.7 lb/watt) = 987 lb

Heat Rejection Penalty - 3 Men (740)(3.414)(.01) = 25 lb

Heat Rejection Penalty - 6 Men (1410)(3.414)(.01) = 48 lb

Total Weight Penalty Less Corrections

Mission Duration (Days)	Fixed Unit + P.P. + H.R.P.	Total Weight Penalty (lb) Three Men	Six Men
0	90 + 518 + 25	633	
	121 lb + 987 + 48		1156
90	99 + 518 + 25	642	
	133 + 987 + 48		1168
180	108 + 518 + 25	651	
	144 + 987 + 48		1179
360	126 + 518 + 25	669	
	168 + 987 + 48		1203
600	150 + 518 + 25	693	
	199 + 987 + 48		1234

If CO_2 reduction is incorporated, the electrodialysis system should be credited with electrolyzing H_2O. This will decrease the size of the electrolysis unit. Conversely, unless electrolysis is required, water make up is necessary to replace the water electrolyzed by the electrodialysis unit, but the oxygen storage requirement can be lessened.

The factors are:

If CO_2 reduction is incorporated, reduce electrolysis weights shown by:

3 Men (2.1 lb O_2 day)(5.35 lb/lb O_2 day) = 11 lb plus
(123 watts/lb O_2)(2.1 lb O_2)(.7 lb/watt) = 172 lb
or 183 lb total

6 Men (4.2 lb O_2 day)(5.35 lb/lb O_2 day) = 22 lb plus
(123 watts/lb O_2)(4.2 lb O_2)(.7 lb.watt) = 344 lb
or 366 lb total

If CO_2 reduction is not used, increase the weight by:

3 Men 2.00 lb O_2/day requires (9/8)(2.0 lb) or 2.36 lb H_2O/day. The storage penalty for H_2O is 1.07 lb total/lb stored or

(1.07) (2.36) = 2.35 lb/day total penalty for water make-up Oxygen storage will be 2.1 lb per day. The storage penalty of 1.12 lb total/lb O_2 gives (2.1) (1.12) or 2.35 lb/day total O_2 penalty reduced per day. The result is 2.35 lb - 2.35 lb or 0.18 lb/day to be added for 3 men.

6 men (0.18) (2) or .36 lb/day to be added.

The results are:

Total Weight Penalty - No CO_2 Reduction in ECS

		Total Weight Penalty (lb)	
Mission Duration (Days)	Correction	Three Men	Six Men
0	(633) + 0	633	
	1156 + 0		1156
90	(642) + (90)(.18)	658	
	1168 + (90)(.36)		1200
180	651 + (180)(.18)	683	
	1179 + (180)(.36)		1244
360	669 + (360)(.18)	734	
	1203 + (360)(.36)		1333
600	693 + (600)(.18)	801	
	1234 +(600)(.36)		1450

Total Weight Penalty - With CO_2 Reduction in ECS

		Total Weight Penalty (lb)	
Mission Duration (Days)	Correction	Three Men	Six Men
0	633 - 183	450	
	1156 - 366		790
90	642 - 183	459	
	1168 - 366		802
180	651 - 183	468	
	1179 - 366		813

Mission Duration (Days)	Correction	Total Weight Penalty (lb) Three Men	Total Weight Penalty (lb) Six Men
360	699 - 183	486	
	1203 - 366		837
600	693 - 183	510	
	1234 - 366		868

Comparison Of CO_2 Removal Systems

Figure 10 illustrates weight penalty as a function of mission duration of the CO_2 removal systems treated in the preceding paragraphs. Figures 11 and 12 illustrate weight penalty comparisons between systems which are difficult to distinguish in Figure 10. Figures 13 through 16 show the weight breakdowns of the various schemes.

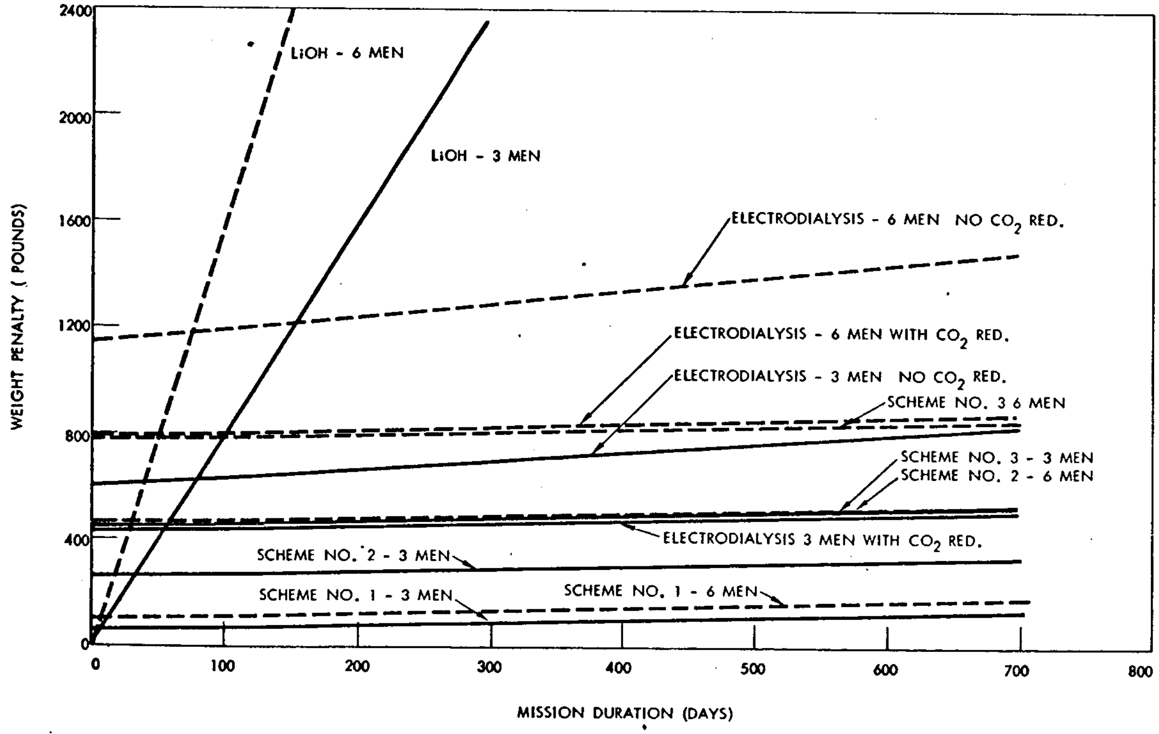

Figure 10. CO_2 Removal Techniques

CONFI[redacted]

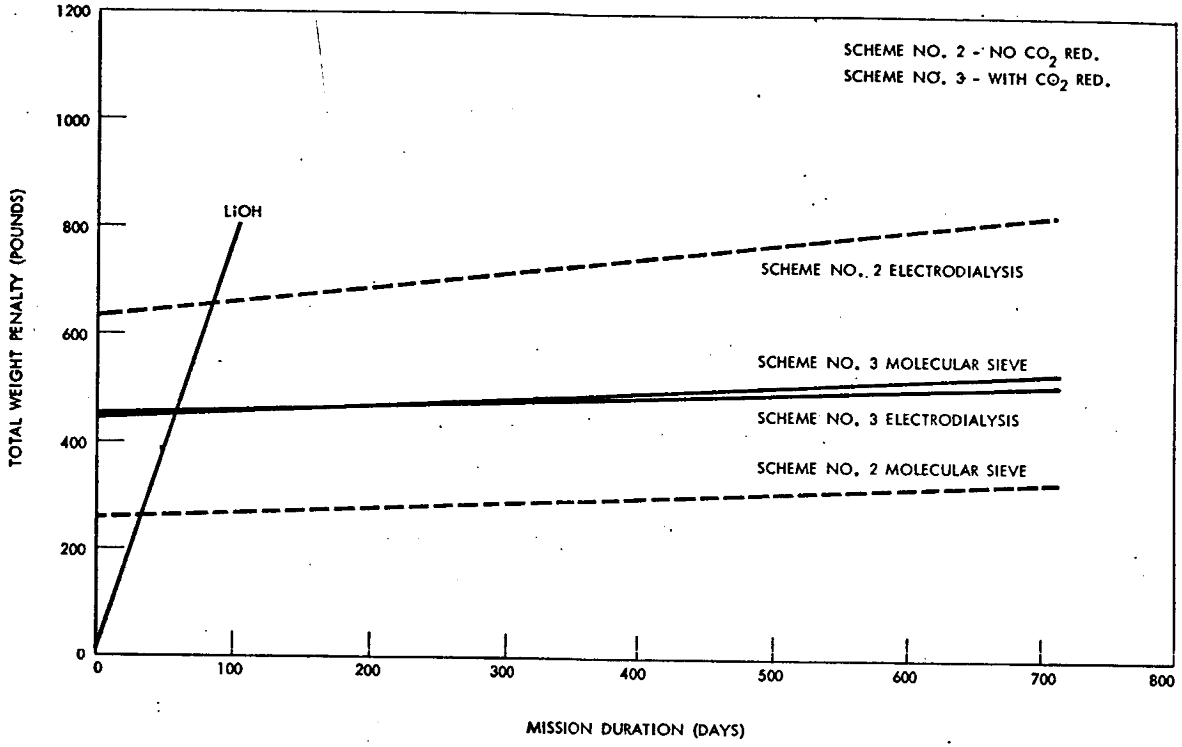

Figure 11. CO_2 Removal - Electrodialysis vs. Molecular Sieve Total Weight Penalties 3 Men

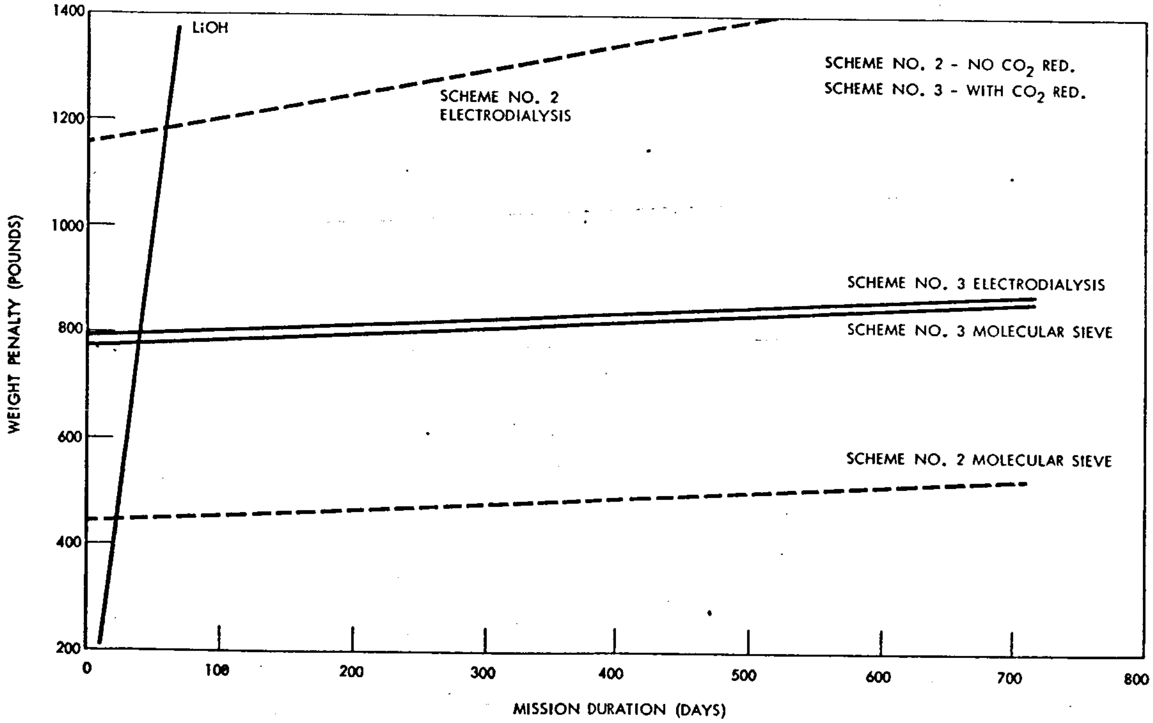

Figure 12. CO_2 Removal Electrodialysis vs. Molecular Sieve Total Weight Penalties 3 Men

[redacted]

CON[redacted]

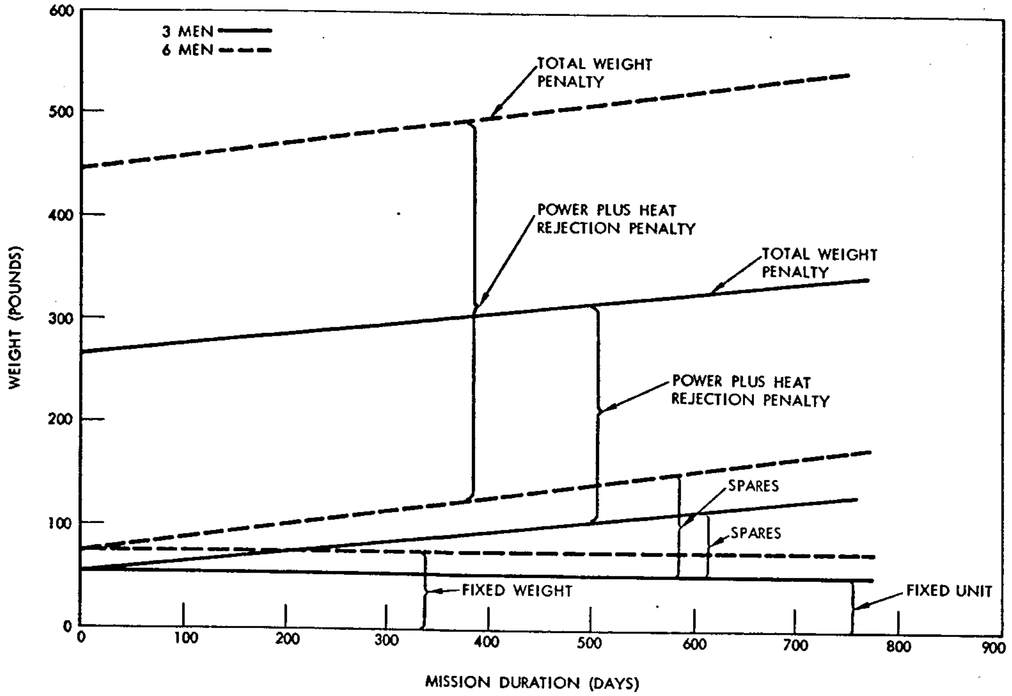

Figure 13. Weight Penalty Breakdown Molecular Sieve No CO_2 Reduction (Scheme #2)

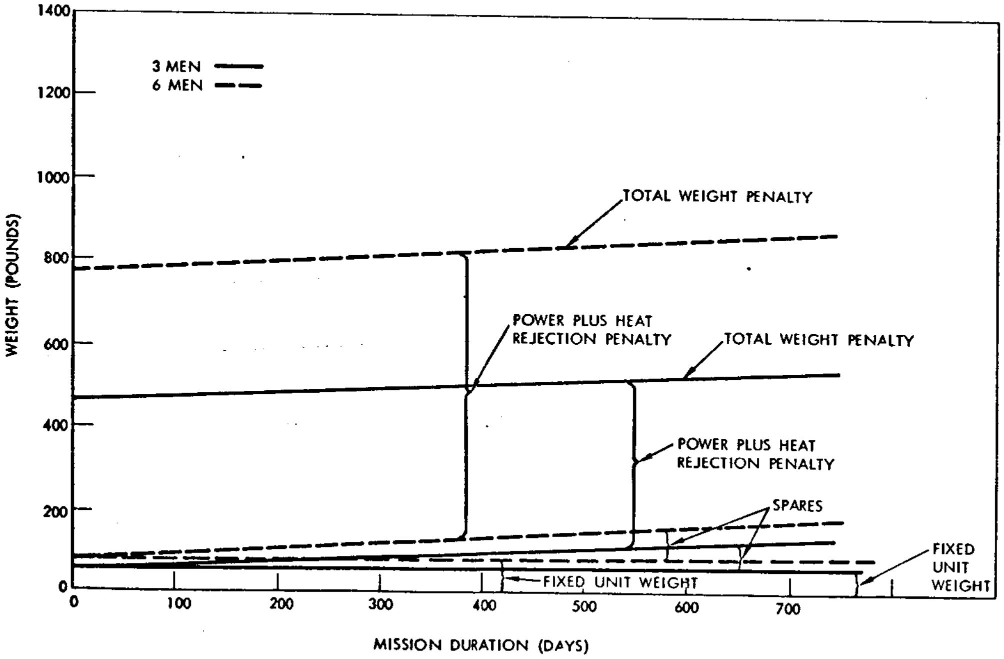

Figure 14. Weight Penalty Breakdown Molecular Sieve CO_2 Reduction Incorporated in ECS

[redacted]

CONFI[redacted]

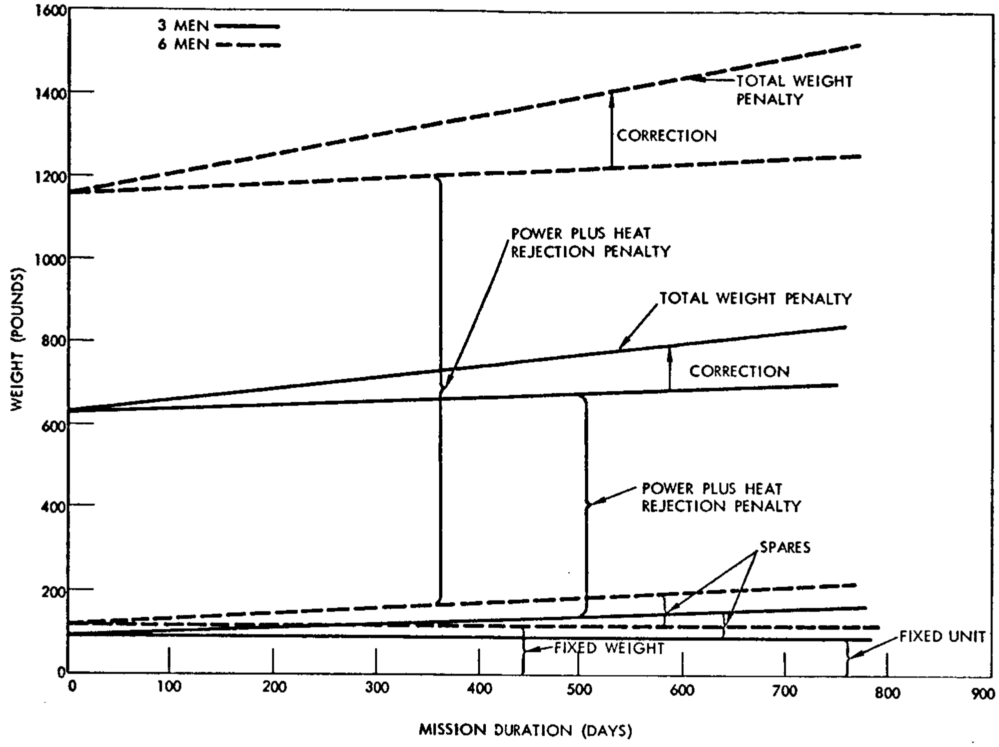

Figure 15. Electrodialysis Weight Penalty Breakdown No CO_2 Reduction

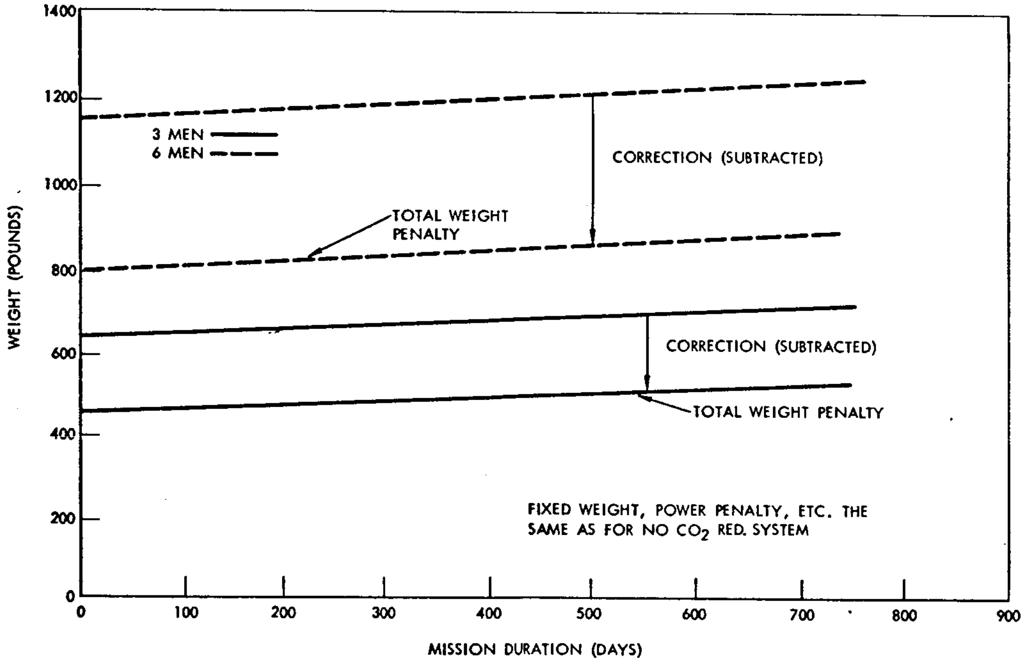

Figure 16. Electrodialysis Weight Penalty Breakdown With CO_2 Reduction in ECS

[redacted]

CO_2 REDUCTION - O_2 RECOVERY

Sabatier Reaction - Without Methane Decomposition

Fixed Unit Weight

Mission Duration (Days)	Basic Unit + Exp. & Spares	Fixed Unit Weight Three Men	Fixed Unit Weight Six Men
0	48 lb + 0	48 lb	
	84 lb + 0		84 lb
90	48 lb + (90)(1.3)	165 lb	
	84 lb + (90)(2.54)		313 lb
180	48 lb + (90)(1.3)	282 lb	
	84 lb + (180)(2.54)		542 lb
360	48 lb + (360)(1.3)	516 lb	
	84 lb + (360)(2.54)		1000 lb
600	48 lb + (600)(1.3)	828 lb	
	84 lb +(600)(2.54)		1610 lb

Power Penalty - 3 Men (15 watts)(.7 lb/watt) = 11 lb

Power Penalty - 6 Men (25 watts)(.7 lb/watt = 18 lb

Heat Rejection Penalty - 3 Men (185 Btu/hr)(.01) = 2 lb

Heat Rejection Penalty - 6 Men (370 Btu/hr)(.01) = 4 lb

Total Weight Penalty - Sabatier System

Mission Duration (Days)	Fixed Wt. & P.P. + H.R.P.	Total Weight Penalty Three Men	Total Weight Penalty Six Men
0	48 lb + 11 + 2	61 lb	
	84 + 18 + 4		136 lb
90	165 lb + 11 + 2	178 lb	
	313 + 18 + 4		335 lb
180	282 lb + 11 + 2	295 lb	
	542 + 18 + 4		564 lb

CONF[redacted]

Mission Duration (Days)	Fixed Wt. & P.P. + H.R.P.	Total Weight Penalty Three Men	Total Weight Penalty Six Men
360	516 lb + 11 + 2	529 lb	
	1000 lb + 18 + 4		1022 lb
600	828 lb + 11 + 2	841 lb	
	1610 + 18 + 4		1632 lb

Sabatier With Methane Decomposition

This system was not investig ted to the length required to determine detail weights and power requirements. The main reason was the preliminary investigation indicated the most logical system is basically a Sabatier reaction with a Bosch type reaction added. This offers no advantage over utilization of a Bosch only. The other systems such as the $C_2H_2 + H_2$ reaction require high power.

Bosch Reaction

Fixed Unit Weight

Mission Duration (Days)	Basic Unit & Spares & Expt.	Fixed Unit Weight Three Men	Fixed Unit Weight Six Men
0	55 lb +	58 lb	
	96 lb + 0		96 lb
90	55 lb + (90)(.268)	80 lb	
	96 lb + (90)(.43)		134 lb
180	55 lb + (180)(.268)	103 lb	
	96 lb + (180)(.43)		173 lb
360	55 lb + (360)(.268)	152 lb	
	96 lb + (360)(.43)		251 lb
600	55 lb + (600)(.268)	216 lb	
	96 lb + (600)(.43)		354 lb

Power Penalty - 3 Men (220 watts)(.7 lb/watt) = 154 lb

Power Penalty - 6 Men (360 watts)(.7 lb/watt) = 252 lb

[redacted]

Heat Rejection Penalty - 3 Men (52 Btu) (.01) = .5 lb
Plus 20% total watts (44)(3.414)(.01) = 1.5 lb = 2.0 lb

Heat Rejection Penalty - 6 Men (104 Btu)(.01) = 1 lb
Plus 20% total watts (72)(3.414)(.01) = 2.5 = 3.5 lb

Total Weight Penalty - Bosch System

Mission Lt., Days	Fixed Unit Wt. & P.P. + H.R.P.	Total Weight Penalty Three Men	Six Men
0	58 lb + 154 + 2	214 lb	
	96 lb + 252 + 4		352 lb
90	80 lb + 154 + 2	236 lb	
	134 lb + 252 + 4		390 lb
180	103 lb + 154 + 2	259 lb	
	173 lb + 252 + 4		429 lb
360	152 lb + 154 + 2	308 lb	
	251 lb + 252 + 4		507 lb
600	216 lb + 154 + 2	372 lb	
	354 lb + 257 + 4		610 lb

Comparison of CO_2 Reduction - O_2 Recovery Systems

Figure 17 compares the weight penalties of these systems. Figures 18 and 19 illustrate the weight break downs of the various systems.

WATER ELECTROLYSIS

Double Membrane Cell (H_2SO_4)

Fixed Unit Weight

Mission Duration (Days)	Basic Unit & Spares	Fixed Unit Weight(lb) Three Men	Six Men
0	33 lb + 0	33	
	50 lb + 0		50
90	33 lb + (.07) (90)	39	
	50 lb + (0.1) (90)		59

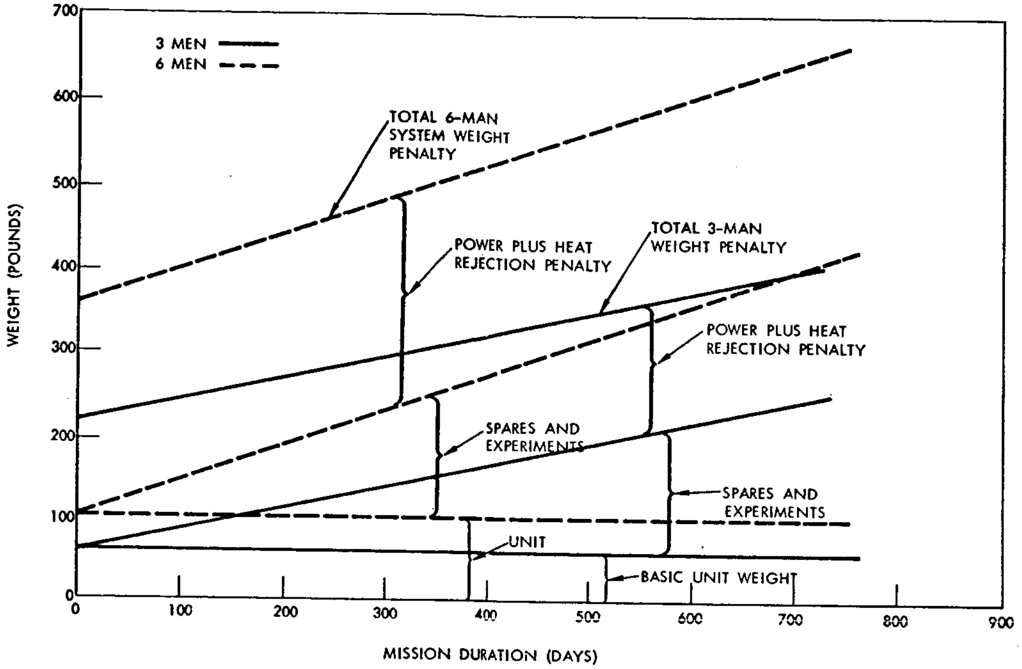

Figure 17. Weight Penalty BOSCH - CO_2 Reduction System

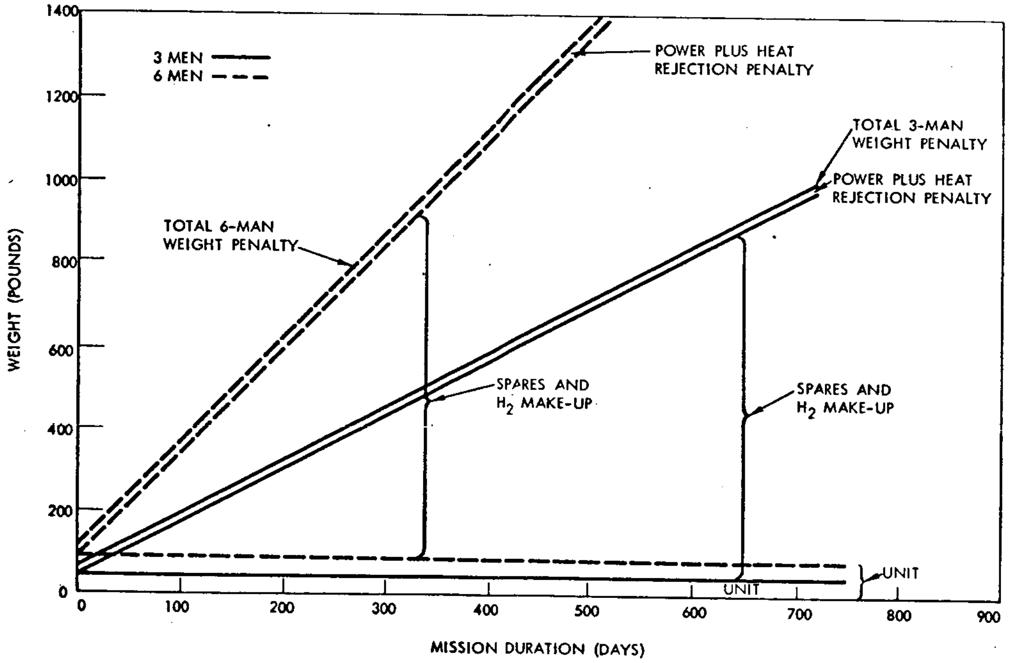

Figure 18. Weight Penalty Sabatier CO_2 Reduction System

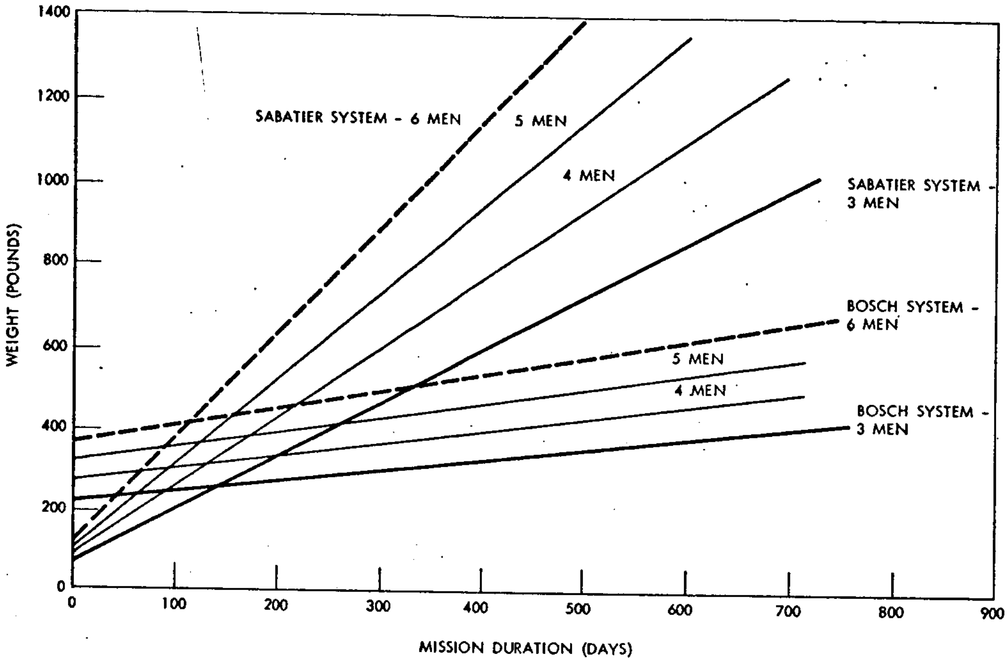

Figure 19. CO_2 Reduction System Weight Comparison

Mission Duration (Days)	Basic Unit & Spares	Fixed Unit Weight (lb) Three Men	Fixed Unit Weight (lb) Six Men
180	33 lb + (.07)(180)	46	
	50 lb + (0.1)(180)		68
360	33 lb + (.07)(360)	58	
	50 lb + (0.1)(360)		86
600	33 lb + (.07)(600)	75	
	50 lb + (0.1)(600)		110

Power Penalty - 3 Men (762 watts)(.7 lb/watt) = 534 lb

Power Penalty - 6 Men (1510 watts)(.7 lb/watt) = 1058 lb

Heat Rejection - 3 Men (880 Btu/hr)(.01 lb/Btu) = 9 lb

Heat Rejection - 6 Men (1760 Btu/hr)(.01 lb/Btu) = 18 lb

Total Weight Penalty - Double Membrane Cell

Mission Duration (Days)	Fixed Wt. & P.P. + H.R.P.	Total Weight Penalty(lb) Three Men	Six Men
0	33 lb + 534 + 9	576	
	50 lb + 1058 + 18		1126
90	39 lb + 534 + 9	582	
	59 lb + 1058 + 18		1135
180	46 lb + 534 + 9	589	
	68 lb + 1058 + 18		1144
360	58 lb + 534 + 9	601	
	86 lb + 1058 + 18		1162
600	75 lb + 534 + 9	618	
	110 lb + 1058 + 18		1186

Phosphorous Pentoxide Cell

Fixed Unit Weight

Mission Duration (Days)	Basic Unit & Spares	Fixed Unit Weight(lb) Three Men	Six Men
0	100 lb + 0	100	
	160 lb + 0		160
90	100 lb + (.12)(90)	111	
	160 lb + (.16)(90)		174
180	100 lb + (.12)(180)	122	
	160 lb + (.16)(180)		189
360	100 lb + (.12)(360)	143	
	160 lb + (.16)(360)		218
600	100 lb + (.12)(600)	172	
	160 lb + (.16)(600)		256

Power Penalty - 3 Men (1270 watts)(.7 lb/watt) = 890 lb

Power Penalty - 6 Men (2540 watts)(.7 lb/watt) = 1780 lb

Heat Rejection Penalty - 3 Men (2600 Btu/hr)(.01 lb/B-H) = 26 lb

Heat Rejection Penalty - 6 Men (5200 Btu/hr)(0.1 lb/B-H) = 52 lb

Total Weight Penalty - Phosphorous Pentoxide Cell

Mission Duration (Days)	Fixed Wt. & P.P. + H.R.P.	Total Weight Penalty(lb) Three Men	Six Men
0	100 lb + 890 + 26	1016	
	160 lb + 1780 + 52		1992
90	111 lb + 890 + 26	1027	
	174 lb + 1780 + 52		2006
180	122 lb + 890 + 26	1038	
	189 lb + 1780 + 52		2023
360	143 lb + 890 + 26	1059	
	218 lb + 1780 + 52		2050
600	172 lb + 890 + 26	1088	
	256 lb + 1780 + 52		2088

KOH with Platinum-Asbestos-Nylon-Wick Unit

Fixed Unit Weight

Mission Duration (Days)	Basic Unit & Spares	Fixed Unit Weight(lb) Three Men	Six Men
0	20 lb + 0	20	
	35 lb + 0		35
90	20 lb + (.07)(90)	26	
	35 lb + (.10)(90)		44
180	20 lb + (.07)(180)	33	
	35 lb + (.10)(180)		54
360	20 lb + (.07)(360)	45	
	35 lb + (.10)(360)		71
600	20 lb + (.07)(600)	62	
	35 lb + (.10)(600)		95

Power Penalty - 3 Men (780 watts)(.7 lb/watt) = 550 lb

Power Penalty - 6 Men (1545 watts)(.7 lb/watt) = 1080 lb

Heat Rejection Penalty - 3 Men (920 Btu/hr)(.01 lb/B-H) = 9 lb

Heat Rejection Penalty - 6 Men (1840 Btu/hr)(.01 lb/B-H) = 18 lb

Total Weight Penalty - KOH With Plat.-Asbestos-Nylon Wick Unit

Mission Duration (Days)	Fixed Wt. + P.P. + H.R.P.	Total Weight Penalty(lb) Three Men	Six Men
0	20 lb + 550 + 9	579	
	35 lb + 1080 + 18		1133
90	26 lb + 550 + 9	585	
	44 lb + 1080 + 18		1142
180	33 lb + 550 + 9	592	
	53 lb + 1080 + 18		1151
360	45 lb + 550 + 9	604	
	71 lb + 1080 + 18		1169
600	62 lb + 550 + 9	621	
	95 lb + 1080 + 18		1193

Comparison of Water Electrolysis

Figure 20 compares the weights of the various water electrolysis techniques. Figures 21 through 23 show the weight breakdowns of the various techniques.

ATMOSPHERIC CONSTITUENTS STORAGE - OXYGEN AND NITROGEN

Storage Requirements

3.1 psia oxygen partial pressure

Total volume 1360 ft^3 + 210 ft^3 = 1570 ft^3

Gas	Press.(mmHg)	% By Vol.	% By Wt.	Leakage(lb/day)	Wt. Invert.(lb)
O_2	160	44.44	47.85	4.79	26.90
N_2	185	51.39	48.42	4.84	27.20
H_2O	10	2.78	1.68	0.17	0.94
CO_2	5	1.39	2.05	0.20	1.16
TOTAL	360	100%	100%	10.00	56.20

STORAGE REQUIREMENTS

	Oxygen		Nitrogen	
	Three Men	Six Men	Three Men	Six Men
Metabolic (lb/day)	6	12	-	-
Leakage Make-up (lb/day)	4.8	4.8	4.8	4.8
Total (lb/day)	10.8	16.8	4.8	4.8
Fixed Weight				
Repressurization (5) times (lb)	135	135	136	136
Emergency Leakage (5) times (lb)	15	15	16	16
Total (lb)	150	150	152	152

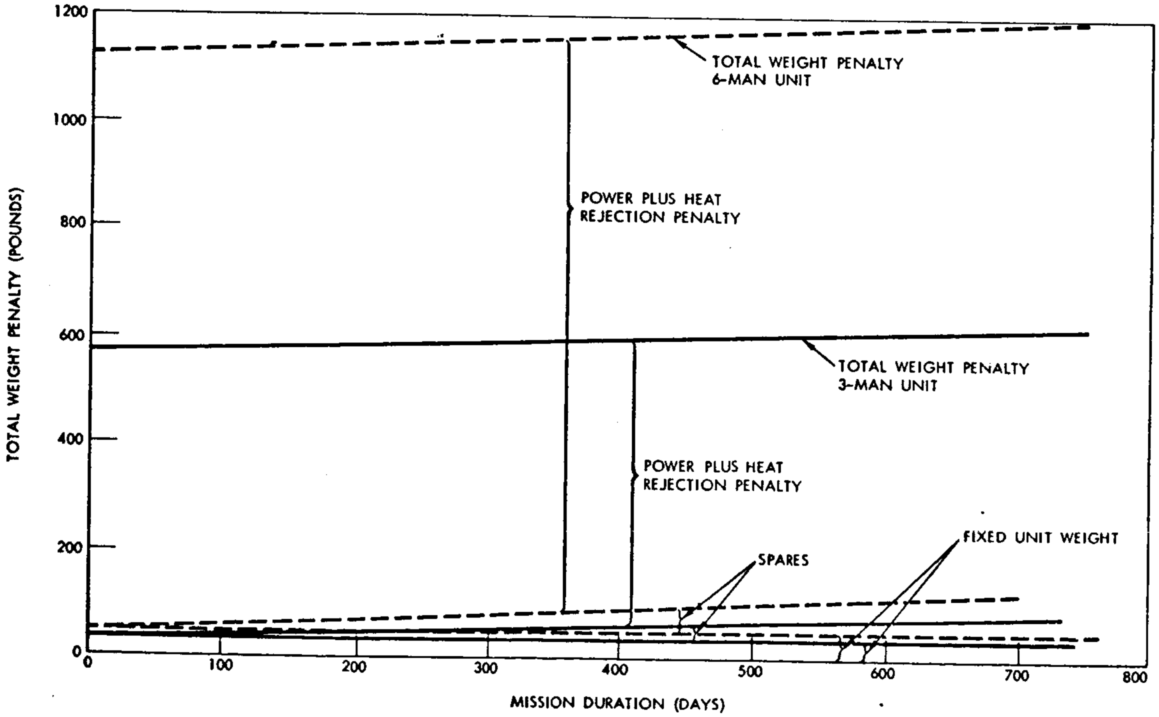

Figure 20. Electrolysis Unit Double Membrane Cell.

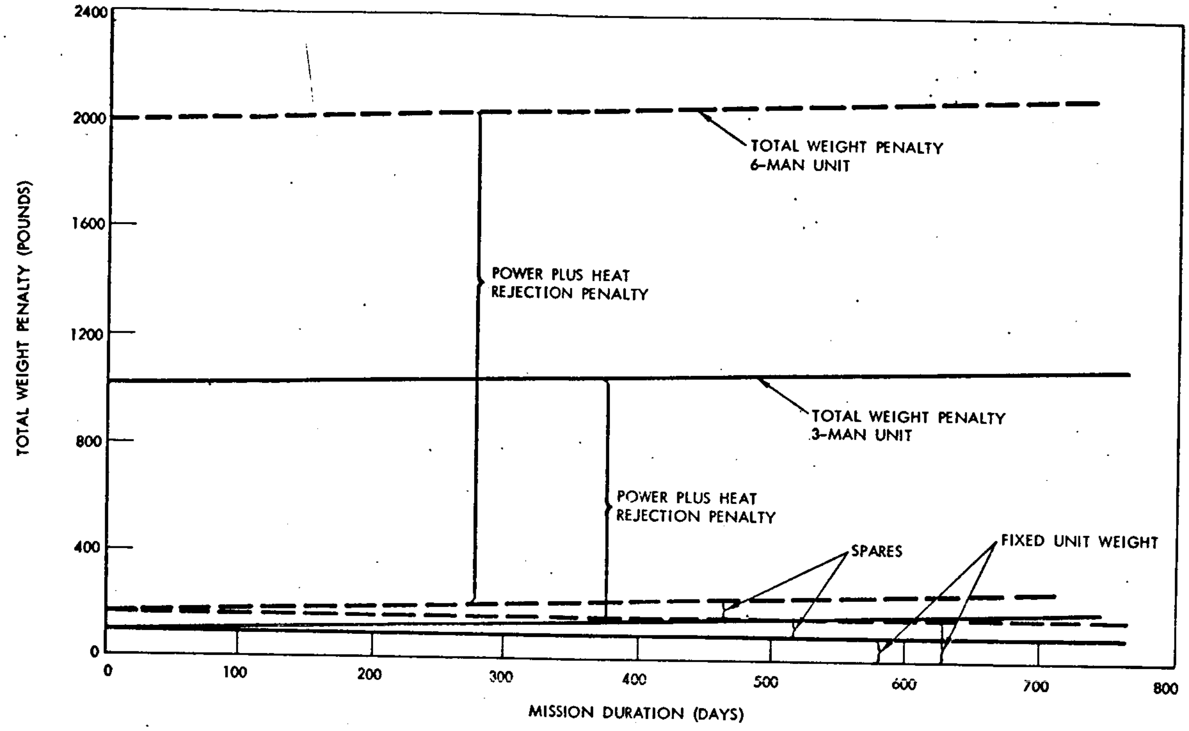

Figure 21. Electrolysis Unit Phosphorous Pentoxide Cell

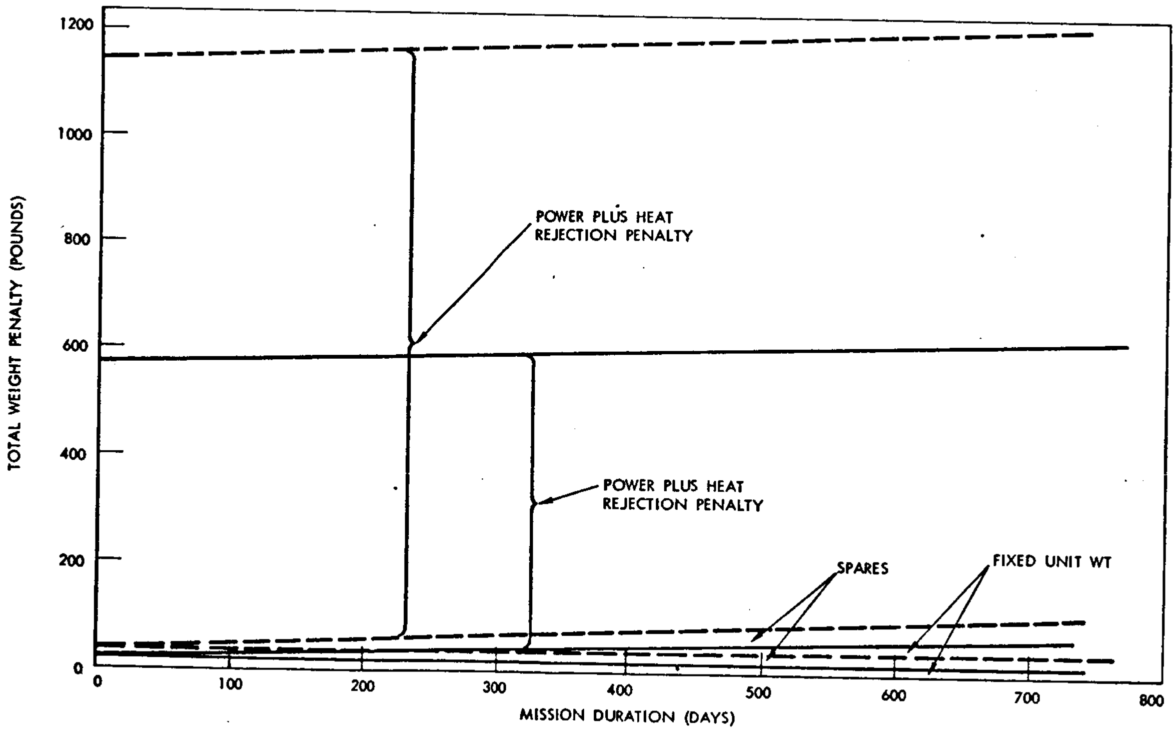

Figure 22. Electrolysis Unit KOH With Plat-ASB-Nylon Wick

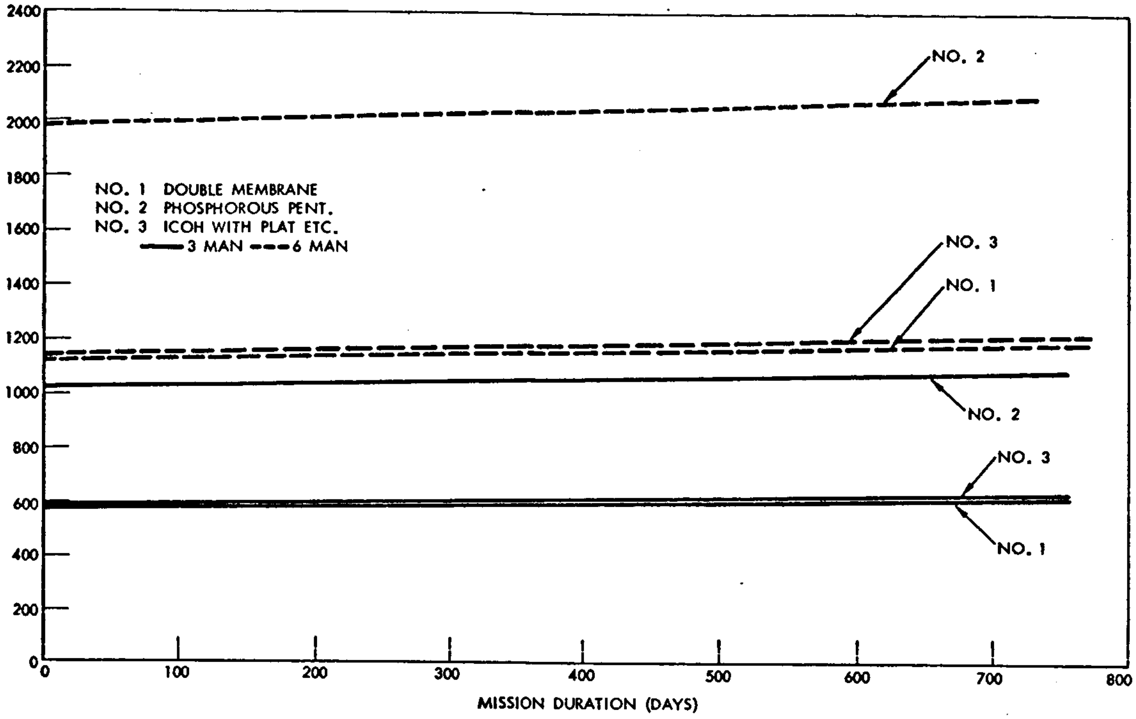

Figure 23. Electrolysis Unit Comparison

PROLONGED MISSIONS ECS RECOMMENDATIONS

This section of the report presents recommended ECS systems for mission durations ranging from 90 to 600 days. The design philosophy adopted was to modify the Block II Apollo ECS by adding regenerative subsystems until the point was reached at which it was more prudent to completely redesign the system.

90-DAY MISSION

An ECS for 90 days was considered, based on the Block II system, the following assumptions for comparisons:

1. LiOH and fuel cell power supply
2. Molecular sieve and fuel cell power supply
3. Molecular sieve, other type of power supply
4. Molecular sieve, water reclamation and other type of power supply
5. Power penalty 1 pound per watt
6. Stored oxygen and nitrogen resupply. Figure 24 shows a comparison of the weights of system hardware plus expendables versus mission duration for these ECS systems.

The weights of the Block II ECS hardware and expendables required for 90 days are listed below. The water requirements for three men were calculated as follows:

Food and Drink	18 pounds/day
Personal Hygiene (sponge bath)	9
Total	27

CON[redacted]

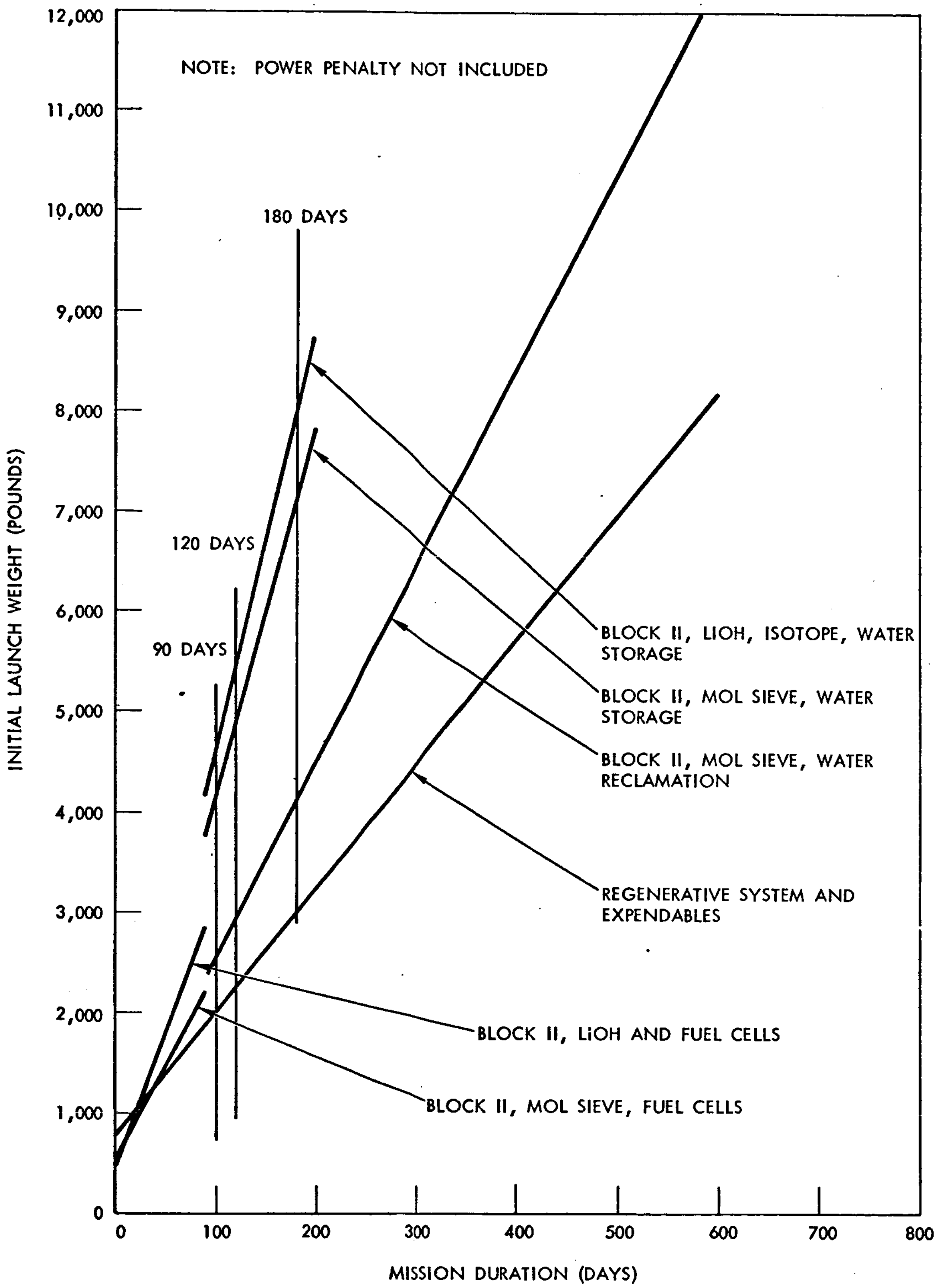

Figure 24. Hardware Plus Expendables Weight Versus Mission Duration

[redacted]

CONFI[redacted]

Recovered from humidity	12.4
Fuel cell production	36
Total	48.4

The water available exceeds the use requirements (assuming the thermal control system will not require a water boiler by the time 90 day missions are attempted), and therefore, no storage of water above the initial launch pad charge is necessary.

ECS dry hardware (Block II)	449 pounds
LiOH	719
Oxygen	967
Nitrogen	436
Oxygen tanks	203
Nitrogen tanks	92
Power penalty 310 (1) =	2866
	310
Total Equivalent Weight =	3176

Molecular Sieve with Fuel Cells

ECS Hardware	449
Molecular sieve	51
Oxygen	976
Nitrogen	445
Oxygen tanks	204
Nitrogen tanks	93
	2218
Power Penalty (595) (1)	595
	2813

[redacted]

Molecular Sieve without Fuel Cells

ECS hardware	449
Molecular sieve	51
Gases and tankage	1718
Water storage	1570
Power penalty	595
	4383

The water storage is necessary because of the absence of fuel cells, resulting in a net requirement of 27 - 9.6 = 17.4 pounds per day storage.

Molecular Sieve, Water Reclamation

ECS hardware	449
Molecular Sieve	51
Water reclamation units	56
Gases and tankage	1718
Expendables for water reclamation	67
	2341
Power Penalty	635
	2976

An inspection of the weight comparisons shows that the ECS total equivalent launch weight depends on the type of power supply. Assuming that fuel cells can be used for the 90 day mission, substitution of a molecular sieve for LiOH gives a saving of 648 pounds in system weight; including the power penalty reduces this saving to 363 pounds. This clearly indicates the choice of a molecular sieve over LiOH on a weight basis alone. In addition, the LiOH requires a storage volume of 29 cubic feet compared with 2.3 cubic feet for the molecular sieve.

If a power supply other than fuel cells, such as solar cells or an isotope, is used, the ECS system choice would be the Block II with a molecular sieve and a water reclamation system. With water reclamation, the system weight saving is 1447 pounds over one using water storage. Inclusion of the power penalty brings the saving in total equivalent launch weight to 1407 pounds.

MISSION LONGER THAN 90 DAYS

The modified Block II ECS systems considered in the previous section used regeneration CO_2 removal (molecular sieve) and water reclamation. The next advance in concept would include the recovery of CO_2, its conversion to water, and the generation of oxygen from the water. The inclusion of oxygen generation results in what is called a regeneration system, which merits a complete redesign, instead of merely adding to the basic Block II ECS.

Based on the subsystems tradeoffs previously reported, a regenerative system was designed using the following subsystems:

1. Airflow loop
    a. Debris trap
    b. Fans and motors (two)
    c. Catalytic burner
    d. Chemisorption bed
    e. Charcoal filter
    f. Main heat exchanger
    g. Water separators (two)
    h. Sensors, valves, etc.
2. CO_2 Management Subsystem
    a. Molecular sieve
    b. Accumulator
    c. Bosch-type CO_2 reduction reactor

   d. Water electrolysis unit

3. Water Reclamation Subsystem
   a. Air Evaporation-two units, one for wash water and humidity condensate, and one for urine recovery.
4. Thermal Control Loop
   a. Heat exchangers (two)
   b. Accumulator
   c. Reservoir
   d. Filter
   e. Pumps (two)
   f. Regenerative heat exchanger
   g. Accessories
   h. Radiator
5. Leakage Makeup Gases

The required flow rates and other process data were calculated, both for 3 and 6 men, and from these data equipment weights and power requirements were found. The weight and power breakdown is given in Table 4. Note that the totals include expendables for 90 days.

Figure 25 shows the relation between the total equivalent launch weight and the mission duration for three of the 90 day systems discussed earlier and for the regenerative system. This figure reveals some interesting trade-off information. If fuel cells are used, a molecular sieve should be substituted for LiOH for missions longer than 44 days. Providing sufficient volume is available for storage of the LiOH, this further substantiates the use of Apollo concepts for 45 day missions. Figure 25 also indicates that when power penalty is included, the regenerative system has no weight advantage at 90 days. The selection of systems for mission durations in excess of 90 days depends upon state-of-the-art and reliability, unless there is a clear advantage in weight and volume required for expendables storage. This will be more fully discussed below.

Table 4. Regenerative Systems Weight and Power Breakdown

	Three Men	Six Men
Hardware		
Air Loop	64.8	97.3
CO_2 Management	330.0	510.0
Water Reclamation	56.0	96.8
Thermal Control Loop	57.0	68.9
Radiator	75.0	100.0
	582.8	873.0
Expendables 90 days		
CO_2 Management	4.0	6.0
Water Reclamation	67.0	139.0
Oxygen (Leak)	436.0	436.0
Nitrogen (Leak)	445.0	445.0
	952.0	1026.0
Storage System		
Oxygen tank	92.0	102.0
Nitrogen Tank	93.0	93.0
Valves, etc.	20.0	20.0
Original water stores	54.0	108.0
Coolant Liquid	90.0	120.0
	359.0	443.0
Total, System Plus Expendables	1893.8	2342.0
Power Requirements, watts		
Air Loop		
Fan	125	200
Catalytic Burner	15	15
Water Separator	6	9
CO_2 System	1100	2200
Water Reclamation		
Urine	15	20
Wash Water	25	36
Coolant Pumps	50	75
	1336	2555
System Equivalent Launch Weight (90 Day Expendables)		
System	1894	2342
Power Penalty Equivalent Weight	1336	2555
	3230	4897

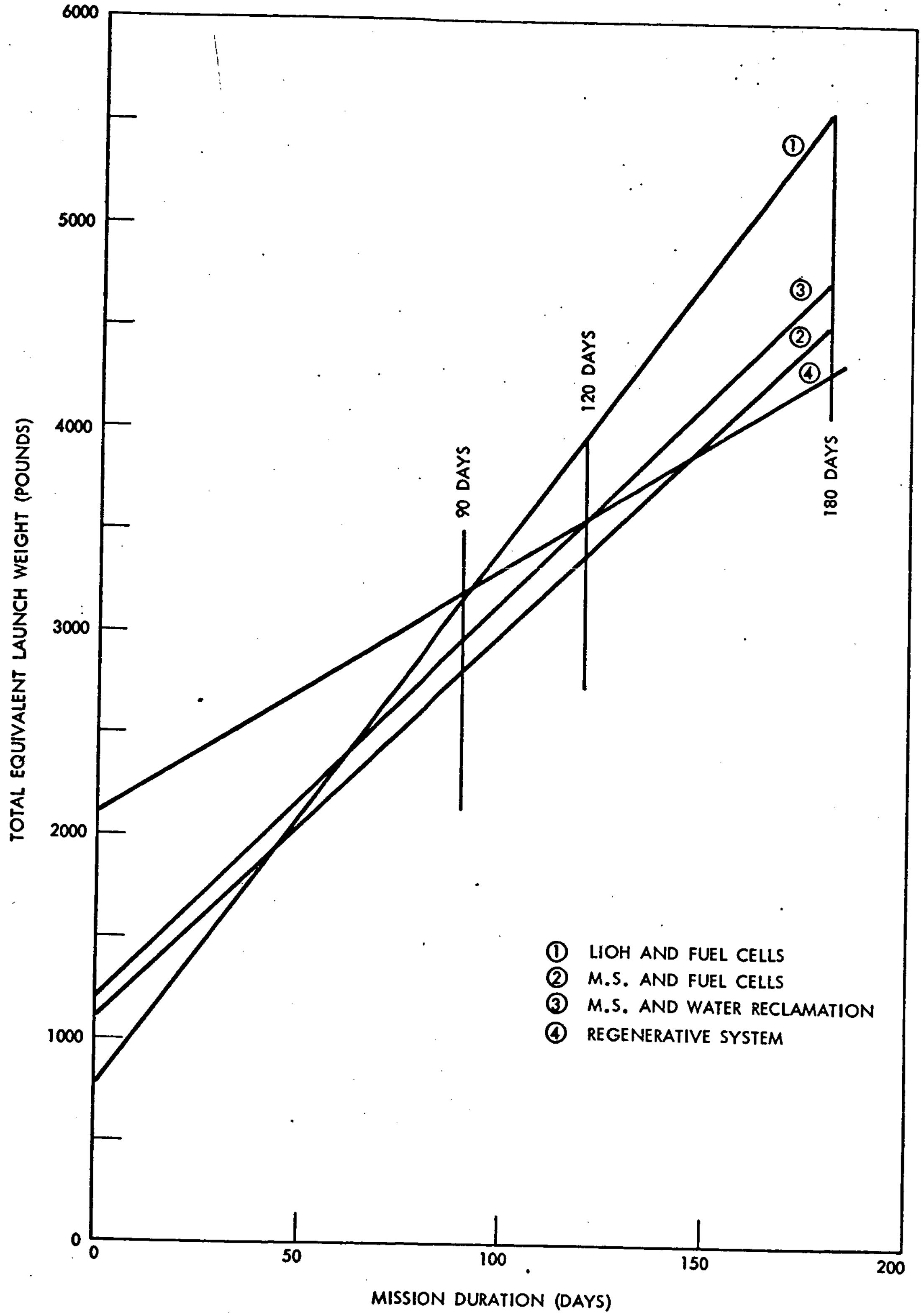

Figure 25. Mission Duration Days

120-DAY MISSION

The trade off point between the system employing a molecular sieve and water reclamation and the regenerative system occurs at 120 days. However, because of the complexity of the regenerative system, its greater operating problems, and inherently lower reliability, the molecular sieve-water reclamation system would be the more likely choice for this mission. Systems availability is also a significant factor; regenerative systems will most likely not be flight qualified before the 1968-1970 period, a fact which will certainly affect ECS system choice.

180 DAY MISSION

For missions of this duration, the regenerative system has a 450 pound weight advantage over its closest competitor. This may not be too great an advantage unless the launch vehicle has a limited payload capacity. However, the point is being approached at which the volume limitations of the Apollo CSM, laboratory, may not permit storing all of the oxygen and nitrogen required by the non-regenerative system. The choice then is the regenerative ECS for this mission duration.

360 AND 600 DAY MISSIONS

It is clear from the foregoing discussion that a regenerative-type ECS system is required for mission durations in excess of 180 days, without resupply.

EARTH LANDING SYSTEM

EARTH LANDING SYSTEM

EARTH LANDING SYSTEM

A two part analysis was performed for the Earth Landing System (ELS) for the prolonged missions study. The first part of the analysis is an extension of the work performed for Apollo X where the existing Block II Apollo ELS was modified to permit missions of up to 45 days duration. The extent of further modifications required to extend the orbital storage lifetime of the ELS up to 600 days is defined and the test requirements established. The second part of the analysis is directed towards the preliminary definition of an ELS capable of providing satisfactory landing performance for a six man vehicle. The orbit storage requirements of this concept are almost identical to that performed for the Block II ELS and therefore are not analyzed separately.

BLOCK II RECOVERY SYSTEM LIFE EXTENSION ANALYSIS

The ELS components and materials were evaluated in terms of compartment environments for a 600 day orbital storage period. The potential effects of the environments on the cold welding and stress cycling of metals, textile strengths, pyrotechnics deterioration, seals degradation, lubricants sublimation, and the prolonged exposure of packed parachutes were investigated. In performing these investigations, literature searches were conducted, methods of calculating deteriorating effects of environments were derived, and information was gathered from other knowledgeable sources in the areas of concern.

As data in many cases were extremely limited, the conclusions derived are based to a large extent on extrapolation of existing data and/or application of theory. Although there are no proven life limiting factors for the ELS components, it is considered mandatory that the analytical findings be substantiated in the future by a comprehensive environmental test program.

RADIATION EFFECTS ANALYSIS

In an earth orbit of 200 nautical mile altitude, the radiation encountered will be primarily trapped electrons and protons; polar protons also will be encountered in polar orbits. All organic polymers are somewhat susceptible to radiation damage. This broad class includes the fabrics, elastomers, and plastics present in the landing system. In general, radiation produces cross linking of polymer chains (which stiffens the product) and scission of the chains (which weakens the structure) as well as various degrees of gas formation. The threshold damage levels for various applicable materials ranges from 2×10^5 to 8×10^8 rads.

Plastics and elastomers in the landing system are stable at least up to 10^6 rads, with the exception of two fluorocarbons; i.e., Teflon, in the sequence controller, and the elastomer Viton, which is used as a seal in the pilot chute and drogue chute systems. Teflon and Viton are very susceptible to radiation, with the formation of corrosive gases and deterioration of physical properties. Effects (in air) on Teflon are noted at about 10^4 rads; effects on Viton are noted at around 5×10^5 rads; however, in the absence of oxygen they can tolerate considerably more radiation. Other than the fluorocarbons, the weaker points would include the chloroprene (neoprene) O-rings and greases. Elastomers under stress have been found to be more susceptible to damage from radiation from unstressed elastomers. Greases, which are generally made from a liquid lubricant plus a soap, have been found to be more susceptible to radiation than the parent liquid lubricant. Versilube G-300 grease (made from Versilube F-50 silicone lubricant plus a lithium soap) is not the most radiation resistant grease available but is reported to have shown no deterioration after exposure to 10^6 rads at a pressure of 10^{-5} torr; however, this is undoubtedly close to its upper limit.

Pyrotechnics and propellants are also radiation sensitive. Gases are generally produced and the properties gradually degrade; however, their tolerance is surprisingly high, with even the most susceptible components being reliable after exposure to a total dose of 10^6 rads.

Inorganic components (glass and metals) are much more radiation resistant than the organic components. Although glass develops a brownish color at relatively low-radiation exposures of 10^4 rads or less, non-optical changes of engineering interest are not expected at doses less than approximately 10^9 rads. Changes in engineering properties of metals occur at levels far in excess of radiation limitations imposed by organic materials within the system.

If a threshold value of 2×10^5 rads is accepted for nylon cord, it then becomes the limiting factor for landing system components. Even though this value is only a tenth to a hundredth of the threshold values usually quoted for other nylon textiles it would still require several years in a 90 degree inclination orbit at 200 nautical miles altitude to reach this dose. At an inclination of 28 degrees, it would take about 250 years.

Functional radiation thresholds for the various components in the sequence controller are given in Table 5. Silicon controlled rectifiers in some cases are less resistant to radiation than a silicon diode or transistor. The epitaxial planar-type employed in the sequence controller, however, is a relatively radiation-resistant silicon controlled rectifier.

Teflon is utilized in the electronic system as an insulator. Difficulties are experienced with this material in a radiation environment at about 10^4 rads because of degradation of physical properties and the release of corrosive gases.

Whereas the sequence controller is located in the crew compartment rather than in the landing system compartment, the nominal shielding will be 5 grams of aluminum per square centimeter rather than 1 gram, which would be the case if it were stored in the recovery system compartment. In addition, electronic components are shielded further by varying amounts of epoxy potting material and metal enclosures for the relays and semiconductors. This degree of shielding is expected to be adequate. It is estimated the silicon semiconductors would have lifetimes (from a radiation standpoint) in excess of 2 years in any earth orbit and that Teflon insulation would be suitable for more than 2 years in a 28 degree earth orbit and for at least 1 year in a 90 degree earth orbit.

TEMPERATURE EFFECTS

In the low altitude earth-orbit mission, parachute recovery system components go through one temperature cycle on each 90 minute orbit. The maximum temperature calculated is no more than 120 F and not less than -40 F at the inside wall of the recovery compartment cover -- well within the limits established for the present Apollo recovery system. A thermal plot of the ELS compartment is shown in Figure 26.

Table 5. Functional Thresholds of Sequence Controller Components

Component	Functional Thresholds (rads)
Silicon controlled rectifier (epitaxial planar)	5×10^4
Relay (with Teflon insulation)	10^4
Wire sleeving (Teflon)	10^4
Silicon diode, zenner diode, transistor	5×10^4
Capacitor, tantalum	5×10^4
Relay, time delay (with nylon insulation)	5×10^6
Connector (with silicon insulation)	5×10^6
Baroswitch (with diallylphthalate insulation)	2×10^7
Connector (with diallylphthalate insulation)	2×10^7
Mylar insulation	3×10^7
Potting (epocast 202, 9617 hardener)	10^8
Bonding material (epoxy resin)	10^8
Resistor (wire wound with silicone paint insulation)	3×10^9
Resistor (graphite with vitreous enamel insulation)	3×10^{10}
Resistor (metal film, with vitreous enamel insulation)	8×10^{10}
Chassis, brackets, etc. (aluminum)	10^{12}
Borosilicate glass	10^9
Silicone rubber	10^6

As temperature decreases, organic polymeric materials generally gain in strength and stiffness and lose in elongation and impact strength. The recovery system components, however, are not expected to function at orbital temperature environments; they are only required to survive storage under these conditions.

Nylon and Dacron have shown no degradation after exposure to -100 F for 24 hours, and cotton yarns have shown no apparent degradation after exposure to -70 F for 24 hours. A minimum continuous service temperature of 0320 F is listed for nylon and -432 F for Dacron. The textiles in the recovery system can be expected to survive the minimum temperatures encountered during the specified earth or lunar orbits.

Resins and plastics such as epoxy, polyurethane foam, melamine, and polyesters are capable of withstanding at least -65 F, as evidenced by various military specification requirements. A temperature of -432 F is quoted as a minimum continuous service temperature for these materials. The service temperature range for the silicone grease Versilube G-300 is given as -100 to 450 F. Elastomers such as neoprene and Viton are relatively vulnerable to reduced temperatures; they are functional, however, at least as low as -65 F and would probably withstand storage as low as -85 F.

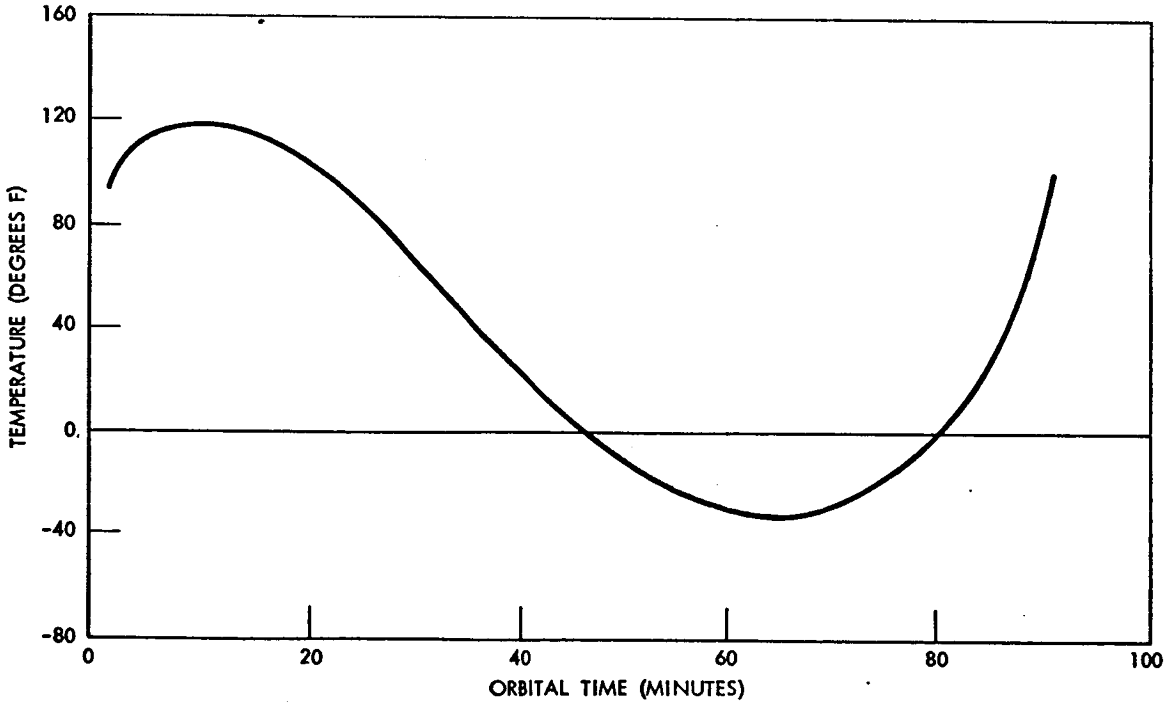

Figure 26. ELS Compartment Inside Wall Temperature vs Orbital Period for 200 nm Earth Orbit

Electronic components in the sequence controller are well protected from temperature fluctuations because of their protected location in the crew compartment and the thermal insulating properties and specific heat of the epoxy block in which they are potted. Expected temperatures are well within acceptable temperature limitations of these components. Withstanding the upper temperature limit of 150 F which occurs for a short period at earth reentry is not expected to present difficulties.

Textile strength is dependent on temperature. As a rule of thumb, the rate of chemical reaction and degradation doubles for each 10 C rise in temperature. Results from recent Apollo tests show that nylon fabric suffers only a 4 percent loss of strength after 46 days of exposure to 150 F at a pressure of 1×10^{-6} torr (tested at ambient temperatures).

The shelf life of pyrotechnics and storable propellants is also dependent on temperature; however, existing evidence indicates that the expected conditions should not present a problem.

It is concluded that the temperatures expected during space storage, or during reentry, will have no adverse effect on the materials and components of the ELS.

ULTRAHIGH VACUUM EFFECTS

The potential effects of ultrahigh vacuum on ELS materials and components have been considered. The 600 day orbital storage period and the 200 nautical mile altitude determine the ultimate levels of vacuum to be considered. Definition of these conditions is basic to this analytical investigation.

The recovery system compartment is vented to space because of mechanical design and structural limitations on buckling strength. The compartment, initially at a pressure of one atmosphere, will reach external pressure in theory a few minutes after lift off. This vent cross-sectional area determines the rate of loss of material to external space and, to a certain extent, the level of vacuum within the recovery system compartment.

The pressure in external space as defined by the "U. S. Standard Atmosphere of 1962," is approximately 10^{-8} torr in the earth orbit. It should be pointed out that molecular concentrations at these pressures are extremely small and differ in chemical composition and kinetic energy from that at the earth's surface.

The pressure within the compartment is dependent upon vapor pressures of the various materials within the compartment, the rates of outgassing of various materials, and leak rate of the compartment.

Estimating the pressures within the recovery system compartment is difficult due to the unknown and variable rates of outgassing of materials and the unknown vapor pressures of the materials within the compartment.

Unless partially pressurized, the vacuum level of the compartment, while in earth orbit, will probably reach 10^{-8} torr, the pressure of external space. Data on ultrahigh vacuum effects for the mission periods are generally not available, therefore estimates of the vacuum stability of materials and major components used in the ELS were made in an analytical manner from existing data and through computation. Vacuum levels of 10^{-6} torr and lower might be expected to produce effects such as (1) loss of material by vaporization or sublimation, (2) decomposition of materials, and (3) cold welding of contacting metal surfaces. Rates of evaporation of pure materials from solid and liquid surfaces can be computed from theory. The rate depends upon vapor pressure of the material, temperature, and area of surface exposed. Under certain conditions, the mass flow through an aperature separating gases at different pressures can be estimated.

The measurable effects on metals of ultrahigh vacuum are loss by vaporization and cold welding of surfaces in intimate contact. The question of cold welding of metal parts and mating surfaces under high vacuum conditions is related to lubrication and friction and to the volatility of the oxide coating. The phenomenon of cold welding has been observed under laboratory conditions. It can be stated that the phenomenon does not occur readily or at all above a pressure of 10^{-7} torr. The adhering surfaces must be extremely "clean" and free of lubricant and oxide coating. Cleanliness can develop by evaporation of lubricant and absorbed gases. Breakdown of the oxide coating is more difficult and will occur slowly by evaporation or by chemical dissociation at very low pressures. It is more likely that oxides are abraided from the surface in moving parts after evaporation of the lubricant, causing them to seize or cold weld.

The occurence of a cold weld could seriously affect the operation of the recovery system. Vulnerable points are the interface between the mortar lid and mortar tube, the swivel fittings at the riser attachments, and the metal strands in the steel riser cables. Provisions, therefore, must be made to assure that an internal pressure of no less than 10^{-7} torr is maintained throughout the storage period.

The effect of a high-vacuum environment on rocket propellant pyrotechnic reefing line cutters and disconnect cartridges is expected to be minimal for the storage period because they are hermetically sealed. As eventual degradation would occur under high-vacuum conditions over extended periods of time, the integrity of the seals and the sealant materials is, therefore, of prime importance.

EFFECT OF PROLONGED PARACHUTE PACKING STRESSES

At the present time, it is not allowable for the Apollo main parachutes to remain packed for longer than six months prior to launch. Of this six months, the parachute is allowed to remain installed on the Apollo ELS deck not more than 90 days prior to the mission. For a 14-day mission, this totals 104 days outside of shape-retention containers.

The pressure-packed parachute is under a considerable compression force during the period of storage. Once removed from the shape-retention container, it has a tendency to swell, and the fabric and cords which make up the constraining corset-like retention cover are under considerable tensile stress. Storage during a mission involves the vacuum, radiation, and temperature environment inside the compartment. Very little is known about the effects of space environments on the storage life of textile materials under compressive and tensile forces.

The U. S. Army, Navy, and Air Force have tested the storage life of several types of parachutes under various conditions. The information obtained has considerable bearing on the question of storage life of pressure-packed landing system parachutes, and is summarized as follows:

1. A U. S. Navy test program was performed by Switlik Parachute Company in 1949 and 1950 on vacuum-packed, hermetically sealed personnel parachutes. No evidence of deterioration or degradation of performance due to the vacuum was noted; however, the maximum length of time between packing and testing did not exceed 60 days.

2. The effect of extended periods of time between packing and use has been investigated by the U. S. Army. Standard packing procedures, rather than pressure packing, were employed. Performance tests following one year of storage in Alaskan weather indicated no degradation of performance. A more recent series of tests has been conducted in Alaska using 64-foot G-12 cargo chutes with temperatures to about -60 F. There was no evidence of deterioration from storage at low temperatures, but the overall results of the long-term storage tests were inconclusive. At the present time, it is standard practice to repack cargo-type parachutes after storage for 6 months under arctic conditions and after 12 months under temperature conditions. Cargo parachutes stored under ambient temperature conditions for 10 years were recently tested. They deployed in a normal manner and showed no performance loss.

3. The U. S. Air Force (ASD) has a current program in which pressure-packed parachutes are stored in containers exposed to ambient temperatures in Northern Maine, Albuquerque, and Key West. Periodically, parachutes are removed and the components tested for evidence of degradation. Tests have been made on parachutes stored up to seven years with no evidence of degradation.

4. The U. S. Air Force (ASD) is also determining the effects of long-term storage on pressure-packed, heavy-duty ribbon parachutes pressure packed to a density of 35 pounds per cubic foot. The parachutes were initially stored in containers under ambient conditions in Pennsylvania; they are now stored under ambient

conditions in Albuquerque, New Mexico. Each 6 months, units are removed from their containers and tested in aerial drops. Parachutes that have been stored in containers for up to two years have been tested without evidence of deterioration. The standard repack interval for operational parachutes of this type is now two years.

Data from these programs indicate that pressure-packed parachutes could be stored in containers under earth ambient conditions for at least two years and that temperatures within the landing system compartment during earth orbit are not detrimental.

COMBINED ENVIRONMENTAL EFFECTS

Very little information is available on the effect of radiation in a hard vacuum. Previous studies tend to indicate that some materials are less affected by radiation while in vacuum. In these cases, it is suspected that oxidation played a role in the observed radiation effects in a normal atmosphere. Other materials appear to show the same radiation effects whether irradiated in air or vacuum.

Tests with nylon tire cords have indicated much less degradation from radiation in vacuum as compared with radiation in air. Dacron and polyurethane likewise show decreased radiation effects in vacuum; however, in the case of cotton and epoxy laminates, the presence or absence of a vacuum appears to be insignificant.

Radiation effects are not expected to be a major factor at 200 nautical miles with the possible exception of some electronic components in a 90-degree orbit; however, vacuum effects could be significant. Whether or not relatively low levels of radiation will accentuate degradation and other effects produced by vacuum is not known. Certainly, in any experimental evaluation of vacuum effects, the additional factor of temperature must be considered.

The important question is not only the combined effects of radiation, vacuum, and temperature, but also whether these combined effects remain after reentry and at the time of ELS initiation. Only a limited amount of test data is available on individual space environmental effects. Data available on combined effects are very limited and generally do not extend beyond 10^{-6} torr. No data are available on combined effects with the subsequent environmental change duplicating reentry conditions. It is realized that these sequential tests are extremely difficult to perform and may lie beyond the present state of the art, relative to available test chambers and test techniques. The fact remains pertinent, nevertheless, that test equipments and techniques should be directed toward accomplishing such tests.

CONTROLLED COMPARTMENT PRESSURE

It is difficult to assess pressure levels precisely in the recovery system compartment, based on outgassing and vaporization of equipment within the compartment and the effects on materials during the logistics spacecraft mission. The recovery system compartment is vented to the outside and filled with air at sea level atmosphere pressure before lift off. While entering the vacuum of space, the air from the compartment will flow in a controlled fashion through the existing aperture which is provided for the baroswitch pressure sensor and the leakage areas of the ELS compartment. Simultaneously, gases and impurities begin to outgas. This outgassing is actually an absorption process involving two materials in close contact with each other. Outgassing should be distinguished from vaporization and sublimation since outgassing refers only to the slow removal of gases (water) and impurities previously absorbed on the contained walls and by the various materials in the compartment. As soon as the vacuum in the compartment decreases to the vapor pressure level of the most volatile material, vaporization will occur. This is a process whereby the material changes its physical state. Silicone oils are probably affected first. Once the vapor pressure of a material is reached, the pressure inside the compartment stabilizes until the volatile component is exhausted. Then, the vapor of this material will be pumped from the compartment into space at a rate depending on the effective cross-sectional area of the aperture in the compartment. This phenomenon will continue until all vaporizing materials are removed; therefore, only outgassing and vaporization are of importance in this analysis.

Vaporization is an equilibrium process and loss rates in the recovery compartment can be calculated. This required knowledge of materials, material vapor pressures, aperture areas, and the volumetric geometry of the compartment and its components. Compartment pressure can be maintained at a level around 10^{-6} torr by adding vaporizing or subliming materials. These materials are available commercially and precise vapor pressure data have been obtained.

Due to the temperature variation within the compartment, the compartment pressure will cycle. As this cycling takes place, the instantaneous loss will change.

As may be seen from Figure 27, which is a plot of vaporizing substance weight as a function of storage time to maintain an internal pressure level of 10^{-6} torr, the size of the leakage area is highly significant.

The 100 cm^2 leakage area is typical of the existing Apollo Block II ELS compartment. For the Apollo X missions, it was recommended that no structural modification be made and that 10 lb of volatile substances be added. However, as may be seen from Figure 27, the weight and volume of the volatile substance would be prohibitive for a 600 day mission.

It has been calculated that a 10 cm^2 aperture is sufficient to provide the required venting to the ELS compartment. Therefore it is recommended that for the prolonged missions better seals be provided in order not to exceed the 10 cm^2 leakage area and that 10 lb of volatile substance be added to maintain the desired pressure level.

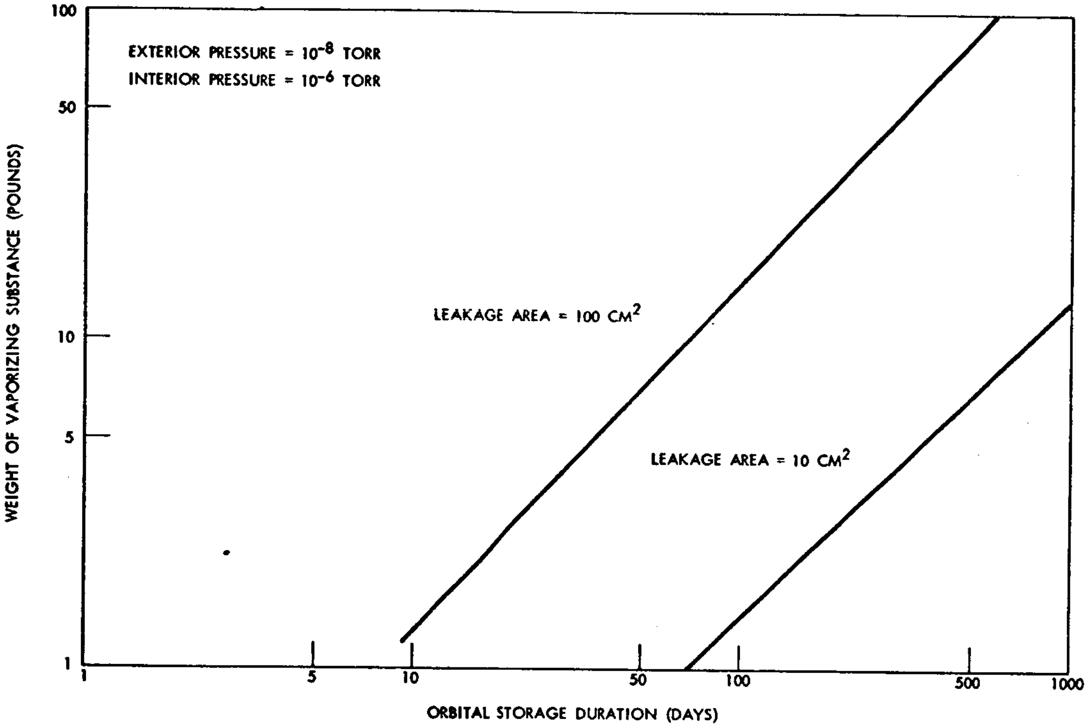

Figure 27. Orbital Storage Duration (Days) Vaporizing Substance Weight as Function of Storage Time

SYSTEM TEST REQUIREMENTS

The proposed approach of maintaining pressure within the recovery system compartment above 7.5 x 10^{-6} torr as a means of extending the life of the Block II recovery system for prolonged missions provides an acceptable solution. The choice of maintaining a minimum pressure within the recovery system compartment rather than to pursue a new component development test and qualification program for very high vacuum levels is based on the ground rule of extending utilization of the Block II configuration to prolonged missions at a minimum cost. Other ground rules observed in planning the development test effort are:

1. The Block II parachute recovery system will have been previously qualified to satisfy the basic Apollo mission environments and performance parameters.
2. The development test effort will encompass only those environments and parameters specified for prolonged missions which differ from those of the basic Apollo mission requirements.
3. Flight qualification test requirements will have been previously satisfied by Apollo Block II system flight tests.

TEST REQUIREMENTS

The proposed approach to maintain compartment pressure at, or above, the minimum level specified for the basic Apollo mission, relieves development test requirements to the level of tests which will confirm components and system suitability for the extended exposure period of up to 600 days. In order to determine suitability with confidence, tests should be performed at exposure durations and pressure levels which represent a safety margin beyond operational criteria. The technique for maintaining compartment pressure at required levels should be checked using realistically simulated conditions and components at the earliest possible date since it constitutes the basis for the suitability of the Apollo Block II parachute system as well as forming the basis for component and materials test. Calculated leak rates and the requirements of sublimated materials must be verified and the contribution of materials outgassing and the effects of gas adsorption must be determined.

Tests of selected system materials and small components are required to verify predicted effects and to support development of recommended life-extension techniques. Tests will normally determine strength or weight loss after exposure to maximum vacuum and temperature cycling for the longest specified mission time plus margins. Where material characteristics differ at storage conditions from operational performance conditions, strength tests of material properties should be determined immediately after space environment exposure. Test conditions should realistically simulate increase in pressure and temperature with time, representative of reentry and descent up to the event of recovery system deployment and operation. Material lost due to exposure represents a permanent change not subject to strength recovery in atmosphere. Strength loss, therefore, may be determined at ambient test conditions.

The following data are to be obtained from tests on materials and components after exposure to space environments:

1. The effect on strength of textiles compressed in storage
2. The effect on strength of textiles in tension
3. The constituent loss and subsequent performance change of textiles
4. The constituent loss and property change of lubricants
5. The effect on strength of polyurethane foam, toughness of polyurethane resin and sealing efficiency of seals.
6. The extent of molecular bonding in textiles and metals (cold welding) and subsequent effect on system performance
7. The outgassing characteristics of materials and components in the recovery compartment
8. The characteristics of sublimating compounds and control of compartment pressure
9. The determination of discontinuities, if any, in material properties within the established margins of vacuum and exposure time beyond mission environment limits

Laboratory Test Parameters

Laboratory development tests will consist of:

a. Tests to determine effects of exposure to vacuum and temperature cycling
b. Tests to determine adequacy of compartment pressure control

Environments proposed for exposure-effects tests on materials and components are a vacuum level of 7.5×10^{-6} torr, temperature cycling between -40 F and 120 F every 90 minutes, and a test duration of 600 days.

Laboratory Development Tests (Parameters to be measured)

Laboratory tests are proposed on materials and small components to determine exposure effects and verify analytical conclusion of Section II. Independent tests will be conducted on textiles, lubricants, pyrotechnics, plastics and seals. At the environment levels considered, cold welding of metals is not expected to occur but confirmation is required. Parameters to be measured are listed below.

Textiles

Textile strength and weight loss at test conditions
Rate of strength recovery after vacuum exposure

Twenty-eight (28) identical specimens will be used in the test series; 24 subjected to vacuum environment, and 4 will be control specimens.

Specimens of 300 pound nylon tape, MIL-T-6134B, type II, have been selected to represent the basic fabric material in an easily tested form.

Lubricant

Weight loss
Change in coefficient of starting friction

Specimen: G-300 lubricant in a representative aluminum container

Pyrotechnics

Residual gas
Post test performance: No-fire power, fire power and energy output

Plastics

Residual gas
Strength and weight change
Recovery of strength with increasing ambient pressure

Seals

Residual gas
Change in elasticity (durometer hardness)
Permanent set

Metal Joints

Degree of cold welding under mission orbital loading
Effect of cold welding on post-test performance
Level of significance: 3 percent change

Compartment Pressure Maintenance Tests

Laboratory tests are required to verify the suitability of the proposed method of maintaining recovery system compartment pressure. These tests are designed to give the total quantity and rate of normal desorption and outgassing of recovery system components and to verify analyses related to vaporizing material quantity needed and leak rates determined for a known aperture between compartment and test vacuum level employed.

The tests proposed involve two identical compartments (A and B) containing recovery materials. Each compartment and contents will duplicate (in proportion to a full-scale system) surface materials, surface area, free volume, weight and volume of textiles, weight of lubricants, plastics and seals. Size of specimen compartment may be as low as one cubic foot in volume. However, the problem of accurately duplicating proportional leak area and material ratios becomes increasingly difficult as size decreases from full scale. A compartment size equivalent to a quadrant of the full scale recovery system compartment is proposed. The following parameters are to be measured:

Compartment A pressure level above test chamber pressure
Compartment B pressure level above test chamber pressure
Amount of polysiloxane loss
Weight loss of compartment contents

NOTE: Polysiloxane to be introduced only into compartment "A" to permit direct comparison of its effectiveness in maintaining compartment pressure.

SIX MAN VEHICLE ELS ANALYSIS

The present Apollo vehicle is designed to perform a lunar mission with a crew of three. The recovery system consists of three vertical descent, noncontrollable parachutes; satisfactory operation of any two of the three parachutes will result in a safe landing. The parachute system is complemented by an impact attenuation system which absorbs some of the impact energy. This system consists of a series of shock struts which support the crew seats in the three axes. This system is further complemented by a crushable honeycomb "toe" which is part of the spacecraft structure to absorb some of the initial landing shock. In the landing attitude, the vehicle longitudinal axis is inclined 30 degrees from the vertical with the "toe" down. Because of the structural deformation which occurs at landing, the spacecraft is not considered to be reusable. Figure 28 is a diagram of the Apollo impact attenuation system. The Apollo Earth Landing System was originally designed to meet certain requirements specified by NASA, the most significant of which are:

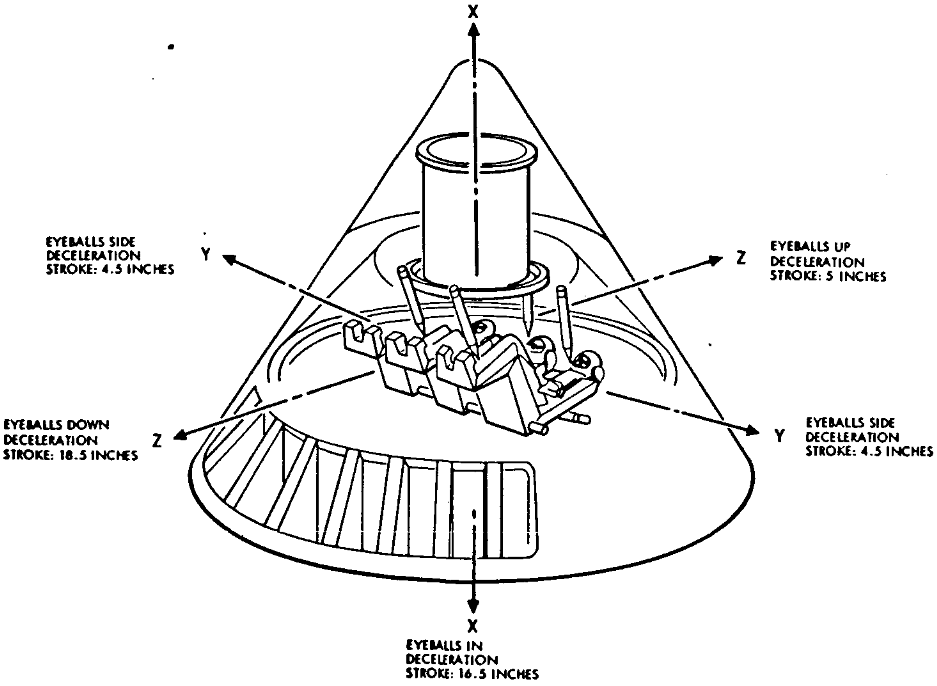
X
EYEBALLS SIDE DECELERATION STROKE: 4.5 INCHES
Y
Z
EYEBALLS UP DECELERATION STROKE: 5 INCHES
EYEBALLS DOWN DECELERATION STROKE: 18.5 INCHES
Z
Y
EYEBALLS SIDE DECELERATION STROKE: 4.5 INCHES
X
EYEBALLS IN DECELERATION STROKE: 16.5 INCHES

Figure 28. Apollo Impact Attenuation System Schematic

1. The spacecraft is to be capable of making a satisfactory water or land landing within nominal design limits under sea state 3 conditions, or on land at an altitude of 5,000 feet with a 20 knot ground wind on slopes not exceeding 5 degrees.

2. Under emergency conditions, the vehicle is to be capable of making a water landing under sea state 4 conditions with ground winds up to 30 knots and on slopes up to 15 degrees.

3. For design purposes, the crew is assumed to be incapacitated and the ELS is to function automatically with no aid from the crew. However, manual overrides are to be provided.

4. Recovery system provisions to permit the vehicle to avoid terrain obstacles, excessive ground slopes, and to negate some of the ground wind during the landing phase are not to be considered.

The Apollo ELS was designed within the preceding constraints, and a test program was performed to demonstrate its capabilities.

In analyzing Apollo system design and reviewing test results, it is concluded that the majority of the landing problems encountered can be attributed to three major factors: (1) the lack of sufficient attenuation stroke in all axes, (2) the relatively high vertical velocity component at impact, and (3) the lack of spacecraft control to avoid excessive slopes and negate ground shear winds.

Therefore, a design philosophy which would eliminate some of these problems is developed for the six man spacecraft.

SPACECRAFT RECOVERY RATIONALE

In order for the spacecraft to make safe operational landings on a routine basis, it appears necessary that system design accommodate primary land landings with a maximum degree of crew safety and possibly spacecraft reuse. It is not economically feasible to mobilize a recovery task force each time a spacecraft is to be recovered, nor is it desirable to subject the crew to loads which stress human tolerance limits to impact shock. Therefore, it is apparent that the Apollo landing philosophy, and some of the ELS components, must be modified to accomplish satisfactory landings with the six man spacecraft. Also to be compatible with overall mission requirements, a water landing capability must be provided.

As presently designed, satisfactory performance of the Apollo impact attenuation system is dependent upon a fixed mass. If for instance, one of the crew couches is removed, the mass to be attenuated is decreased and the resulting g loads at landing would proportionally be higher unless the couch struts were redesigned. If, on the other hand, additional crewmen or cargo are added to the basic Apollo complement of three, the available stroke is insufficient to attenuate the crew within their physiological limits because of volume limitations of the crew compartment. Therefore, it appears highly desirable that the impact attenuation system be designed in a manner which, while providing maximum volumetric efficiency, will also permit suitable attenuation of the total spacecraft, regardless of the number of crewmen and-or the amount of cargo on board. This system design must provide an impact load profile and dynamic characteristics which, under normal landing conditions, can be tolerated by the crew, and which would not impose loads on the spacecraft structure in excess of the design limits dictated by the boost and reentry phase of the flight profile.

This approach will result in a universal design that (1) can provide for varying combinations of crew and cargo, (2) will not impose severe impact loads on the structure and the crew, and (3) will provide for nominal spacecraft reusability (by not relying upon irreversible structural deformation of the spacecraft's primary structure).

An essential requirement is to provide a certain degree of vehicle control during the descent phase following reentry to permit selection of a landing site free of boulders, high power lines, and other ground obstructions. Therefore, it is necessary for some member of the crew to physically control the terminal flight of the spacecraft, and for the recovery system to be of a type that permits directional vectoring.

The preceding implies that two of the current Apollo ground rules - no recovery system control, and no active crew participation - cannot be imposed as recovery requirements. However, these requirements should be deleted only for the nominal recovery case; it appears entirely feasible to design a recovery system that would function automatically in event of a disabled crew and be nominally passive until activated by the crew. By eliminating these two Apollo ground rules, other system constraints can partially be eliminated since spacecraft control implies that excessive ground slopes and ground winds can either be avoided or negated, thus, making the landing phase of the spacecraft less hazardous.

To accomplish the required objectives for recovery control and landing site selection, several candidate landing recovery system concepts were investigated, including paraglider, rotor system, balloons, and gliding parachutes. To compare these candidate systems parametrically, certain common design criteria and preliminary ground rules were established and are discussed in subsequent paragraphs.

The following landing requirements are partly based on Apollo requirements and on the recovery rationale previously defined. They are used as a common baseline for design analysis of the various candidate recovery systems.

Nominal landing conditions (normal mission):

1. Recovery and landing will nominally occur during daylight hours over the San Antonio, Texas, Apollo recovery area. The backup land landing area will be the Woomera range, Australia.

2. For design purposes, the maximum ground wind will be assumed not to exceed 20 knots which is representative of 95 percent of the time for San Antonio during the worst month (April), and 90 percent of the time for Woomera during the worst month (November).

3. For design purposes, the terrain slope will be assumed not to exceed 5 degrees and be free from local obstacles.

4. The terrain altitude shall not exceed 2,000 feet, and the maximum ambient temperature considered is 120 F.

5. The ELS will be designed to attenuate landing loads to a nominal maximum of 10 g on the crew and the vehicle.

Contingency landing conditions (mission abort):

1. Recovery and landing may occur over either land or water during daylight hours, but only over water during night hours.

2. The maximum sea state for water landing will be sea state 4, and the maximum ground winds to be considered for ground landings shall be 30 knots.

3. The surface of the terrain will include hummocks, boulders, etc., similar to a rockstrewn desert area.

4. The terrain altitude shall not exceed 5,000 feet and the terrain slope shall not exceed 5 degrees.

5. The ELS will be designed to attenuate emergency landing loads to a maximum of 20 g on the crew and spacecraft.

6. Crew provisions will be supplied for a seven-day post-landing survival period.

Emergency provisions (primary landing system failure):

1. The ELS will be equipped with either redundant provisions or a fully automatic backup system which requires no crew control.

2. The emergency system shall be designed to land the spacecraft within suitable crew tolerance limits on either land or water during either daylight hours or night under conditions of sea

state 4, ground winds up to 20 knots, and ground slopes up to 15 degrees.

General considerations:

1. The recovery system must be capable of providing a safe landing from all aborts.
2. No more than one landing emergency condition is considered at one time. No more than one system failure mode in conjunction with one landing emergency condition is to be considered.
3. Failure of any component of the recovery system will not compromise satisfactory performance of the other components. An emergency backup system will be provided if the primary system is not redundant.

RECOVERY SYSTEM PARAMETRIC ANALYSIS

Four main recovery system concepts were parametrically analyzed. The concepts selected for analysis are in accordance with the previously developed landing rationale, which requires a certain measure of control over vertical and horizontal velocities. The normal parachute system, which has no vectoring potential, was not analyzed as a prime system due to its limitations. However, it was considered for the emergency backup system requirements.

The four concepts studied include paraglider, rotor system, hot air balloon (Paravulcoon), and steerable parachute. These systems have been analyzed with respect to deployment characteristics, aerodynamic performance, landing characteristics, and required redundancy or backup provisions. A comparative evaluation of the candidate systems identified significant parameters such as weight, volume, reliability, and state of the art.

Paraglider

Paraglider is an inflatable structure which is stored in a manner similar to a parachute. Upon deployment, three structural members extend under pressure. These members support a sail membrane in a triangular pattern providing aerodynamic lift. The spacecraft is suspended beneath the paraglider by five suspension lines; three lines are attached to the center keel and one to each leading edge boom. By varying the length of the control cables, the spacecraft cg can be shifted with respect to the wing center of pressure, thus causing an unbalanced moment in either or both the longitudinal and lateral directions to produce the desired pitch and bank maneuvers. A schematic of the Paraglider system is shown in Figure 29.

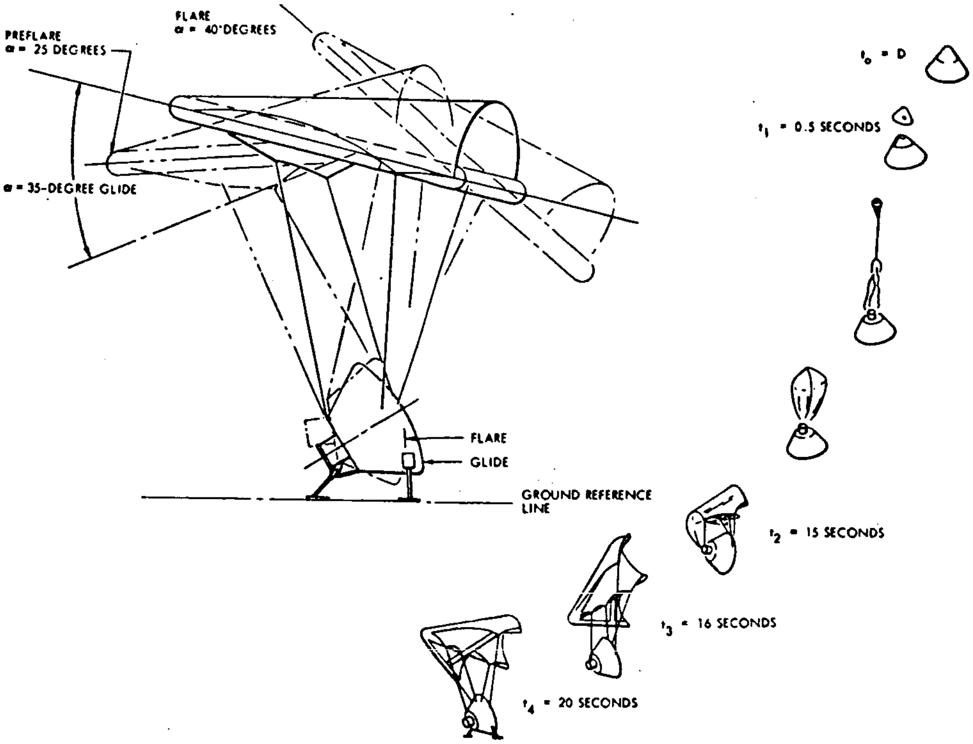

Figure 29. Paraglider Deployment and Landing Sequence

Rotor Recovery System

The rotor recovery system operates similar to a helicopter in unpowered flight, permitting maneuvering during descent and near zero-zero velocity touchdowns. The rotor group consists of a hub and four blades controlled in cyclic and collective pitch. The blades, stored during reentry, begin to deploy from the fully coned or trailing position, rotating as they pick up load. Figure 30 is a system schematic and deployment sequence of the rotor.

Balloon System

The characteristics of two balloon systems (hot-air balloon and helium or hydrogen balloons) were studied in the Modified Apollo Study. It was established that the gas (helium or hydrogen) required to provide sufficient buoyancy resulted in a high weight penalty and that the rate of inflation required to satisfy the pad abort requirement could not be achieved. Therefore, this balloon concept was rejected in favor of the hot-air balloon. The system considered is a cluster of three redundant balloons complemented by heating units and a control system. This concept is not new and some development drop tests have been sponsored by NASA to study deployment, inflation, and terminal descent characteristics of a 54-foot-diameter balloon. In addition, wind tunnel testing of smaller diameter balloons has been performed. A system deployment sequence is shown in Figure 31.

CON[redacted]

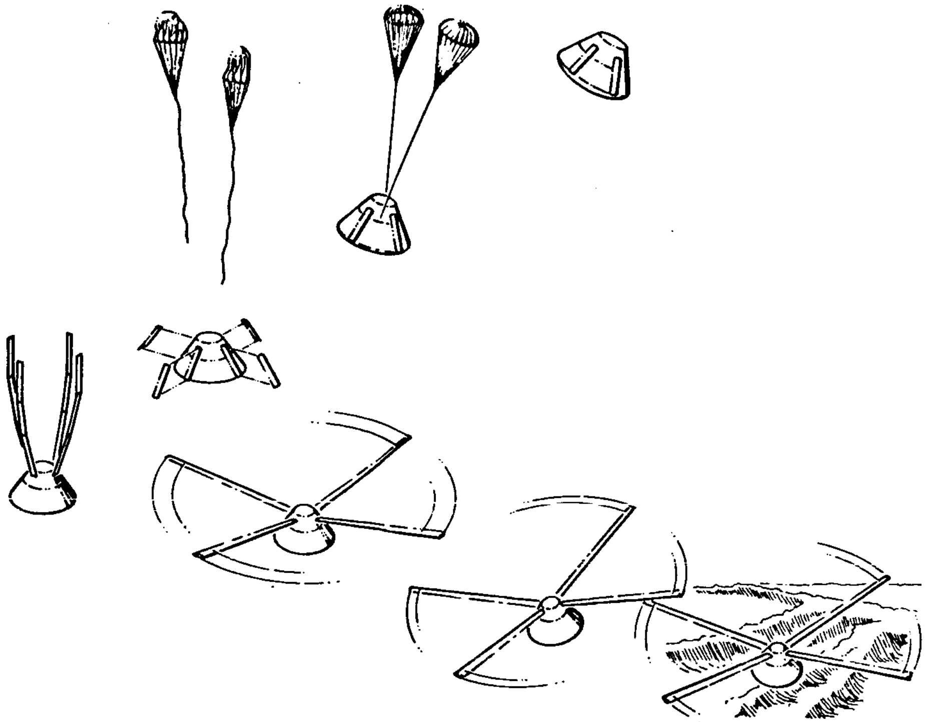

Figure 30. Rotary Wing Deployment and Landing Sequence

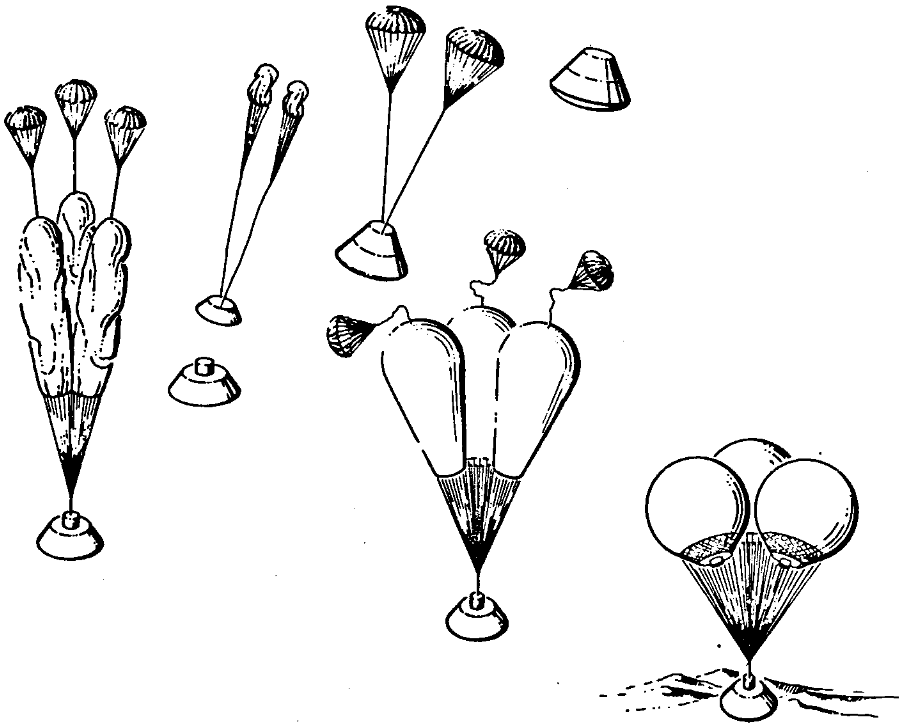

Figure 31. Special Purpose Balloon Deployment Sequence

[redacted]

Parachutes

All space flights to date have used parachutes for final descent. Primarily parachutes have been used because of the high degree of reliability within the state of the art, ease of packaging, low weight, and low volume. The recovery systems presently being developed for Gemini and Apollo are parachute systems. Terminal descent parachutes may be generally classified in two categories: standard parachutes and steerable parachutes.

Standard Parachute

The standard recovery parachute system is generally composed of a single or cluster of solid or ringsail parachutes. This concept is the most highly developed and reliable recovery system currently available. It has been man-rated on spacecrafts and has been used for many years as the final landing state for recovery of missiles and drones, and for aerial delivery of personnel and cargo.

Although the standard parachute system is attractive from the standpoint of simplicity, reliability, low weight, and volume, its performance is severely limited. To keep weight within reason, descent velocities on the order of 25 to 30 feet per second must be tolerated. This system is at the mercy of ground winds, and high horizontal velocities equal to the wind speed are to be expected at impact. Pendulum stability of the high drag configurations used for recovery of manned spacecraft is generally poor for single parachutes.

The standard parachute system has no translational or rotational capability to permit landing site vectoring and obstacle avoidance. Because of these drawbacks, it appears that in future spacecraft the standard parachute system will not be considered suitable as a primary system, but will be retained as a backup system capable of automatic operation.

Steerable Parachute Types

In recent years, new parachutes have been developed to give the parachute some maneuverability potential. Among these are glidesail, aerosail, parasail, and cloverleaf parachutes. The glidesail parachute was an early version of the steerable parachute which utilized a split or vented flap. Raising and warping of the flap provided glide and turn capability. Lift-to-drag ratios on the order of 0.7 to 0.8 for single parachutes and 0.9 to 1.0 for a cluster of three parachutes were obtained for this configuration. The Aerosail parachute, which is a modified circular canopy with shaped leading edge and two flaps, was developed in 1962. This configuration exhibited L/D ratios on the order of 1.4. During the same period the Parasail type was developed and has demonstrated L/D ratios on the order of 1.2 and turn rates up to 70 degrees per second. Because of timely development, this particular parachute was selected for possible replacement of Paraglider on Gemini.

The performance of steerable parachutes was substantially improved in 1963 with the development of the Cloverleaf parachute. Wind tunnel and free flight tests of this configuration have demonstrated L/D ratios in excess of 2.0 with good stability and turn-control characteristics.

In this report, only the cloverleaf and parasail parachutes will be analyzed as candidate steerable parachute systems since they represent the latest development in this area. Figures 32 and 33 graphically depict the aerodynamic characteristics of these parachutes in terms of L/D and velocity.

RECOVERY SYSTEM SELECTION

In this section the candidate system designs are compared and evaluated in terms of landing characteristics, crew safety and system reliability, weight and volume, adaptability to the basic logistics spacecraft configuration, and development risk. The combination of these factors provides the yardstick for measuring the suitability of these systems for the logistics spacecraft.

Landing Characteristics

Of the candidate systems, the hot-air balloon concept is the only system that cannot provide a programmed glide-landing capability. On the other hand, this concept is capable of landing on earth at near-zero vertical velocity. This is advantageous from an impact attenuation design standpoint. However, the lack of lateral control during descent makes this system highly susceptible to wind drift and does not always provide the capability of selecting a landing site smooth and free from obstacles. It is generally agreed that the vertical velocity forces generated at impact can be dissipated by a suitable impact attenuation system; however, it is extremely difficult to design a system capable of attenuating the forces that result from uncontrolled spacecraft tumbling. To achieve a high degree of crew safety with a reusable spacecraft, tumbling cannot be allowed under nominal landing conditions. Therefore, the balloon system is considered to be incompatible with the recovery requirements.

The other three candidate system approaches (rotors, steerable parachutes, and Paraglider) all possess the capability of accomplishing a programmed glide landing. The primary disadvantage of a relatively high horizontal velocity and low vertical velocity landing, as is the case for Paraglider, is that the landing surface must be a conventional runway or dry lake bed. This restricts the suitable ground landing areas for this type system. This high horizontal velocity component is also detrimental in case of an emergency water landing because of spacecraft tumbling possibilities and high-g forces generated by suddenly decelerating the spacecraft at water impact.

On the other hand, the rotor system and the steerable parachute concepts, that land with a relatively low horizontal velocity, are highly suitable to the zone landing concept - a cleared area 300 feet square. The one advantage of both the rotor system and paraglider over the

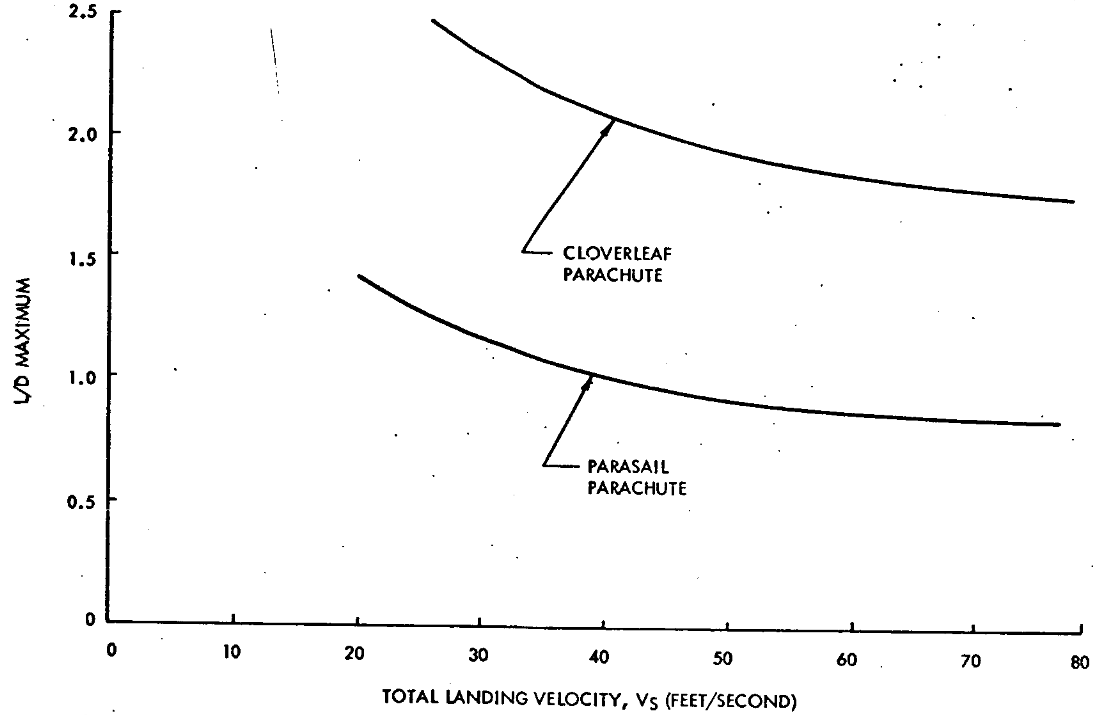

Figure 32. Lift-to-Drag Ratio Versus Landing Velocity for Cloverleaf and Parasail Parachutes

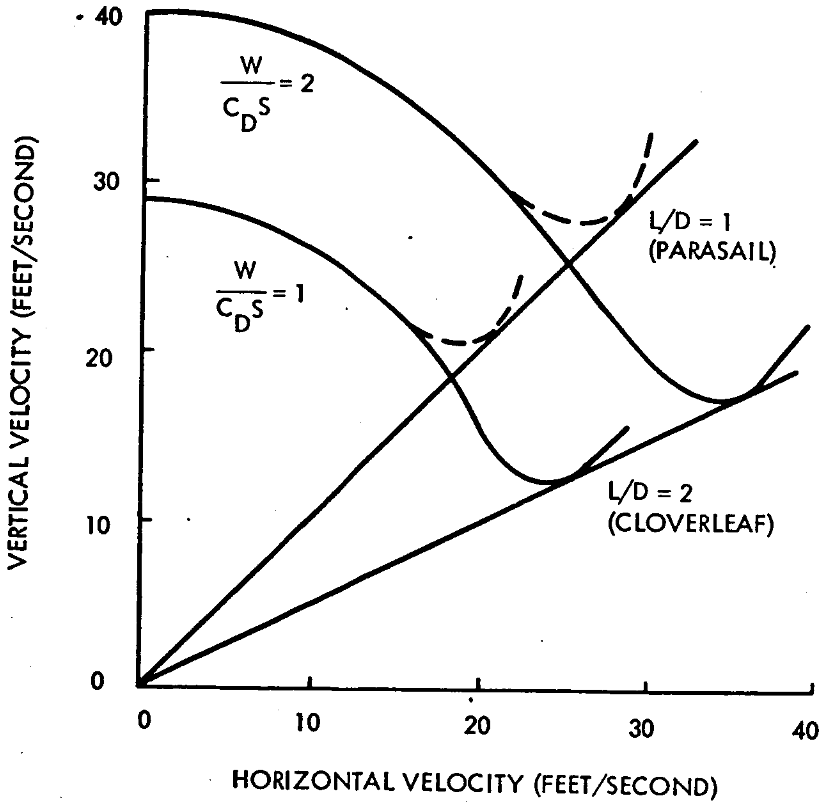

Figure 33. Vertical Velocity Versus Horizontal Velocity for Steerable Parachute

steerable parachute is the greater slant range that can be achieved due to their higher L/D ratios. However, a high L/D ratio capability is not required for the zone landing because many zones are assumed to exist within the landing CEP.

To date system tests performed on steerable parachutes have demonstrated their ability to deploy, inflate, and glide to a preselected landing site and to negate ground winds and obstacles while under remote control. Some of these tests were performed with the controller flying the spacecraft remotely by a vehicle-mounted TV system located as far as 8 miles away.

Crew Safety and System Reliability

Available test data concerning deployment of rotors is insufficient to assess the problems that might be involved. However, existing data does indicate that the spacecraft must be stable to within ± 10 degrees for reliable blade deployment. It is also known that all blades must be simultaneously deployed. The failure of any blade to deploy would cause severe imbalances in the system resulting in catastrophe unless it is immediately jettisoned and a backup system is deployed. Although the reliability of a deployable rotor system is yet to be established, it is reasonable to assume that when successful deployment is achieved, the system will function similar to a helicopter.

Data on Paraglider development tests have shown that major problems exist during deployment and wing inflation. Major structural problems have resulted from the unpredictable transient loads that occur during deployment.

To a certain degree reliability of deployment and inflation of hot-air balloons has been demonstrated. However, clusters of balloons of the size discussed for the logistics spacecraft have never been tested and test data exists only on much smaller balloons. In general, experience with aerodynamic decelerators has shown that many problems of a minor nature on small scale systems are often greatly magnified when the system is scaled up. To date, drop tests have been performed on a 70- and an 80-foot diameter parasail and a 40-foot diameter cloverleaf parachute. Although some development problems have been encountered, the systems have generally demonstrated a high degree of reliability.

Only the balloon, rotor, and parachute system concepts are presently capable of being deployed for a pad abort. All of these systems can inflate in a sufficiently short time to ensure recovery from a boost abort apogee of 5,000 feet. However, it has been calculated that in event of a rotor system malfunction, there is insufficient time for a backup parachute to be sequentially deployed. The Paraglider, as presently designed, is not capable of being deployed, inflated and converted to glide in the altitude range provided by the LES.

Only the balloon system, because of its redundancy provisions, and the steerable parachute with an independent, simultaneously deployed standard parachute backup appear to satisfy the crew safety requirements for pad abort.

System Weight and Volume

Figure 34 shows a plot of total recovery system weight as a percent function of spacecraft recovery weight. As shown, the steerable parachute system is by far the most efficient concept in terms of weight and volume. The system weight shown includes primary recovery system, backup provisions, drogue parachute system, and required attenuation system.

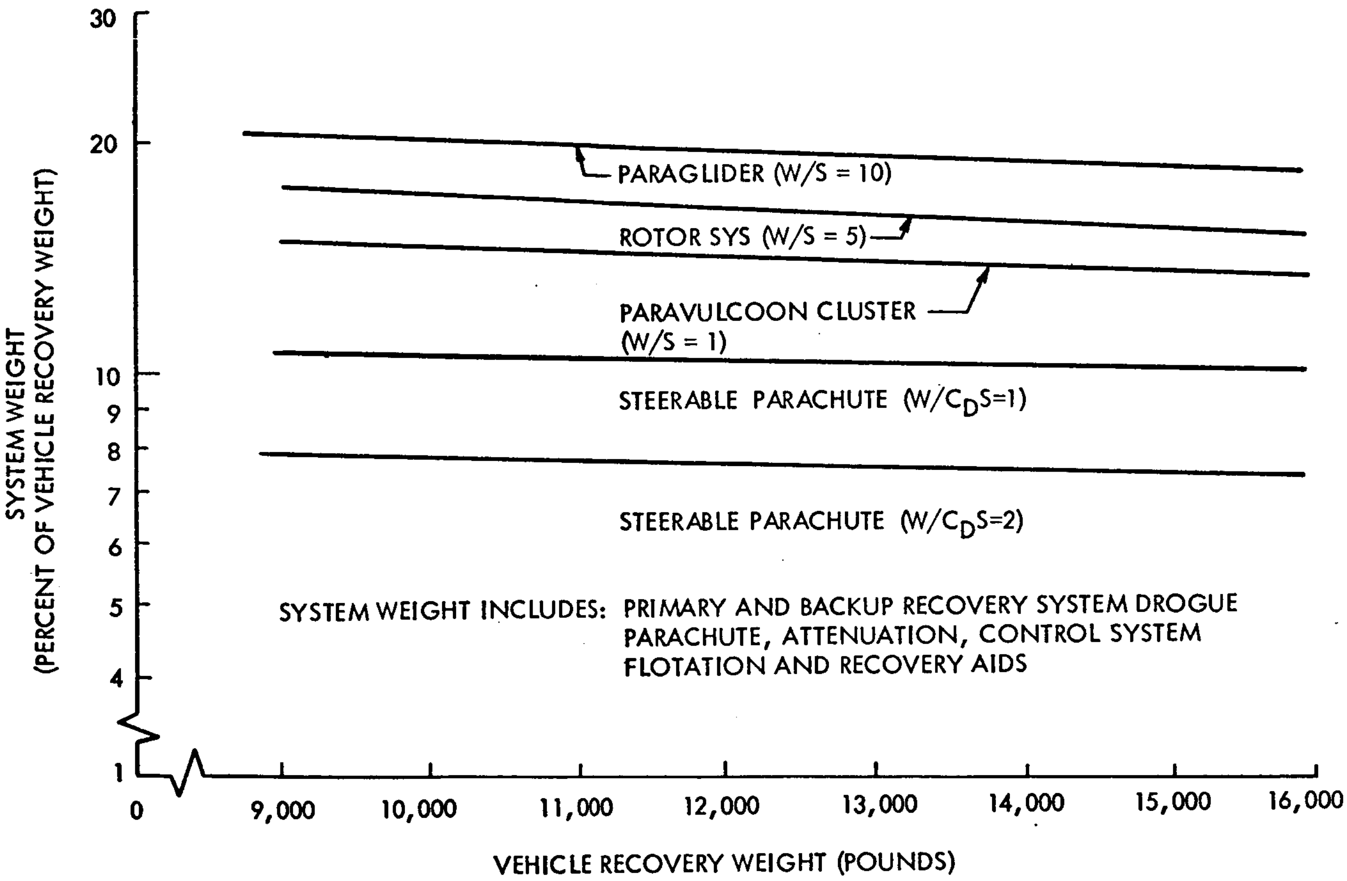

Figure 34. Earth Landing System Weight Comparison

Development Risk

Since the present Apollo vehicle uses a standard parachute for recovery, a direct evolution of this system would be the easiest to adapt to a ballistic-shape vehicle. The main differences between the standard system and the steerable parachute system are the control and vision provisions that must be incorporated. The required control provisions are relatively simple and are presently being refined in steerable parachute test programs. Aerodynamic control is accomplished by flap deflection that requires less power than Paraglider which must displace the vehicle center of gravity with respect to the wind to obtain control.

The deployable rotor system is by far the most complex concept to integrate in a vehicle shaped for low L/D ratio because provisions must be made to extend, inflate, or unfold the blades. To date, none of the helicopter manufacturers have had any degree of success with folding or telescoping blades. Remaining problem areas include designing a hub around the docking collar, providing an antitorque stabilizer, and making provisions for jettisoning the system and deployment of a backup system in event of failure.

The biggest disadvantage of the Paraglider, rotor, and balloon concepts is the lack of data on deployment problems and system reliability. A large gap exists between theoretical analyses of the performance of these systems and their practical application as recovery systems. Therefore, if any of these concepts are used, an extensive drop test qualification program will have to be undertaken to man-rate them.

Selected System

Performance of the candidate systems is compared in Table 6. On the basis of the considerations previously discussed, the steerable parachute concept is recommended as the most promising solution to recovery system requirements of the logistics spacecraft.

The selected system will provide the crew with the capability of selecting a suitable landing site relatively flat and free of obstacles and offsetting ground winds up to landing criteria limits. It is the most efficient system in terms of weight and volume and the most highly developed and tested of the candidate concepts. By providing the required landing control, maximum crew safety will be assured since both water and ground landings can be performed. In addition, the system can satisfactorily operate in a passive mode and can accomplish a vertical landing without crew assistance, which further increases its crew safety advantage. Of the candidate approaches, the selected system will be the least costly in terms of design, test, and vehicle integration because of its relative simplicity and high degree of development. The specific system design and operational characteristics are analyzed in detail in a subsequent section of this report.

CON[redacted]

Table 6. Recovery Concepts Comparison

	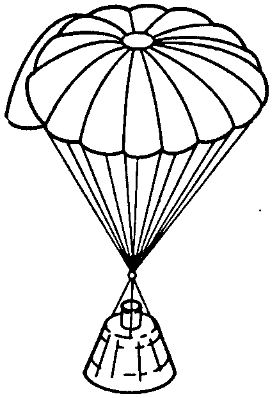 **STEERABLE PARACHUTE** **(L/D=1 TO 2)**	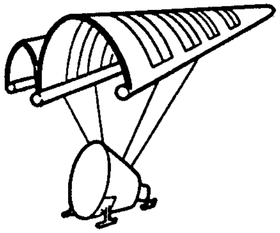 **PARAGLIDER** **(L/D=3)**	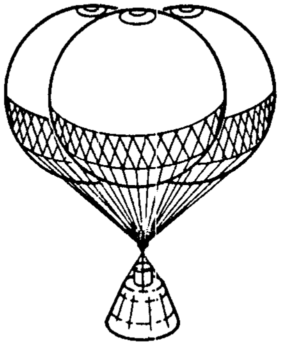 **PARAVULCOON** **(L/D=0)**	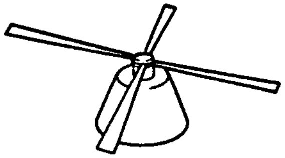 **ROTOR** **(L/D=3)**
Comparison	Steerable Parachute* (L/D - 1 to 2)	Paraglider (L/D = 3)	Paravulcoon (L/D = 0)	Rotor (L/D = 3)
Advantages	Low weight and volume High reliability Within state of the art Unimproved site acceptable	Good glide range Low vertical velocity Partially developed	Redundant System No backup required Zero vertical velocity Partially developed	Zero/zero landing High L/D Mimimum attention required
Disadvantages	Limited range Attenuation required	Improved site required Pad abort marginal Water landing critical High weight and volume	No roll control High horizontal velocity Explosion hazard High weight and volume	Flare critical Rotor deployment problematical Complex Low development status

*This concept was selected

[redacted]

IMPACT ATTENUATION SYSTEMS

Different impact attenuation systems, including honeycomb pads or struts, airbags, and hydraulic or mechanical attenuators were reviewed. Velocity attenuators such as retrorockets, ballistic reels, and canopy pressure devices that complement the actual attenuation devices were also analyzed. From this review basic candidate approaches were selected for further study and their compatibility with the landing requirements were defined in terms of landing stability.

The spacecraft impact attenuation system must be designed to provide a satisfactory landing under normal and emergency conditions within the framework of the landing considerations previously mentioned. The nominal design requirements for the impact attenuation system are not as stringent as Apollo because the L/D ratio of the selected recovery system concept will provide a capability to reduce vertical velocity and will be capable of offsetting ground winds. However, since the possibility of a primary system failure must be considered, design constraints are dictated by landing conditions resulting from the use of the backup system. Under normal recovery conditions, the primary recovery system will provide a capability of offsetting the ground winds to the extent required by vehicle stability limits. However, under emergency recovery conditions, where the standard backup parachute is used, it must be assumed that the vertical velocity will be on the order of 40 feet per second, and that the wind shear velocity will be the maximum nominal condition (34 feet per second) at landing.

The vehicle may be allowed to tumble if the wind or slopes are outside stability envelope limits—if impact acceleration loads on the crew can be kept within emergency limits. An emergency landing may occur on either land or water with ground landings imposing the most stringent design conditions on the attenuation system. Therefore, it is assumed that if attenuation system performance is satisfactory for ground landings, it will be more than adequate for water landings.

Landing conditions for both normal and emergency modes are summarized in Table 7. From the standpoint of impact attenuation, the emergency recovery conditions present the most stringent constraints in terms of crew safety.

ATTENUATOR CONCEPTS

The energy of a falling vehicle may be dissipated in three ways. It can be absorbed by the deformation of material, counteracted by an opposing reactive force, or dissipated by a combination of the two. Crushable honeycomb, struts, and air bags are commonly used impact attenuators; retrorockets are a good example of reactive devices.

The use of absorbing systems by themselves require that a long stroke be provided to achieve the desired load factor. The stroke requirement is

Table 7. Impact Attenuation System Conditions
(No Double Emergencies Assumed)

Landing Consideration	Recovery System Type		
	Primary System		Backup System
	Cloverleaf (L/D = 0 to 2)	Parasail (L/D = 0 to 1)	Ringsail or Solid Parachute (L/D = 0)
Canopy loading	$W/C_DS = 2.0$	$W/C_DS = 2.0$	$W/C_DS = 2.0$
Nominal groundwind	0 - 34 fps	0 - 34 fps	0 - 34 fps
Emergency groundwind	34 - 51 fps	34 - 51 fps	-
Nominal groundslope	5 deg	5 deg	5 deg
Emergency groundslope	-	-	15 deg
Design Conditions Prior To Impact			
Vertical velocity (fps)	$V_v = 32$	$V_v = 32$	$V_v = 40$ fps
Horizontal velocity (fps)	$V_h = 0 - 16$ fps	$V_h = 0 - 26$ fps	$V_h = 34$ fps

further complicated by the stroking efficiency of the device and the combinations of horizontal velocity and slope at landing. The long stroke of these systems is disadvantageous in terms of vehicle stability at landing, since the cg is high off the ground.

Velocity attenuators such as retrorockets, which reduce the energy of the vehicle prior to impact, are lightweight and volumetrically efficient. However, it is nearly impossible to design a system to dissipate all energy at impact because of variables such as ground slope, altitude sensing error, landing attitude, thrust variation, and burning time.

Considerable analytical data exists indicating that the optimum attenuation system in terms of weight, volume, and crew safety is a combination of the two systems; therefore, this type system will primarily be considered.

Velocity Attenuators

Candidate velocity attenuation systems which were considered to combine with energy absorbing systems include:

1. Ballistic reel
2. Ballistic pulley
3. Explosion in canopy
4. Retrorockets

Ballistic Reel

The ballistic reel is a device for accelerating the spacecraft upward toward the parachute canopy just prior to impact. This is done by reeling in the parachute riser lines by utilizing the energy of a gas-generator-powered rotating flywheel. This device was initially proposed for use on the Apollo command module but was not developed further than the preliminary design stage. A detailed study of this concept was performed in the modified Apollo study and it was found that the system weight is high and that the complicated rotating mechanisms make this device unreliable. Also it is impractical to make this device mechanically redundant. However, one advantage is that no upsetting moments are produced during reel-up with this concept.

Ballistic Pulley

The ballistic pulley appears to have merit. The action is the same as the ballistic reel, but instead of reeling in the risers onto a drum, two pulley sheaves are employed. By moving the pulley sheaves apart by a cartridge activated piston cylinder arrangement, the riser is effectively shortened. This device could be integrated into the parachute riser lines by providing one pulley for each riser. One disadvantage of this device is that the mechanism will suffer from the effects of space environment, such as cold welding. Another problem is the limited stroke for acceleration which, in turn, requires greater accuracy from the sensing device. Also it is difficult to design mechanical redundancy into the system.

Pressure Increase in Canopy

The USAF developed and tested a prototype device which consists of a TNT charge or gas generator mounted in the center of each parachute skirt. Just prior to impact, this device was actuated by a very short probe and the high pressure generated by the explosion decelerated the vehicle to zero vertical velocity for about 50 milliseconds. After that time, the vehicle started to accelerate again, but never resumed its initial velocity because of the higher drag of the parachutes resulting from the residual hot air. No parachute damage was recorded during these tests. From the center of gravity standpoint, the force vector on the vehicle is advantageous and no upsetting moment can result. In addition, the potential weight savings of this device over other methods is considerable. However, the installation reliability, maintenance, and development requirements for such a device are not presently defined.

Retrorockets

Retrorockets considered for this application fall into two categories: above the crew module cg (tractor type), and below the crew module center of gravity (pusher type). Primarily, the tractor type advantages lie in alignment of thrust through the crew module center of gravity and the fact that the motor nozzles cannot be blocked by contact with the ground. However, the possibility of rocket exhaust impingement on the riser lines is a problem which must be overcome. In addition, rocket suspension will be complicated by the two riser lines required for the selected gliding parachute design. Deployment problems exist because there are two separate parachutes, the primary and backup. If the primary chute fails during deployment, the redundant or backup parachute is deployed and, at the same time, the risers of the primary parachute must be disconnected from the tractor retrorockets and the backup parachute connected. If both parachutes are simultaneously deployed during pad abort, the problem is further complicated.

The pusher retrorocket concept can be divided into two types: conventional solids and skirt jet. The skirt jet system uses an annular rocket engine attached to the periphery of the vehicle. This rocket attenuates velocity by providing a pressure force on the base of the vehicle as well as momentum thrust at the vehicle edge. The pressure force is a ground effect phenomenon which occurs when the vehicle operates in proximity to the ground. Gas is trapped within the annular curtain between the ground and the vehicle, and it is the compression of this gas which provides a decelerating force.

The skirt jet velocity attenuation system provides a distinct performance advantage over the equivalent conventional retro arrangement and has been analytically and experimentally proved. As a measure of efficiency, it can be shown that about half as much propellant as a conventional retro is needed to accomplish the velocity attenuation maneuver. It can also be shown that the skirt jet vehicle requires only a third as much propellant to hover in close proximity to the ground.

The motor itself consists of a toroidal chamber with a two-dimensional slot nozzle. When using liquid propellant, the chamber is the mixing chamber; for solids, the chamber is packed with propellant. The diameter of the motor, for the vehicles considered, is in excess of 150 inches, leading to a small cross sectional area of solid propellant. Assuming a propellant weight of 60 pounds, the cross sectional area would only be 2 inches.

The major disadvantage of this system is the requirement for the two thrust-to-weight ratios which must be provided to account for the landing variables. This would mean either using liquid propellant where the thrust-time can be changed or using solid propellant with thrust deflection. In both cases, added complexity results. Another disadvantage is that the heat shield must be jettisoned to expose the peripheral motors. It is concluded that the skirt jet velocity attenuator, while providing a significant weight savings over conventional retrorockets, has a significant development risk, particularly when the impulse must be varied. Thus, this device is considered less attractive than a conventional retrorocket system.

From a development risk and reliability standpoint the conventional retrorocket mounted below the crew module center of gravity is advantageous. This system can consist of either a centrally located rocket or a cluster of rockets mounted around the periphery of the heat shield. Ideally, the rocket should have a two-step thrust level. To keep the ignition altitude within reason, a thrust-to-weight ratio of approximately three is required, stepping down to a thrust slightly below vehicle weight a few feet from the ground to prevent rebound after ground contact. The lower thrust value also serves to compensate for variations in vehicle weight, descent velocity, and timing within the limits of the attendant mechanical attenuation system. For simplicity, it is desirable to retain a single rocket burn time for varying rates of descent. Thus, a trade off is necessary between the number of rockets fired, the initiation altitude, and the residual velocity at impact.

A conventional pusher retrorocket landing gear system has been successfully tested for Gemini in conjunction with the parasail parachute. This rocket system consists of two retrorockets with an initial thrust-to-weight ratio of 3 which is reduced to 0.9 just before touchdown. Probably the best known example of retrorocket-parachute application is the NAA Redhead/Roadrunner final landing system which has been highly successful.

Operational Tolerances

Residual vertical velocities can be expected when using a velocity attenuator. This velocity is a result of various combinations of conditions which exist at the start of the landing sequence. Errors in the altitude at which velocity attenuation begins, air density, variations in vehicle weight, variations in velocity attenuator performance, and drift over ground slopes are examples of conditions that dictate the value of residual velocity.

Previous studies have shown that the velocity will be on the order of 12 to 16 feet per second for the worst combination. Even at this low velocity, the vehicle must be provided with impact attenuation to achieve the required deceleration limit.

Energy Absorbing Systems

The energy attenuation techniques reviewed include air bags, fixed honeycomb, foam-filled bags, and shock struts. The location of the energy absorbing medium is an important consideration. The method selected must be suitable for integration into the structural concept and, equally important, it must resist tumbling. The heat shield provides an excellent skidding surface with a fairly low coefficient of friction between the ablative material and the ground. It is the ability to skid which decreases the tendency to tumble.

Air Bags

Air bags have been extensively used by the armed forces as impact attenuation for aerial delivery of cargo. The bags are nonporous bladders generally fitted with a blowout plug which bursts at a preselected pressure. Air bags could be used if stored between the heat shield and the internal structure of a vehicle which lands with heat shield down. However, they have low stroke efficiency and are not capable of resisting shear forces. Weight of the air bag system is high compared with other energy absorbers, particularly if the air is stored on board.

A modification of this principle is possible with recent developments in polyurathane foams and aerosol foaming equipment which achieve 50 percent of their strength within 4 minutes. The efficiency of foam-filled bags will be greater than air-filled bags; however, foam cannot be used for an impact system with the existing pad abort requirements until curing times of the foams are reduced to less than 1 minute.

Fixed Honeycomb

There is considerable data to indicate that among the absorbers, balsa wood ranks as the most efficient, followed closely by metal honeycomb. Honeycomb provides the highest inherent reliability and the lightest weight of those crushable materials that can be used for spacecraft. Aluminum alloy appears to be the best choice and is most efficient when subjected to a stress of 65 psi or greater.

Shock Struts

Shock struts constitute the most widely known methods of absorbing energy in the aircraft industry. The characteristics of hydraulic or pneumatic struts are well known and consistently reproducible. Other energy absorbing materials are possible, including crushables, frangible, and friction devices. Shock struts can be used between the heat shield and the inner structure or extended to act as landing gear. The major disadvantages of struts are their relatively high concentrated loads at the attachment points and the unpredictable behavior of certain elements, such as seals, to prolonged space exposure.

Landing Attitudes

Two basic landing attitudes are immediately apparent. One is landing heat shield down; the other consists of landing in a manner proposed for Gemini, with a Paraglider where the longitudinal axis of the vehicle is parallel to the ground at touchdown. This configuration uses a three-legged landing gear and rocket motors mounted on the bottom as shown in Figure 35.

A family of concepts are applicable to the heat-shield-down landing attitude. This configuration lends itself to providing either a centrally mounted base retro, radially mounted multiple retros, or a suspended retro for velocity attenuation. These various retro concepts can be used in conjunction with either the extended or nonextended heat shield concepts.

In the extended heat shield concept, attenuation is provided by extendable honeycomb blocks. Figure 36 shows an extendable heat shield configuration that uses periphery mounted retros and honeycomb blocks.

In the nonextendable heat shield concept, the honeycomb pads are sandwiched between the crew compartment floor outer mold line and the heat shield inner mold line.

Landing Dynamic Analysis

The landing stability limits of the two candidate landing attitudes were analyzed by computer runs. A review of empirical data obtained from early Apollo drop tests and scale models of the extended heat shield configuration was also performed to verify the validity of computer results. Figure 37 shows the tentative stability envelope for the three-legged configuration; Figure 38 shows the approximate stability envelope of the vehicle landing on its base.

The three-legged configuration is stable in the forward direction but highly susceptible to side forces caused by lateral winds or side slopes. This configuration does not appear suitable for landing with the backup parachute system, since horizontal velocity is not controllable and the landing direction cannot be predicted. It is also doubtful if a suitable landing could be accomplished even with the primary system, since at least 5 degree slopes and wind gusts in excess of the stability limits shown are to be expected.

The heat-shield-down attitude stability profile shown in Figure 38 indicates that the vehicle will remain stable within ±20 feet per second in any direction for the nominal slopes considered. These stability limits are compatible with the performance capability of the primary parachute system that permits offsetting the ground winds.

Attenuation System Selection

Figure 39 presents a summary comparison of candidate attenuation system configurations considered. Configuration 1 is quite advantageous in that it affords the pilot direct vision during the recovery phase and allows for a natural flying position. In addition, the retro installation presents a minimum number of problems. However, because of its poor landing stability characteristics, this concept is considered to be unacceptable.

Configuration 2 (Figure 39) provides a very efficient retrorocket system because of the ground effect; however, the mechanical complexities of the landing gear, and the inherent difficulty of providing a step thrust function makes this concept unattractive. Another major disadvantage is the fact that the heat shield must be jettisoned. In event of premature actuation prior to reentry, this would be catastrophic.

The suspended retro concept in Configurations 3A and 4A (Figure 39), is highly attractive from the standpoint of thrust alignment standpoint and thrust cutoff stability at impact. From a reentry heating standpoint, its stowed location is also advantageous, and maintenance and installation requirements are minimum. To prevent rocket impingement upon the vehicle, the nozzles must be canted, thus, resulting in loss of thrust efficiency. Its major problem involves the danger of collision at deployment; however, this can probably be overcome by good design practice.

The base mounted retros, Configurations 3B and 4B (Figure 39), provide high efficiency and are advantageous from a mechanical complexity standpoint. Their major disadvantage is the difficulty providing thrust cutoff capability.

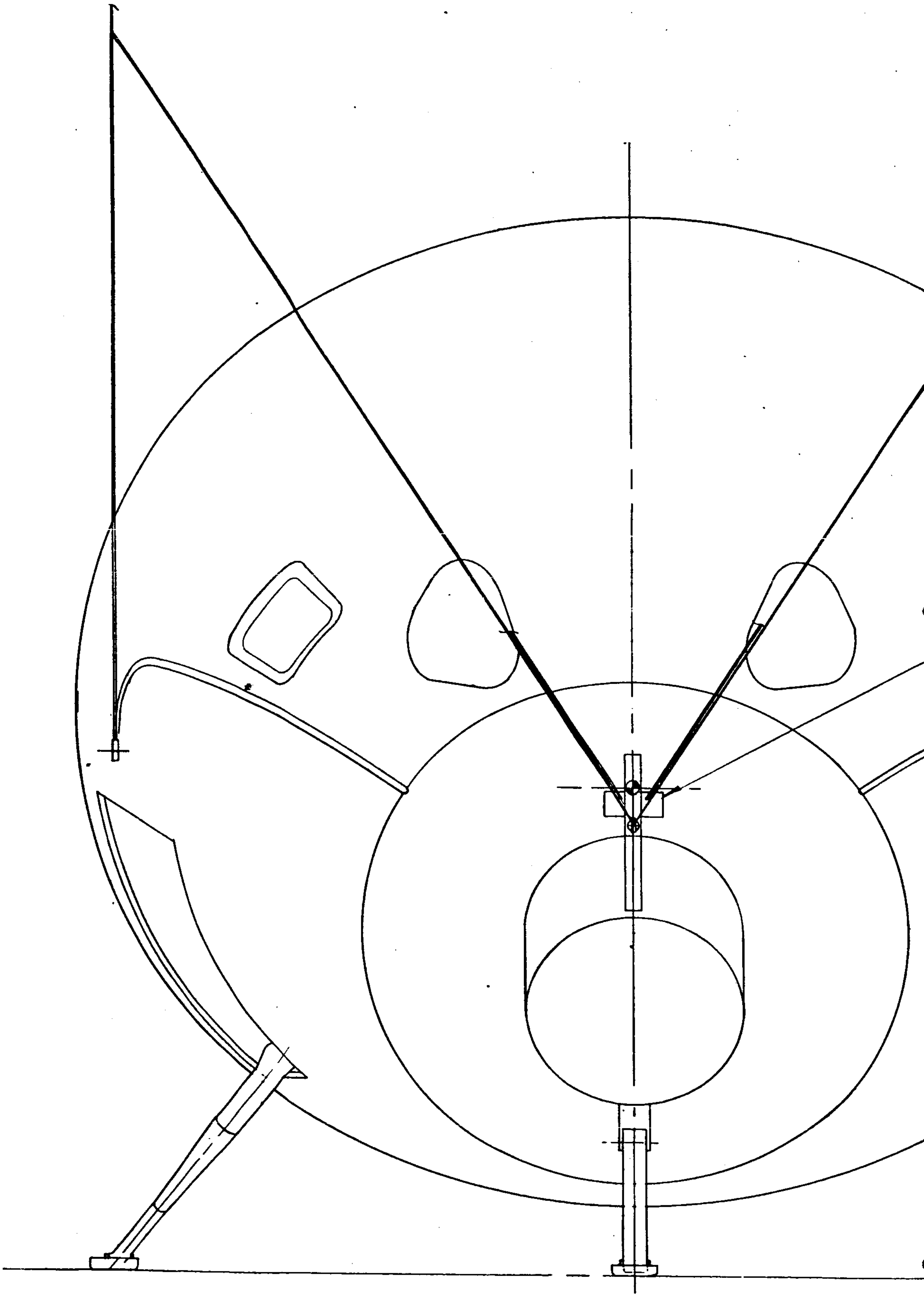

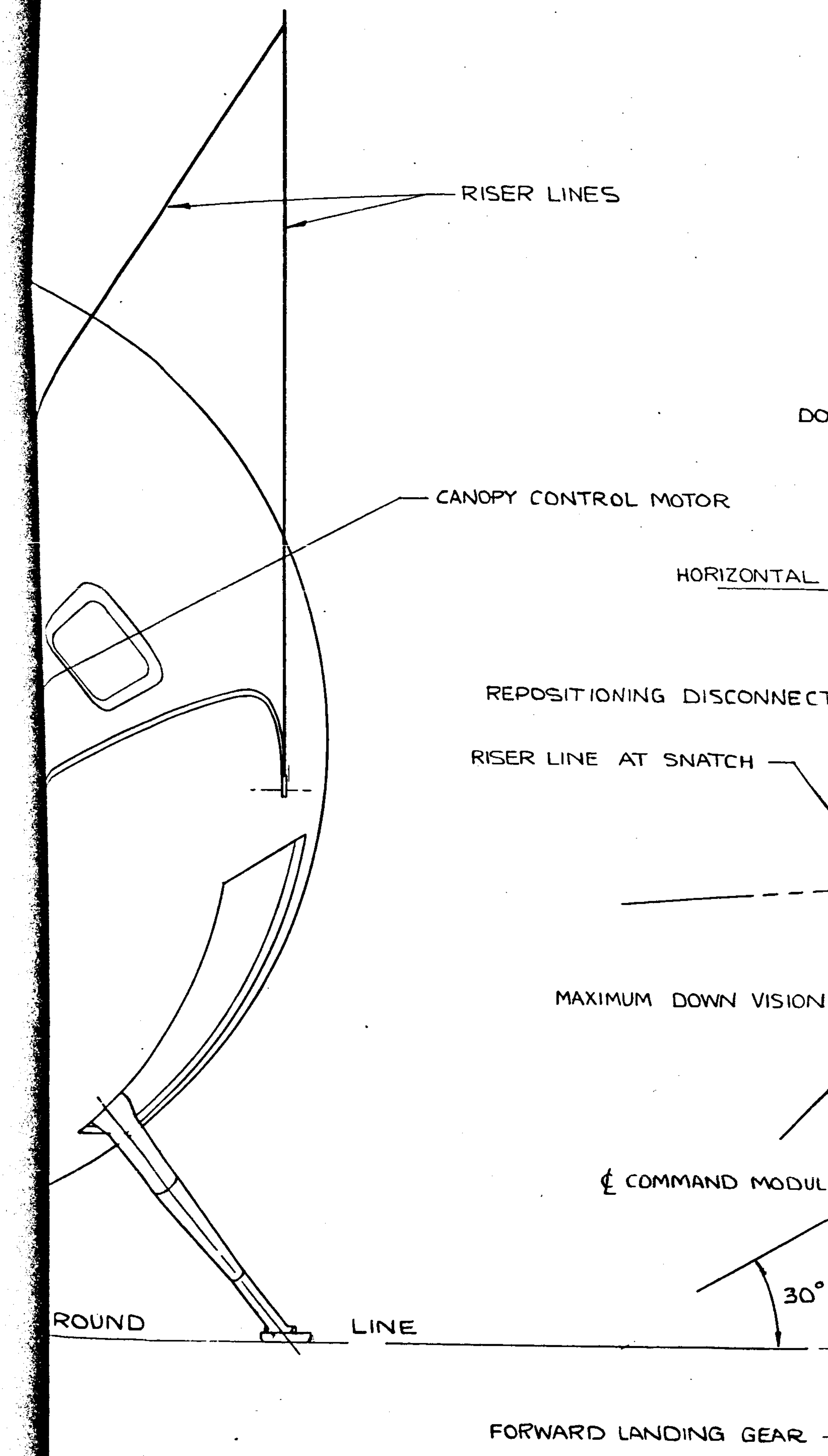
RISER LINES
DO
CANOPY CONTROL MOTOR
HORIZONTAL
REPOSITIONING DISCONNEC
RISER LINE AT SNATCH
MAXIMUM DOWN VISION
℄ COMMAND MODUL
30°
ROUND
LINE
FORWARD LANDING GEAR

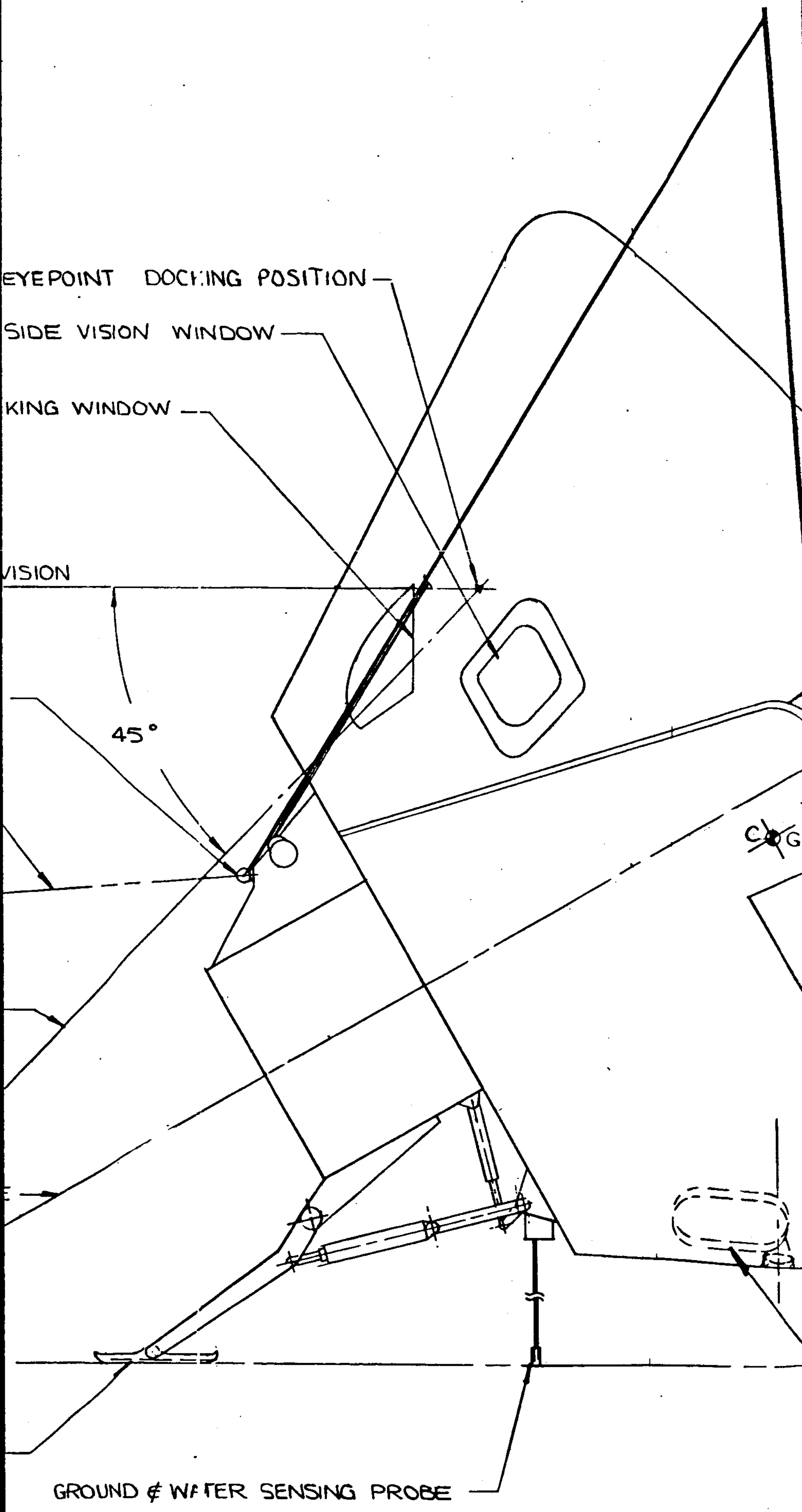
EYEPOINT DOCKING POSITION
SIDE VISION WINDOW
KING WINDOW
VISION
45°
C G
GROUND & WATER SENSING PROBE

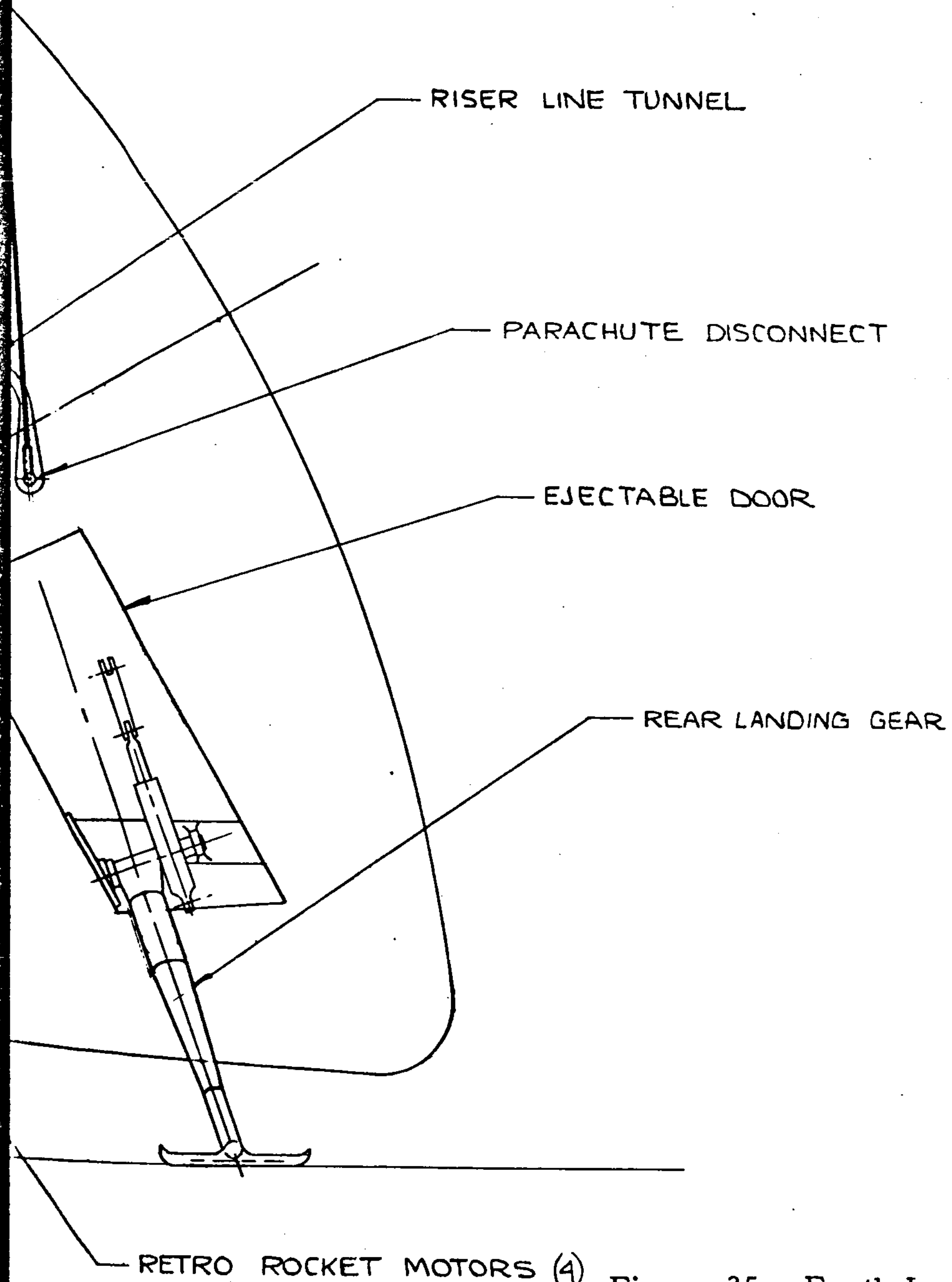
RISER LINE TUNNEL
PARACHUTE DISCONNECT
EJECTABLE DOOR
REAR LANDING GEAR
RETRO ROCKET MOTORS (4)

Figure 35. Earth Lan

5198-20

ing System Configuration - Three-Legged Gear and
Retrorockets

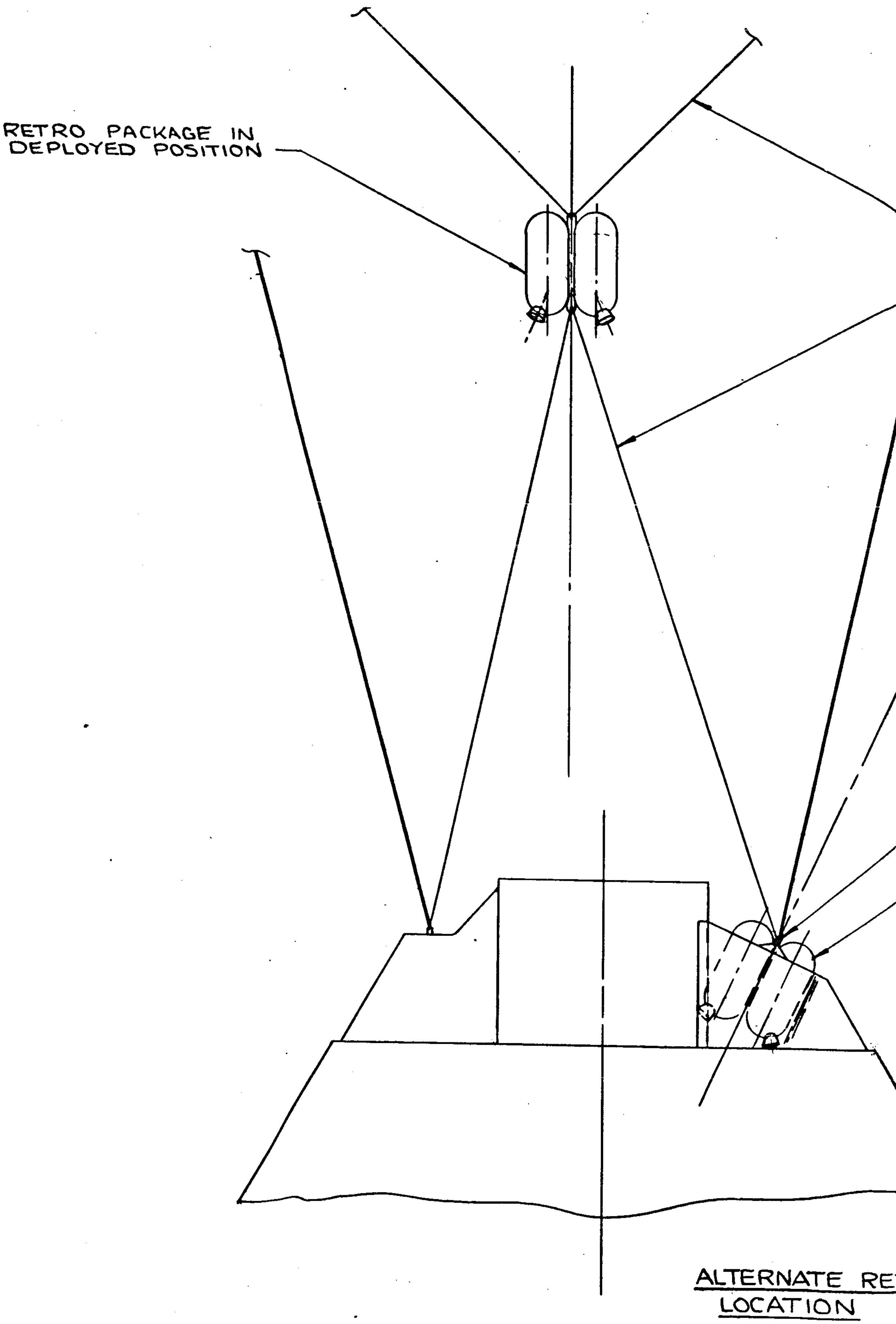
RETRO PACKAGE IN DEPLOYED POSITION
ALTERNATE RE
LOCATION

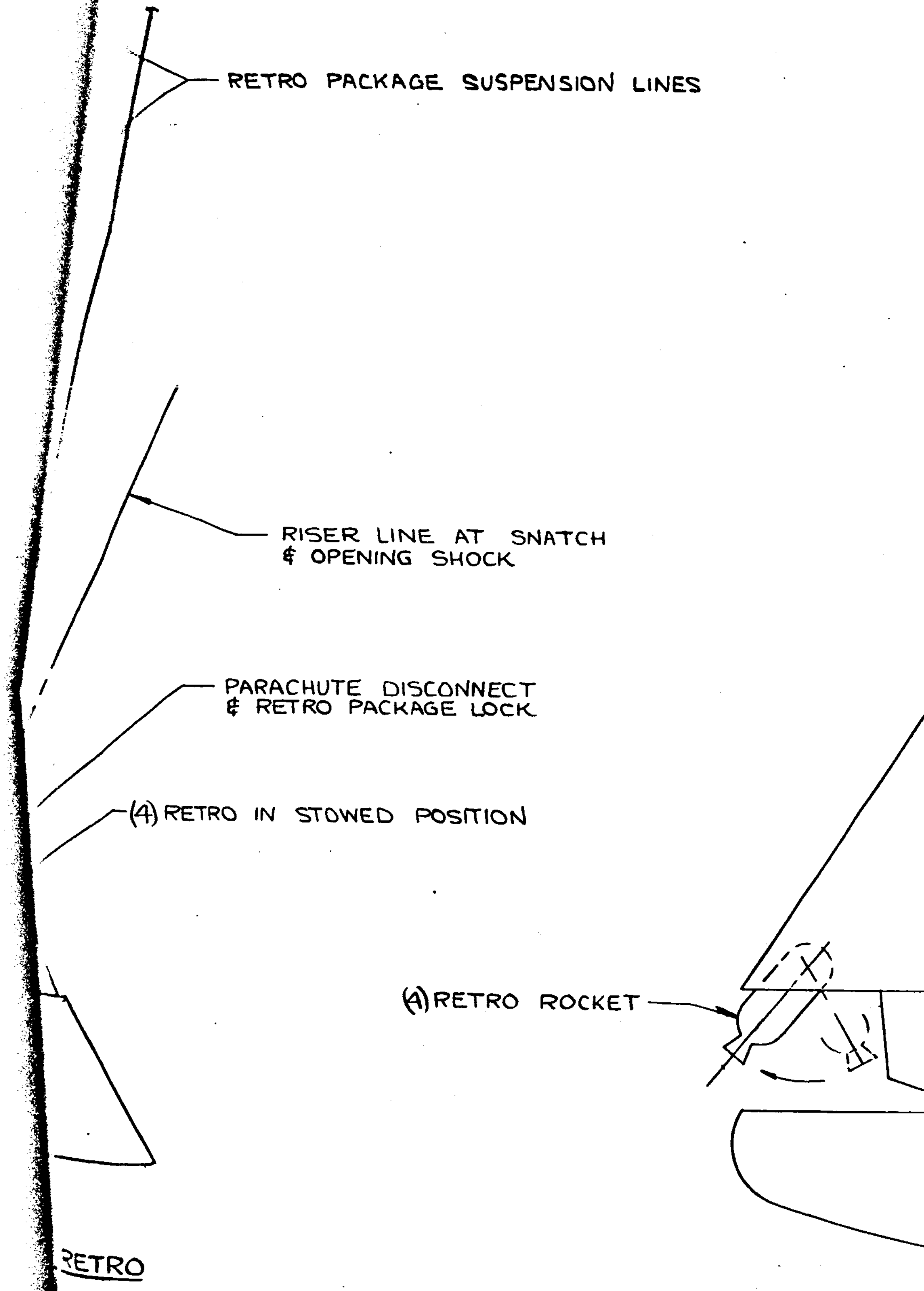
RETRO PACKAGE SUSPENSION LINES
RISER LINE AT SNATCH & OPENING SHOCK
PARACHUTE DISCONNECT & RETRO PACKAGE LOCK
(4) RETRO IN STOWED POSITION
(4) RETRO ROCKET
RETRO

RO PACKA
OTED PO

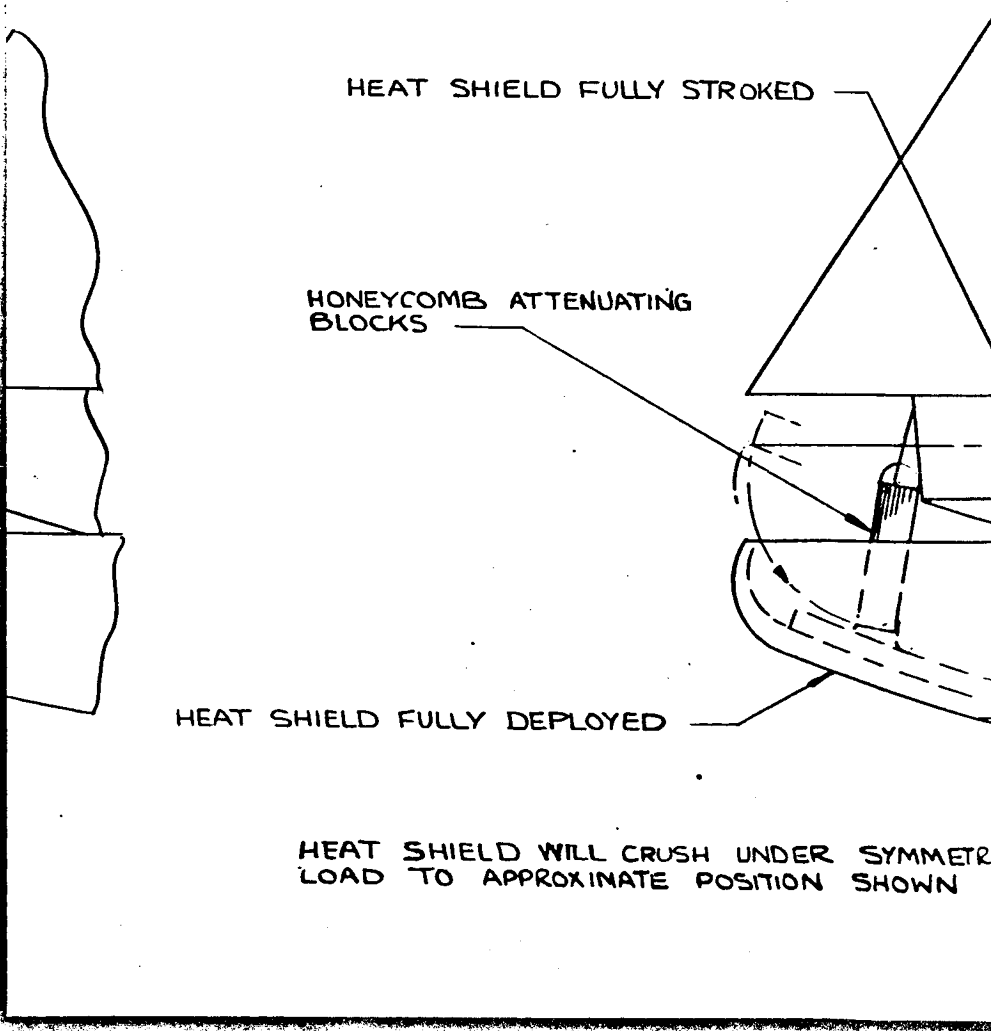
HEAT SHIELD FULLY STROKED
HONEYCOMB ATTENUATING BLOCKS
HEAT SHIELD FULLY DEPLOYED

HEAT SHIELD WILL CRUSH UNDER SYMMETR
LOAD TO APPROXINATE POSITION SHOWN

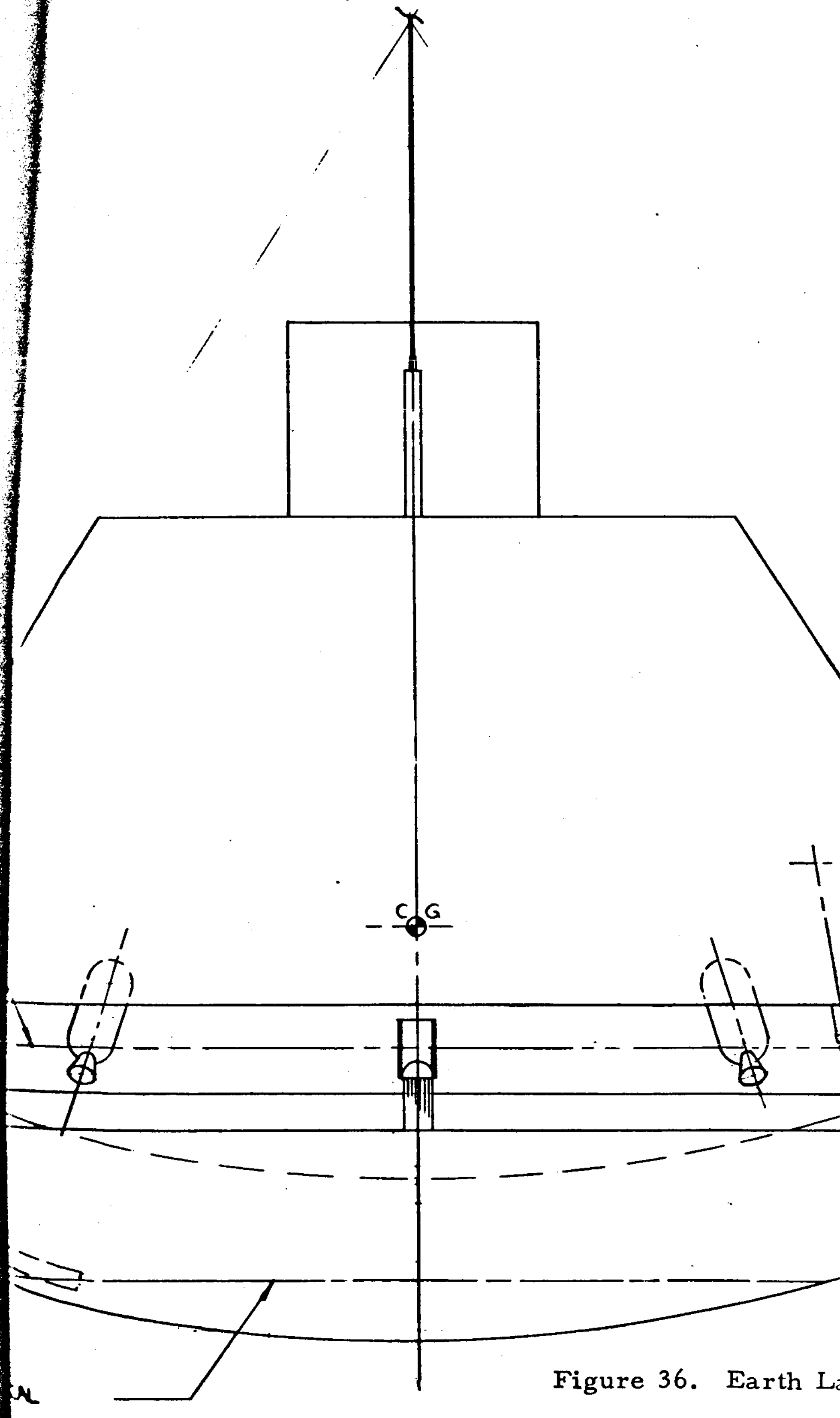

Figure 36. Earth La

5198-21

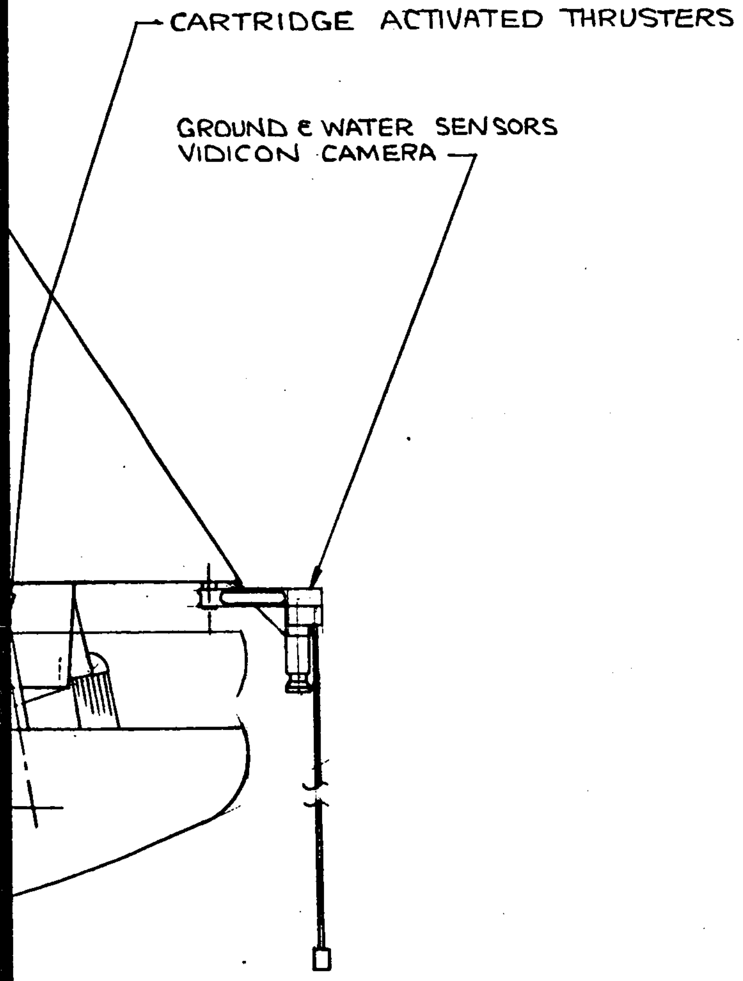
CARTRIDGE ACTIVATED THRUSTERS
GROUND & WATER SENSORS
VIDICON CAMERA

nding System Configuration - Extended Heat Shield and Retrorockets

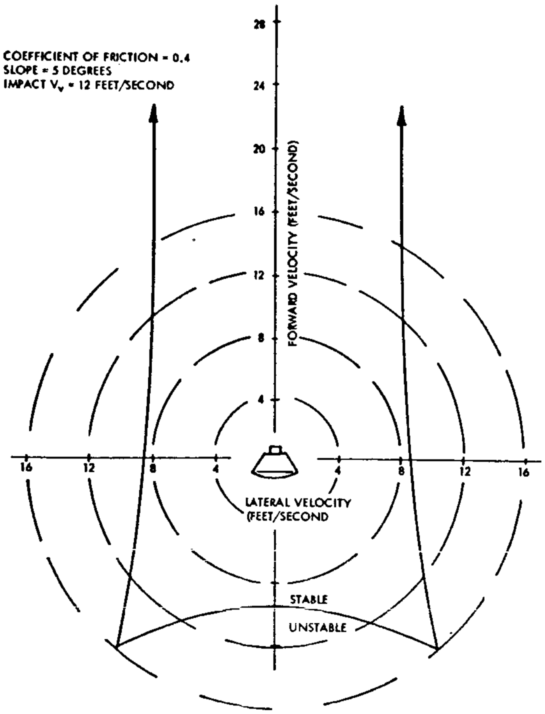

Figure 37. Landing Stability Envelope of Three-Legged Landing Configuration

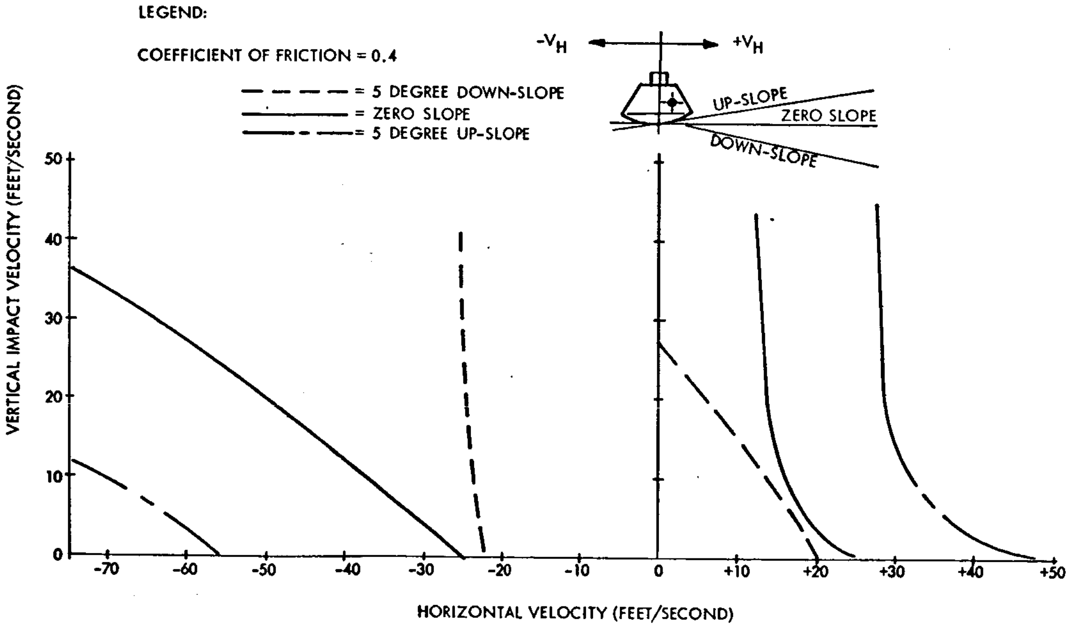

Figure 38. Landing Stability Envelope for Heat Shield Down Configuration

CONF[redacted]

BASIC LANDING ATTITUDES	IMPACT ATTENUATION CONCEPTS	RETRO ROCKET CANDIDATE CONCEPTS	ADVANTAGES	DISADVANTAGES
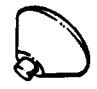	CONFIG NO. 1 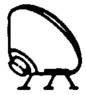 THREE LEGGED LANDING GEAR	A) 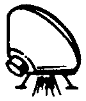 BASE RETROS	DIRECT LAND. VISION NAT. FLYING POSITION SIMPLE RETRO INSTAL	POOR LAND. STABILITY COMPLEX LAND. GEAR HIGH STRUCT LOADS
		B) 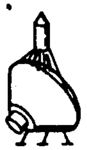 RISER SUSP RETRO	SELF ALIGN. RETRO GOOD DIRECT VISION SIMPLE THRUST CUTOFF	COMPLEX RETRO EXTRACT. IMPINGMENT PROBLEM
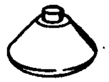	CONFIG NO. 2 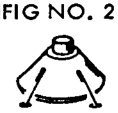 FOUR LANDING LEGS	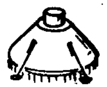 PERIPHERAL SKIRT JET RETRO	HIGH EFFICIENCY ROCKET LOW RETRO WEIGHT GOOD STABILITY	HEAVY LANDING GEAR JETTISONED HEAT SHIELD TWO STEP THRUST DIFFICULT
	CONFIG NO. 3 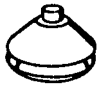 EXTENDED REAR HEAT SHIELD	A) 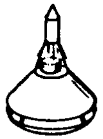 RISER SUSP RETRO	RETRO THRUST THRU C.G. SIMPLE THRUST CUTOFF LOW ATTN SYS WT GOOD REENTRY C.G.	ROCKET DEPL. PROBLEMS THRUST EFFICIENCY LOSS ACTIVE ATTENUATION
		B) 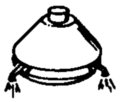 PIVOTED MULTI RETROS	EASY STOWAGE & DEPL SIMPLE DESIGN LOW ATTN LOADS	RETRO BLOCKAGE AT IMPACT C.G. ALIGNMENT PROB. UPSETTING MOMENT CAUSED BY SINGLE FAILURE
	CONFIG NO. 4 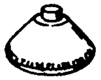 FIXED HEAT SHIELD (INTERNAL ATTENUATION)	A) RISER SUSP RETRO SAME AS ABOVE	PASSIVE ATTENUATION	
		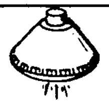 CENTRAL BASE RETRO	GOOD RETRO STOWAGE PASSIVE ATTENUATION DEPL. OF SENSORS NOT REQD	HIGH STRUCT PENALTY POOR REENTRY C.G. LOC. THRUST CUTOFF DIFFICULT

Figure 39. Summary Comparison of Candidate Attenuation Concepts

~~CONFIDENTIAL~~

The extended heat shield concept results in a mechanically simple lightweight attenuation system. Its major disadvantage is the susceptibility of space storage and lower reliability.

The fixed heat shield attenuation concept, Configuration 4 (Figure 39), is completely passive and highly desirable from a standpoint of reliability and orbital storage. Its main disadvantage is a reduction in vehicle aerodynamic and stability because of the higher center of gravity location and the additional structure and heat shielding that must be added for the attenuation stroke.

It is concluded that Configuration 4A—the fixed heat shield concept—embodies several outstanding advantages. Impact attenuation is passive, thus, resulting in high reliability and overall system design simplicity. However, results of a weight analysis show that the increased base diameter and added conical heat shield necessary for the attenuation stroke adds about 360 pounds to the spacecraft in addition to the basic attenuation system.

Another disadvantage of the fixed heat shield concept is that even though the stroke has been minimized as much as possible, a minimum of 10 inches of stroke must be provided to prevent the buckling heat shield from puncturing the inner shell. Adding this additional stroke of 10 inches results in a net cg shift of 8 inches in the +X direction. The effect of the cg shift on reentry stability was analyzed with respect to the two-point stability problem. Results from the computer run conclusively indicate that this cg shift prevents elimination of the two-point stability problem. Therefore, the fixed heat shield is rejected in favor of the extendable heat shield concept because of weight and cg considerations.

From the standpoint of impact stability, it is highly desirable that the retro thrust be cut off at the moment of impact to prevent rebounding and to minimize crew module toppling tendencies. From a thrust termination standpoint, the most suitable retro concept is the suspended retrorocket. This concept also provides self-alignment with respect to cg, and is more readily serviceable. This concept has previously been successfully used in recovery of the NAA Redhead/Roadrunner drone and it is selected as the most promising retro configuration for the logistics spacecraft.

From a standpoint of system simplicity and weight the best configuration consists of a multi-nozzle, single retro motor similar to the launch escape motor in design features and initiation provisions. The retro motor is suspended sufficiently high and the canted nozzles are designed to prevent impingement of thrust upon the structure. Therefore Configuration 3A, the extended heat shield/suspended retro concept, is selected as the most promising configuration.

It is apparent from the analysis of retrorocket velocity attenuators that the method of sensing ignition altitude plays an important part in the final impact velocity. Choice of an electronic primary rate-of-descent sensor with a mechanical backup probe offers the most reliable system since each component relies on a different working principle, and the malfunction of one is not likely to affect the function of the other. The selected extendable probe is a variation of the DeHavilland Stem, with a water and ground impact switch at its end. This device had been developed for the Gemini and parasail landing system. The unit can be either mechanically or electrically powered, but mechanical actuation is preferred because it does not rely on another spacecraft system. The rate-of-descent sensor required is an all-electronic system that measures velocity and altitude with reference to the earth's surface. These units are available off the shelf for aircraft and helicopter use, and with modifications, can be adapted to meet spacecraft recovery requirements. Since both the probe and electronic equipment are armed during descent, it is important that the probe not interfere with the more sensitive electronic unit. Because of redundancy requirements, and to provide a backup system of high reliability and low complexity, a fixed length probe with a single time delay element is selected. Under low vertical velocity conditions, ground contact of this 13-foot probe will initiate a timer which will activate the retro 8 feet above ground. For the high velocity case (40 feet-per-second), the timer is bypassed and retro initiation occurs at probe-ground contact. This concept, although not optimal for all cases, is an excellent compromise which will permit a safe landing under all conditions short of triple emergencies.

GUIDANCE AND NAVIGATION SYSTEMS

GUIDANCE AND NAVIGATION SYSTEMS

The primary function of the Guidance and Navigation (G&N) system is to generate commands to guide the spacecraft during thrusting and reentry maneuvers. The G&N system can also be used to provide a precise attitude reference and to control the attitude of the spacecraft. During booster thrusting phases, the G&N system is used in a guidance monitor and backup mode. The G&N system can be used as the prime source or as backup to ground tracking networks for navigation data.

The purpose of this section is to present data on several typical G&N systems as applied to extended duration earth orbit missions. This data consists of system descriptions, parametric reliability data and key performance parameters.

Parametric data is presented for the Apollo Block II G&N system, the N35-S G&N system and a strapdown system configuration. The reliability data is presented parametrically as a function of the type of orbit for the transit phases and as a function of the daily system use time and the mission duration for the orbital phases. The reliability data can be used to determine the level of sparing which is required for specific missions. In the performance sections, emphasis has been placed on presenting the key performance parameters since the performance of an error analysis is dependent on a specific maneuver and is not parametric in nature. Data is also presented on the attitude reference capabilities of the systems.

Much of the material presented in this section is based on data supplied by AC Spark Plug on the Apollo G&N and a strapdown configuration; by Raytheon on the Apollo computer and by Autonetics on the N35-S G&N system.

DESIGN FACTORS

The suitability of a guidance and navigation system for a specific mission is strongly influenced by such mission peculiar requirements as the system operating time, accuracy for maneuvers and vehicle control requirements. To determine the requirements which are imposed by the mission, it is necessary to first derive a detailed mission profile. To reflect this mission dependence the mission can be divided into transit (boost and reentry) and orbital phases.

System operating time and requirements for boost and reentry are virtually constant and independent of orbital operations. The most significant factor is whether it is a polar, low inclination, or synchronous earth orbit. The major variable during transit is the duration of the parking orbit. The transit phase also differs from the orbital phase in that time is more critical. Since the crew is constrained in their couches except during part of the parking orbit, the detection and replacement of malfunctioned equipment can only be achieved automatically. Due to the difficulty in sparing, the transit reliability acts effectively like a bias in determining system reliability. Also, the environment during transit phases is more severe than for orbital operations due to the presence of thrust or atmospheric forces.

Based on the mission profile, requirements which must be met during orbital phase can then be defined. The vehicle will be required to perform orbital maneuvers if it is necessary to change orbits during the mission, to accurately maintain the present orbit to support an experiment, or to periodically increase orbital altitude to counter the effects of atmospheric decay. The primary orbital requirement is to stabilize the spacecraft either inertially or in a rotating coordinate frame for experiments. The mission profile is used to define the required stabilization accuracy, time duration, frequency, and reference. Also, it may be necessary to establish the line of sight to aid visual tracking of space or earth targets or to direct sensors.

Due to the overlap of functional capabilities between the G&N and SCS, it is possible to trade-off some experiments between the two systems. Due to the greater reliability problem associated with the G&N system, it is desirable to minimize G&N system use time by assigning less stringent experiments to the SCS.

In addition to the time directly associated with the experiments, the G&N system will be operated for certain necessary tasks. These include:

(1) IMU Alignment: A nominal time of 15 minutes is required for warmup and initial alignment of the platform. Realignment of the inertial platform would require 5 minutes. Realignment would be required after one orbit of continuous use or more often if greater accuracy is required.

(2) Optical Measurements: For earth orbit navigation, optical measurements can be made by landmark tracking, star-horizon measurements, or star refraction measurements. The time available for landmark tracking is approximately 5 minutes in low earth orbit. This is equivalent to the time that the landmark is visible (i.e., nearly horizon to horizon passage).

For orbital operations, system operating time can vary greatly between missions. However, time will in general be available for maintenance so that manual detection and replacement of malfunctioned units can be performed. With the provision of adequate spares, system reliability for orbital operations may be kept near unity.

In addition to the mission imposed requirements on system operating time and functional capabilities, long term storage requirements and the possible large number of on-off cycles will also effect system suitability. The main problem associated with long term storage is the possibility of physical or chemical change in a part which will effect system reliability or performance. This factor can be minimized by subjecting most parts to a screen and burn-in test program to induce failure in inferior parts prior to component assembly. For missions as long as 600 days, it is not feasible to subject the actual hardware to real time simulation of the mission to evaluate the effects of storage or cycling. Degradation during storage is sometimes estimated by using a percentage of the equipment operating failure rate as the failure rate during non-operation. Since this degradation factor is based on experience with comparable equipment for storage on the ground, it is not possible to correlate this data with the effects of storage in space under zero g and different environmental conditions (radiation, pressure, temperature, etc.). Since this degradation factor is small and is partially nullified when system spares are provided, in the following discussion it is assumed that there is no degradation of non-operating equipment. The effects of cyclic system operation can be minimized by proper design of relays and switches and by taking into account the effect of transients on other system components. The required number of on-off cycles can be minimized by designing the mission so that several experiments can be run simultaneously or by grouping shorter experiments so that they can be run sequentially wherever possible.

Moisture sealing requirements will also have an effect on system sparing or redundancy provisions. Some hardware redesign may be required to provide an in-flight maintenance capability under moisture sealing conditions. This is especially true in the case of the Apollo G&N system which is moisture sealed and contains no provisions for in-flight maintenance. Although sparing is more efficient at the module level, it may not be feasible due to restrictions imposed by moisture sealing and by malfunction isolation time. Data in the following sections is based primarily on box-level sparing but the use of module-level sparing is also considered for components like the Apollo computer where the gain unreliability is significant.

Severity factors are generally used in finalized reliability analyses to reflect the effect of environment on reliability. Since severity factors are dependent on vibration and shock levels which are both mission and vehicle dependent, they are not included in the following analysis although it is recognized that transit reliability may be effected when more definitive mission and vehicle data is available.

APOLLO BLOCK II G&N SYSTEM

The Apollo Block II G&N System is capable of independently performing guidance and navigation. In conjunction with the Reaction Control System, the G&N System is capable of controlling spacecraft attitude. In conjunction with the Service Propulsion System, the G&N System provides control of spacecraft thrusting.

The Apollo Block II G&N System is divided into three major subsystems: inertial, computer, and optical. The inertial subsystem consists of an inertial measurement unit (IMU), three electronic coupling units (ECU), portions of the power and servo assembly (PSA), the navigation base and portions of the display and control panels. The IMU is a three gimbal inertial platform which contains three 25 IRIG Mod 2 stabilization gyros and three 16 PIPA accelerometers. The ECU's are electronic analog-to-digital and digital-to-analog converters. The inertial ECU's are used to transfer gimbal angular data between the IMU and the digital computer. The PSA contains the power supplies and electronics for the inertial and optical subsystems.

The computer subsystem consists of the Apollo Guidance Computer (AGC) and two display and keyboards (DSKY). The AGC is a parallel, single address, stored program, general purpose computer. The computer contains 36,864 words in fixed (core rope) memory and 2,024 words of erasable (scratch pad) memory. A word contains 16 bits including sign and parity. There are 36 instructions. The DSKY's are used by the astronaut to enter data into the AGC and to initiate various program functions. Also, the DSKY's display the program routine which is being executed and specific stored data.

The major elements of the optics subsystem are the optics head, two ECU's, and portions of the display and control panels. The optics head contains the sextant, telescope and optical base. The telescope is a single line-of-sight, 1-power, 60 degree field of view instrument. The telescope is used for the measurement of angles to earth landmarks for orbital navigation and as an aid to the sextant for coarse acquisition of stars. The sextant is a dual line-of-sight, 28-power, 2 degree field of view instrument. The sextant is used for making sightings of two stars for IMU alignment. A horizon photometer and automatic star tracker, which are incorporated in the sextant head, are used to provide an alternate method for earth orbit navigation based on the angle between the horizon blue line and a star. The optics ECU's are used to transmit the shaft and trunnion angles for the optics. These units are time shared and are also used to transmit the commanded Service Propulsion engine gimbal angles.

The Apollo Block II G&N system does not have an active terminal rendezvous sensor. Therefore, for missions which require rendezvous, an interface between the G&N system and the rendezvous radar, which would be added to the Communications System, would be required. Based on previous studies which assumed the use of the LEM radar, an additional 14 pounds would be required for an electrical interface for range, range rate and analog angle data. The two optics ECU's would be used to transmit the commanded radar angles and for receiving the radar gimbal angles. The mechanization of the rendezvous maneuver would be done in the AGC with the DSKY's used to provide rendezvous displays for the astronauts.

RELIABILITY ANALYSES

During the Apollo X study, several modifications to the Apollo Block II G&N system were recommended to improve its reliability for extended missions. These modifications include: (1) energizing the inertial components' suspension only when the inertial subsystem is in operation, (2) adding a redundant heater power slip ring, and (3) deleting the AGC standby mode. These modifications result in a significant system reliability improvement by reducing reliability degradation during non-operating periods. A comparison of equipment failure rates for the G&N system with and without modifications is shown in Table 8.

Table 8. Apollo G&N Failure Rates

Unit	Mode	Failure Rate per 10^6 hours	
		Block II	Apollo X
AGC	Operate	274.7	274.7
	Standby	37.6	0.0
IMU	Operate	132.0	130.0
	Standby	18.65	1.6
PSA	Inertial Operate	105.7	105.7
	Inertial Standby	9.5	0.2
	Optical	59.5	59.5
ECU	Inertial	217.9	217.9
	Optical	145.4	145.4
Optics	Operate	78.0	78.0
Displays and Controls	Operate	29.9	29.9

The following discussion is based on the system with these modifications included.

G&N system reliability is shown in Figure 40 for boost into low inclination, polar and synchronous earth orbits as a function of parking orbit duration. For missions which involve rendezvous, the effect on reliability can be determined by adding half an hour to nominal parking orbit duration to compensate for additional time required for terminal maneuvering and docking. G&N reliability for reentry from the various orbits is shown below:

Mission	Reentry Reliability
Low Inclination Orbit	0.9995
Polar Orbit	0.9995
Synchronous Orbit	0.9960

For orbital operations, the most significant parameter is system operating time. The daily operating time for each subsystem (inertial, computer and optical) can be determined based on the system operations (IMU alignment, optical measurements) which have been previously described and the mission requirements (mapping duration, etc.). Figures 41 and 42 can then be used to determine reliability for orbital operations for each major

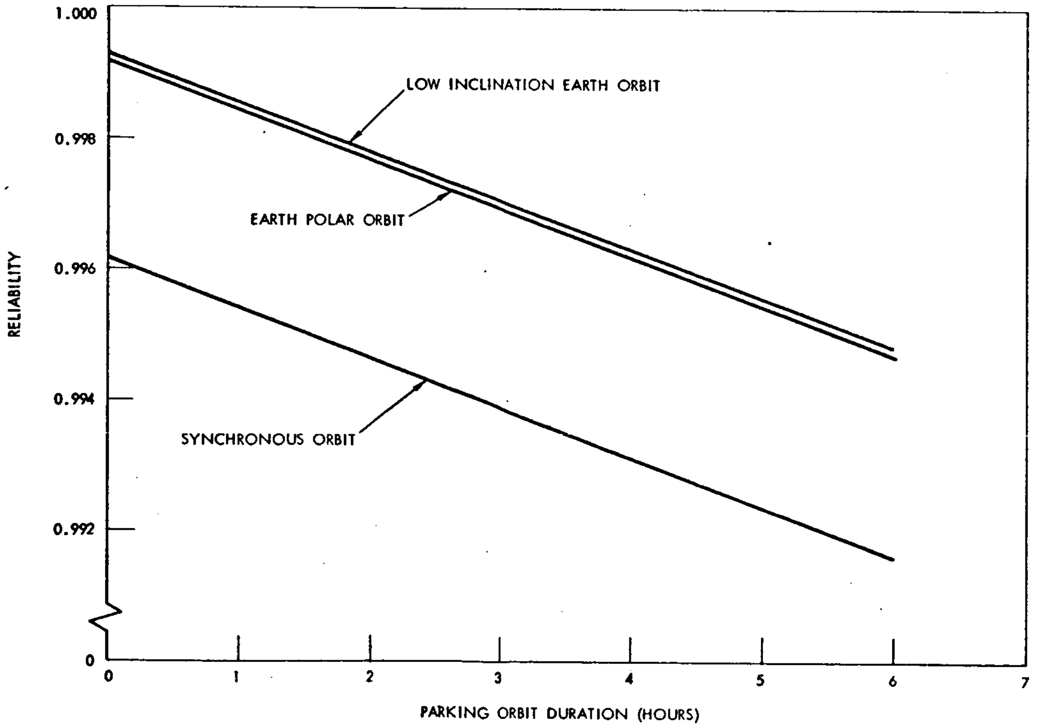

Figure 40. Apollo G&N Boost Reliability

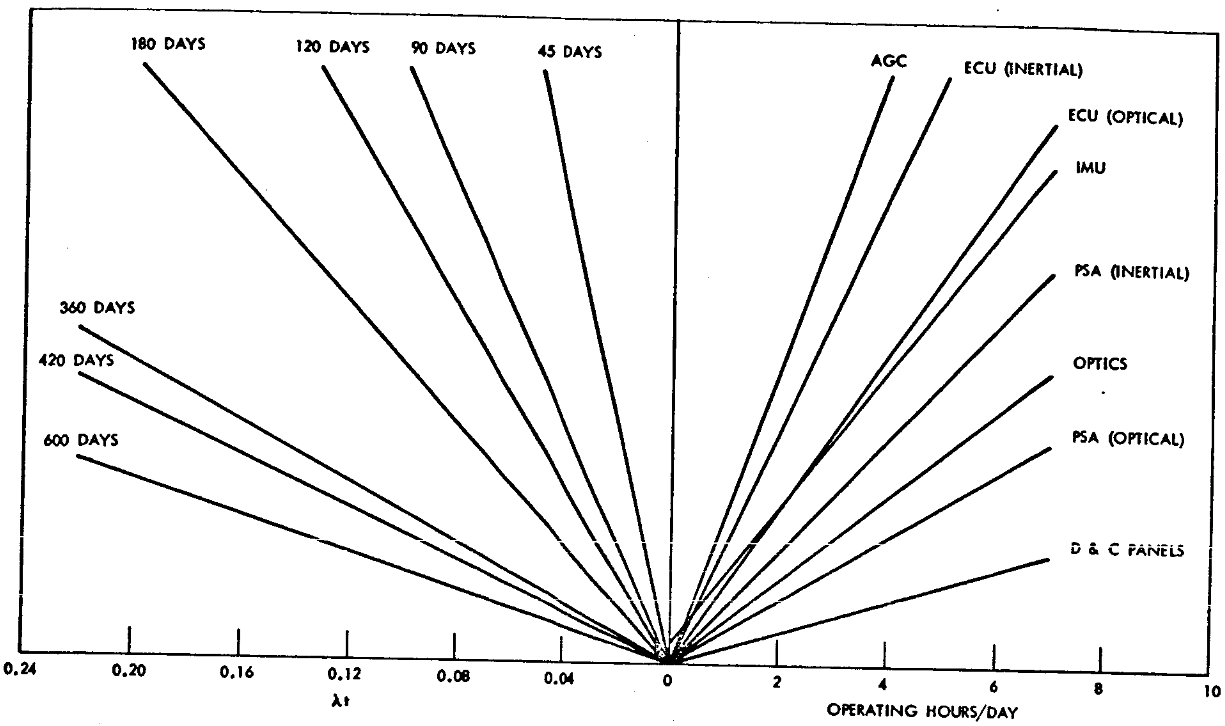

Figure 41. Apollo G&N Parametric Reliability

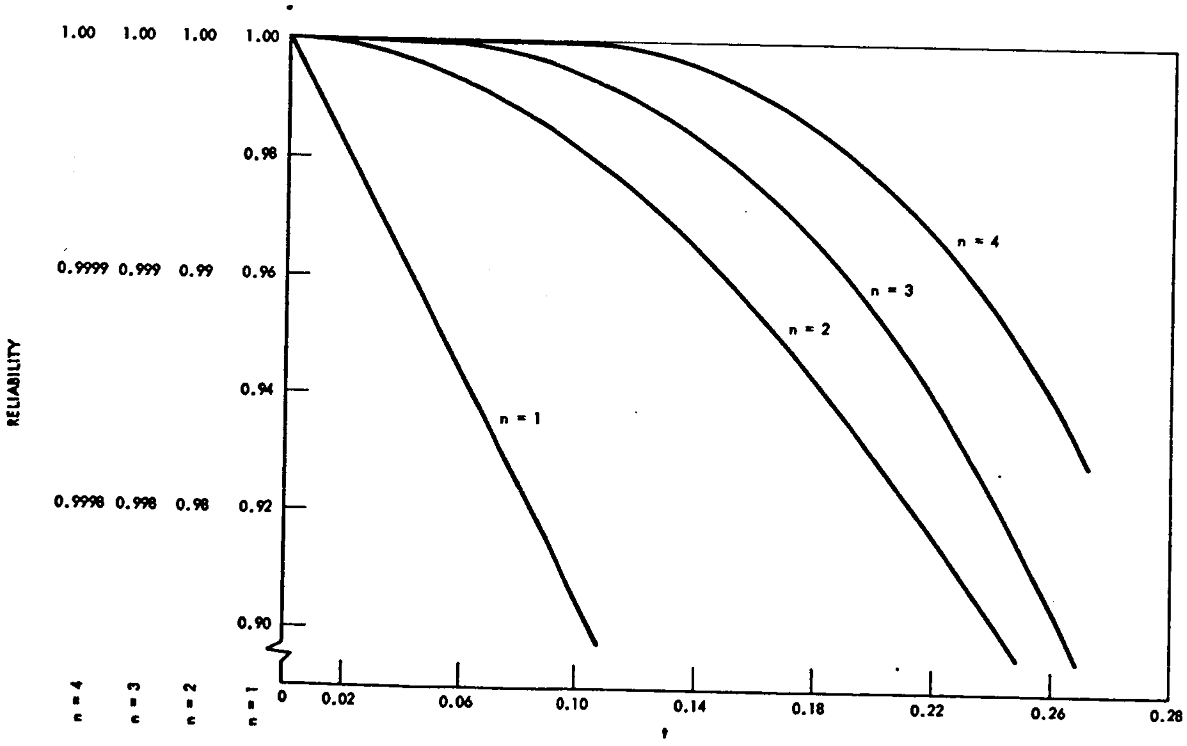

Figure 42. Probability of Success for Box Level Sparing

assembly as a function of daily operating time, mission duration and the number of spares (n minus one in Figure 42) which are provided.

Figure 41 is used to determine the value of λt for each major assembly. This is accomplished by entering the plot with the daily operating time for each subsystem and drawing a vertical line to the corresponding assembly. From this intersection, a horizontal line is then drawn to the line corresponding to mission duration. The value of λt for each assembly is then determined by drawing a vertical line. It should be noted that two lines are required for both the ECU and PSA since these assemblies are used in both the optical and inertial subsystems. Also the line for the IMU does not intersect zero since the inertial component heaters continue to operate during the standby periods. An expanded version of Figure 42 for shorter missions is presented in Figure 43.

Given a reliability goal for a specific mission, the spares required for each assembly can then be determined from Figure 42. As a first step, spares must be provided so that the reliability of each assembly is above the system reliability goal. Additional spares can then be chosen so that the reliability goal (orbital plus transit) is attained with minimum system weight. Other selection criteria such as minimizing the sparing of the IMU and optics can also be applied. Based on the data of Table 9, the weight of the selected system can then be determined.

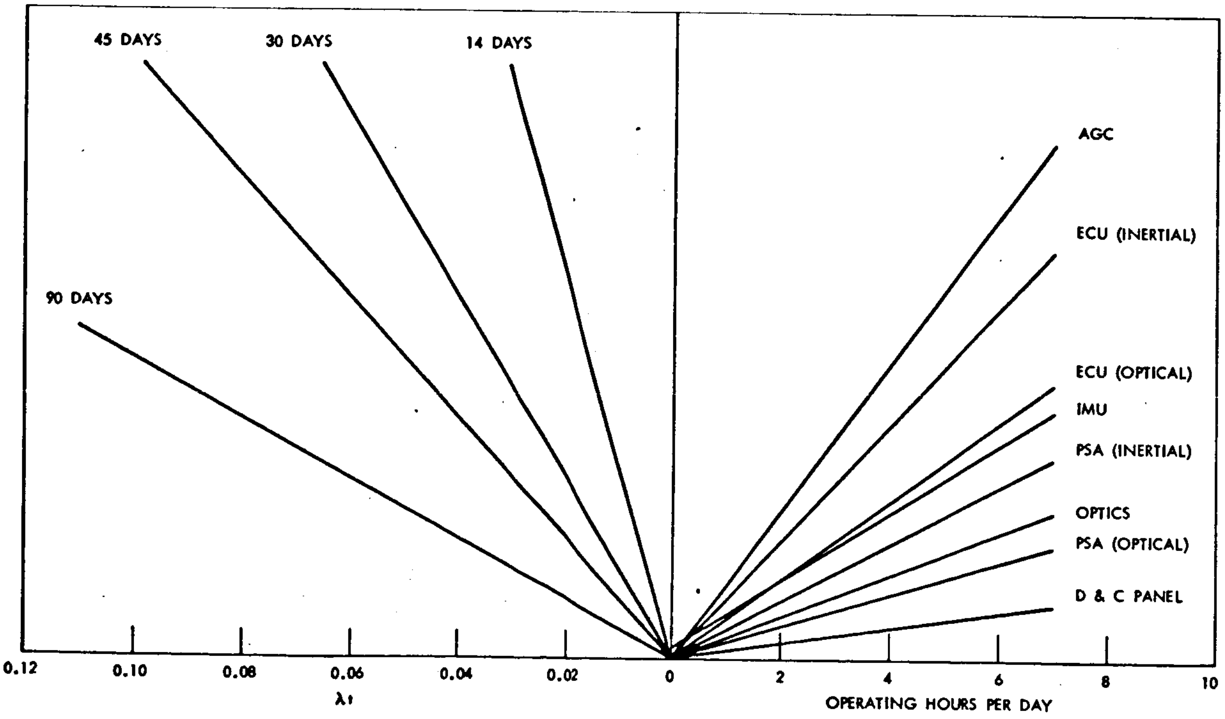

Figure 43. Apollo G&N Parametric Reliability (Expanded)

CON[redacted]

Table 9. Apollo Block II G&N Equipment Weights

Unit	Weight (lbs.)
Electronics	(239.7)
IMU and Coolant Hoses	42.9
Power and Servo Assembly	58.2
Electronic Coupling Unit	36.0
Apollo Guidance Computer	69.0
Navigation Base	17.0
Bellows Assembly	12.7
Signal Conditioning Assembly	3.9
Optics	(57.3)
Optics Head	50.0
Eyepieces	4.2
Optical Shroud	3.1
Displays	(58.6)
Displays and Controls - Navigation	12.1
Display and Keyboard (2)	35.0
Map and Data Viewer	11.5
Loose Stored Equipment	(5.6)
Film Cartridges	2.5
Eye Relief Eyepieces	1.5
Optics Cover	1.6
Cabling	(38.8)
Cabling MIT	38.8
G&N System Total Weight	400.0

[redacted]

Reductions in the weight of spares can be achieved for some units by sparing below the box level. Figures 44 and 45 can be used to determine the reliability of the ECU and AGC for subassembly and module level sparing respectively. The weight of an ECU subassembly is approximately 7 pounds. Each AGC module weighs approximately 1.5 pounds.

In addition to the units previously described, the DSKY will also effect system reliability. On the Apollo LOR mission, a dual DSKY configuration is used. However, only one DSKY is required for operation at any one time. For the extended duration missions, Raytheon recommended the use of a single operating unit. With the addition of 11 spare modules (comparable in weight to a second unit), the reliability of the DSKY will be maintained near unity for all operating conditions considered in this section.

The AGC has the capability of being operated in a standby mode during which it continuously provides a time sync signal to the communications system. For extended duration missions, more reliable methods of accomplishing this function can be provided within the communications system. The AGC is the only major system unit which can be readily modified or deleted to reflect specific mission requirements. For missions in which the G&N system is primarily operated only during the transit phases, the memory capacity required is considerably reduced. A comparison between the Block II AGC and a

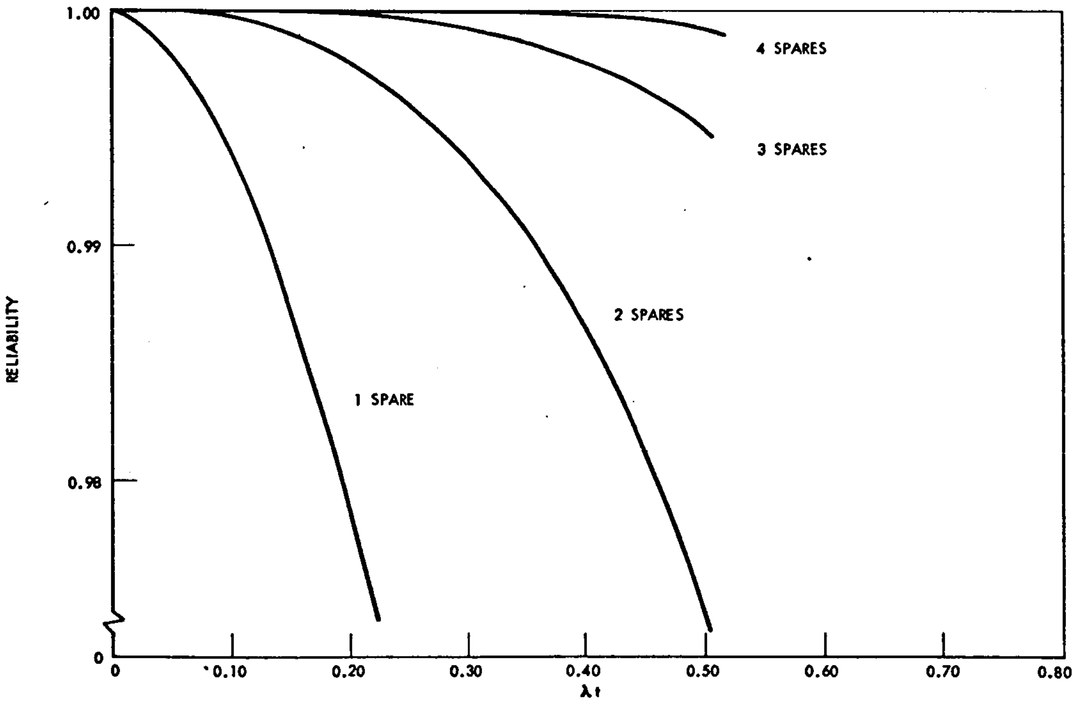

Figure 44. Electronic Coupling Unit - Subassembly Sparing

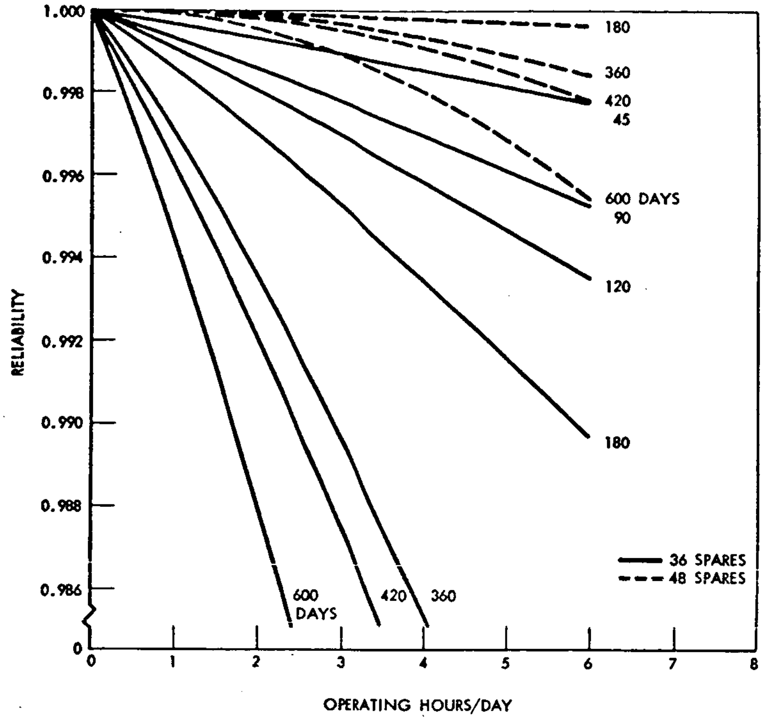

Figure 45. Apollo Guidance Computer-Module Level Sparing

reduced-capacity version is presented in Table 10. It can be seen that the improvements in reliability and reductions in weight are not large in comparison with the memory size reduction.

Table 10. AGC Variations

		AGC	Reduced
Memory Capacity	Fixed	36,864	12,288
	Erasable	2,024	1,012
Failure Rate per 10^6 Hrs.		274.7	226.8
Weight (lb)		69.0	60.2

The following example is presented to demonstrate the method of determining system configurations. The mission is assumed to last 90 days in low inclination earth orbit. The parking orbit duration is 30 minutes. During the orbital phase, the G&N system would be used for half an orbit (45 minutes) per day for experiment support. An additional 15 minutes per day would be required for alignment. It is assumed that the reliability goal for this mission is 0.994 for the G&N system.

Based on the assumed mission requirements, the operating time for the computer and inertial subsystems is one hour per day and for the optical subsytem it is 15 minutes per day. Either Figure 41 or 43 is then used to determine the value of λt associated with each major component. Figure 42 is used to determine the reliability associated with a specific λt. Figure 40 is used to determine the boost reliability. The results are presented below:

Phase	Unit	λt	Basic Reliab.	Reliab. with Spares	Spares Wt.(lbs)
Boost		---	.9989	.9989	---
Orbital	AGC	.0250	.9755	.9997	69.0
	ECU	.0235	.9775	.99975	36.0
	IMU	.0150	.9860	.9999	42.9
	PSA	.0115	.9890	.9999	58.2
	Optics	.0025	.9975	.9975	---
	D&C	.0010	.9990	.9990	---
Entry		---	.9995	.9995	---
Total		---	.9251	.9942	206.1

As can be seen, spares were required for the AGC, ECU, IMU and PSA in order to meet the reliability goal, increasing system weight by 206.1 pounds. The sensitivity of sparing levels to the reliability goal is evident since even a moderate increase in the goal would necessitate the sparing of the optics. If the experiment support was performed in three separate intervals of 15 minutes each, the G&N system operating time would be effected since three alignments per day would be required even though the total duration of the experiments was not changed.

PERFORMANCE

The primary areas of interest in terms of performance are: (1) guidance accuracy during thrusting and reentry maneuvers, (2) navigation accuracy, and (3) attitude reference or control capability. With the exception of transfer to synchronous orbit and large plane change maneuvers, most earth orbit thrusting maneuvers will be of short duration and the thrust accelerations will be less than 1-g. For a short term maneuver, the ΔV will generally be applied along a straight line in inertial space. The guidance error due to the maneuver will primarily depend on the initial alignment error, the accelerometer bias and the velocity pulse scaling. For the first two error sources, the velocity error in each component can be determined as a function of the magnitude of the ΔV and the burn time from Figure 46. The velocity error due to velocity pulse scaling will be on the order of 0.1 feet per second.

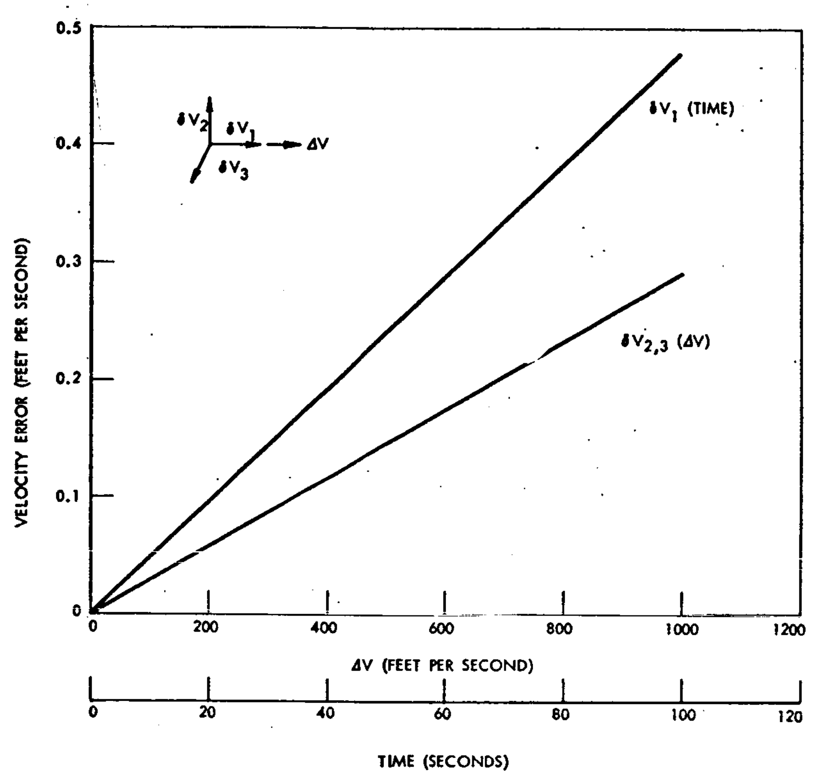

Figure 46. Velocity Errors for Short Term Maneuvers

Since error build-up due to these sources is small, the initial error will still be the dominant term. For more complex maneuvers, the data of Table 11 can be used for performance evaluation.

The Apollo Block II G&N system has a guidance uncertainty (1σ) of 5 n.mi. at parachute deployment for reentry from lunar orbit. The conditions encountered on reentry from synchronous orbit will be similar to those for lunar return. The conditions for reentry from low earth orbit will be less severe. The data (acceleration versus time profile) required for a reentry error analysis is dependent on conditions at atmospheric entry, vehicle L/D, and the reentry range. Navigation accuracy depends on the measurement accuracy frequency and number of measurements, and the navigation mechanization.

The Apollo G&N system has at present the capability of controlling vehicle attitutde to ± 0.5 degrees and attitude rate to 0.05 deg/sec. However, by modification of the computer program, it is possible to achieve an attitude deadband of ± 0.1 degrees with an attitude rate of 0.01 deg/sec. Based on previous studies, precise vehicle stabilization for experiments will be required generally for less than one earth orbit. The local vertical reference capability is dependent on the initial IMU alignment accuracy (60 arc-seconds), the gyro bias drift rate (1 Meru) and the spacecraft orbit position uncertainty. Since these error sources are independent and random, they were combined by root-sum-square technique to obtain the overall standard

Table 11. Apollo Block II G&N Error Sources

Error Source	1σ Value
Gyro	
Bias Drift	1 meru*
Unbalance	10 meru/g
Compliance	1 meru/g^2
Accelerometer	
Bias	1.5×10^{-4}g
Scale Factor	6×10^{-5}g/g
Nonlinearity	2×10^{-5}g/g^2
Sensitive Axis Misalignment	20 arc-seconds
Initial Alignment or Realignment	
Orbital	60 arc-seconds
Optics (Navigation)	
Star-to-horizon "Blue" Line	6 arc-minutes
Landmark Track	6 arc-minutes
*milli earth rate unit	

deviation. The local vertical uncertainty is shown in Figure 47 as a function of orbit position accuracy for a 200 n.mi. orbit.

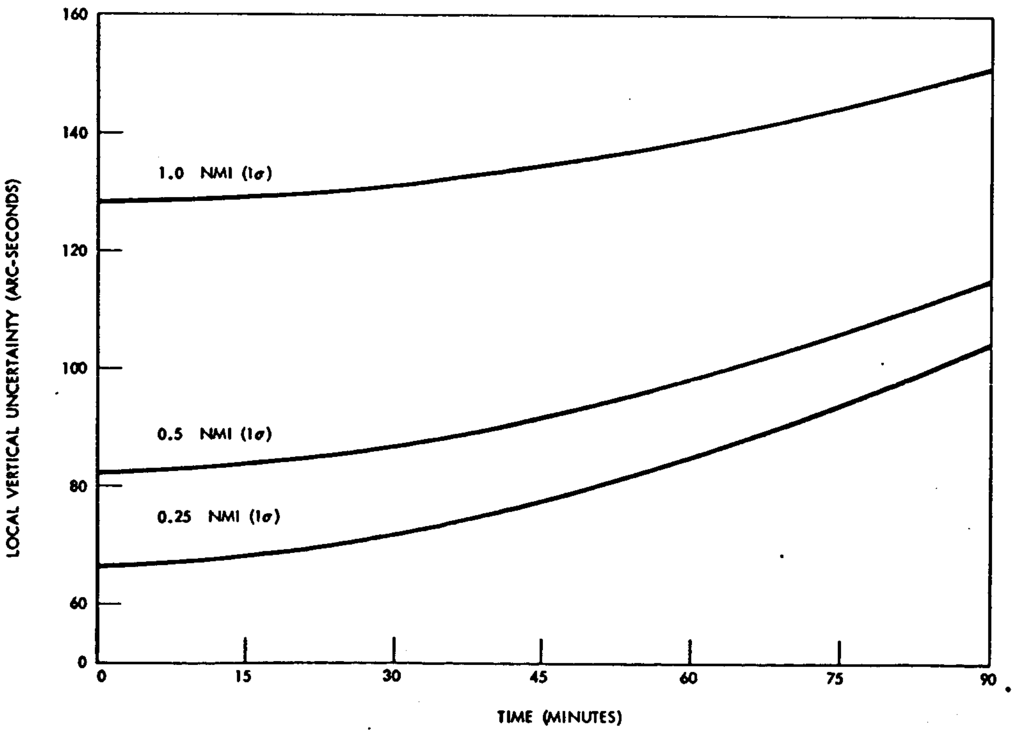

Figure 47. Local Vertical Uncertainty (1 σ) versus Orbit Position Accuracy

N35-S G&N SYSTEM

The N35-S is a self-contained, automatic guidance and navigation system. The major elements of the system are the inertial measurement unit, an optical tracker, a digital computer, and the associated electronics and power supplies.

The IMU is a four-axis, three-gimbal platform with 2 two-axis free-rotor, gas spin bearing G14 stabilization gyros and three VM8S velocity meters. The optical tracker consists of a miniature telescope and solid-state photosensor mounted in a two-axis gimbal system. The digital computer is a general purpose, stored program, single address computer. In its expanded form, the computer has a memory capacity of 16,384 twenty-eight bit words with 42 basic instructions.

The major features are (1) high system reliability which is attainable by the use of electronic components and circuits derived from the Minuteman reliability program, (2) the use of digital-type optical angle readouts for increased precision in tracker and platform gimbal axes readings, and (3) dual mode (two speed) gyros which can be run at low speed (20 rps) during lower-g orbital operations with large reductions in power.

The system physical characteristics are presented in Table 12. Since the previously described assemblies only constitute a bare guidance system, provisions have been made for auxiliary equipment (controls, displays, cabling, etc.) which is vehicle-dependent based on comparable Apollo G&N equipment.

RELIABILITY

The parametric reliability data for this system is presented in a similar manner to that used for the Apollo G&N system. The system reliability for boost into low inclination, polar and synchronous earth orbits is presented in Figure 48 as a function of the duration of the parking orbit. The reliability for reentry from these orbits is shown below:

Mission	Reentry Reliability
Low Inclination Orbit	0.9999
Polar Orbit	0.9999
Synchronous Orbit	0.9993

Table 12. N35-S Physical Characteristics

Assembly	Weight (lbs)	Volume (ft^3)	Power Consumption (Watts)			Failure Rates (per 10^{-6} hrs)
			Ascent	Orbital	Reentry	
Platform	30	1.0 (12" dia. x 15")	64	6.4	64	25.8
Platform Electronics & Power Supplies	5	0.17 (6" x 4" x 12")	29	3.5	29	24.1
Optical Tracker & Electronics	5	0.43 (10" dia., x 8")	5	5	5	9.0
D62A Computer	15.9	0.22 (14" x 7.2" x 3.7")	61	61	61	64.2
Computer Power Supply	14.9	0.22 (14" x 7.2" x 3.7")	24	24	24	7.6
Auxiliary Equipment	151.6	3.0	-	-	-	-
Rendezvous Radar Wiring	14	0.2	-	-	-	-
Total System	236.4	5.24	183	99.9	183	130.7

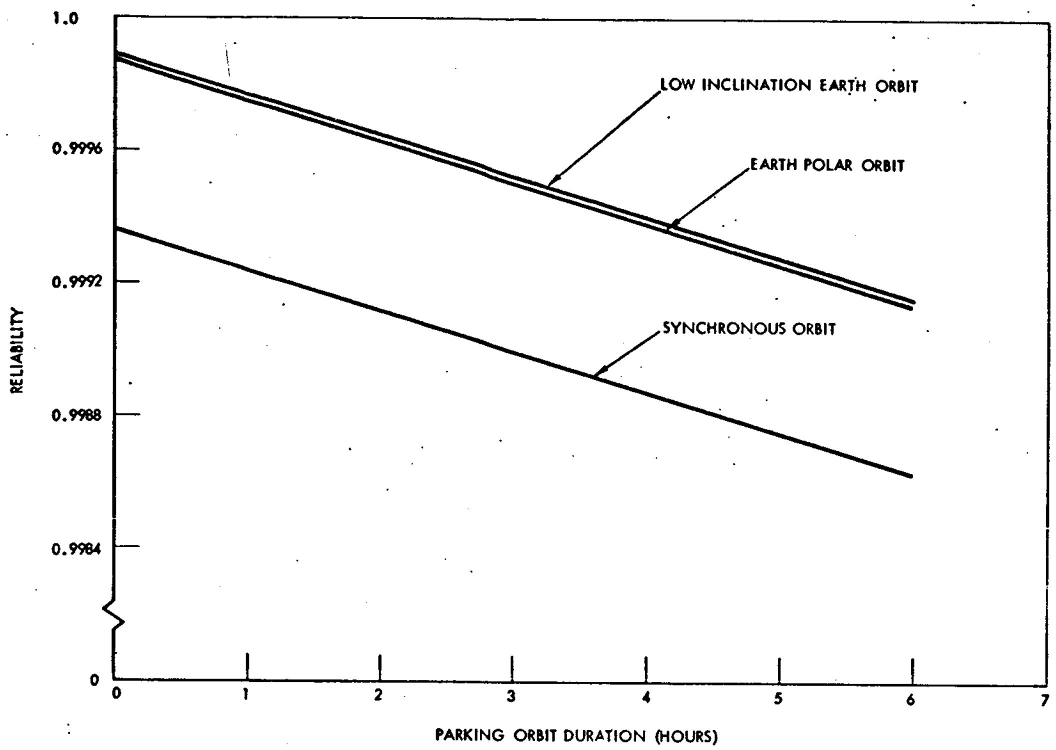

Figure 48. N35-S Boost Reliability

For orbital operations, the system operating times will be essentially equal to those of the Apollo system. In a similar manner, Figure 49 is used to determine the value of λt for each major assembly. During standby or storage modes, the N35-S does not require heater power. For a specific mission reliability goal, Figure 42 is then used to choose the required number of spares for each assembly. Because of the type of design used, Autonetics recommends sparing at the box level only. Since only basic system components are included in the reliability analysis, some provision for displays and controls is also required. The weight of the selected system can then be determined from Table 12.

The digital computer described in the previous discussions is the expanded version of the D62A computer. For applications where the system is used only during transit, the memory capacity of the nominal version of the D62A computer would be adequate. Two versions are compared in Table 13. The computer power supply is not affected.

Table 13. D62A Computer Variations

	Expanded	Nominal
Memory Capacity	16,384	8,192
Failure Rate per 10^6 hr	64.2	42.5
Weight (lb)	15.9	12.4

PERFORMANCE

System error sources required to perform a performance analysis are shown in Table 14.

The local vertical reference capability of the N35-S G&N system is presented in Figure 50 as a function of orbit position accuracy. Due to the greater precision of the IMU gimbal angle readouts, the N35-S can achieve a more precise initial IMU alignment than the Apollo G&N system. There, the N35-S system can provide a more precise local vertical reference or alternatively it can achieve the same reference capability with less precise navigation data.

Table 14. N35-S Error Sources

Error Source	1σ Value
Gyro	
Bias Drift	0.67 meru
Unbalance	2.0 meru/g
Compliance	4.0 meru/g^2
Accelerometer	
Bias	7×10^{-6} g
Scale Factor	8.7×10^{-6} g/g
Non-linearity	5×10^{-6} g/g^2
Sensitive Axis Misalignment	2 arc-seconds
Initial Alignment or Realignment	
Orbital	8.5 arc-seconds
Optics (Navigation)	
Telescope Measurements	6.5 arc-seconds

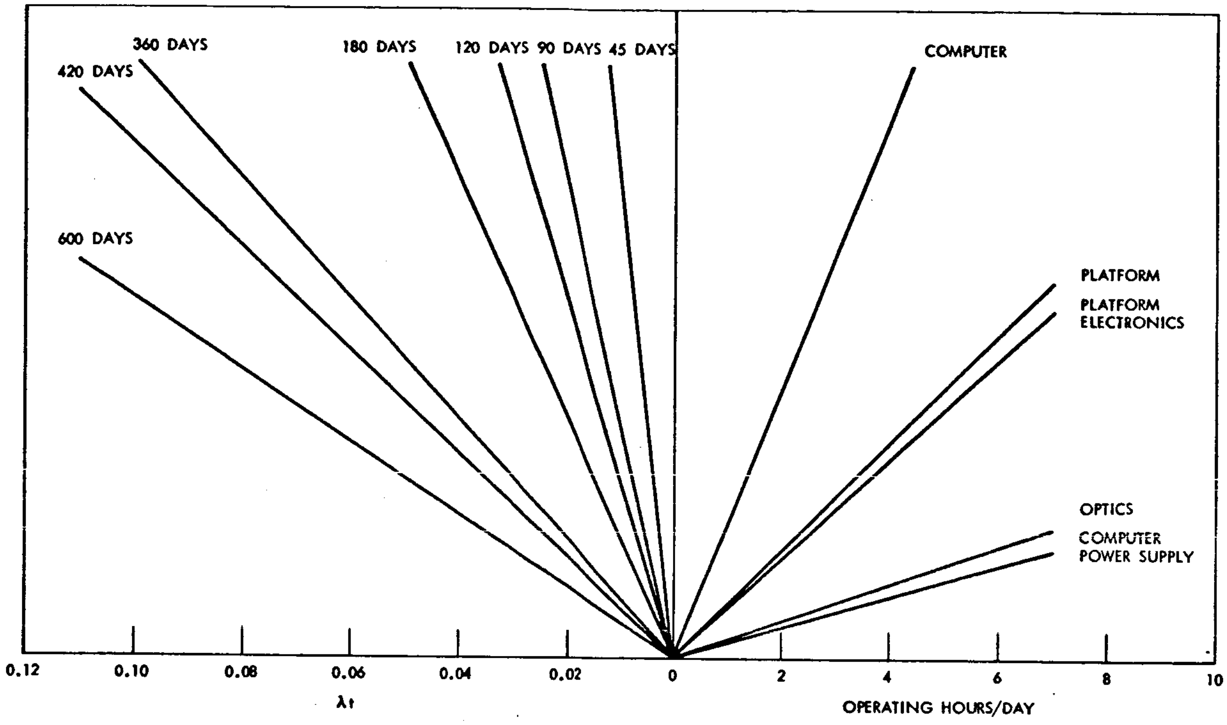

Figure 49. N35-S Boost Reliability

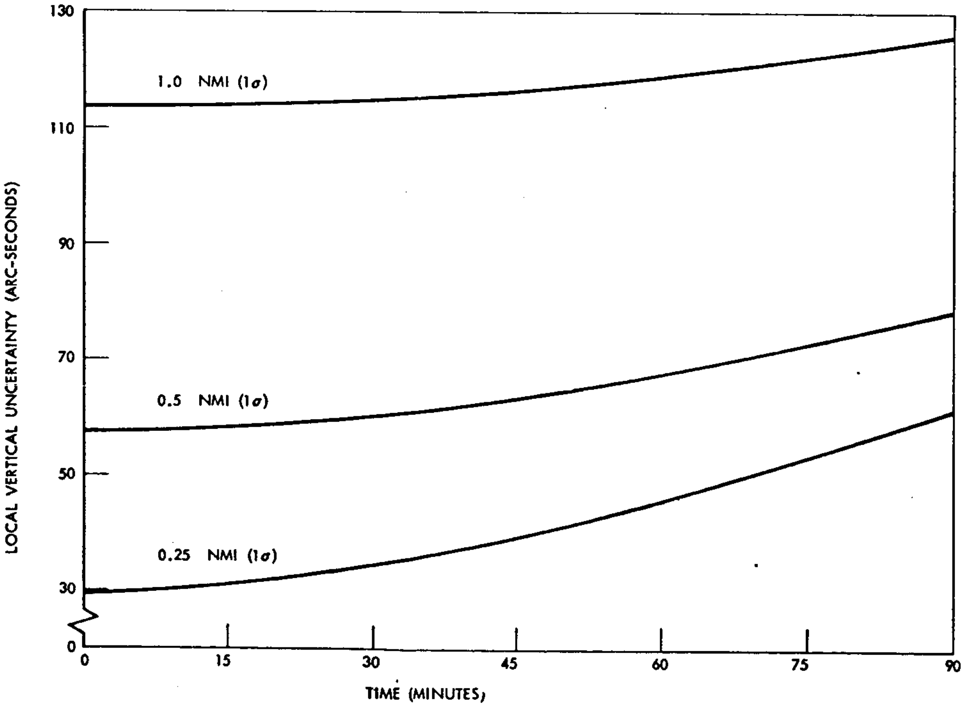

Figure 50. N35-S G&N System Parametric Reliability

STRAPDOWN SYSTEMS

For a large class of future extended duration missions, it is anticipated that the precision capabilities of an inertial guidance system similar to either of the two preceding systems would not be required in orbit. These missions would involve biomedical and behavioral experiments which require only coarse vehicle stabilization and no precise vehicle orbital maneuvers. For these missions, it is possible to consider the use of separate systems during the transit and orbital phases.

Because of the precise vehicle maneuver requirements and high accelerations encountered during transit, the use of an inertial guidance system during these phases would still be desirable. Since the prolonged missions will, in general, require periodic resupply, the vehicle's inertial guidance system must only meet an orbital life equal to the ascent and descent period rather than the total mission duration (up to 600 days). This will simplify the reliability problem associated with long mission durations for complex inertial guidance systems. By providing suitable interfaces, it would be possible to make limited use of the vehicle's guidance system for precise vehicle stabilization or maneuver requirements in orbit.

For most orbital requirements, a strapdown system configuration is adequate. The primary requirements during the orbital phase are: (1) vehicle stabilization for experiments, (2) guidance during short-term maneuvers, and (3) backup navigation.

Both local vertical and attitude hold stabilization modes will be required for experiments. Because of limitations on propellant available for vehicle attitude control, gross vehicle stabilization will often be achieved passively by orienting the vehicle with respect to local vertical in order to use the gravity gradient effect. Therefore, active local vertical stabilization will only be required by experiments which impose more stringent requirements than can be met passively. For stellar observations, an attitude hold mode will be required to orient the vehicle in inertial space. Due to instrument field of view limits and eclipsing effects of the earth, this mode will only be used for periods of approximately half an orbit period or less.

The primary guidance maneuver will be to maintain a certain orbit altitude to counter the effect of atmospheric drag. Since the orbital altitude is not critical for biomedical and behavioral experiments, the primary criterion for determining the frequency of this event will be the propellant allocation. Assuming a Hohmann transfer, the total velocity increment ΔV (impulses at perigee and apogee) can be determined as a function of the perigee altitude, r_0, and the allowable altitude loss, Δr.

Assuming $\Delta r \,/\, r_o \ll 1$, the ΔV is given by:

$$\Delta V = \frac{\Delta V}{2} \sqrt{\frac{\mu}{{r_o}^3}}$$

Figure 51 shows the velocity increment for unit change in Δr for various perigee altitudes. These results can be extended to other values of Δr due to the linearity of the results. For example, the impulsive incremental velocity would be 35 feet per second for transfer from a circular orbit at 180 n.mi. to a circular orbit at 190 n.mi.

Since the Hohmann transfer is accomplished by two almost equal impulses and the required ΔV's are low, the time period of active vehicle guidance and control will also be low. The duration of the attitude hold mode for orbit maneuvers and experiment support is short in either case.

In addition to the guidance and stabilization functions, the other major orbital requirement is navigation. The primary source of navigation data would be the MSFN. The navigation data would be supplied to the astronaut by the up-data link in the communications system. Depending on mission requirements, it may be necessary to provide an on-board navigation capability so that a backup navigation system would be available in the event of failure in the communications system. To provide precise navigation data, it would be necessary to add a digital computer to perform the data processing. The addition of a digital computer to the on-board equipment will have a significant effect on system cost and reliability. A less precise navigation capability can be provided by stellar sightings and hand calculations by the astronaut. The choice between the two approaches depends on mission requirements.

SYSTEM DESCRIPTION

A strapdown system is capable of satisfying the requirements of many missions. For thrusting maneuvers and attitude hold, gyroscopic instrumentation is desirable due to its response and ability to control to an arbitrary inertial attitude. Since this capability is required only for short durations, a gimballed system is not necessary. Three mutually orthogonal rate gyros in a strapdown configuration would be adequate. A manual star tracker would be required for alignment. The required system attitude accuracy would depend on the mission. The system attitude error is a function of such factors as the MSFN error in defining the required attitude, system quantization levels, astronaut set-in errors, and gyro drift rate. The allowable gyro drift rate is presented in Figure 52 as a function of the duration and the portion of total error which is allocated to this source. During thrusting maneuvers, acceleration can be measured directly by an accelerometer (one or three) or indirectly by a timer. One accelerometer with its sensitive axis aligned with the vehicle's longitudinal axis will be sufficient for many applications.

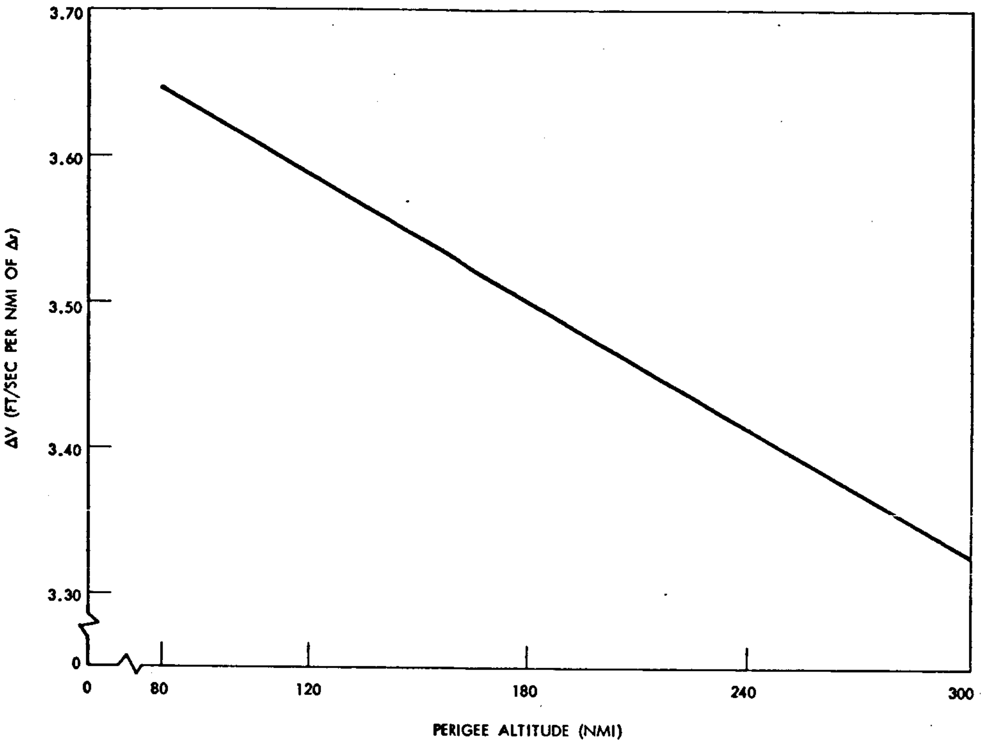

Figure 51. Velocity Increment vs. Perigee Altitude

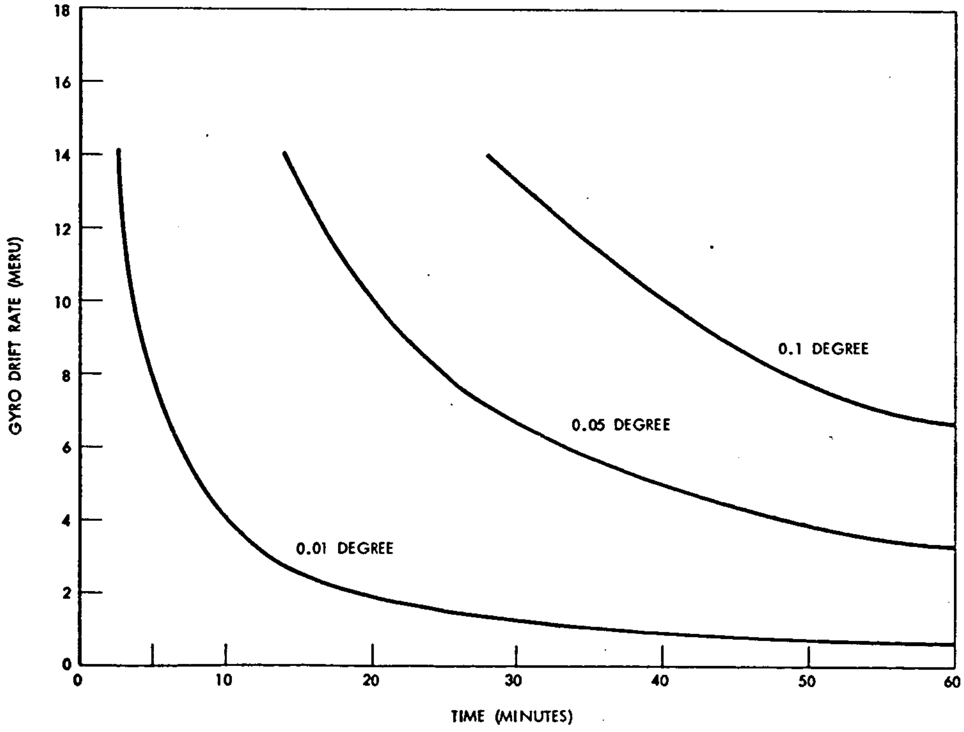

Figure 52. Gyro Drift Rate vs. Attitude Error Allocation

Local vertical stabilization for experiments or during free fall would be based on horizon sensor data. This would provide stabilization about two axes. Stabilization about the third axis, if desired, can be provided by gyros. Currently available horizon sensors have an accuracy capability of approximately 0.5 degrees including both instrument accuracy and horizon variations. Horizon sensors which are now in development have a goal of 0.1 degree attitude accuracy. This is to be achieved by the use of narrow band techniques in the 15 micron region. In addition, electronics power supplies, cabling and displays would be necessary to complete the basic system configuration. Typical physical characteristics for the basic system components are presented below.

Component	Wt (lb)	Vol (ft^3)	Power (watts)	Failure Rate per 10^6 hours
Strapdown Gyros	18	0.3	23	30
Accelerometer	4	0.1	5	6
Star Tracker	25	0.4	--	40
Electronic & Power	10	0.2	20	10
Horizon Sensor	15	0.3	12	5-50
Displays	10	0.2	10	10

As indicated previously, a digital computer would also be required if a precise on-board navigation capability is needed. Either the manual star tracker or the horizon sensors can be used to make the navigation measurements. Either of the two reduced memory capacity versions of the digital computers which were described previously would be adequate for the on-board navigation task.

The digital computer would be programmed with the following basic routines to provide a navigation capability during both thrusting and free-fall intervals.

1. Initial attitude determination
2. Direction cosine updating
3. Computation of velocity during thrust intervals
4. Navigation during thrust intervals
5. Orbital navigation and guidance

The bulk of the computations are contained in the last block. First, the nominal trajectory and state transition matrix would be computed. Then, the filter equations would be solved to obtain a "best" estimate for the orbit. There would also be equations for the computation of the velocity correction increment which is required to achieve a new orbit.

Figure 53 presents strapdown configurations for various modes of operation. The dotted lines indicate backup or alternate mechanizations. Since this system is not in existence, it is possible to select the components to meet specific mission requirements.

An additional consideration is the redundancy and/or sparing provisions that must be provided. This is especially true for the hard mounted components (i.e., horizon sensors and manual star tracker). Redundant horizon sensors will be required due to the long operating time associated with their use.

CON[redacted]

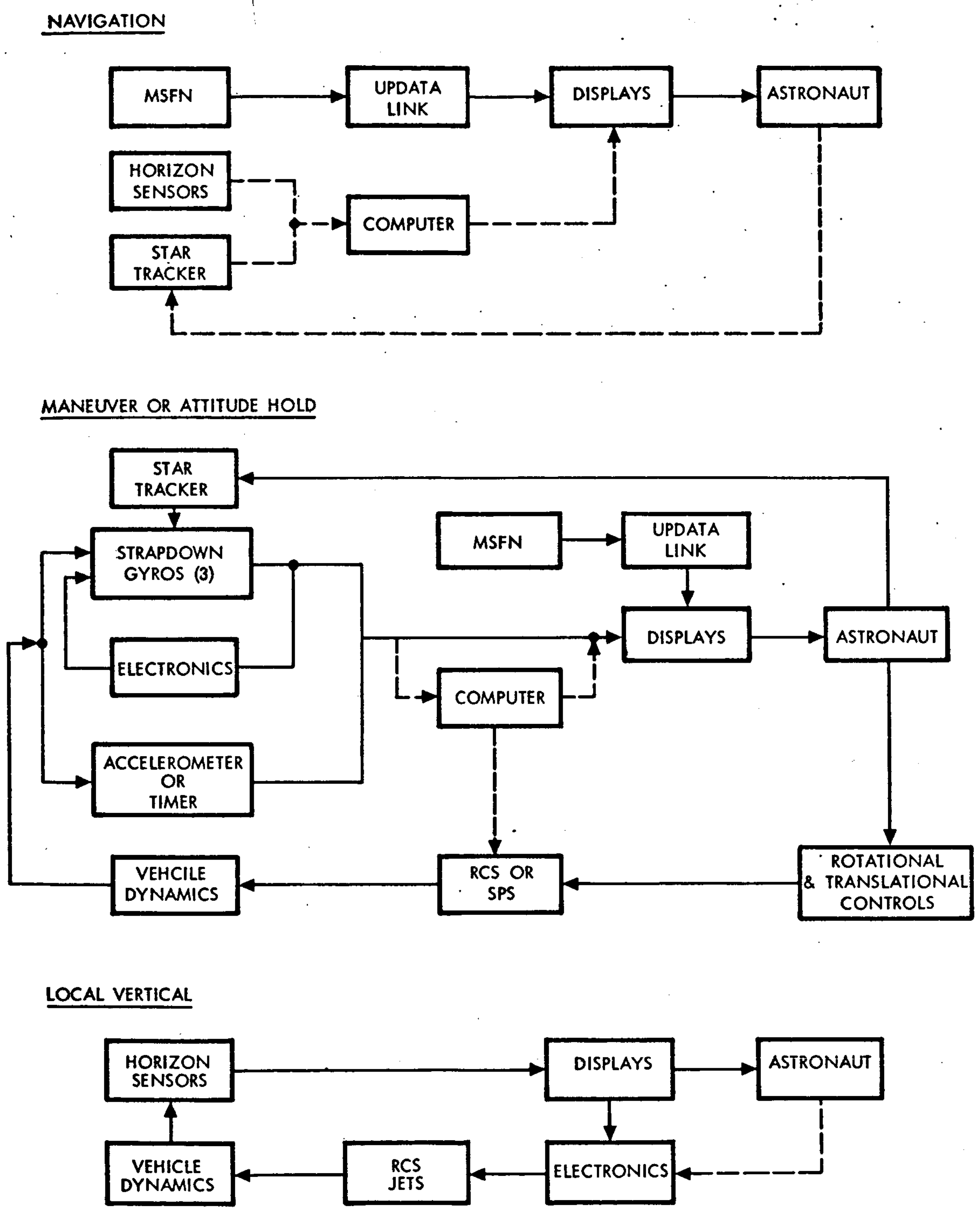
NAVIGATION
MSFN
UPDATA LINK
DISPLAYS
ASTRONAUT
HORIZON SENSORS
COMPUTER
STAR TRACKER
MANEUVER OR ATTITUDE HOLD
STAR TRACKER
STRAPDOWN GYROS (3)
MSFN
UPDATA LINK
ELECTRONICS
DISPLAYS
ASTRONAUT
COMPUTER
ACCELEROMETER OR TIMER
VEHCILE DYNAMICS
RCS OR SPS
ROTATIONAL & TRANSLATIONAL CONTROLS
LOCAL VERTICAL
HORIZON SENSORS
DISPLAYS
ASTRONAUT
VEHICLE DYNAMICS
RCS JETS
ELECTRONICS

Figure 53. Strapdown Configuration Block Diagrams

[redacted]

CONCLUSIONS

The extension of the Apollo G&N system for experiment support for missions up to 45-day duration was investigated during the AES studies. The results indicated that determination of the G&N's suitability is totally dependent on specific mission requirements. Although the use of the Apollo G&N is desirable due to the many hours of experience that will be accumulated on the Apollo and other programs, its use on prolonged missions will be limited due to a reliability problem on the longer missions. Based on previous studies, it is not anticipated that there will be any performance problems associated with its use. Extreme precision requirements on sensor pointing will, in general, be accommodated as part of the experiment requiring the sensor.

The use of Minuteman rather than burned-in parts will result in a reliability improvement as indicated by the N35-S G&N system. It is doubtful if any significant reliability improvement beyond Minuteman parts could be achieved without an extensive reliability development program. An alternate approach would be to use a simpler system such as the strapdown system configuration for the longer missions which do not have stringent performance requirements.

POWER SYSTEMS

POWER SYSTEMS

Several interrelated NASA studies were being conducted at S&ID during the time period of the Prolonged Missions Apollo activity, including the Apollo X portion of Extended Apollo Systems Utilization (published in report SID 64-1860), Ballistic Orbital Support Operations (SID 65-179), Experiments Pallet (SID 65-226), and Apollo Extension Systems (SID 65-500). In the power system area, data generated in support of these studies were often applicable to the Prolonged Missions study. For example, the energy source requirements and space storage effects for the Prolonged Missions logistics spacecraft are similar in many respects to those of the Ballistic Orbital Support Operations (BOSO) spacecraft. The general interrelationship of these programs together with the activity of concern to Prolonged Missions is shown in Figure 54.

In some cases, data applicable to Prolonged Missions were discussed in detail in the final reports of the BOSO and Experiments Pallet studies and will not be repeated in this report. Specifically, the reader is referred to those reports for greater technical detail concerning the prime energy source for logistics spacecraft, the effects of space storage on primary batteries and power distribution equipment, and the performance and thermal control of primary batteries.

During the Extended Apollo Systems Utilization study, the major effort in the vehicle requirements and experiments integration area was directed toward the 45-day vehicle rather than Prolonged Missions. Consequently, the power requirements analysis that was accomplished for Concepts II and III during the Extended Mission Apollo study was not significantly changed. The power system design considerations, however, were extended up to a net load of 4 KW to show the effect of increased power loading from the base point.

The selection of solar cells as the prime power source for Extended Mission Apollo spacecraft was based on the extended Apollo program definition and power system status as of October 1963. Since that time, changes have been made in the program (including operational dates) and in power system technology. Specifically, the feasibility of using a radioisotope power system deserved attention, although contract funds were to be directed toward analysis of the previously selected system. For this reason, Atomics International was invited to direct their company sponsored effort toward this specific application. The results of their work is presented in detail in Appendix B. This section treats solar cell systems and radioisotope systems in some detail. In addition the results of a study of power conditioning, distribution and control system are presented.

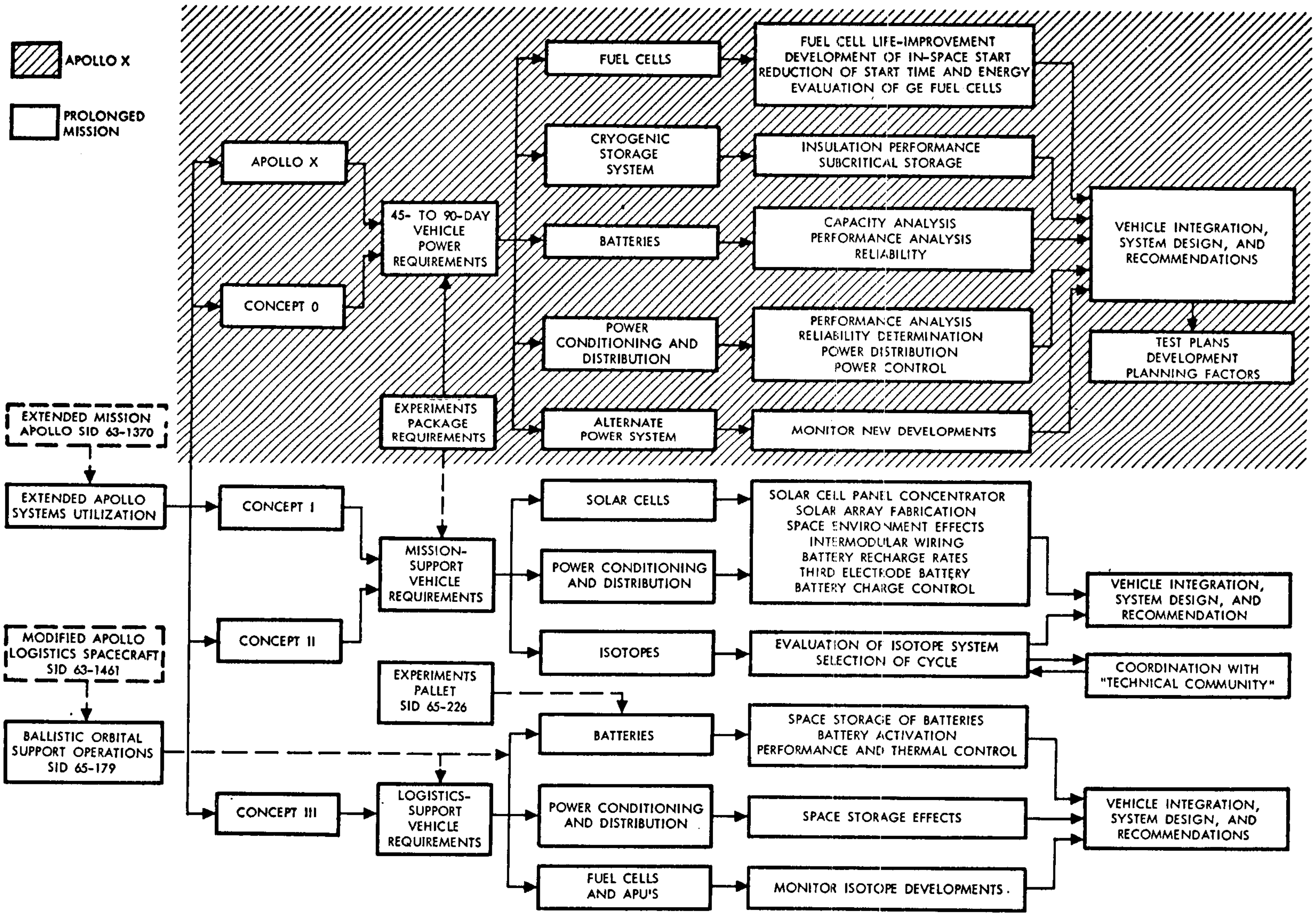
APOLLO X
PROLONGED MISSION
APOLLO X
CONCEPT 0
45- TO 90-DAY VEHICLE POWER REQUIREMENTS
EXPERIMENTS PACKAGE REQUIREMENTS
FUEL CELLS
CRYOGENIC STORAGE SYSTEM
BATTERIES
POWER CONDITIONING AND DISTRIBUTION
ALTERNATE POWER SYSTEM
FUEL CELL LIFE-IMPROVEMENT
DEVELOPMENT OF IN-SPACE START
REDUCTION OF START TIME AND ENERGY
EVALUATION OF GE FUEL CELLS
INSULATION PERFORMANCE
SUBCRITICAL STORAGE
CAPACITY ANALYSIS
PERFORMANCE ANALYSIS
RELIABILITY
PERFORMANCE ANALYSIS
RELIABILITY DETERMINATION
POWER DISTRIBUTION
POWER CONTROL
MONITOR NEW DEVELOPMENTS
VEHICLE INTEGRATION, SYSTEM DESIGN, AND RECOMMENDATIONS
TEST PLANS DEVELOPMENT PLANNING FACTORS
EXTENDED MISSION APOLLO SID 63-1370
EXTENDED APOLLO SYSTEMS UTILIZATION
CONCEPT I
CONCEPT II
MISSION-SUPPORT VEHICLE REQUIREMENTS
SOLAR CELLS
POWER CONDITIONING AND DISTRIBUTION
ISOTOPES
SOLAR CELL PANEL CONCENTRATOR
SOLAR ARRAY FABRICATION
SPACE ENVIRONMENT EFFECTS
INTERMODULAR WIRING
BATTERY RECHARGE RATES
THIRD ELECTRODE BATTERY
BATTERY CHARGE CONTROL
EVALUATION OF ISOTOPE SYSTEM
SELECTION OF CYCLE
VEHICLE INTEGRATION, SYSTEM DESIGN, AND RECOMMENDATION
COORDINATION WITH "TECHNICAL COMMUNITY"
MODIFIED APOLLO LOGISTICS SPACECRAFT SID 63-1461
BALLISTIC ORBITAL SUPPORT OPERATIONS SID 65-179
EXPERIMENTS PALLET SID 65-226
CONCEPT III
LOGISTICS-SUPPORT VEHICLE REQUIREMENTS
BATTERIES
POWER CONDITIONING AND DISTRIBUTION
FUEL CELLS AND APU'S
SPACE STORAGE OF BATTERIES
BATTERY ACTIVATION
PERFORMANCE AND THERMAL CONTROL
SPACE STORAGE EFFECTS
MONITOR ISOTOPE DEVELOPMENTS.
VEHICLE INTEGRATION, SYSTEM DESIGN, AND RECOMMENDATIONS

Figure 54. Power System Flow Diagram

SOLAR CELL POWER SYSTEM

The analysis of a solar cell power system was primarily concerned with three general areas: (1) design of the solar panel and particularly the relative merits of flat panels versus concentrators; (2) mechanical interface between the solar panel and the spacecraft; and (3) secondary energy storage system, and particularly the selection of the optimum battery type.

Cost, always an important criterion for system optimization, is especially important in the selection of the type of solar array and was therefore considered in the analysis. The cost figures shown in this report, however, are for power system comparison purposes only.

SOLAR CELL ARRAY EVALUATION

During the Extended Mission Apollo Study (SID 63-1370-4), the Hoffman Trough Type solar cell concentrator was selected as the means of converting solar energy into primary electrical power. Both flat and concentrator type solar cell panels were investigated in general with major emphasis being placed on the weight, area, and cost analysis and with minor emphasis on detailed electrical and mechanical layouts.

In this section of the report, a more detailed analysis of both the flat and concentrator type solar cell arrays is described, including detailed electrical and mechanical layouts and updated costing allocations pertaining to the requirements of the Prolonged Mission.

Solar Cell Array Types

Three types of solar cell arrays may be considered as suitable for the prolonged mission Apollo laboratory. These are the conventional solar panel, usually a flat rigid surface on which are mounted a maximum number of solar cells (400 to 440 1 x 2 cm cells per square foot). Essentially all experience in space applications has been on solar arrays of this type. Secondly, there are concentrator arrays of which the trough type array has received the greatest attention and development. At present, there is no experience whatever on the performance of concentrator type solar cell arrays in space. Finally, less attention has been given to flexible type arrays of very low weight, which can be rolled up on diameters as small as 8 inches. (Panel and concentrator arrays, of course, are also readily hinged to wrap around somewhat larger diameters. Such arrays may be said to be articulated to distinguish them from the flexible type.)

It appears that solar cell array types that have shown the greatest potential for cost and weight savings have had proportionately less development and testing so that the more favorable cost and weight estimates of these designs must be accepted with less confidence.

Active work on trough type concentrators has been recently confined to three companies: Boeing, Westinghouse, and Hoffman Electronics. The present state and prospects for their designs have been ascertained from technical papers, reports and personal inquiry. Models of each of these three designs are planned to be tested by the MSC Direct Conversion Power Section under simulated space conditions.

The Boeing Company has built a trough concentrator array for JPL under Contract No. NAS 7-100. This array of 18.7 square feet weighed only 14.61 pounds and was designed to be used ultimately with the Mariner spacecraft. The theoretical value of concentration ratio is 1.90; the value measured was 1.89. As regards temperature, the design was optimized for the Mars mission. In earth orbit, due to increased temperature arising from the earth's proximity, the Mars design would incur an area penalty of about 40 percent over that of a flat panel.

Since the efficiency of a solar cell decreases with increasing temperature and since concentrated sunlight tends to raise the temperature, there is a point where increased concentration may actually produce less output. A means of cooling is essential if the benefits of concentration are to be preserved. In principle, if the reflectors can be made efficient radiators, it is possible to increase light concentration with negligible increase of solar cell temperature. As a first step, a small scale concentrator is used to shorten the heat conduction path between the solar cell and its radiator. Next the emissivity of the reflector must be increased.

The effect of reflector emissivity on concentrator efficiency for the Boeing design is as follows: the Mars design with an emissivity of 10 percent would entail a 40 percent area and weight penalty in earth orbit. At 30 percent emissivity the penalty is only 30 percent and at 80 percent emissivity the penalty is only 7 percent. The Boeing Co. feels confident, however, that 80 percent emissivity can be achieved by application of suitable coatings on their aluminum reflectors.

The Boeing design uses slightly curved reflectors to increase misorientation tolerance; the loss in output follows the cosine law out to 10 degrees of misorientation, after which it drops abruptly.

The present Boeing design uses a trough base width of about 2 cm in which two solar cells are laid side by side in pairs. The overall height is $1\frac{1}{4}$ inches and the array can readily be wrapped around a 30-inch radius. The substrate is made of a continuous sheet of polished aluminum 0.010 inch thick with stiffeners spotwelded across the troughs.

The Hoffman concentrator array was developed by Hoffman Electronics as a team member on several S&ID space station proposal efforts. As such it was directed from the start toward earth orbit space station applications. Three square feet of this array with a theoretical concentration ratio of 2.6 (2.39 effective and verified in test) were built. The design weight of this array using honeycomb core construction was 1.45 pounds per square foot. An improved design using a core of sheet metal formers is stronger, stiffer and has been weighed out at 1.0 pounds per square foot.

Like the Boeing array, the Hoffman design is a trough type. The principal differences in optical geometry are a higher concentration ratio (entailing an overall height of 2 inches), and a misorientation tolerance of only ±7.5 degrees (as against 10 degrees for Boeing) achieved by overheight rather than by curved reflector surfaces.

Physically, the principal difference between the Boeing and Hoffman concentrator is the use of silvered glass mirrors rather than polished aluminum. The glass used is the same used on solar cells as filters and performs the same function; i.e., it is a highly efficient radiator of heat having an emissivity of 0.83. The solar cell temperature of the Hoffman design in earth orbit is calculated to be a maximum of 65 C.

The Hoffman design manages to avoid the loss due to inactive areas of the solar cell. The mirrors, installed after the solar cells, overlie the inactive contact area for a gain of 5 percent. The 1 x 2 cm solar cells span the trough base 1.9 cm in width. The overall width of a trough is 2 inches.

The individual trough lengths are manufactured and tested separately and assembled into an array by being hinged together at the peak of the trough. Thus these arrays are well adapted to being wrapped about a body of any reasonable radius with only the weather side exposed.

Although silvered microsheet, used in the Hoffman design, is an ideal reflector-radiator combining the highest reflectivity (silver) with the highest emissivity (microsheet) available, it does have some problems. First, there is the weight of the glass mirrors, about 0.2 pounds per square foot of array including adhesive. The mirrors also have a tendency to crack with a rise in temperature due to expansion of the aluminum backing. Several remedies have been proposed for mirror cracking: assembly at high temperature, fire polishing of the glass edges, use of smaller mirror sections and the use of a Kovar rather than aluminum backing. None of these methods have, however, been tried.

Hughes Aircraft is actively pursuing the development of a flexible array concept called LASCA (Large Area Solar Cell Array). One by two cm solar cells are connected in flexible cell assemblies of approximately seven cells in parallel. The cell assemblies are bonded either to Dupont H-film, a 2 mil thick glass reinforced polyamid — or to Tekonic EX317, a 1 mil glass reinforced teflon. The tensile strength of the latter material is 34 pounds per lineal inch. The assembled flexible array can be wrapped about an 8 inch diameter with an interweaving layer of foam cushion. This stowed configuration is highly resistant to vibration and acoustic noise. Life tests on flexing small sections of array show no cell breakage and even 2 x 2 cm solar cells appear to be of no problem. The wire loop cell assembly interconnections have successfully withstood more than 200,000 bending cycles on a 4-inch radius.

A disadvantage of the flexible array is the wider cell spacing required to obtain flexibility so that only 270 to 300 solar cells per square foot can be accommodated as against 400 per square foot for a rigid substrate. This lower packing factor may however contribute to a lower solar cell temperature in space since the ratio of radiating to absorbing area is increased. In any case, the area penalty over a rigid panel is likely to be about 30 percent. This area factor must be taken into account in making weight comparisons with a rigid panel. The estimated weight is quite low, only 0.5 pounds per square foot of array.

The third type of array considered, the conventional rigid panel can be made with a weight below one pound per square foot. It is difficult to reduce the weight much further than present technology since the solar cells, filters and wiring alone will weigh about 0.5 pounds per square foot. An example of a light weight panel is the Ryan Mariner/Mars class, qualified for Atlas Agena Launch. The weight of this panel is 0.58 pounds per square foot including hinges, actuator fittings and antenna mounts. With the thinner and lighter solar cells now available, the assembled weight, including solar cells is very nearly 1 pound per square foot. The light weight construction does require deeper spars, however, so that the overall thickness of this panel is several inches.

Solar Array Selection Factors

If the factors entering into the determination of optimum array type are extremely complex, involving as they do solar array costs, launch costs due to weight, the effects of area on orbit lifetime, and requirements for deployment and orientation — these factors also are so interacting that their direct benefits are usually offset by indirect effects. In short, no factor seems to be particularly sensitive and an optimum design point is not particularly critical. Thus, for example, though a concentrator array uses only one-half the solar cells required by a conventional array, the cost saving is not 50 percent if launch costs are taken into account. The launch cost of a solar cell in a conventional array exceeds the cost of the solar cell; in a concentrator array the launch cost per solar cell will at least double. If the price of solar cells decline, as it appears they will, concentrator arrays will appear even less attractive as compared to conventional arrays.

Some of these relationships are brought out in Table 15 where launch costs of $1000.00 per pound were added to the price of solar cells assuming 1.6 pounds per square foot both for conventional and concentrator arrays. Four hundred cells per square foot were assumed for the conventional array and 175 for the concentrator. The only costs considered were solar cell and launch costs; costs of assembly and of other components were not taken into account. Assuming that these latter costs do not depend on solar cell efficiency, we obtain a valid curve for the cost of either array as a function of solar cell efficiency (but not a valid comparison of concentrator versus conventional panel costs). Based on present day solar cell prices, the lowest cost conventional array is one made with 9 percent cells, whereas the concentrator array optimizes at a little over 10 percent.

As one would expect, the present day solar cell price curve, which rises steeply at 12 percent, would simply readjust itself should a demand for 9 percent solar cells arise since present day prices are based on a demand centered at 11 percent. It costs just as much to make a 9 percent cell as it does a 12 percent one and when cells are bought by substantially a single customer, he will have little choice but to pay for all cells produced regardless of price structure.

If area drag penalties had been taken into account, the minimum cost point would have shifted upward, perhaps to a 10 percent cell for a conventional array and a 11 percent cell for a concentrator array. As regards the costs of other components, such as filters, panels, concentrators, and cost of assembly, those costs associated directly with the solar cell, such as filters, would tend to make conventional arrays more expensive because a larger number of them are required. This factor is likely to offset any reasonable estimate of the higher cost of a concentrator array due to its greater complexity. Thus, in Table 16 are added to Table 15 a fixed cost of $2.50 per solar cell for filters, substrate, and assembly and an additional $175.00 per square foot for the concentrator substrate.

CON[redacted]

Table 15. Cost vs. Solar Cell Efficiency For Conventional And Concentrator Arrays

Solar Cell Efficiency (Percent)	Solar Cells Only			Conventional Array			Concentrator Array		
	mw/1x2 cm cell at 28 C AMO	Cost/ cell, 1964 large quantity prices	price/ mw	price/ cell incl. launch cost at $1000/lb	mw/1x2 cm cell in orbit	price/mw in orbit	price/ cell incl. launch cost at $1000/lb	mw/1x2 cm cell in orbit	price/mw in orbit
8	19.6	$1.50*	$0.076	$ 5.10	17.8	$0.286	$10.50	38.5	$0.273
9	22.0	2.00*	0.091	5.60	20.0	0.280	11.00	43.3	0.254
10	24.5	2.75*	0.112	6.35	22.2	0.286	11.75	48.0	0.245
11	27.0	4.30	0.159	7.90	24.5	0.322	13.30	53.0	0.251
12	29.4	7.00	0.238	10.60	26.7	0.397	16.00	57.7	0.277

*To the extent available as a by-product of the production of more efficient cells

~~CONFIDENTIAL~~

Table 16. Cost Comparison, Conventional Versus Concentrator Arrays with Solar Cell Efficiency

Solar Cell Efficiency Percent	Cost of Conventional Array in Orbit, per milliwatt	Cost of Concentrator Array in Orbit, per milliwatt
8	$0.426	$0.364
9	.405	.335
10	.398	.318
11	.384	.317
12	.490	.398

In this instance, the optimum point for both arrays is shifted upwards to a 11 percent solar cell design, the concentrator retains a cost edge but it is not great: $317.00 per watt in orbit as against $384.00 for a conventional array.

The expected trend of solar cell prices will make concentrators somewhat less advantageous. Estimates of the price of an 11 percent solar cell procured in large quantities in 1969-70 range from $1.85 to $2.50 each, compared to today's price of from $4.00 to $5.00. Thus, it is not as economical as formerly thought to use solar cell concentrators in space; the solar cell is indeed expensive, but still, when all costs are considered, it alone represents less than a third of the total cost of an array.

Although, on the basis of the foregoing cost analysis, the advantage of a concentrator array over a conventional array is not decisive, it is well to remember the assumptions on which it is based. The first of these, regarding weight and launch cost, essentially penalized either type of array a fixed launch cost of $1600 per square foot (from 1.6 pounds per square foot and $1000 per pounds). If the vehicle is not weight limited and in fact no cost saving can be realized by reducing launch weight, then this penalty disappears. A concentrator array would then appear to be more attractive. If the weight and cost associated with a solar cell increase, as would happen if 60 mil quartz filters were prescribed for radiation protection, then the conventional array would be heavily penalized since it would use more than twice the number of these heavier and more expensive components. Any factor, on the other hand, tending to reduce the cost and weight associated with each solar cell would further decrease any advantage that a concentrator array may have had. Trends in cell-associated costs are discussed in the following paragraphs.

Cell-Associated Cost Trends

Several factors have combined recently to reduce the cost of solar cells. First, the cost of the raw material silicon of solar cell grade has dropped to about $10.00 per pound. This price, a temporary market low, is not likely to drop further. A second factor in cost reduction has been the adoption of the sintered electrical contact and grid in preference to solder. This contact is much more reliable than the solder connection and has eliminated the variation in series resistance that prevailed with solder contacts and grids. The principal effect has not been a reduction in the cost of fabrication — this is higher — but an improvement both in yield and efficiency. The mean of solar cell efficiency has advanced to 11 percent from the previous 10 percent. The cost of fabrication is increased since the solar cells must be polished in preparation for vacuum deposition of titanium and silver prior to sintering.

A secondary cost reducing effect of sintered contacts is the lower weight per cell in the absence of solder. Thus, a 0.015 inch thick 1 x 2 cm solder-less solar cell weighs only 0.18 grams compared to 0.25 grams. Cell thickness may be reduced to 0.012 inch for further weight saving.

With regard to solar cell filters for solar arrays to be used for manned space application, the requirement for radiation protection can be dismissed since the radiation exposure threshold for biological injury is far lower than it is for solar cell degradation. Thus, the conventional 6-mil thick Microsheet UV filter should be adequate for the purpose. The present price of a standard Microsheet filter is about 50 cents each and is not expected to drop below 40 cents each in the 1969-70 period. In other words, the cost of the filter will be a substantial fraction of the cost of the solar cell it cools.

Prospects for reducing solar cell filter costs lie in determining the optimum filter characteristics, an extremely complex problem which must take into account the solar cell spectral sensitivity, the spectrum of AMO (air mass zero) sunshine, the anticipated orbit environment, the solar array thermal characteristics and, what is most crucial, the effect of these factors on solar cell temperature. It is well known that solar cells rapidly degrade in efficiency with temperature rise. It is the purpose of the solar cell filter to absorb little energy to which the cell is insensitive and to be an efficient radiator of heat, for such energy absorbed raises the solar cell temperature and reduces its efficiency at all wavelengths.

Currently, the solar cell filter response is optimized by the mathematically simplifying assumption that the filter response curve is rectangular; i.e., having a sharp cut-on and cut-off wavelength. The optimizing computer program adjusts cut-off and cut-on frequencies, computes temperature and power output and searches for the optimum.

The objections to the simplifying assumption of rectangular filter response are the following:

1. The optimum response is probably not rectangular but may show a gradual transition from stop-band to pass-band.
2. The rectangular characteristic is very difficult to obtain and requires many (about 20) superimposed vacuum deposited dielectric layers.
3. The rectangular characteristic is extremely critical and requires close tolerances in fabrication; consequently, production yield is low.
4. The rectangular optimum may also be critical in its effect on the solar cell and this may explain why filters with apparently identical characteristics show substantial differences in effect when applied to the same solar cell.
5. A smooth response curve, if it is optimum, would be cheaper to produce, be less critical, and yet more efficient than the rectangular response curve.

It appears that an economically significant improvement in the performance and cost of the solar cell filter can be achieved with a moderate investment in more sophisticated computer optimization; for example, using the technique of dynamic programming.

Weight, Area and Cost Comparisons of 4 KW Arrays

The data presented in Tables 15 and 16 can be used to derive estimates of area, weight, and cost for the 4 KW array required by the prolonged mission Apollo. Minimum cost was obtained using 11 percent solar cells for both the conventional and the concentrator array. A comparison between the two types of solar array at the point design of 4 KW using 11 percent cells is given in Table 17.

Table 17. Comparison of 4 KW Conventional and Concentrator Arrays

	Conventional Array	Concentrator Array
Cost per array	\$886,000	\$568,000
Number of solar cells	163,200	75,400
Area	408 sq. feet	432 sq. feet
Weight	650 lb	700 lb
Thickness	1 inch	2 inches

The assumptions upon which this comparison are based should be reviewed:

1. The use of 1 x 2 cm N/P 11 percent silicon solar cells at projected prices
2. The use of standard 6 mil microsheet glass slips at 50 cents each
3. Four kilowatts to be delivered at maximum temperature of array in a 260 n.m. earth orbit
4. Both types of array figured at 1.6 pounds per square foot based on present experience. This weight is to be considered an upper limit for either design and includes wiring, fittings, and associated structure

The principal factor which may modify the estimates in Table 17 for the 1969-70 time period, is a further decline in the price of a solar cell in large quantity production. Such a price cut would further undermine the reason for using a concentrator array, the "high cost" of solar cells, and reinforce the conclusion that the conventional solar cell array is competitive on a cost basis with other power sources for the Prolonged Missions Apollo laboratory.

SOLAR ARRAY - SPACECRAFT MECHANICAL INTERFACES

Beside the electric power subsystem there are three mechanical interfaces that must be resolved to fully integrate a solar array into a spacecraft design. These are stowage for launch, deployment and orientation. Several concepts of solar array and spacecraft integration are shown in Drawings 5177-107B, 5177-108B, and 5177-113. If the array is to be part of the Apollo Service Module, a very large and adequate array, of either the concentrator or conventional type can be stowed within the shelter of Sectors 1 and 4 as shown in Drawing 5149-14B. (Originally shown in SID 63-1370-4 Extended Mission Apollo). Further, it would not be difficult to deploy such an array or to orient it about one axis with respect to the service module after deployment. However, there is one strong argument against installing solar arrays on the service module exclusively and that is, for every return trip of personnel to earth one must sacrifice a 4 KW solar array. There may be some advantage to installing a smaller array on the service module for redundancy, or backup of other power sources, but this is another consideration altogether. The ensuing discussion will therefore be restricted to integration of the solar array with the portion of the vehicle that stays in space, i.e., the prolonged missions Apollo laboratory.

Stowage of the Solar Array for Launch

Most of the preliminary study configurations for the Apollo orbital research laboratory have a major outer surface that is a section of a cone because the laboratory in these configurations is an adaption of the Spacecraft LEM Adaptor. A solar array design that could be stowed upon a conical surface would therefore incur a minimum of interface problems with the laboratory. Such a concept was previously developed for the Extended Mission Apollo laboratory and the layout of this solar array is shown in SID 63-1370. The array consisted of 2 X 2 inch Hoffman type concentrator modules stowed so that each lies on an element of the cone and deployed into a fan shaped plane figure. A similar concept is advantageous for a conventional solar array. As a fundamental building block for this array, a rectangular module 1 X 3 inches in cross section and 120 inches long is shown in Figure 55. The basic components of an array module are the substrate, the solar cell submodule, and the associated wiring and hardware.

The module substrate would be a fully skinned (for stiffness) aluminum honeycomb core stringer. Embedded into the honeycomb as required would be electrical terminal inserts and attachment fittings. Since the stringers will be assembled side by side into an array it may be advisable to use one of the cross sections shown in Figure 56 to allow space for wiring. Of the three configurations shown, the chamber (a) and the taper (b) would present difficulty in bonding the honeycomb core to the sides, whereas configuration (c) would allow a very satisfactory close out of the sides and provide clearance for cabling. Either extrusions or roll-formed aluminum alloy sheet could be used for the sides.

~~CONFIDENTIAL~~

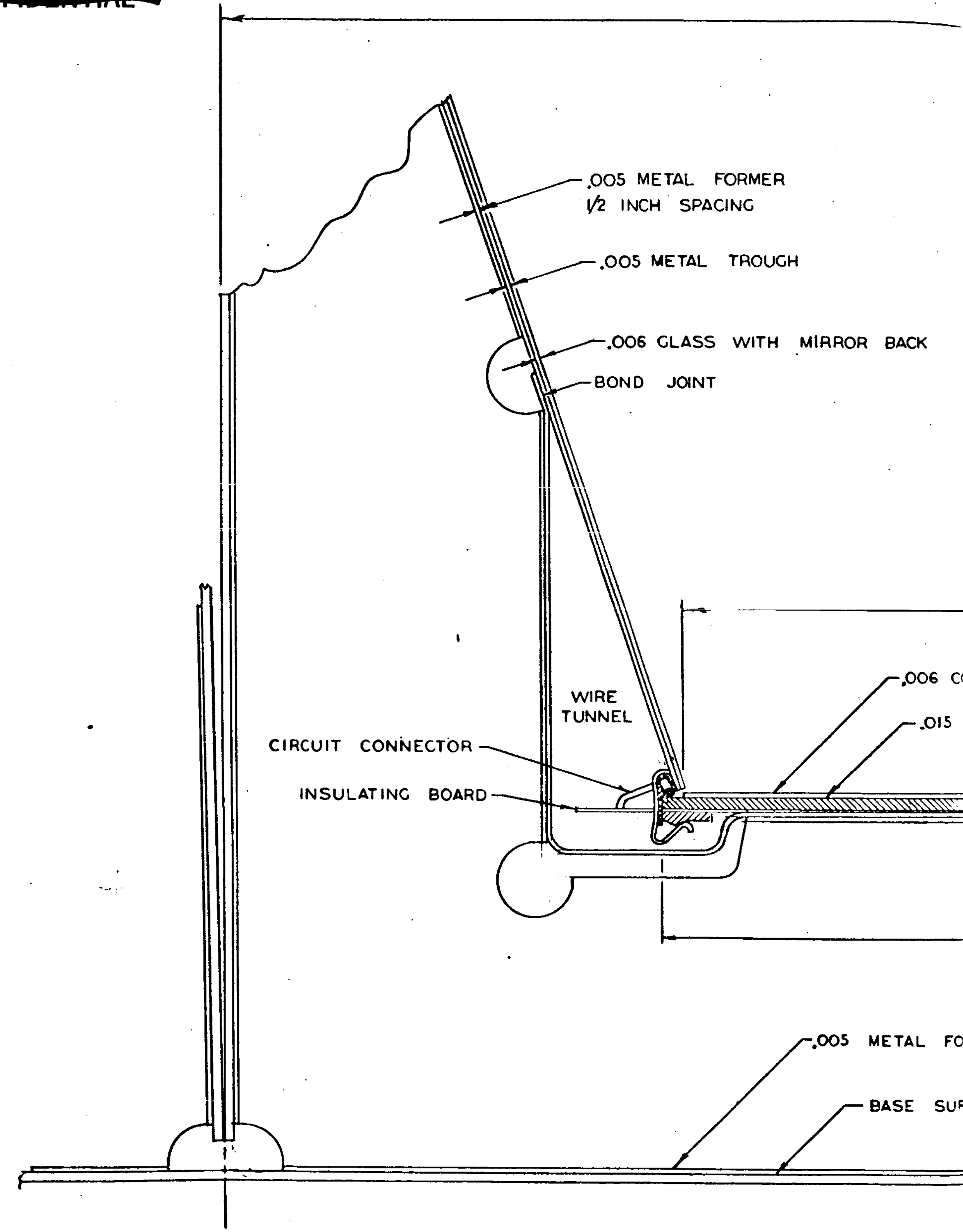
.005 METAL FORMER
1/2 INCH SPACING
.005 METAL TROUGH
.006 GLASS WITH MIRROR BACK
BOND JOINT
.006 C
.015
WIRE TUNNEL
CIRCUIT CONNECTOR
INSULATING BOARD
.005 METAL FO
BASE SU

DETAI
TEN TIMES F
SECTION THROUGH

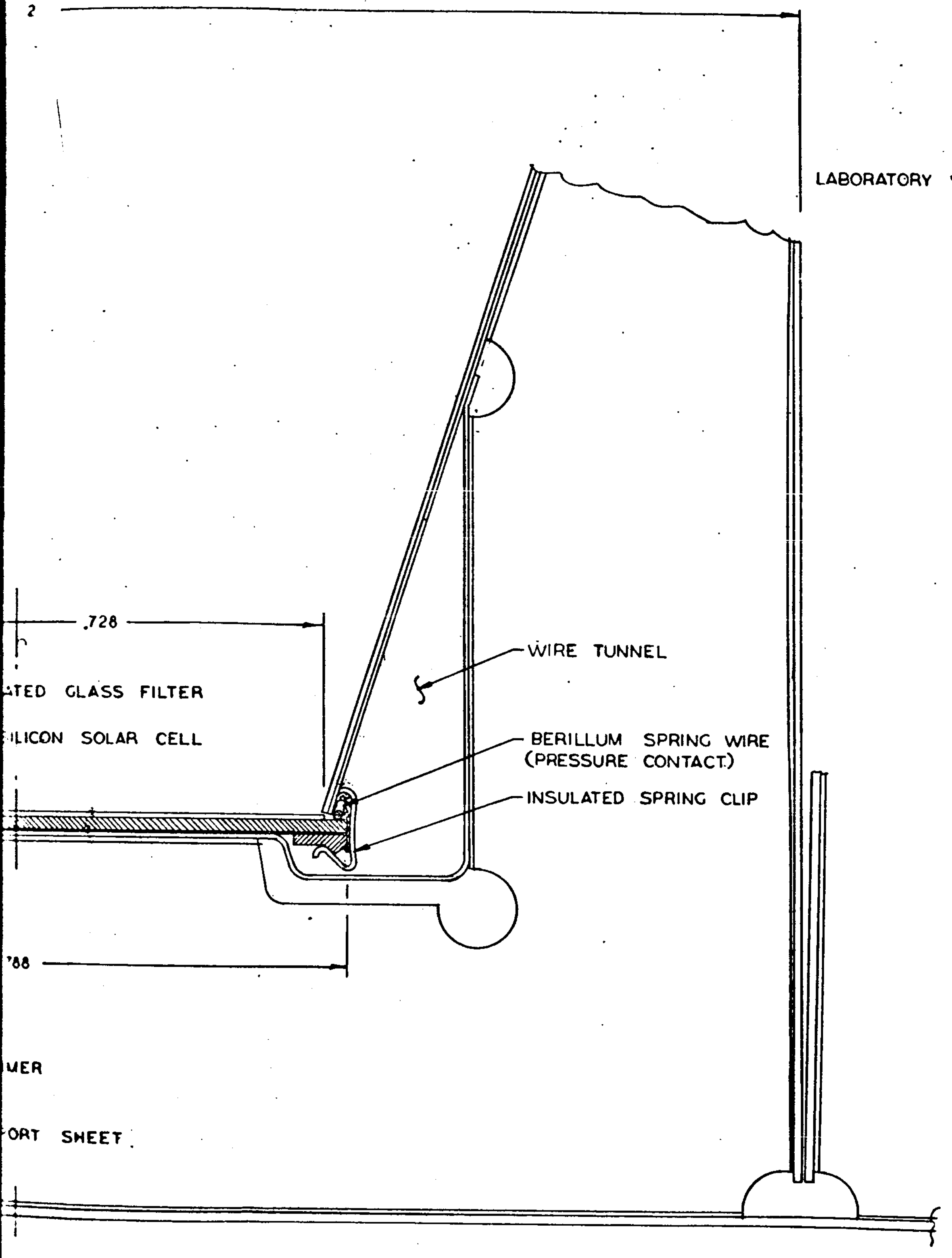
2
LABORATORY
.728
TED GLASS FILTER
ILICON SOLAR CELL
WIRE TUNNEL
BERILLUM SPRING WIRE
(PRESSURE CONTACT)
INSULATED SPRING CLIP
88
MER
ORT SHEET

B

L SIZE
CONCENTRATOR

~~CONFID~~

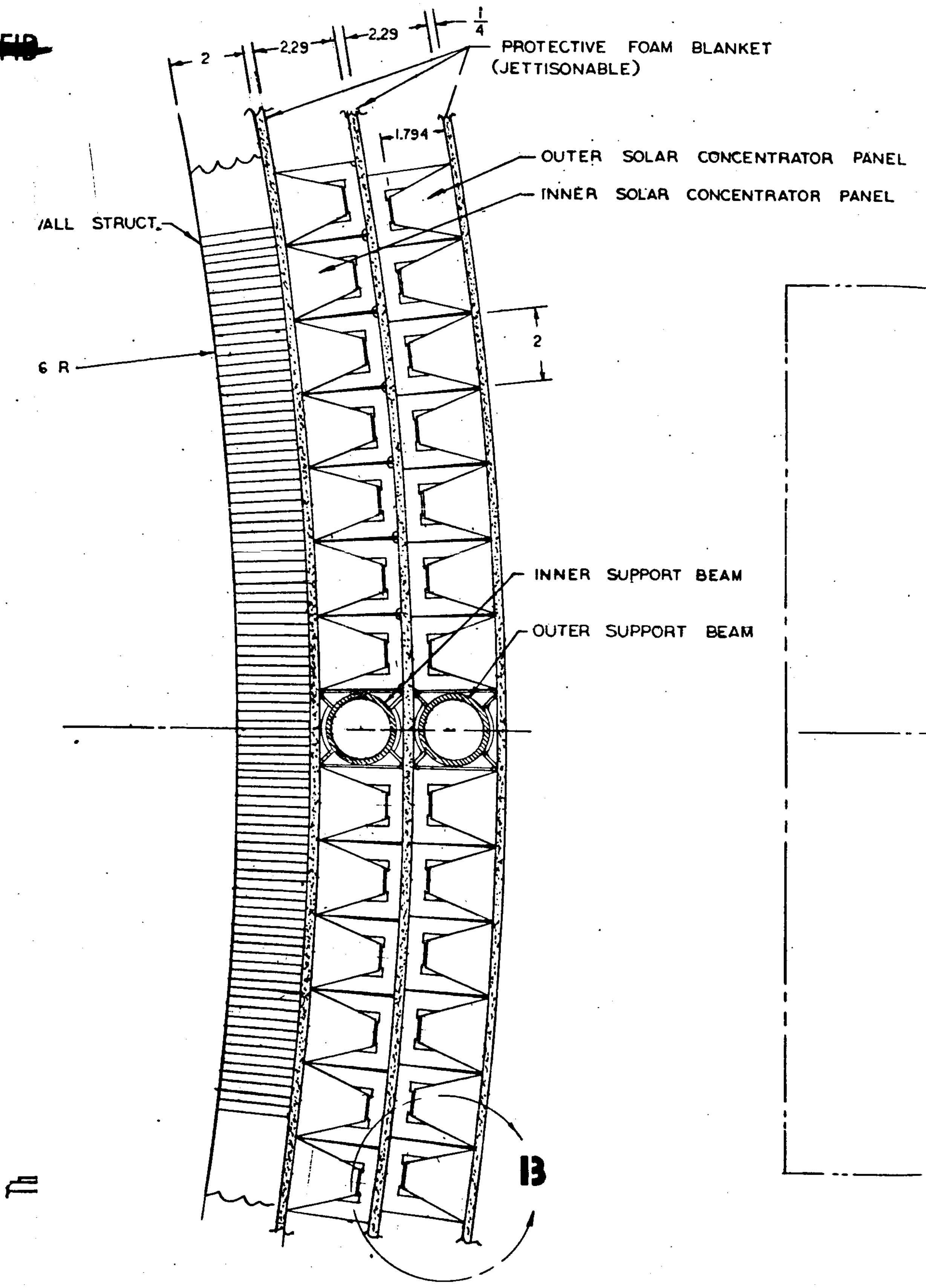
2
2.29
2.29
1/4
PROTECTIVE FOAM BLANKET
(JETTISONABLE)
1.794
OUTER SOLAR CONCENTRATOR PANEL
INNER SOLAR CONCENTRATOR PANEL
/ALL STRUCT.
6 R
2
INNER SUPPORT BEAM
OUTER SUPPORT BEAM
B

DETAIL A

HALF SIZE

SECTION THROUGH PANEL

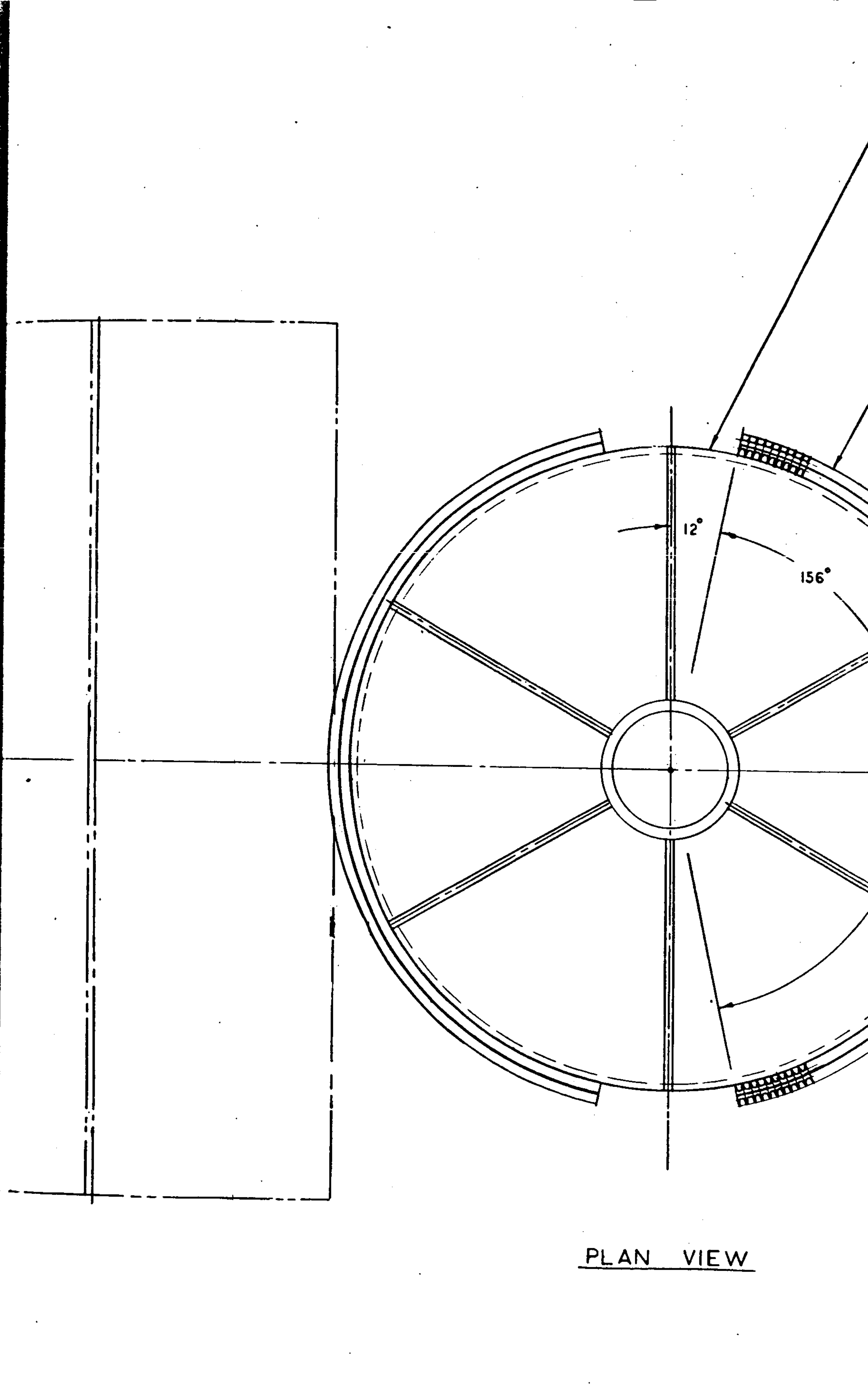

PLAN VIEW

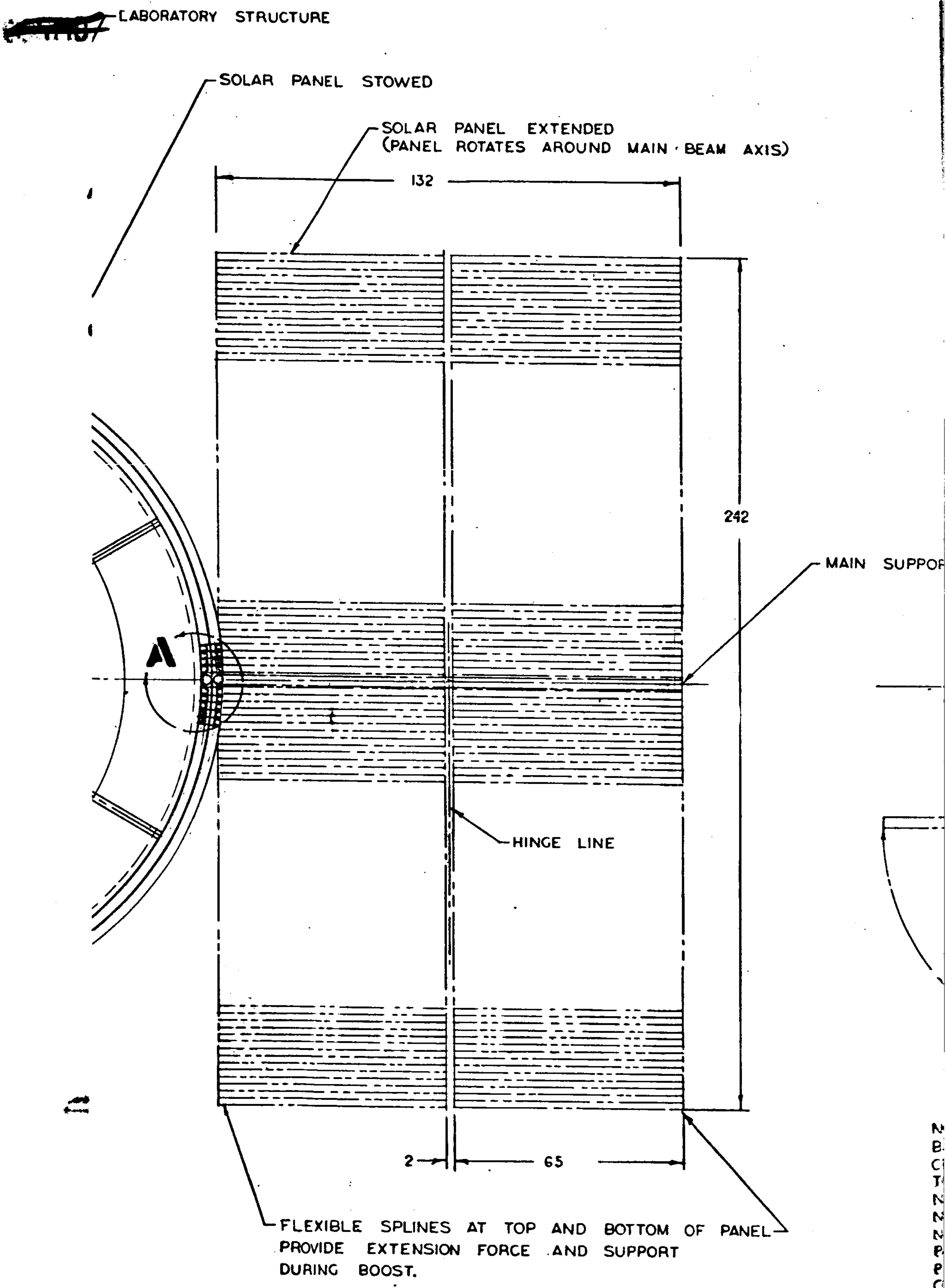
LABORATORY STRUCTURE
SOLAR PANEL STOWED
SOLAR PANEL EXTENDED (PANEL ROTATES AROUND MAIN · BEAM AXIS)
132
242
MAIN SUPPOR
A
HINGE LINE
2
65
FLEXIBLE SPLINES AT TOP AND BOTTOM OF PANEL PROVIDE EXTENSION FORCE AND SUPPORT DURING BOOST.

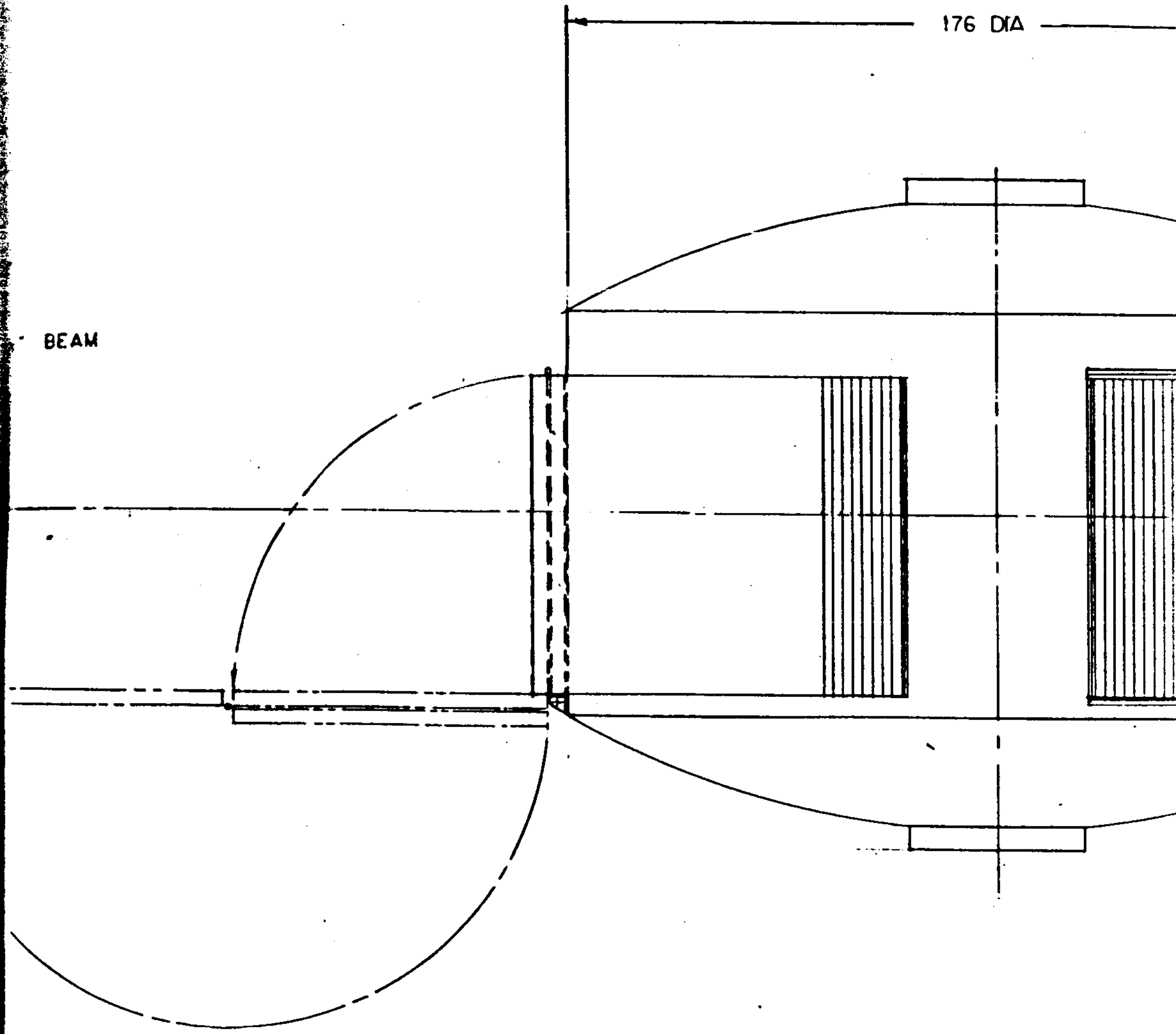

SIDE VIEW

PANEL DESIGN DATA

MINAL POWER OUTPUT	4.0 KW
SIC SILICON CELL RATING	11%
LL SIZE — 1 CM X 2 CM X .015 INCH	
TAL NUMBER OF CELLS	75,400
UMBER OF CELLS PER PANEL	37,700
UMBER OF CELLS PER TROUGH	316
UMBER OF TROUGHS PER PANEL	120
NEL ACTIVE AREA	73.25 SQ FT
NEL GROSS AREA	31,680 SQ. IN. (220 SQ. FT)
NCENTRATION RATIO	2.16/1
IENTATION TOLERANCE	± 7.5°
TIMATED PANEL WEIGHT	352 LBS / PANEL *

CLUDING SUPPORT STRUCTURE, ACTUATOR AND WIRING

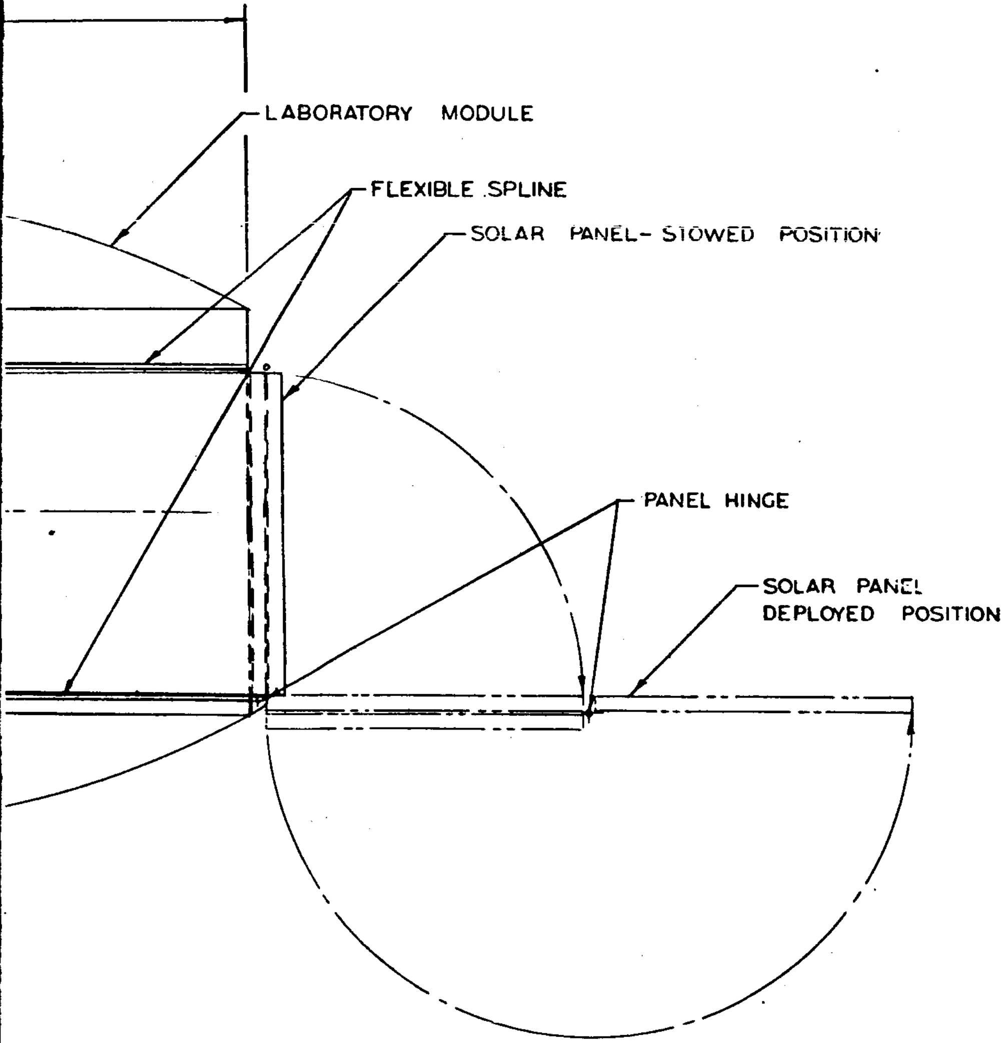
LABORATORY MODULE
FLEXIBLE SPLINE
SOLAR PANEL- STOWED POSITION
PANEL HINGE
SOLAR PANEL DEPLOYED POSITION

RE-DRAWN

A.E.SMITH
4 DEC. 64

NORTH AMERICAN AVIATION, INC.
SPACE and INFORMATION SYSTEMS DIVISION
12214 LAKEWOOD BLVD., DOWNEY, CALIFORNIA

SOLAR PANEL- CONCENTRATOR
ARRANGEMENT - 4 KW OUTPUT

5177-107 B

~~CONFIDENTIAL~~

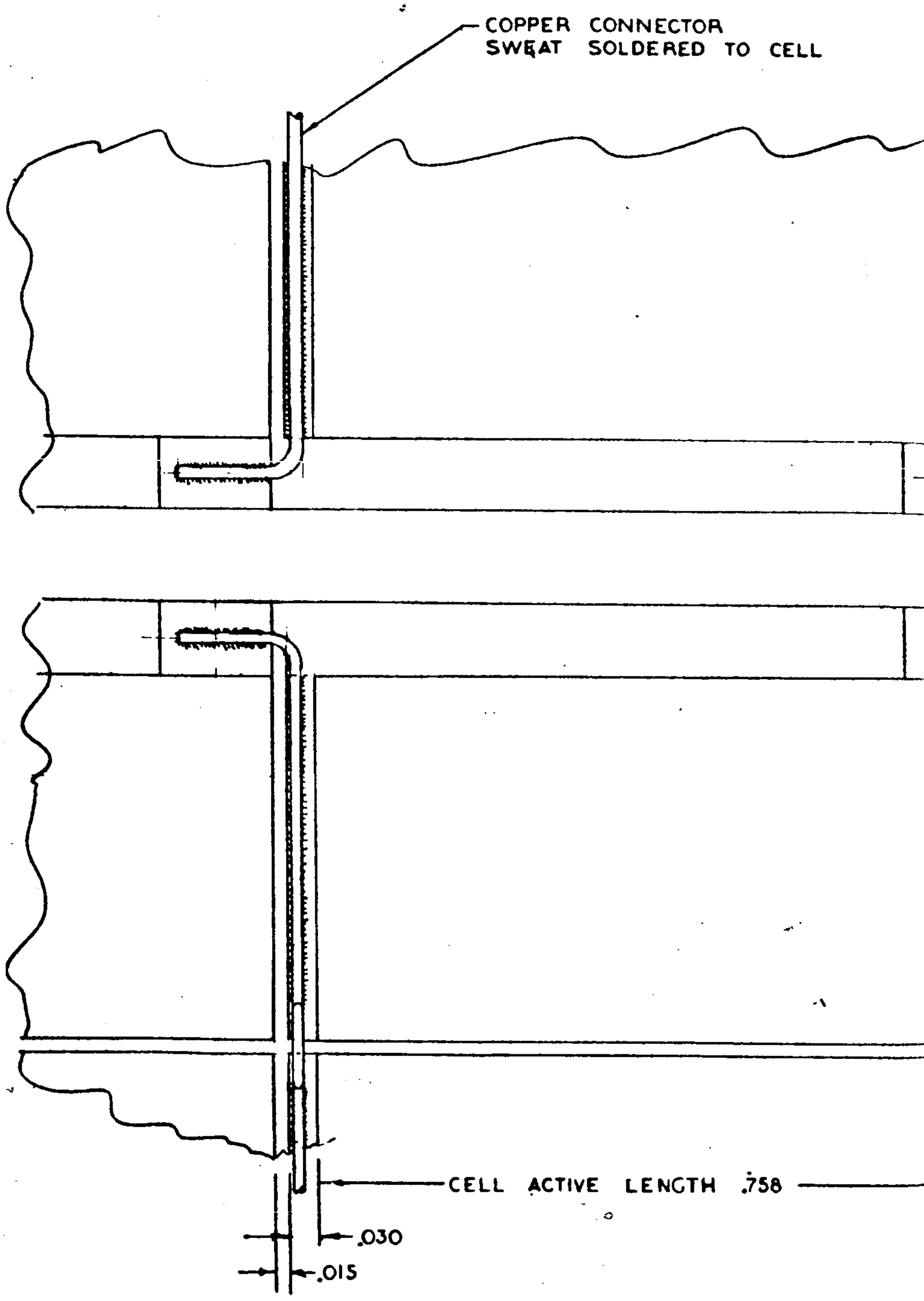
COPPER CONNECTOR
SWEAT SOLDERED TO CELL
CELL ACTIVE LENGTH .758
.030
.015

DETAIL C TEN X

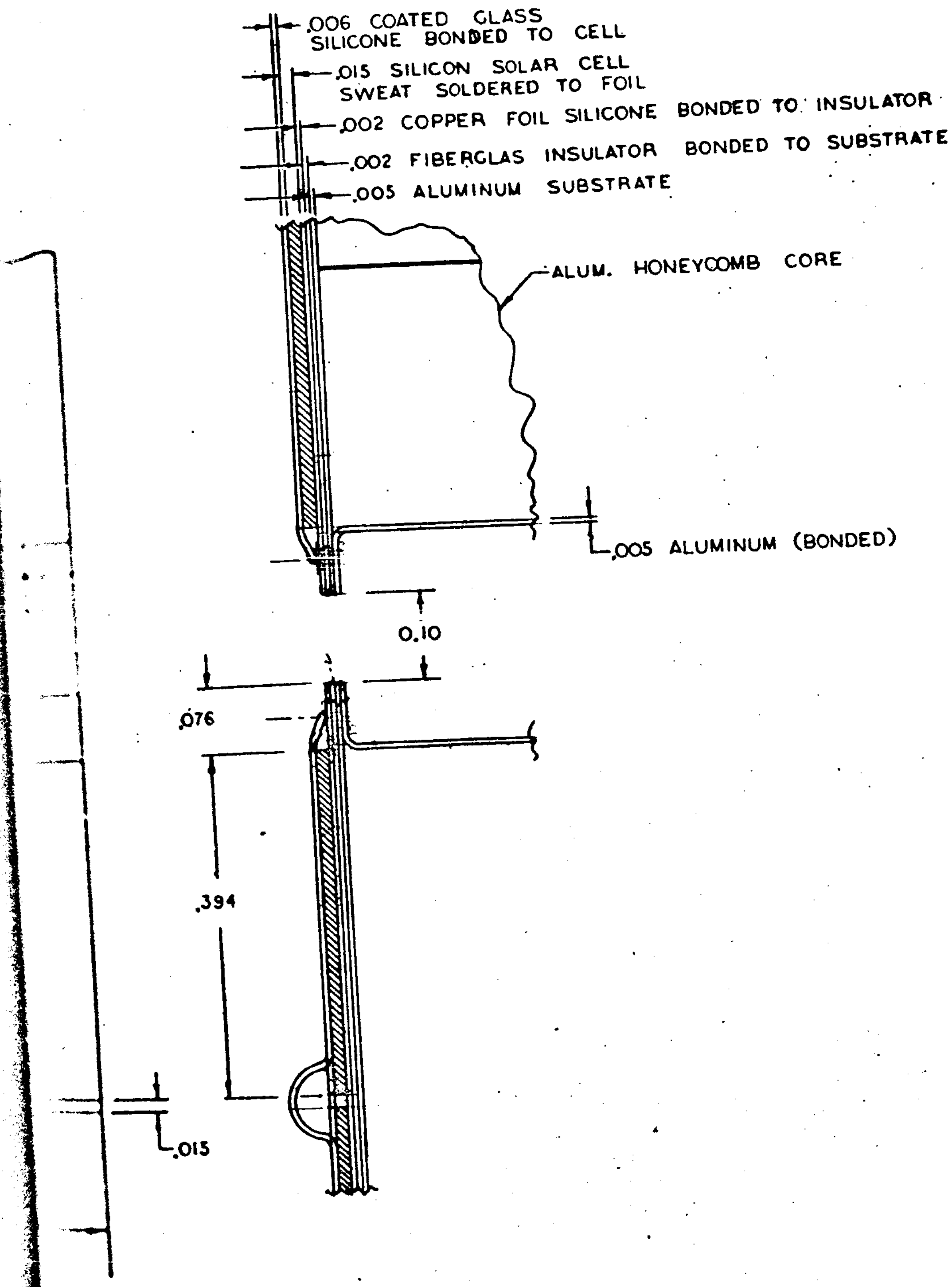
.006 COATED GLASS SILICONE BONDED TO CELL
.015 SILICON SOLAR CELL SWEAT SOLDERED TO FOIL
.002 COPPER FOIL SILICONE BONDED TO INSULATOR
.002 FIBERGLAS INSULATOR BONDED TO SUBSTRATE
.005 ALUMINUM SUBSTRATE
ALUM. HONEYCOMB CORE
.005 ALUMINUM (BONDED)
0.10
.076
.394
.015

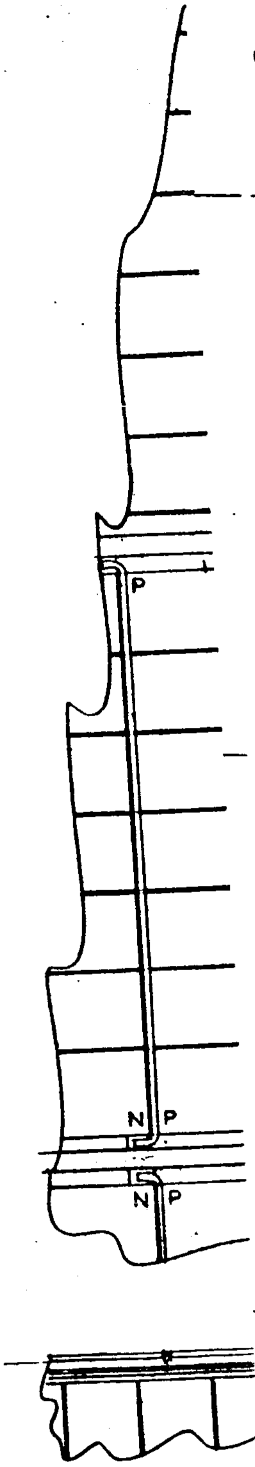
P
N P
N P

SIZE

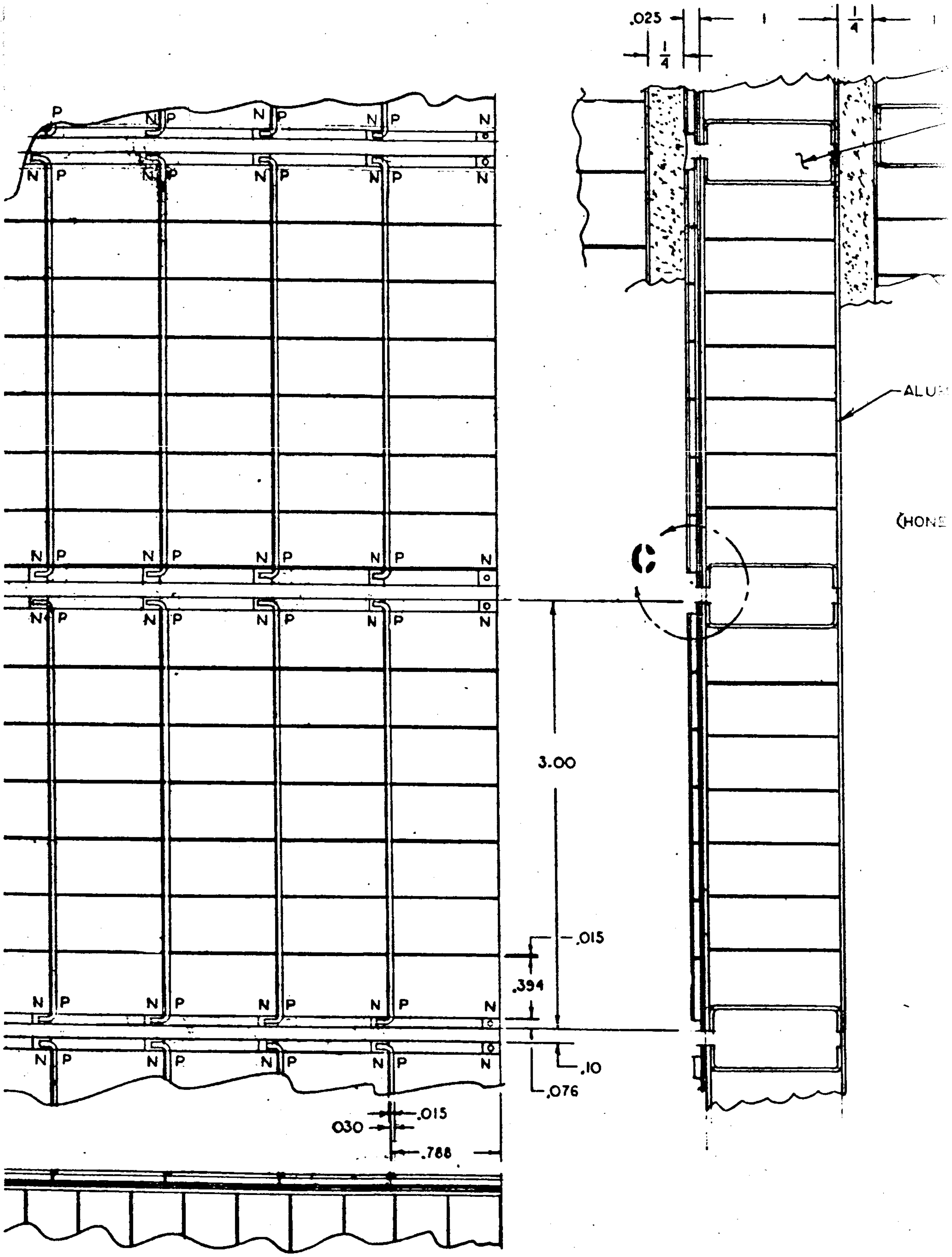
.025
1/4
1
1/4
1
N
P
C
3.00
.015
.394
.10
.076
.015
030
.788
ALU
(HONE

DETAIL B TWICE FULL SIZE

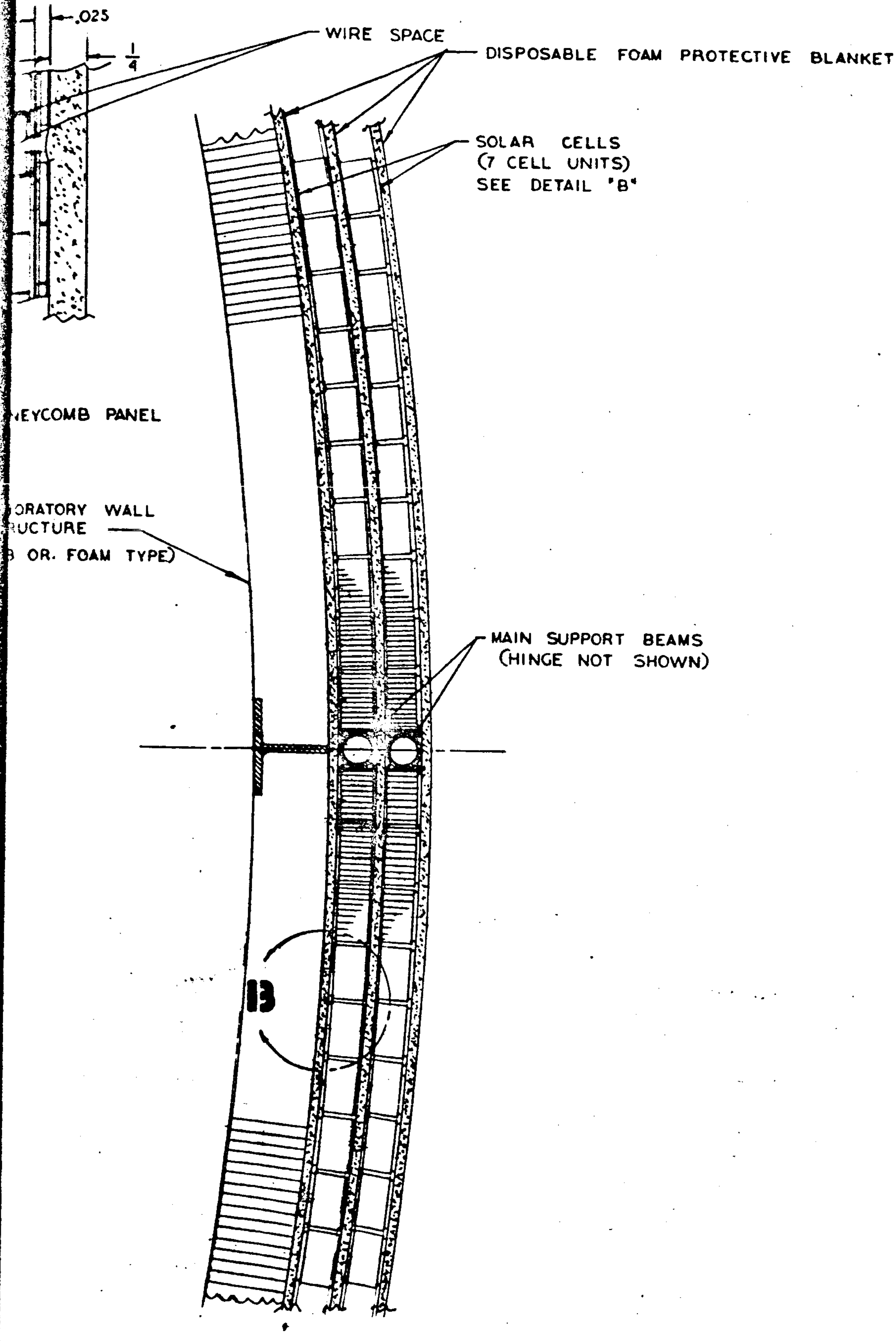
.025
1/4
WIRE SPACE
DISPOSABLE FOAM PROTECTIVE BLANKET
SOLAR CELLS
(7 CELL UNITS)
SEE DETAIL 'B'
EYCOMB PANEL
ORATORY WALL
UCTURE
OR. FOAM TYPE)
MAIN SUPPORT BEAMS
(HINGE NOT SHOWN)
B

DETAIL A HALF SIZE

TYPICAL SECTION THRU PANEL

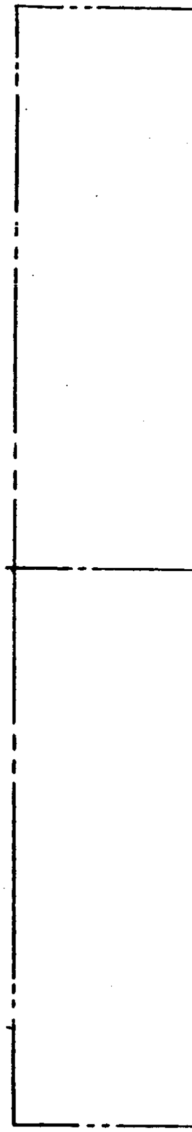

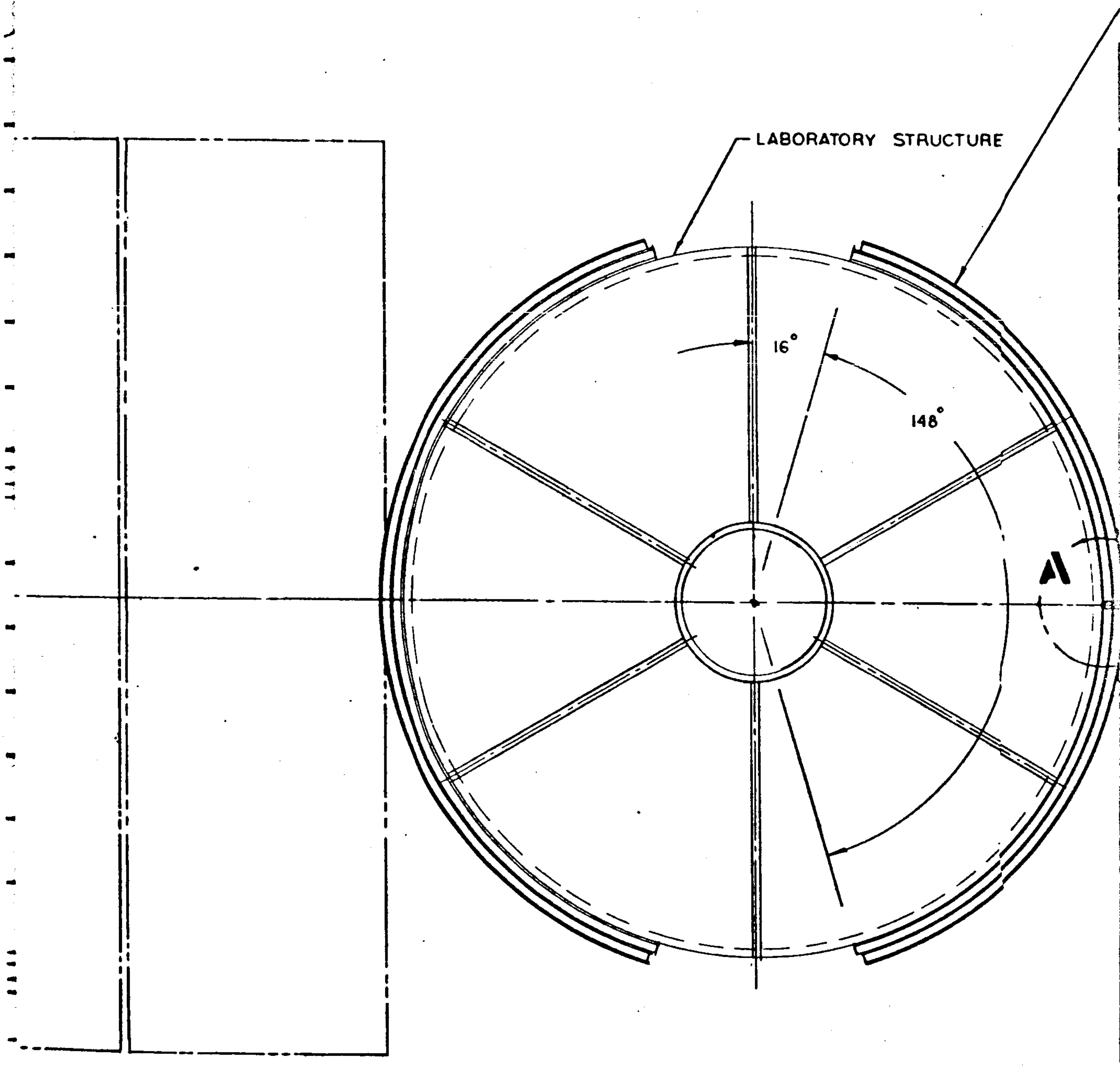
LABORATORY STRUCTURE
16°
148°
A

PLAN VIEW
1/20 SIZE

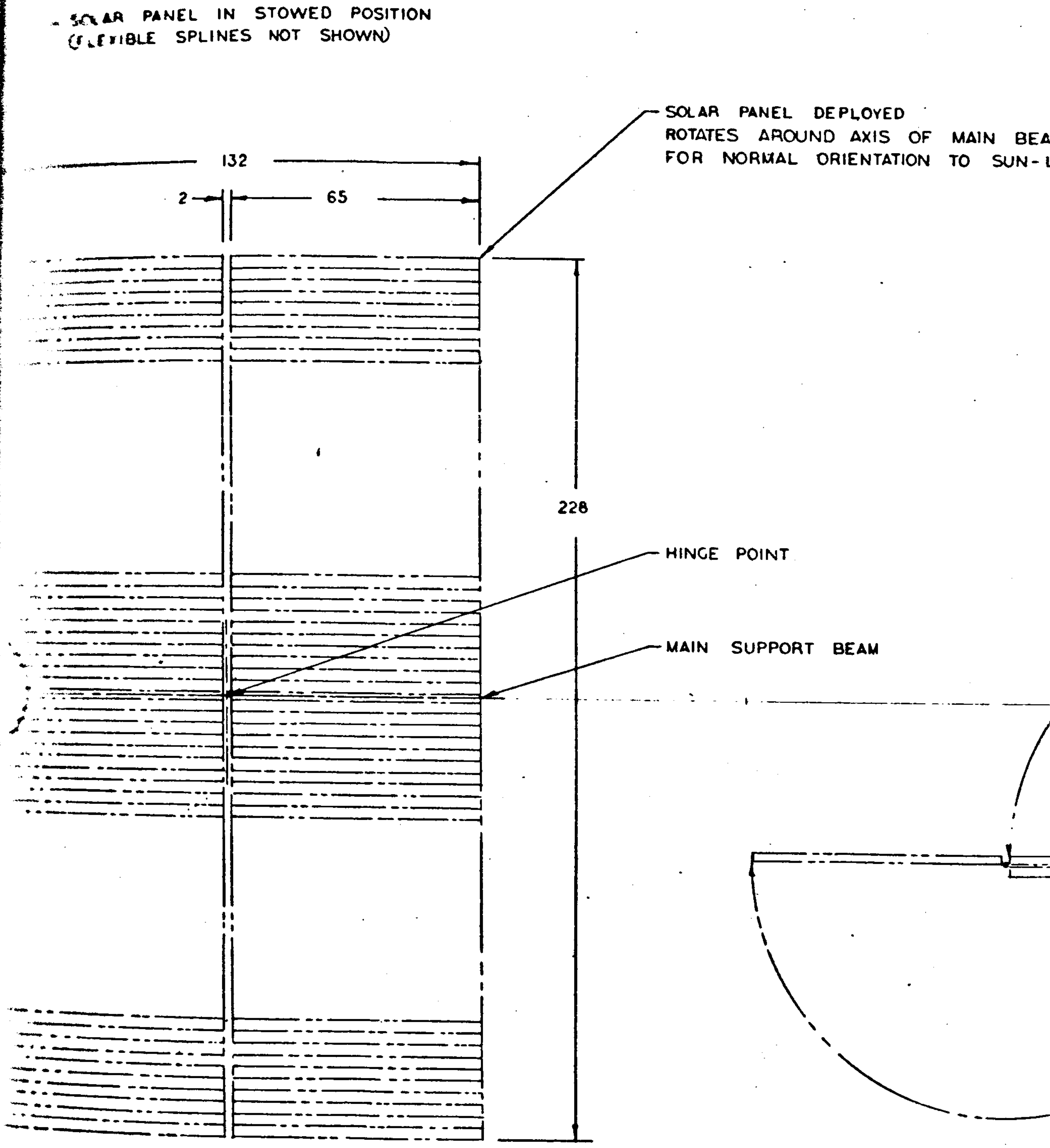
SOLAR PANEL IN STOWED POSITION
(FLEXIBLE SPLINES NOT SHOWN)
132
2
65
SOLAR PANEL DEPLOYED
ROTATES AROUND AXIS OF MAIN BEA
FOR NORMAL ORIENTATION TO SUN-
228
HINGE POINT
MAIN SUPPORT BEAM

CONFI

NF

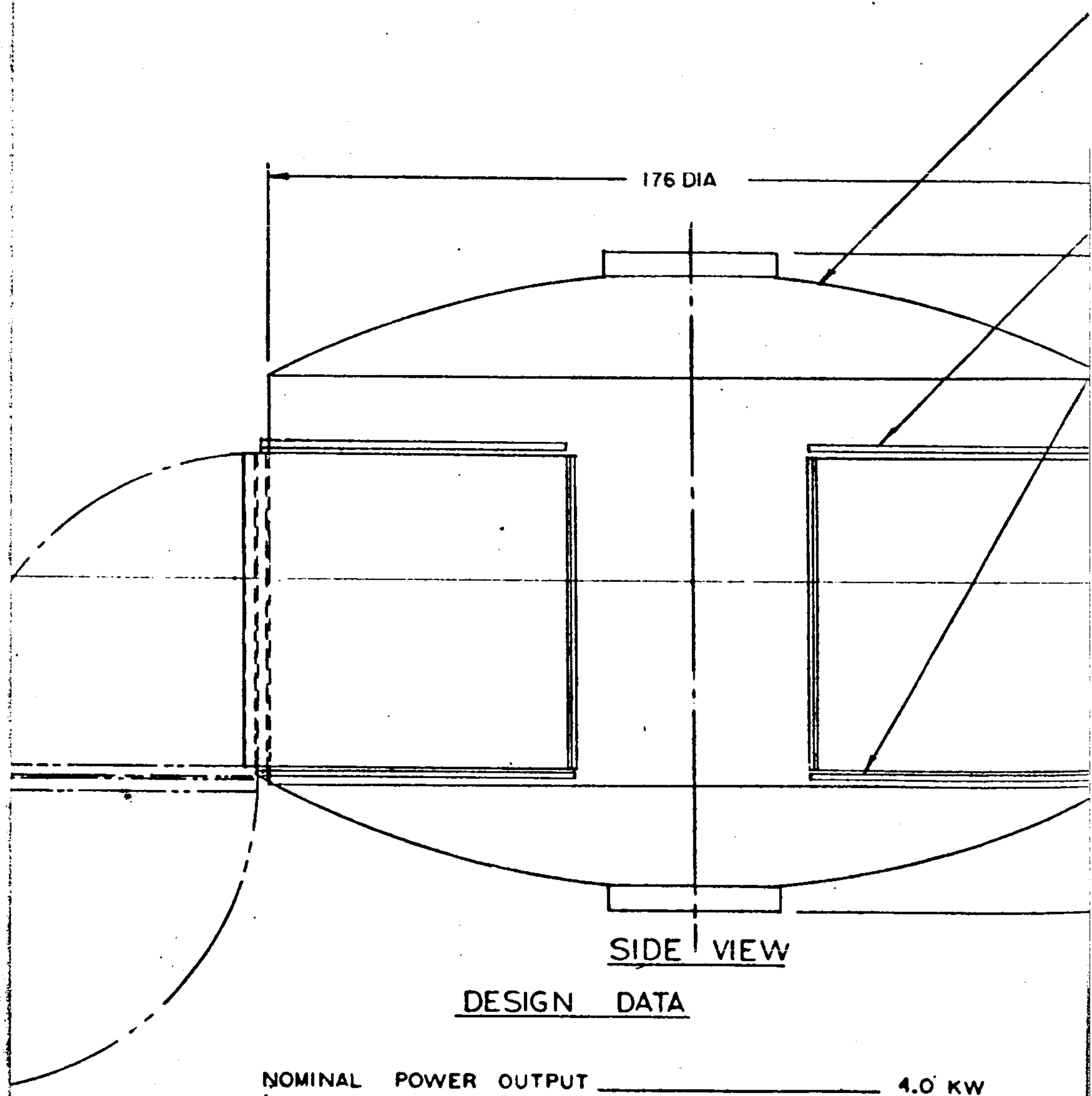

SIDE VIEW

DESIGN DATA

NOMINAL POWER OUTPUT	4.0 KW
BASIC SILICON SOLAR CELL RATING	11%
CELL SIZE — 1 CM X 2 CM X .015 INCH	
TOTAL NUMBER OF CELLS	163,800
NUMBER OF CELLS PER PANEL	81,900
NUMBER OF 7 CELL ROWS PER UNIT	78
NUMBER OF 65 X 3 INCH UNITS PER PANEL	150
ACTIVE AREA EACH PANEL	159 SQ. FT.
DEPLOYED AREA EACH PANEL	209 SQ. FT.
OUTPUT - WATTS PER SQ. FT.	9.57
ORIENTATION TOLERANCE	±15°
ESTIMATED WEIGHT PER PANEL INCLUDING SUPPORT STRUCTURE ACTUATOR AND WIRING	335 LBS
STANDARD UV FILTERS	

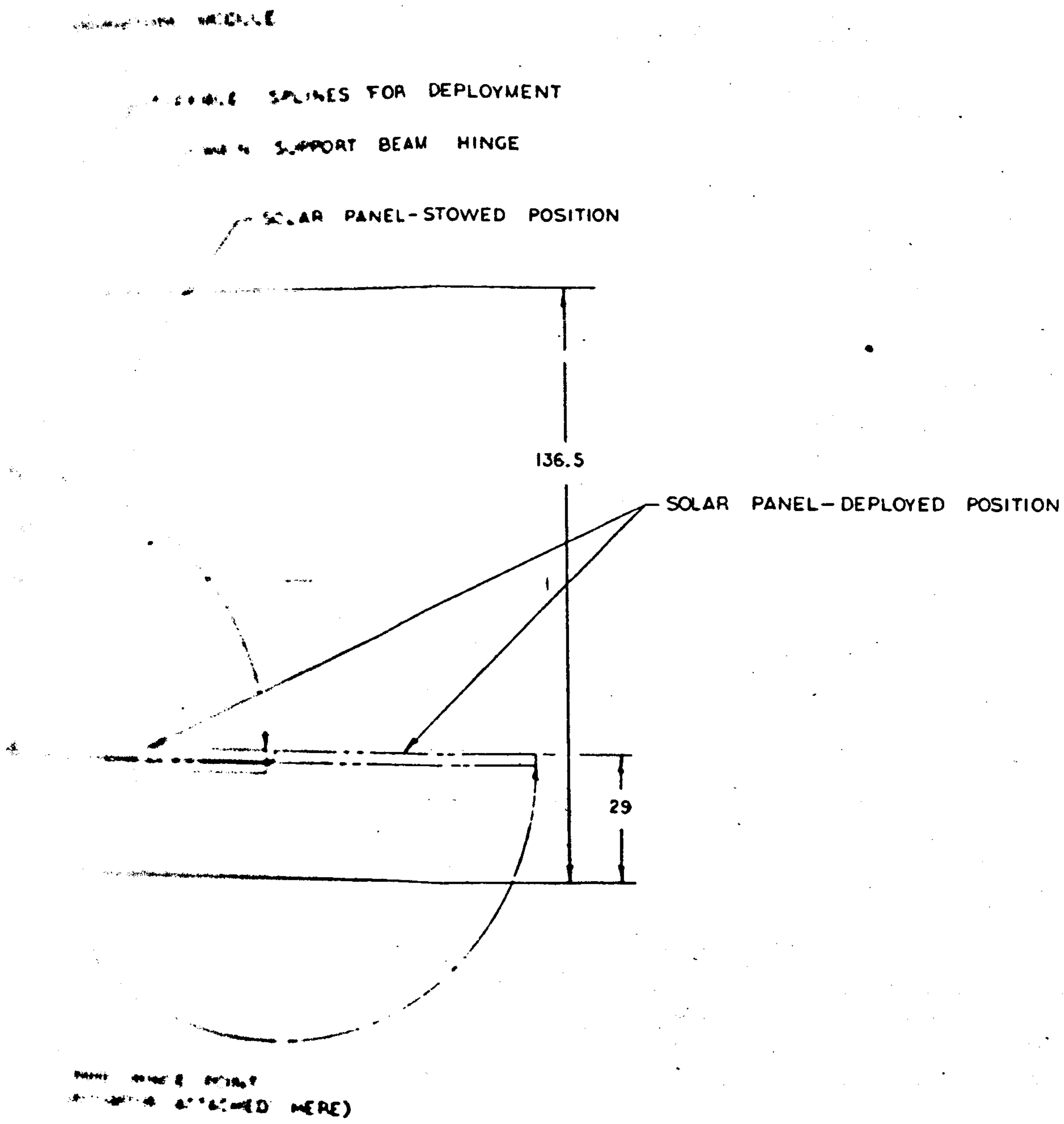
MODULE
SPLINES FOR DEPLOYMENT
SUPPORT BEAM HINGE
SOLAR PANEL-STOWED POSITION
136.5
SOLAR PANEL-DEPLOYED POSITION
29
ATTACHED HERE)

RE-DRAWN

NOTED	9 DEC 64	NORTH AMERICAN AVIATION, INC. SPACE and INFORMATION SYSTEMS DIVISION 12214 LAKEWOOD BLVD., DOWNEY, CALIFORNIA	
SOLAR PANEL ARRANGEMENT - 4 KW FLAT PANEL ARRAY			5177-108 B

C[redacted]

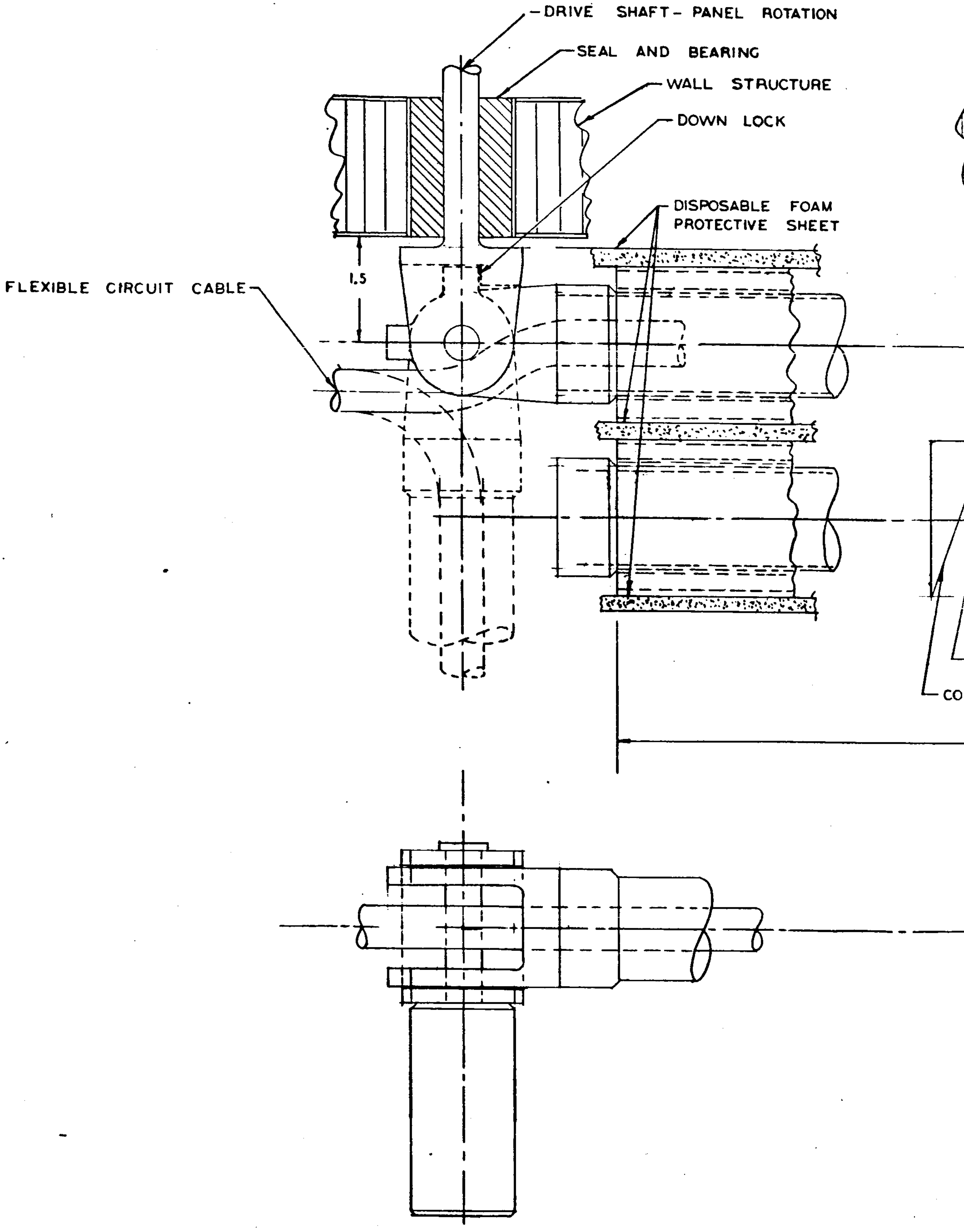
DRIVE SHAFT - PANEL ROTATION
SEAL AND BEARING
WALL STRUCTURE
DOWN LOCK
DISPOSABLE FOAM PROTECTIVE SHEET
FLEXIBLE CIRCUIT CABLE
1.5
CO

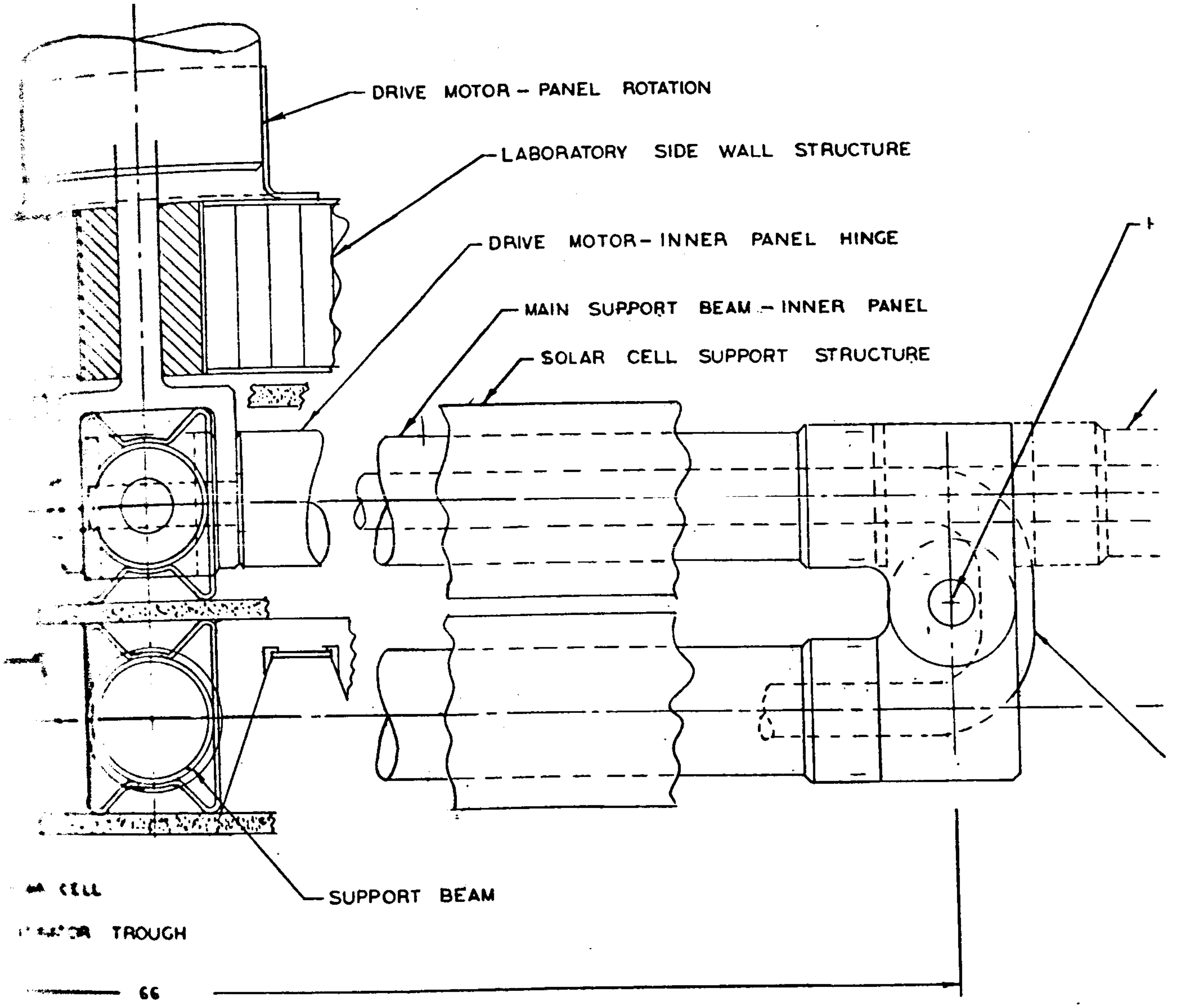
DRIVE MOTOR – PANEL ROTATION
LABORATORY SIDE WALL STRUCTURE
DRIVE MOTOR – INNER PANEL HINGE
MAIN SUPPORT BEAM – INNER PANEL
SOLAR CELL SUPPORT STRUCTURE
SUPPORT BEAM
CELL
TROUGH
66

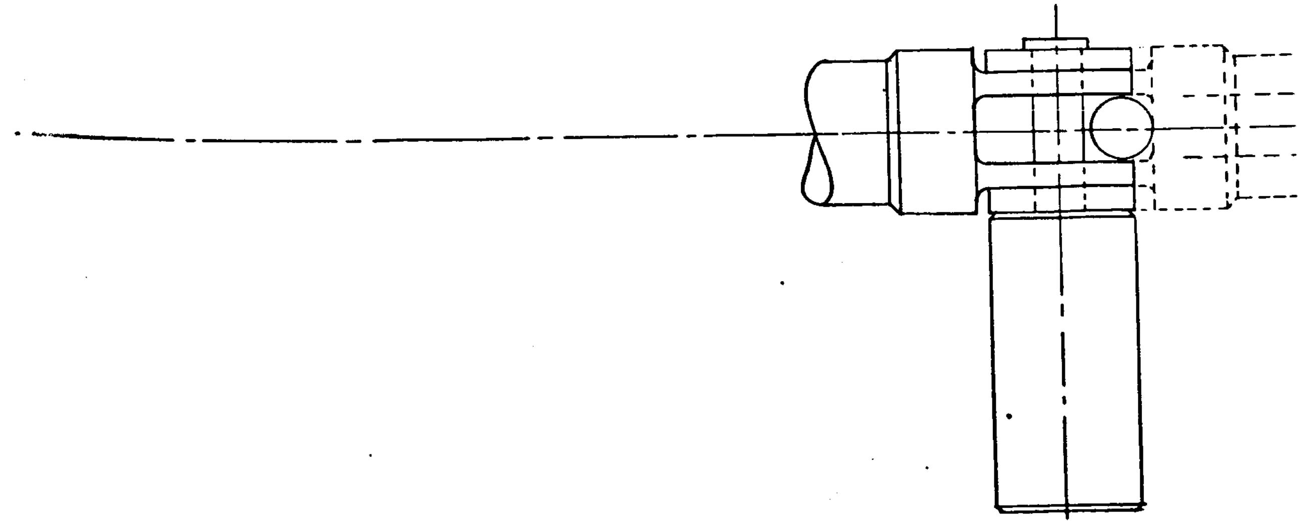

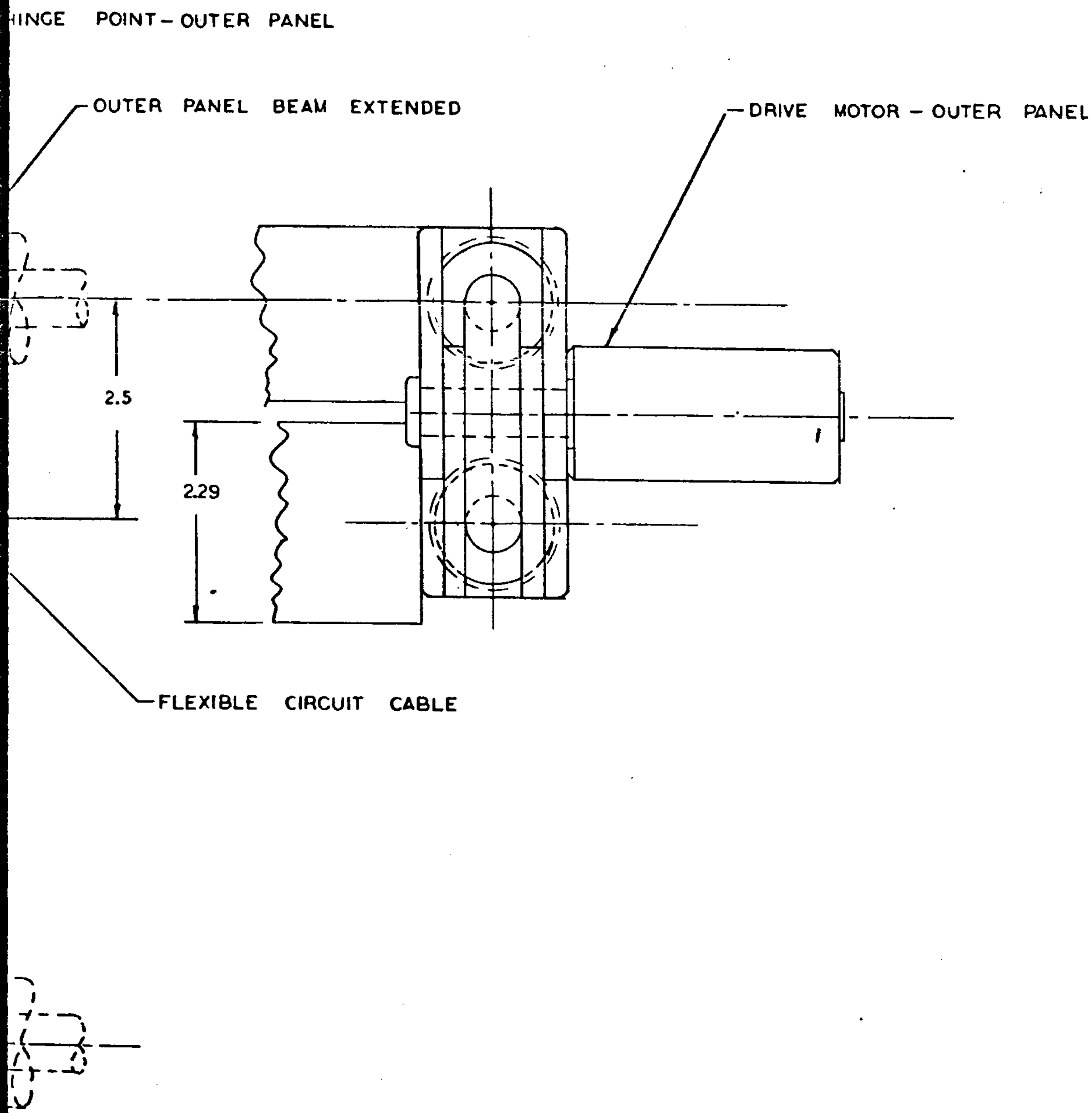
HINGE POINT – OUTER PANEL
OUTER PANEL BEAM EXTENDED
DRIVE MOTOR – OUTER PANEL
2.5
2.29
FLEXIBLE CIRCUIT CABLE

FULL

NORTH AMERICAN AVIATION, INC.

MAIN SUPPORT BEAM DETAILS – EASUS SOLAR PANELS

5177-113

~~CONFIDENTIAL~~

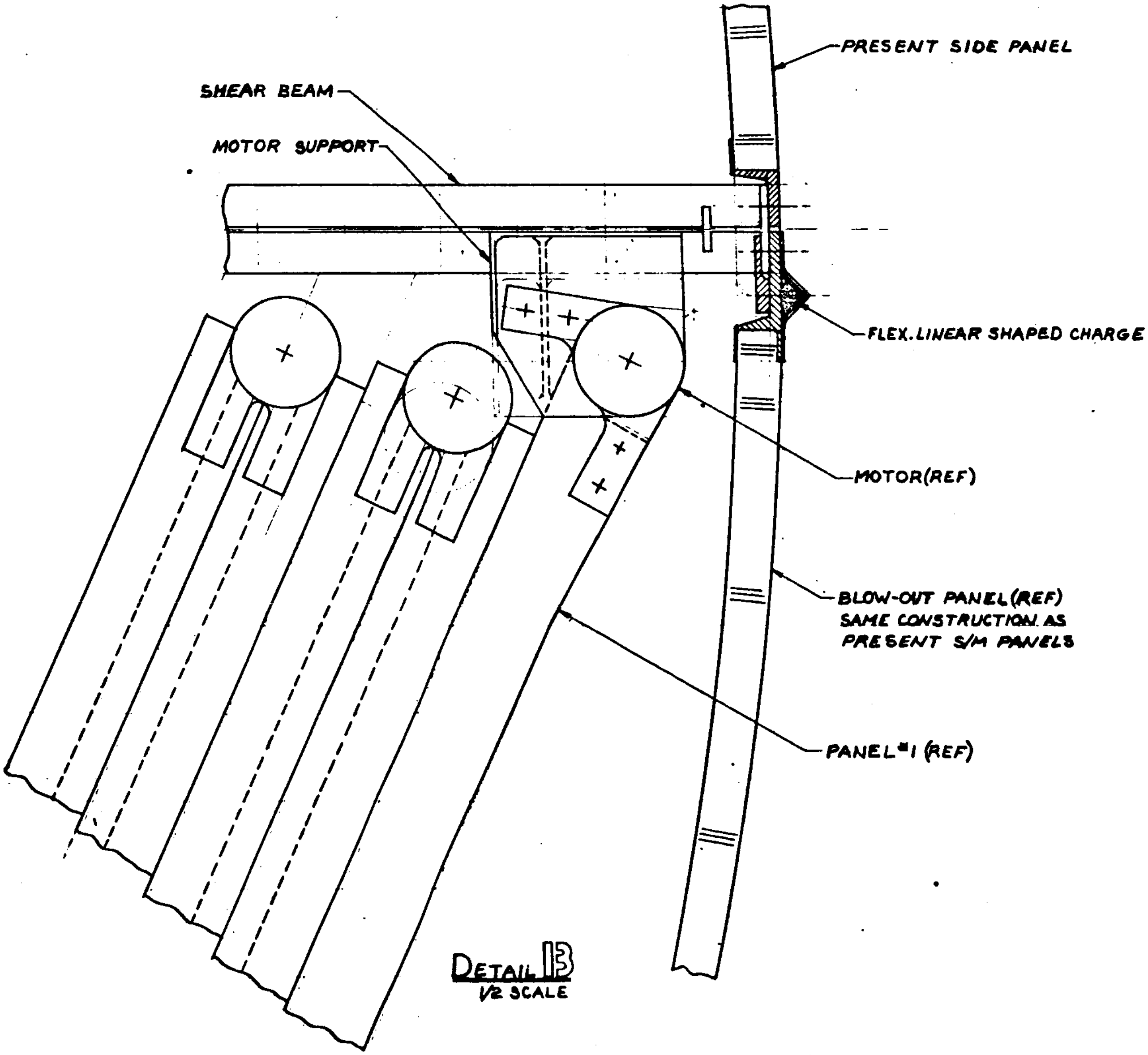
PRESENT SIDE PANEL
SHEAR BEAM
MOTOR SUPPORT
FLEX. LINEAR SHAPED CHARGE
MOTOR (REF)
BLOW-OUT PANEL (REF) SAME CONSTRUCTION AS PRESENT S/M PANELS
PANEL #1 (REF)

DETAIL 13
1/2 SCALE

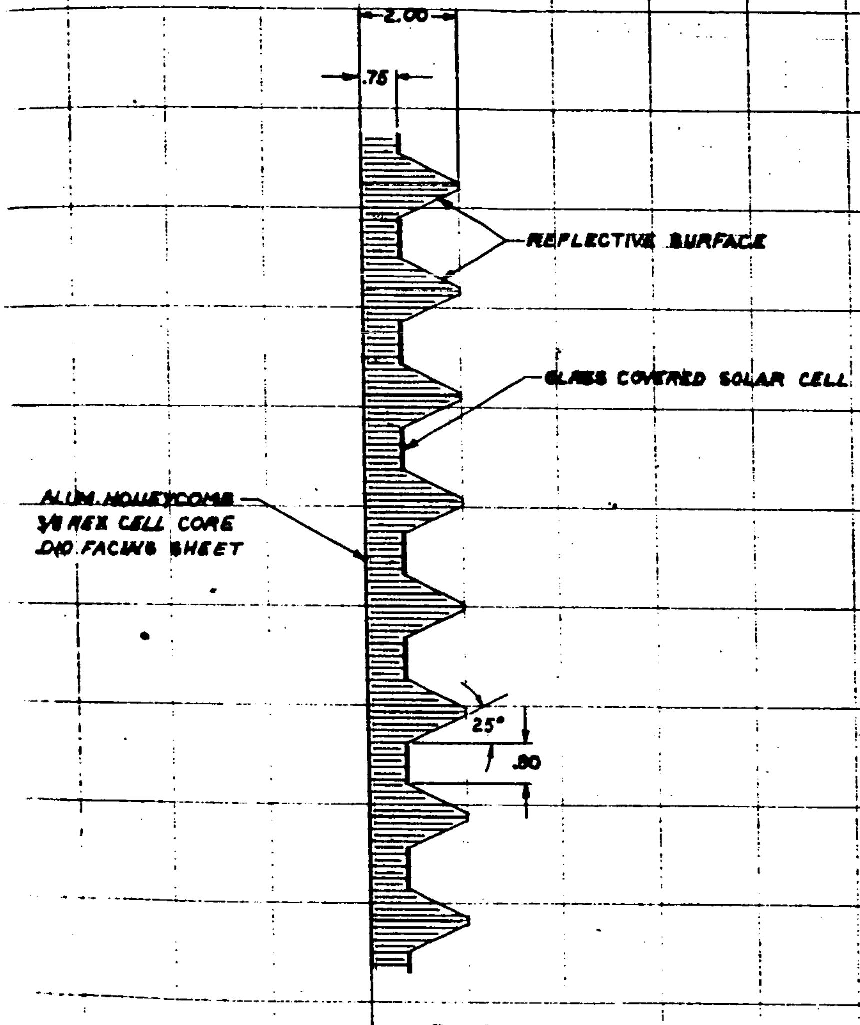
2.00
.75
REFLECTIVE SURFACE
GLASS COVERED SOLAR CELL
ALUM. HONEYCOMB
3/8 HEX CELL CORE
.010 FACING SHEET
25°
.80

SECTION A-A
1/2 SCALE

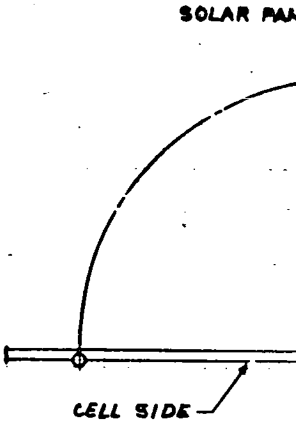
SOLAR PA
CELL SIDE

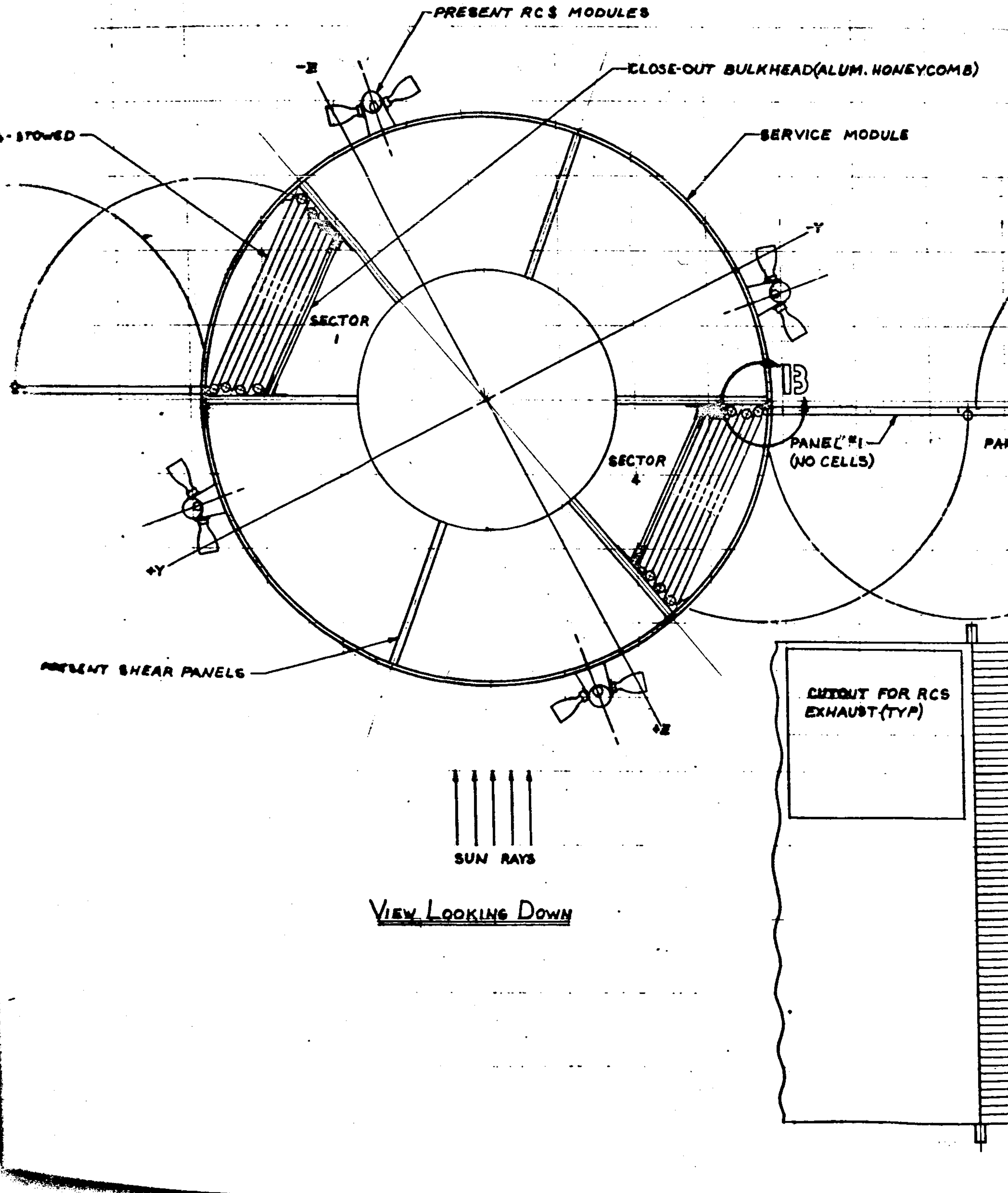
PRESENT RCS MODULES
-Z
CLOSE-OUT BULKHEAD(ALUM. HONEYCOMB)
℄-STOWED
SERVICE MODULE
-Y
SECTOR 1
℄
13
PANEL #1 (NO CELLS)
SECTOR 4
+Y
PRESENT SHEAR PANELS
+Z
CUTOUT FOR RCS EXHAUST (TYP)
SUN RAYS

VIEW LOOKING DOWN

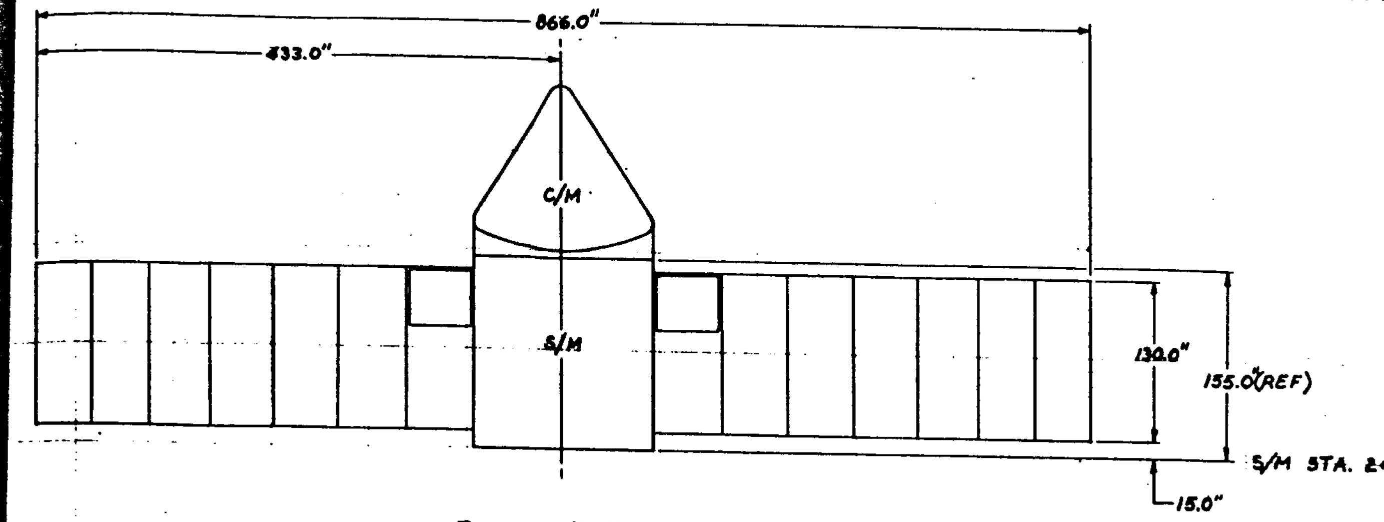
866.0"
433.0"
C/M
S/M
130.0"
155.0"(REF)
S/M STA. 2
15.0"

CONCEPT I ~ ELEVATION
NO SCALE

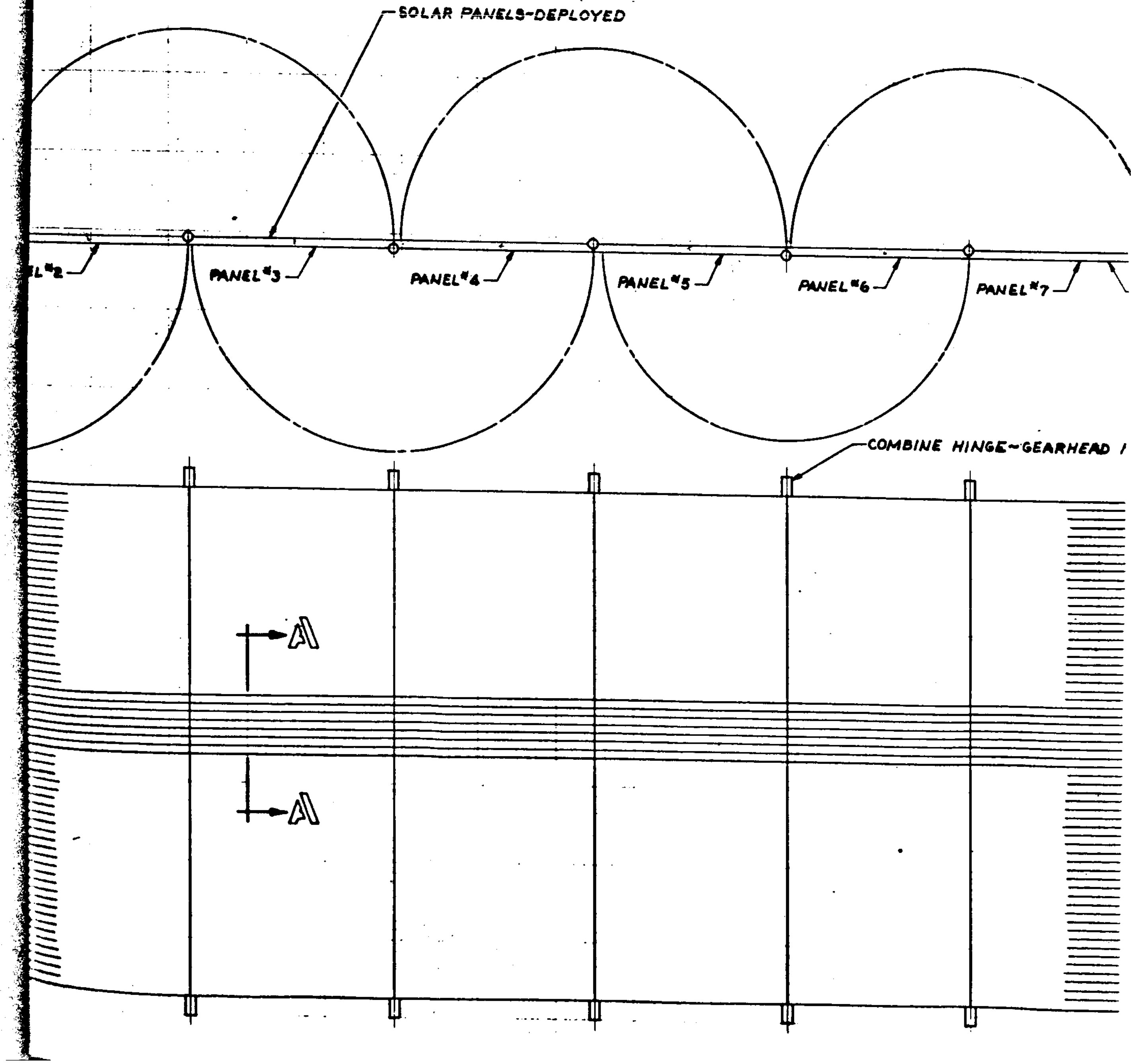
SOLAR PANELS-DEPLOYED
L#2
PANEL #3
PANEL #4
PANEL #5
PANEL #6
PANEL #7
COMBINE HINGE-GEARHEAD /
A
A

~~CON~~

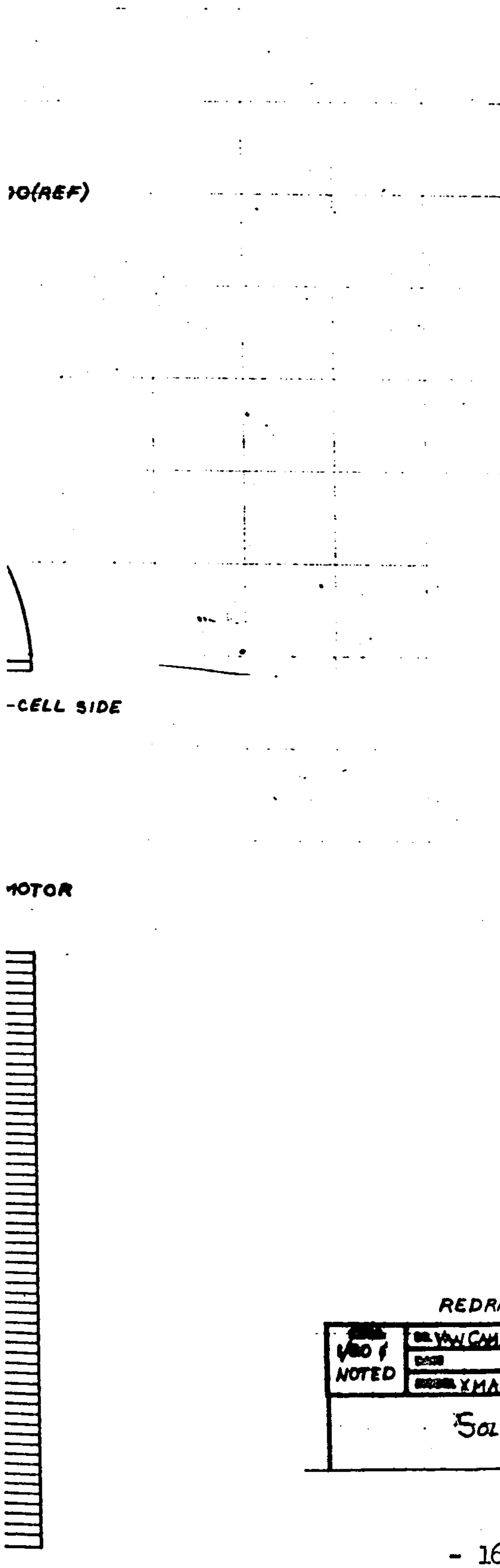

PARAMETERS:

TOTAL DEPLOYED AREA	601 FT²
AVAILABLE CELL AREA	548 FT²
NUMBER OF CELLS	88,800
REQUIRED LOAD	1.5 KW
UTILIZATION FACTOR	.88
INCIDENCE ANGLE	7.5° MAX

REDRAWN

NOTED	VAN CAMP	NORTH AMERICAN AVIATION, INC. SPACE and INFORMATION SYSTEMS DIVISION 12214 LAKEWOOD BLVD., DOWNEY, CALIFORNIA	
	DATE		
	XMAS		
		SOLAR PANEL ARRANGEMENT CONCEPT I ~ XMAS	5149-14B

~~CONFIDENTIAL~~

CON[redacted]

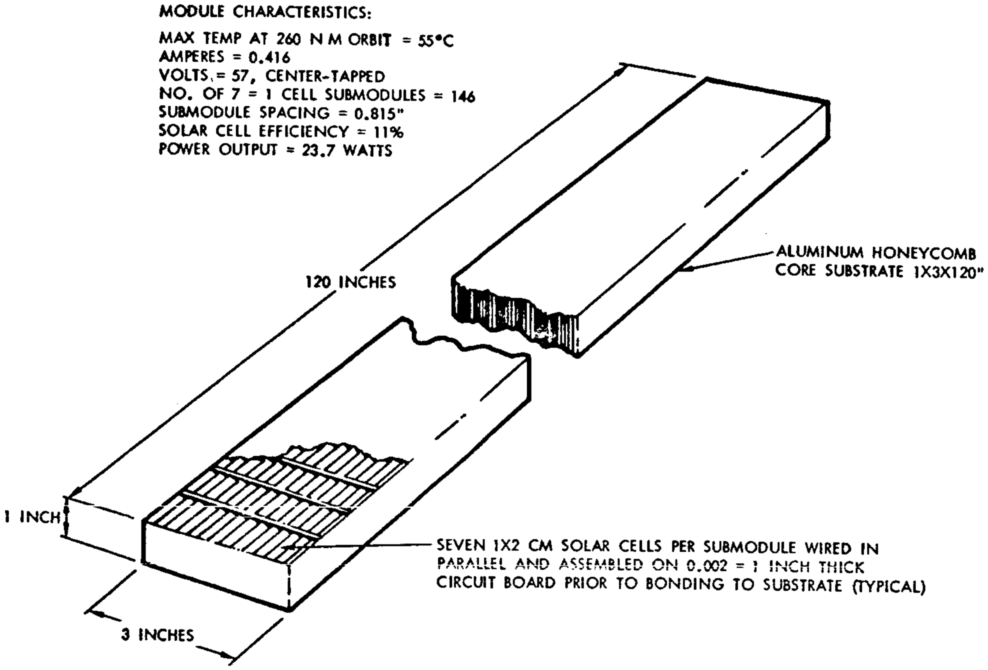
MODULE CHARACTERISTICS:
MAX TEMP AT 260 N M ORBIT = 55°C
AMPERES = 0.416
VOLTS = 57, CENTER-TAPPED
NO. OF 7 = 1 CELL SUBMODULES = 146
SUBMODULE SPACING = 0.815"
SOLAR CELL EFFICIENCY = 11%
POWER OUTPUT = 23.7 WATTS

120 INCHES
ALUMINUM HONEYCOMB CORE SUBSTRATE 1X3X120"
1 INCH
3 INCHES
SEVEN 1X2 CM SOLAR CELLS PER SUBMODULE WIRED IN PARALLEL AND ASSEMBLED ON 0.002 = 1 INCH THICK CIRCUIT BOARD PRIOR TO BONDING TO SUBSTRATE (TYPICAL)

Figure 55. Basic Solar Array Module

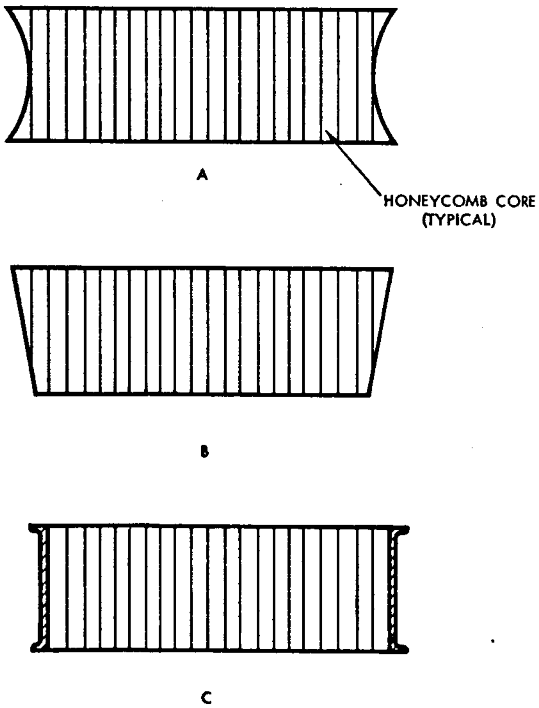
A
HONEYCOMB CORE (TYPICAL)
B
C

Figure 56. Solar Array Module Gross Sections

[redacted]

The basic solar cell submodule would consist of the following components:

1. Seven 1 x 2 cm N/P 11% solar cells
2. Seven microsheet filters
3. A 2 mil fiberglass reinforced circuit board
4. An expanded metal silver upper terminal

The seven solar cells are sweat-soldered to the 0.8 x 3 inch circuit board; simultaneously with this operation the expanded metal upper terminal would be sweated into place. The seven solar cells are by this means wired electrically in parallel and both the circuit board and the expanded metal terminal have provisions for wiring adjacent submodules in series.*

The seven cell submodules after being individually tested are assembled with silicone adhesive to the substrate on approximately 0.815 inch centers as shown in Figure 55 and electrically connected in series. In a 260 n.m. orbit, using 11 percent solar cells and taking into account temperature and fabrication losses, the assembled module 120 inches long will provide 57 volts at 0.416 amperes (23.7 watts). This voltage may be conveniently center tapped to provide DC voltages of plus and minus 28.5 volts at the maximum power point.

Prior to being assembled in an array, each array module would be tested for defects and power output. Because the module is narrow (only 3 inches wide) and the solar cell submodules are attached to it with a soft adhesive, any defective submodule is easily located, removed and replaced without damage to remaining adjacent solar cells. Only three electrical terminals are required: one at each end and one at the center. Each array module contains 146 7-cell modules or 1022 solar cells.

These array modules are to be assembled so that in the stowed position they will lie along the conical elements of laboratory surface with the solar cells facing the surface. A layer of foam ½ inch thick between the stowed array and the laboratory would serve to protect the solar cells. The means of storage must be compatible with deployment of the array into a flat plane which can be oriented when deployed about one axis with respect to the spacecraft.

---

*The expanded metal terminal was recommended by Mr. W. Cherry of NASA, Goddard, as being more reliable than a crimped wire interconnection. He also recommended the use of fused silica instead of microsheet solar cell filters because of darkening of the glass on exposure to UV and radiation; whether the extra expense is warranted for the Apollo laboratory has not been determined.

Solar Array Configuration

Since each array module produces 23.7 watts, 170 modules will be required to deliver 4000 watts, 85 to each side of the laboratory. If a minimum of 1/16 inch is allowed between modules (to permit wrapping around the laboratory) 85 modules laid side to side will occupy 260 inches at the upper (narrower) end of the laboratory. A radius of 86 inches allows 270 inches for each half of the array. Because the stowed array modules will diverge toward the bottom of the laboratory, (where the half circumference is 326 inches) the space between adjacent modules at that end will be about 5/8 inches.

A simple means of assembling the array modules is to bond them to a large sheet of aluminum having the shape when flat of the developed surface of the cone on which the array lies in the stowed position. This shape will be a section of a circular annulus having radii of 650 and 770 inches as shown in Figure 57 but will be, nevertheless, nearly rectangular. As seen, the array modules will be spaced further apart inboard than at the extremity of the array. Though a slight area penalty is incurred, this type of spacing is advantageous from the standpoint of temperature. Due to the view factor

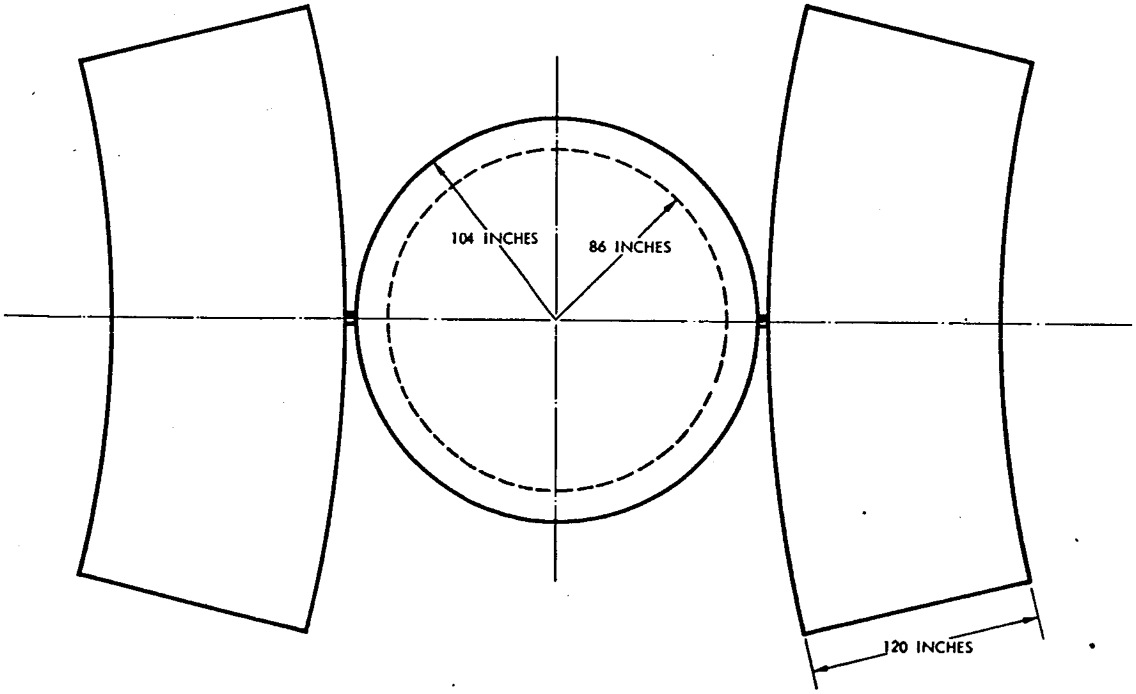

Figure 57. Plan View of Laboratory and Extended Solar Array

of the laboratory the outer portion of the array would normally be cooler than the closer portions. By wider spacing of solar array modules close to the laboratory, more radiating area is achieved to compensate for the unfavorable view factor.

Solar Array Structure

If only thin aluminum sheet (0.005 to 0.020) were used as a structural mounting for the stringer type array modules, it would be difficult to provide sufficient stiffness to hold the array in the flat position and more difficult still to orient the array about its axis. The requirement of flatness and stiffness can be met by elastic aluminum or steel ribs at inner and outer arcs of the extended array, the two ribs joined by a "spine" or torsion member as shown in Figure 58. The elastic ribs are designed to be wrapped with the stowed array about the laboratory and to spring open and flat when released. The 1 x 3 inch aluminum torsion spine joins the two ribs and keeps them in one plane. The base of the structure continues on to the motor driven shaft by which the array is rotated to face the sun.

It is clear that a rigid attachment of the solar array (modules and sheet) to the basic structure may cause destructive stresses when the array is curved into the stowed position and when it is released. A loose

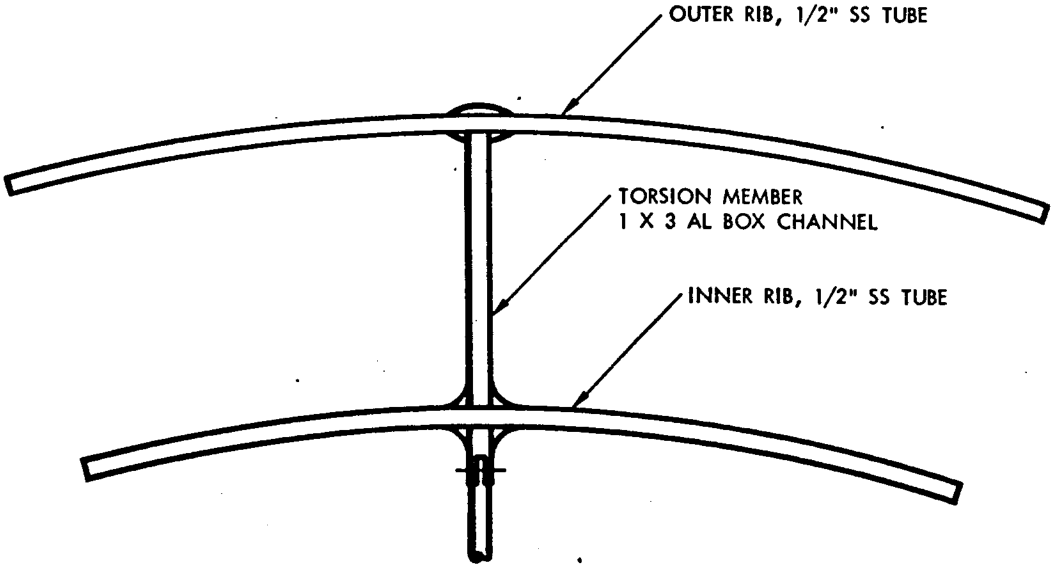

Figure 58. Skeletal Structure of Solar Array

attachment, analogous to a curtain rod is all that is required; for example, at end of each array module there may be an eye by which each array module would be loosely attached at both ends to the ribs with a wire loop.

Orientation of the Solar Array

Full orientation of the solar array to the sun first requires orientation of the laboratory about the roll axis. The orientation of the roll axis itself is completely arbitrary; thus, the laboratory has considerable freedom in this respect. Secondly, the array is oriented about its axis to face the sun. An array oriented about two axes with respect to the spacecraft not only would be far more complicated but such a scheme is plagued by shadowing by the spacecraft. Shadowing does not occur in single axis orientation.

To avoid the use of slip rings, orientation will not be continuous but be restricted to a total of about 540 degrees. On the dark side of the earth an array maneuver will therefore be required to reset the array to a new start position. Such an array maneuver is advisable in any case to minimize drag. Thus, upon onset of the dark period the array is oriented for minimum drag area and just prior to the start of the light period it is oriented to the sun. If the array is a conventional solar cell array, the orientation tolerance is very broad (about ±15 degrees). A concentrator array requires more accurate orientation (about 7.5 degrees).

SECONDARY ENERGY STORAGE

During the Extended Mission Apollo study, a comparative analysis was conducted between nickel-cadmium and silver-cadmium type secondary batteries. Battery characteristics of recharge rate, discharge rate, overcharge rate, percent depth of discharge, weight, volume, and cost were compared. The results indicated that the silver-cadmium battery will save in weight as much as 65 percent, over a 120-day period, and 45 percent over a one-year mission duration.

The objective of this study was to investigate, further, the differential in battery characteristics in order to explicitly select the most optimum secondary energy storage system. The investigation also included the various recharge schemes including the method of recharge using a third gas reference electrode.

Battery Characterization

The most recent information on nickel and silver-cadmium type secondary batteries was surveyed so as to prevent a relatively close comparison between battery characteristics. The relatively large capacity (100-120 AH) required of the sealed battery packs has not, as yet, been qualified but has been theoretically designed; therefore, a performance comparison, at these capacities, is not available for this study.

Space Technology Laboratories, performed a series of tests on 12 and 20-amp-hr nickel-cadmium cells for the Orbiting Geophysical Observatory. The tests included overcharge equilibrium tests, characterization tests, pressure tests, and various method of charge control.

In the characterization tests, it was concluded that the terminal voltage of a nickel-cadmium cell on charge is a function of the temperature of the cell, the charging current, and the state of charge of the cell. The relationship between voltage, current, and temperature of a cell at full charge was derived as

$$E_F = E_0' - (0.00056 + 9.9 \times 10^{-5}\ I)(t - 59) + 0.011I - 6.32 \times 10^{-5}\ I^{2.33}$$

NAA-S&ID developed a similar equation for Ag-Cd cells. By this equation, the voltage, E_b, of a battery having N-series-connected, 12-ampere-hour, Ag-Cd cells with a total interconnecting lead resistance of R_L, is described by

$$E_b = IR_L + N\ 1.443 - (0.00115 + 8.0 \times 10^{-5}\ I)(t - 60) + 0.047\ I - 68.0 \times 10^{-5}\ I^{3.02}$$

Figure 59 shows the relationship between charge rate, terminal voltage, and temperature for both the empirical NiCd equation and the derived AgCd. The charge rate scale is based on that of a 20 AH capacity rating battery. In the utilization of other capacity ratings, the scale should be modified corresponding to the basepoint capacity. It should be noted that the battery internal resistance will vary with varying capacities, but in this case has been assumed constant for sake of battery comparison.

Estimated Cyclic Life

Figure 60 (based on Inland Testing Laboratory test data and Gulton estimates of cycle life) depicts the cyclic life of both nickel and silver-cadmium batteries as a function of percent depth of battery discharge.

CONFI[redacted]

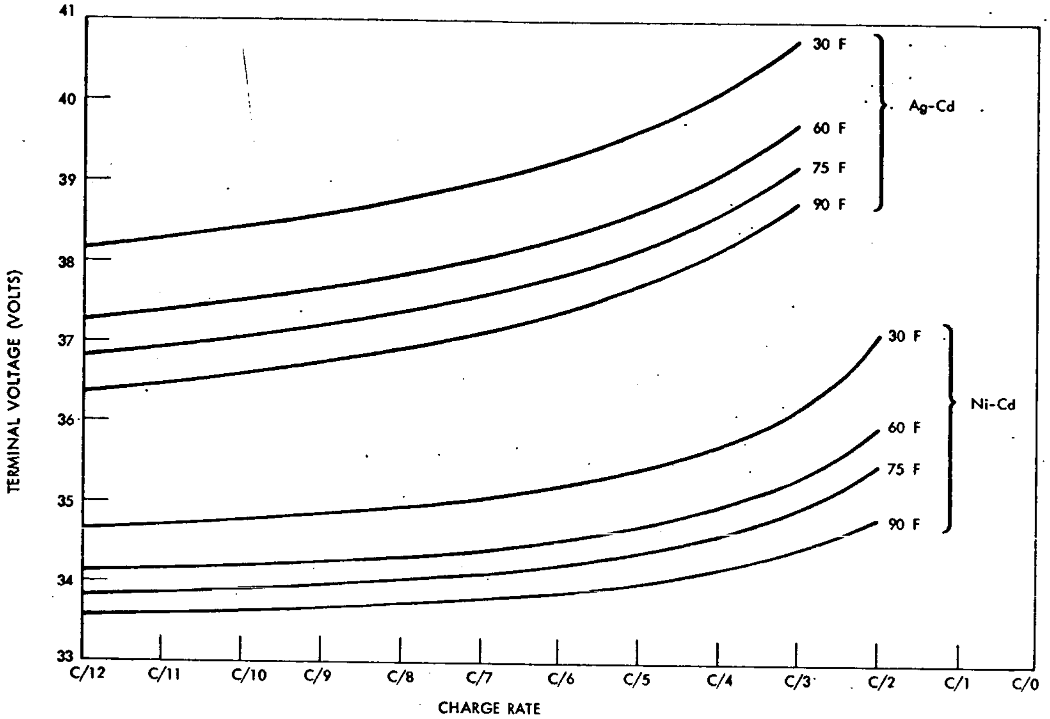

Figure 59. Change Rate as Function of Terminal Voltage

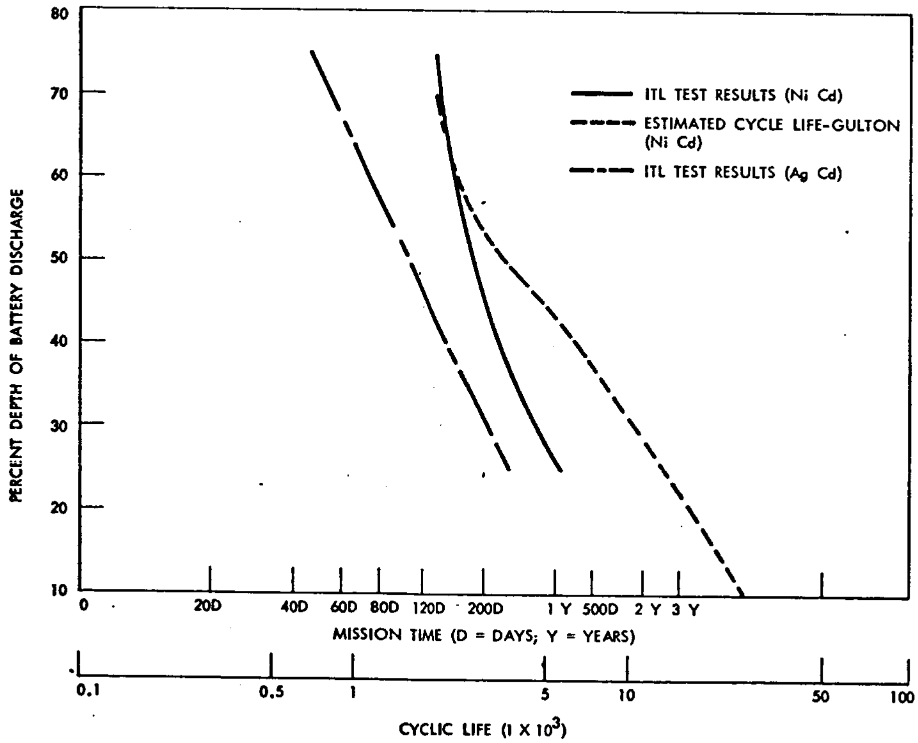

Figure 60. Cycle Life of Hermetically Sealed Nickel and Silver-Cadmium Cells as a Function of Varying Percent Depths of Discharge (25°C)

~~CONFIDENTIAL~~

Charge Rate

Figure 61 depicts cyclic life of both nickel and silver-cadmium cells as a function of charge rate, redundancy, and operating temperature.

Charge rates are based on the amount of energy required to replace discharged capacity during one recharge period. For example, assuming ambient temperature conditions (25 C), to accomplish a 200-day mission at the prescribed Prolonged Mission power level of 1185 watts would require:

a. (1) 55AH capacity NiCd battery at a C/1.98 charge rate (Gulton estimated) or

b. (1) 60 AH capacity NiCd battery at a C/2.16 charge rate (ITL test results) or

c. (1) 110 AH capacity AgCd battery at a C/3.96 charge rate (ITL test results)

If the above charge rates could be tolerated, then the above results could be utilized, based strictly on a percent depth of battery discharge basis. However, this is not the case. These rates can be accepted until the point where electrolytic decomposition of the electrolyte begins and then the cell is maintained at this voltage by means of trickle charging the battery. In the ITL test results, the charge rates varied from 1.22 C (75% depth) to C/3.06 (25% depth) for the NiCd cells and C/2.45 (75% depth) to C/7.35 (25% depth) for the AgCd's. The nominal values which are usually quoted for overcharge rates are C/6 for NiCd and C/10 for AgCd. If these values were used for the Prolonged Mission analysis, it is then evident that at least triple over-capacity is required for both NiCd and AgCd for a mission time of 200 days. Projected life indicates that 100 percent over capacity occurs at around 4100 cycles for NiCd and, if projected, 5500 cycles for AgCd.

Battery Pack Weight and Volume

Figure 62 depicts total battery pack weight as a function of cyclic life, overcapacity, and temperature. The weights were based on actual and proposed hardware values.

After establishing the temperature and charge rate required, the percent capacity required can be obtained from the previous set of figures and the weight from Figure 62. For example, at ambient temperature (25C) consider a 200-day mission with a maximum charge rate of C/4 and C/9, respectively, for NiCd and AgCd. Two hundred percent capacity is required for NiCd whereas 300 percent is required for the AgCd cell. In this case,

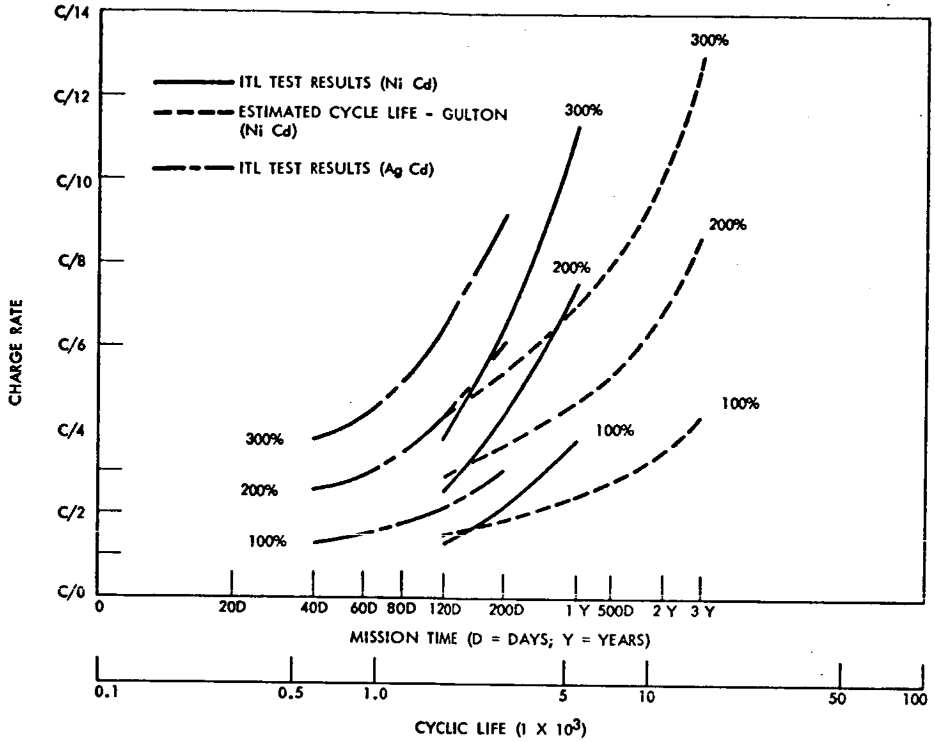

Figure 61. Cycle Life of Hermetically Sealed Nickel and Silver-Cadmium Cells as a Function of Charge Rate - (25°C)

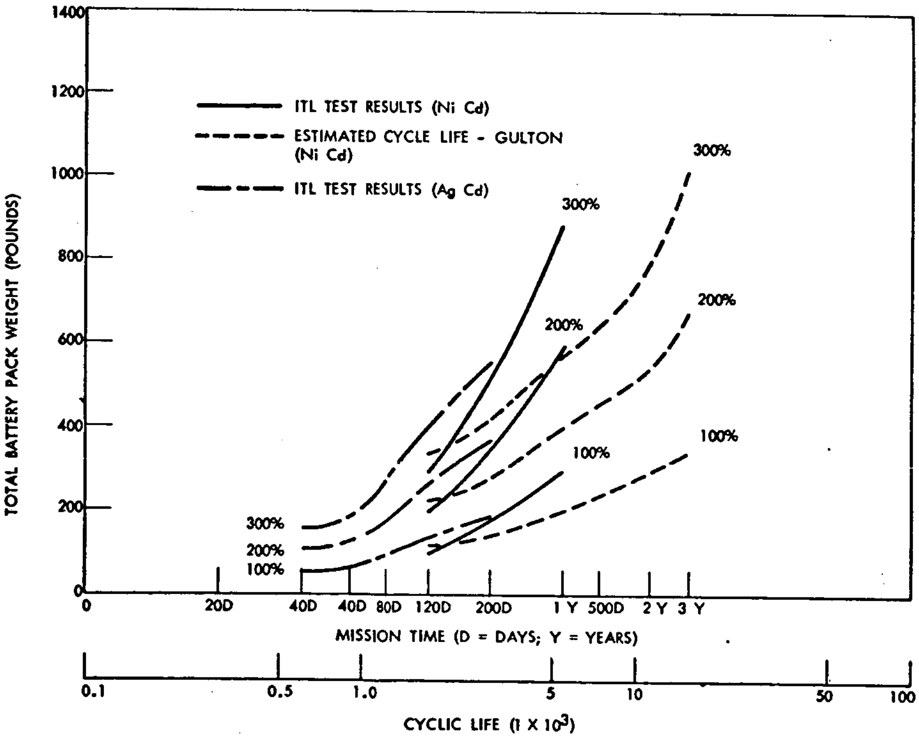

Figure 62. Cycle Life of Hermetically Sealed Nickel and Silver-Cadmium Cells as a Function of Total Battery Pack Weight - (25°C)

a NiCd system of 340 pounds is required in contract to a 500 pound AgCd system for the same mission. Whereas, if a C/6 charge rate was imposed on the NiCd system, the total system weight would have resulted in value of 520 pounds.

At longer mission times than 200-days, it appears as though the AgCd curves will tend to cross those of the NiCd's and thereby exhibit considerable weight savings. At present, however, cyclic life information has not been compiled which will allow establishing the cross-over point.

Figure 63 depicts battery pack volume as a function of cyclic life, overcapacity, and temperature. The philosophy used in selecting a battery pack volume is the same as that used in the selection of a battery pack weight.

Power Required to Recharge Battery

There have been several methods suggested in determining the required recharge power of a battery including constant voltage, constant current, efficiency, assumed overcharge, etc. For example, by knowing the required recharge current, the end point recharge voltage of the battery can be determined from Figure 59. The required power can then be established from the values of the current and voltage. As can be seen from Figure 59, the lower the recharge rates, the lower is the end point voltage; whereas at high charging rates of C/2 or greater, the end point voltage rises rapidly.

The acceptance efficiency of a battery will vary as to charge rate and temperature such as that shown in Figure 64. However, this is based on the assumption that the battery be allowed to be recharged at this rate indefinitely, which, as mentioned previously, is erroneous at high charge rates. This, therefore, leads to establishing the recharge power as that which was utilized by ITL. The percent overcharge required to replace the battery capacity within one orbit was established as 120 percent at 5C, 130 percent at 25C, 140 percent at 35C, and 150 percent at 50C for NiCd and 103 percent for AgCd at all temperature ranges. From the established overcharge required and the charging voltage, the constraints on the solar cell panels can be determined.

Battery Selection

The most recent information available indicates that the silver-cadmium battery does not exhibit the advantage anticipated in the original Extended Mission Apollo study. The major differences in the results occurs in the presumed AgCd percent depth of discharge as a function of mission time. The most recent data was conducted on larger capacity batteries whereas the

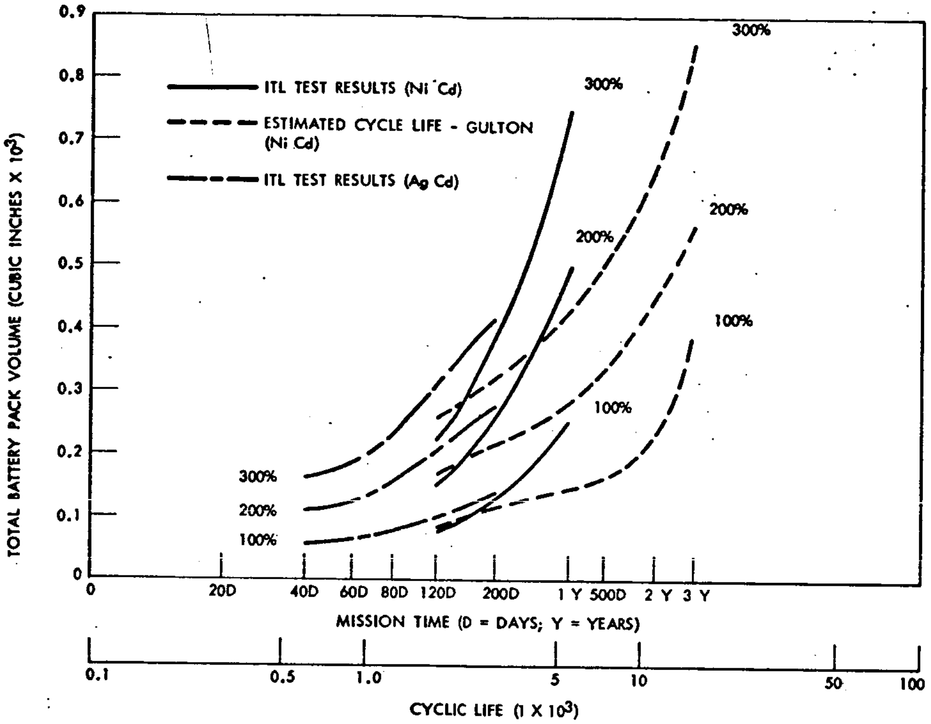

Figure 63. Cycle Life of Hermetically Sealed Nickel and Silver-Cadmium Cells as a Function of Total Battery Pack Volume (25°C)

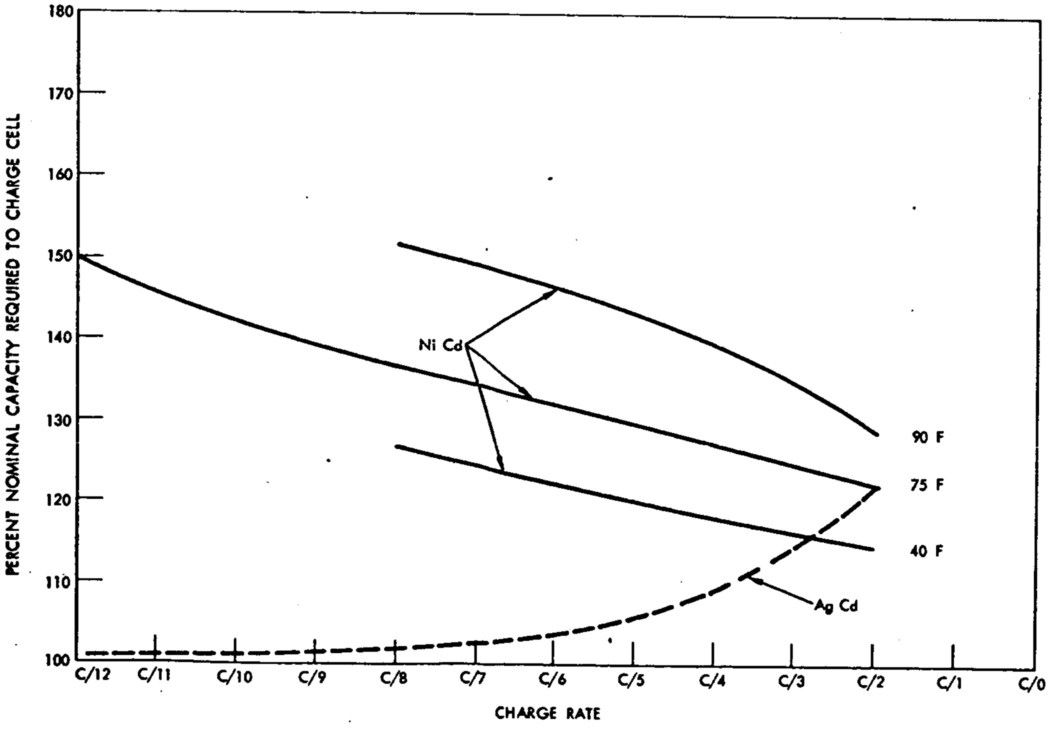

Figure 64. Typical Charge Acceptance Curves for Nickel and Silver-Cadmium Secondary Batteries

Boeing test results were conducted on a variety of cells ranging from 3 AH to 12 AH. The long cyclic lives of 1800-20,000 at percent depth of from 65 to 25 percent were performed at room temperature on 5 AH cells. Test data performed on 12 AH cells more closely approach those of the ITL data with 1350 cycles, 35 percent depth at 20 C and 903 cycles, 35 percent at 40 C.

Until more cyclic life information becomes available on AgCd cells, a definite crossover point between NiCd's and AgCd's cannot be determined. However, it appears reasonable to project the actual data curves upwards of one year for Prolonged Mission Apollo considerations.

The curves presented were based on a system load of 1184 watts. These curves, however, with the appropriate scale factor can be utilized for any projected load level.

For a one year lifetime, ambient conditions and a limiting C/6 and C/10 charge rates respectively for NiCd and AgCd, the total battery capacity, weight, volume, recharge voltage and recharge power are:

	NiCd	AgCd
Required Capacity	170 AH	240 AH
Required Weight	480 lbs	490 lbs
Required Volume	4050 in.^{3}	3950 in.^{3}
Required Recharge Voltage	34.3	37.2
Recharge Power	1260 watts	1080 watts

SOLAR CELL POWER SYSTEM DESIGN

The state of knowledge and development of the solar cell power systems is such that the design approach alternatives presently being considered promise only small advantages from one to the other. There are no breakthroughs expected in the technology discussed in this report, either in solar cell efficiency, solar panel weight, or secondary battery characteristics.

Although the basic comparisons were based on power loads and system requirements derived from the Extended Mission Apollo study described in report SID 63-1370-4, extrapolation of data over the power range from 0.5 to 4 KW is reasonably accurate. For a one year mission, the solar panel area, total system weight, and system cost (excluding R&D) are shown in Figures 65, 66, and 67. As the figures show, the lower charge efficiency of Ni-Cd

CONF[redacted]

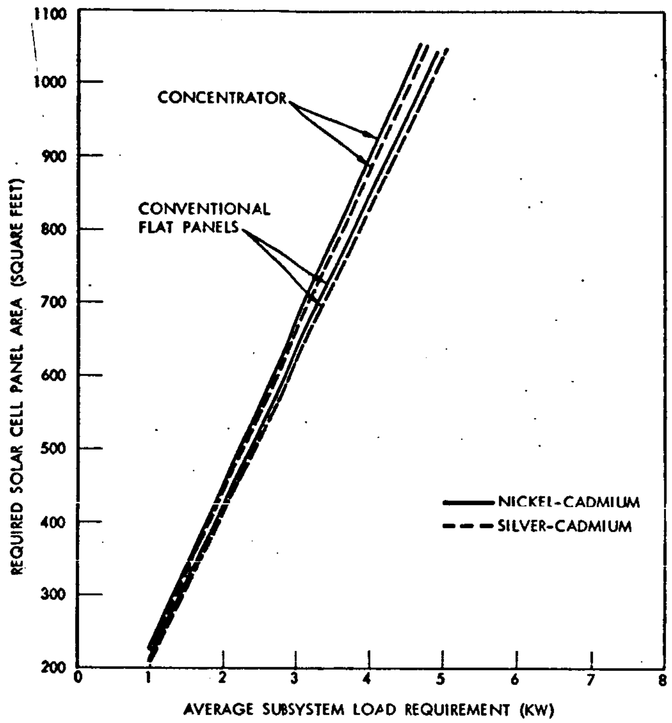

Figure 65. Solar Cell System Area

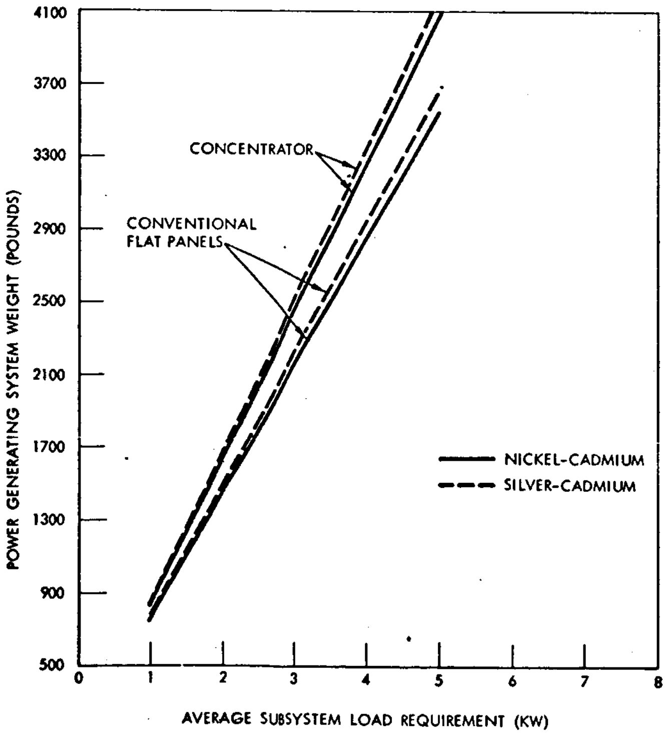

Figure 66. Solar Cell Power System Weight

[redacted]

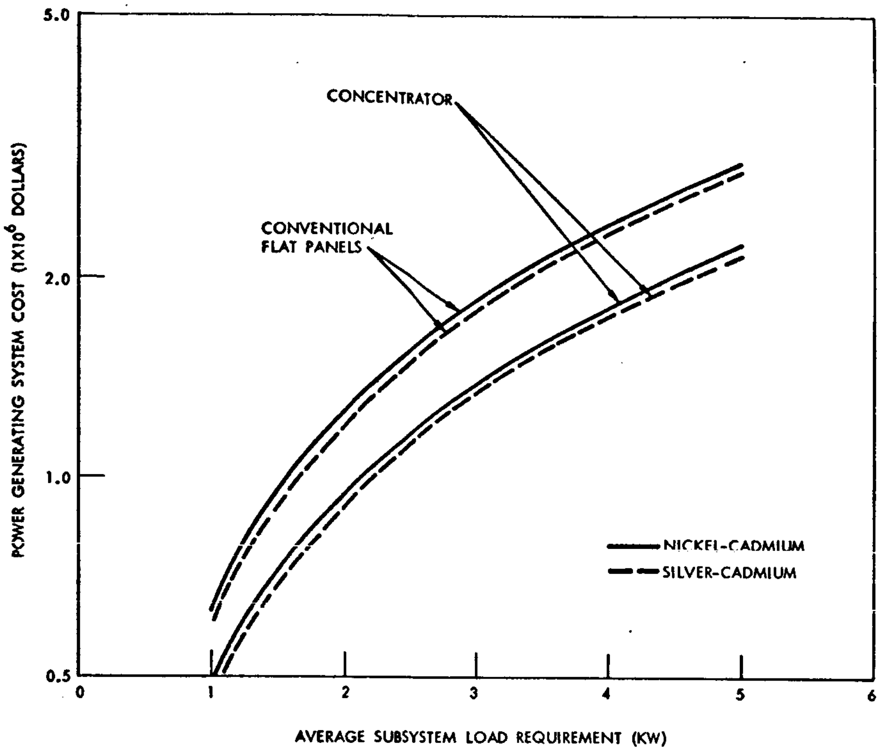

Figure 67. Solar Cell Power System Cost

batteries necessitates a larger solar array, whose weight more than overcomes the slight weight advantage of Ni Cd batteries over Ag-Cd. The difference, however, is not considered conclusive, particularly since the effect of this larger area has an almost negligible effect on atmospheric drag as shown in Figure 68. A more pronounced effect, although still not very conclusive from an overall program standpoint, is the difference between flat and concentrator arrays. The area and weight penalties of concentrators are, of course, offset by a lower system cost but even this difference becomes insignificant as the cost of solar cells becomes small in relation to total system cost.

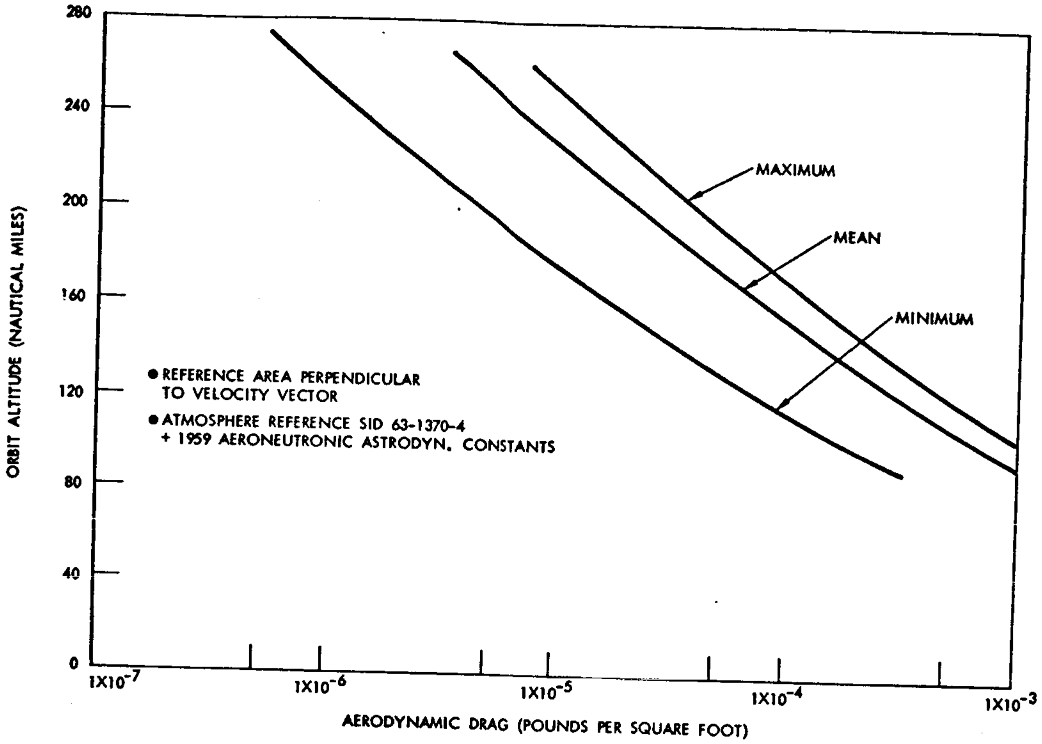

Figure 68. Relationship Between Orbital Altitude and Aerodynamic Drag

ISOTOPE POWER SYSTEM

In cooperation with S&ID, the Atomics International division of North American Aviation has made a preliminary study of the feasibility of integrating an isotope heat source electrical power system into the AORL system. The results of their study are presented in detail in Appendix B. During the first phase of the study, various system concepts were evaluated, and parametric studies were made to point out advantages and limitations for possible configurations of a dynamic power conversion system. It was determined early in the study that, due to the vehicle limitations on available radiator area, and excessive isotope inventory requirements, a thermoelectric power conversion system to produce the desired electrical power levels is not feasible.

On the basis of the parametric studies, a reference configuration was established for more detailed analysis. This reference system is a 3 KWe Mercury Rankine Dynamic Conversion system using a heat source of Po^{210} isotope. The isotope source and boiler may be located in the Apollo Command Module, and the rest of the system located in the service module; or the entire system located in the service module, if the re-entry trajectory insures a water landing of the service module.

The only major differences between the reference system and present Mercury Rankine technology are CRU turbine performance, and the use of an isotope heat source. All other considerations represent only minor (if any) variations on the present Mercury Rankine development program.

Because of the present development status of Mercury Rankine Program components, it is feasible to provide systems for earlier Apollo missions at a lower electrical power level. For this reason development schedules and costs have been estimated for providing systems before the beginning of the Prolonged Missions program; it is feasible to provide this type of system for 1971 AES flights. A reliability demonstration plan was assumed to provide a test cost estimate, and cost versus reliability demonstration trade offs are provided.

The more significant results of this study are summarized in the following table:

Isotope Power System Summary

Configuration	1 active power conversion subsystem + 1 standby PCS, Isotope heat rejection through NaK heat exchanger loop, Po^{210} isotope heat source

Isotope Power System Summary (Cont)

System Overall Efficiency	12% (10.4% after conditioning)
System Power	3.3 KWe net, 1% regulated 28 V dc
System Weight	1839 lbs.
Reentry Weight	563 lbs.
Re-supply Interval	120 days
Cost through delivery of two systems	$35 million less isotope
Availability	1.7 KWe system delivered in 48 mo; 2.25 KWe system delivered in 60 mo; 3.0 KWe system delivered in 65 mo; 3.3 KWe system delivered in 72 mo.

POWER CONDITIONING, DISTRIBUTION, AND CONTROL

The detailed design of a power conditioning, distribution, and control system must necessarily be performed after the characteristics of the power source and the requirements of the spacecraft and mission are accurately known. In this study, more detailed design than was performed during the Extended Mission Apollo study would reflect only minor changes in requirements. Therefore, for a solar cell power source, the power conditioning and distribution schematics shown for Extended Apollo Concepts II and III are still generally applicable to this program. If an isotope system whose net product is regulated d-c is used, the system is also basically the same with the exception of voltage regulators and battery charging circuits. If the net output of the isotope system is both d-c and 400 cps a-c, the inverters are, of course, eliminated.

Rather than make interim changes to the system design each time a requirement change is proposed, it was the intent of this study to examine, in more detail, the power conditioning and control equipment to determine its basic compatibility with Prolonged Missions performance and reliability requirements. As will be discussed later in this section, the reliability of d-c to a-c inversion is the major factor in overall life extension of Apollo type systems. To alleviate this problem, three approaches were studied; (1) improvement in inverter reliability; (2) simplification of the inverter by changing the a-c power characteristics to something other than an accurately controlled sine wave; and (3) elimination of a-c power requirements. Westinghouse Electric (the manufacturer of the Apollo inverter), examined the first approach. The results, presented in Appendix A, indicate that significant improvements in reliability are feasible by (1) normal component improvement under Apollo Quality Control efforts; (2) by upgraded components; (3) by circuit simplification; and (4) by incorporation of in-flight maintenance provisions. The other two system reliability improvement approaches (mitigating or eliminating a-c requirements) were considered by examining the characteristics of those components that are the primary users of spacecraft a-c power.

RELIABILITY OF THE POWER CONVERSION AND DISTRIBUTION SYSTEM

Several factors combine to make advisable a review of the reliability of the electrical power distribution for a prolonged mission Apollo spacecraft. First, the prolonged mission Apollo will not use fuel cells, and though these are not part of the power distribution system as such, they do enter into the reliability analysis of the standard Apollo electrical power distribution system. Secondly, the successful use of redundancy to attain reliability may be very sensitive to mission duration; an exponential failure distribution cannot be applied in such cases even though all the components exhibit exponential failure statistics. Finally, it would be desirable to determine PDS reliability as a function of mission duration, to discover weaknesses that develop when mission time is prolonged, and evaluate possible remedies.

Figure 69 shows a simplified reliability diagram for the prolonged mission Apollo electrical power distribution system. This diagram was adapted from the present Apollo PDS reliability diagram by replacing the fuel cells with solar power. No change was made in the failure rate of the remaining components except for a reduced failure rate for a more reliable version of the DC-AC inverters.

In Table 18 this diagram is further simplified by combining all series-reliabilities into one failure rate; the redundant reliabilities are brought out separately. The reliability of the redundant groups was separately computed for time intervals from 45 days to three years. Net system reliability is the product of these reliabilities and is shown in the last column.

Two conclusions may be drawn from the analysis. The expected PDS reliability is good for perhaps 45 days but then degrades rapidly, primarily because of the typical "wearout characteristic" of a redundant group. Secondly, for all practical purposes the PDS reliability is the DC-AC inverter reliability--even if all other components were perfect, no measureable improvement in reliability would be realized. It is clear from the analysis that the present DC-AC inverter concept will not do for prolonged missions.

Figure 70 shows the expected PDS reliability as a function of mission duration.

POWER CONVERSION

The DC-AC Inverter used on Apollo is a static inverter which provides a sinusoidal 3-phase 400-cycle output with high efficiency and very low harmonic content by means of high frequency switching. The reliability of this unit is based on failure rates and parts count of individual components rather than on tests of completed assemblies. In order-of-magnitude the failure rates of the more critical components of this inverter are:

Filter Capacitors	1.80×10^{-5} per hour
Power Transistors	1.20×10^{-5} per hour
Power Diodes	0.96×10^{-5} per hour
Micro-module Preamps	0.75×10^{-5} per hour
Balance of components	7.55×10^{-5} per hour
Net failure rate	12.26×10^{-5} per hour

From the net failure rate of the inverter we arrive at a MTBF (average life) of 8,156 hours. It is evident that improving the inverter reliability will not be a simple matter of improving or avoiding the use of a few weak components; even if the four most critical component types were eliminated the MTBF would only be increased by 60%. Thus there is almost no hope that the present inverter concept will meet the requirements of

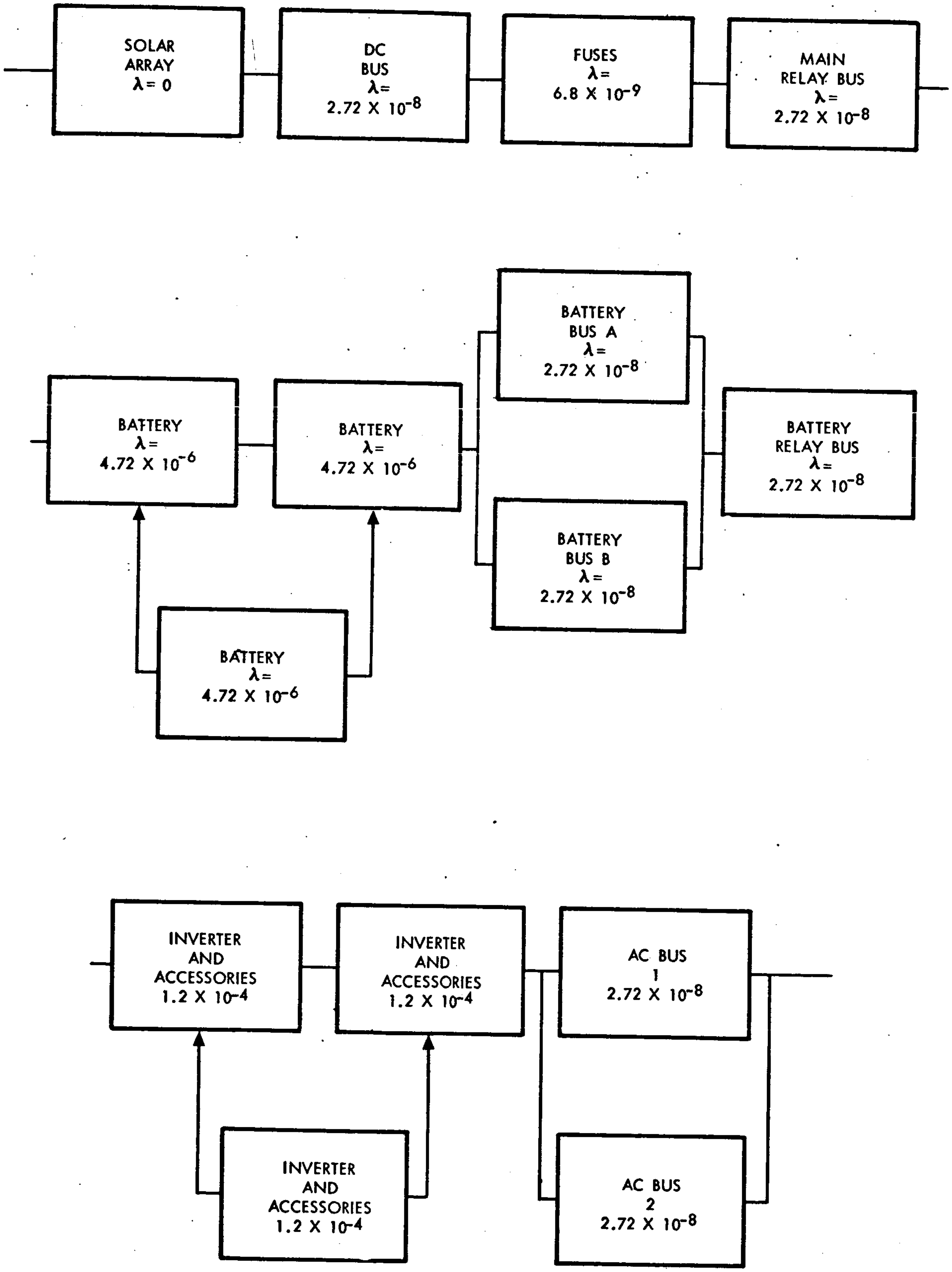
SOLAR ARRAY λ= 0
DC BUS λ= 2.72 X 10-8
FUSES λ= 6.8 X 10-9
MAIN RELAY BUS λ= 2.72 X 10-8
BATTERY λ= 4.72 X 10-6
BATTERY λ= 4.72 X 10-6
BATTERY BUS A λ= 2.72 X 10-8
BATTERY BUS B λ= 2.72 X 10-8
BATTERY RELAY BUS λ= 2.72 X 10-8
BATTERY λ= 4.72 X 10-6
INVERTER AND ACCESSORIES 1.2 X 10-4
INVERTER AND ACCESSORIES 1.2 X 10-4
AC BUS 1 2.72 X 10-8
AC BUS 2 2.72 X 10-8
INVERTER AND ACCESSORIES 1.2 X 10-4

Figure 69. Power Distribution Reliability Diagram

[redacted]

[redacted]

All Series Elements
Busses, Fuses, Circuit Breakers
$\Sigma \lambda i = 8.84 \times 10^{-8}$

Time	Series Elements $\lambda = 8.84 \times 10^{-8}$
45 Days	.99999045
90 Days	.99998090
6 Months	.999621
One Year	.999224
2 Years	.998448
3 Years	.997672

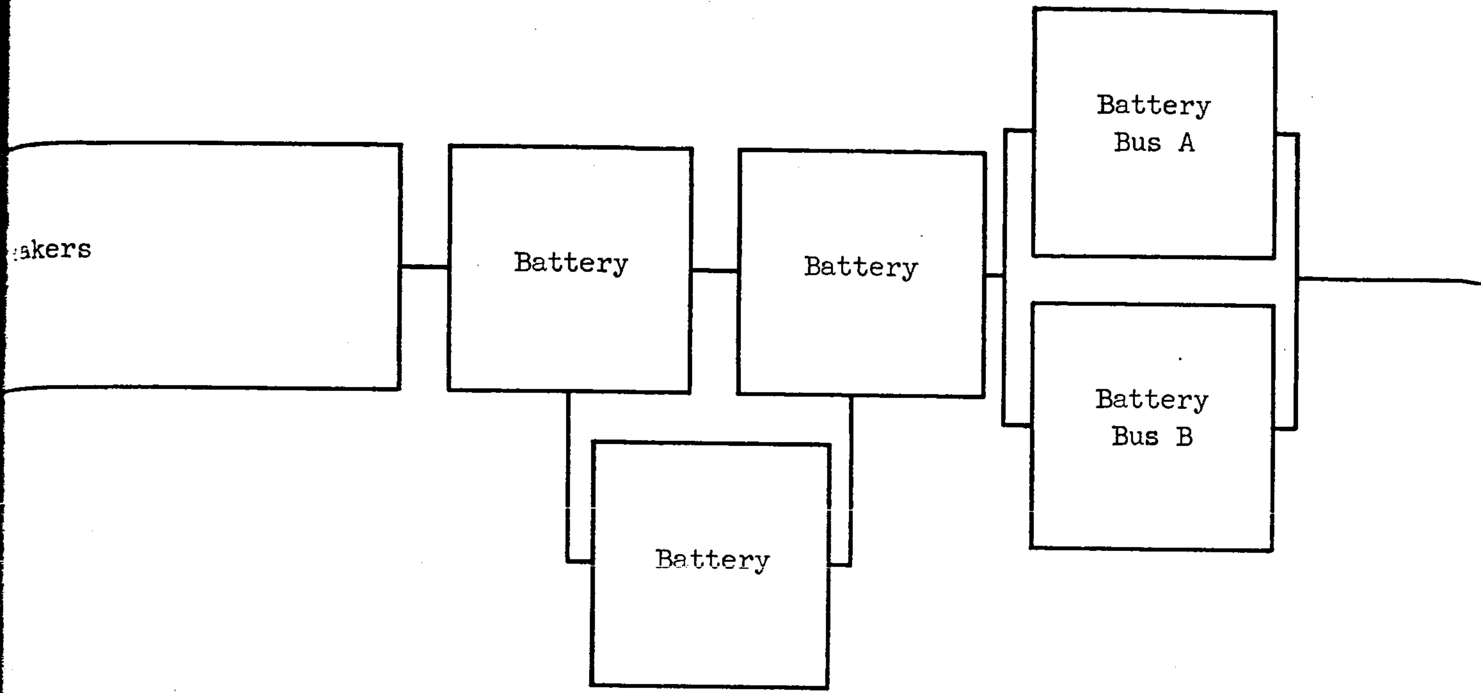
akers
Battery
Battery
Battery
Battery Bus A
Battery Bus B

	3 Standby Redundant Units, $\lambda 1 = 4.72 \text{ X } 10^{-6}$	2 Operating Redundant Units, $\lambda 1 = 2.72 \text{ X } 10^{-8}$	3 Standby Redundant Units, $\lambda 1 = 1.2 \text{ X } 10^{-4}$
	.999999978	.99999999956	.9997833
	.99999916	.99999999655	.997426
	.99999872	.9999999858	.983078
	.99998871	.9999999432	.909472
	.9999136	.9999997728	.648118
	.9997215	.9999994882	.39060

TABLE 18. PDS RELIABILITY ANALYSIS FOR PROLONGED MISSION APOLLO

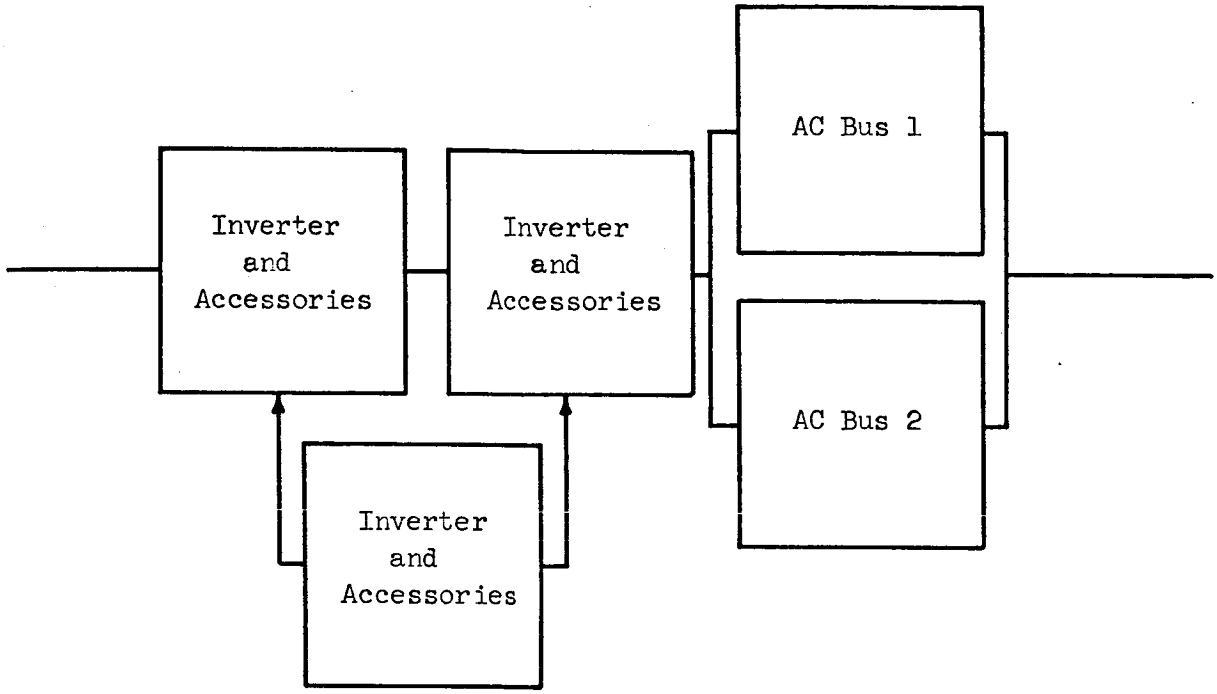
Inverter and Accessories
Inverter and Accessories
AC Bus 1
AC Bus 2
Inverter and Accessories

2 Operating Redundant Units, $\lambda 1 = 2.72 \times 10^{-8}$	P.D.S. Net Reliability
.99999999956	.9997737
.99999999655	.997406
.9999999858	.982704
.9999999432	.908756
.9999997728	.647056
.9999994882	.38958

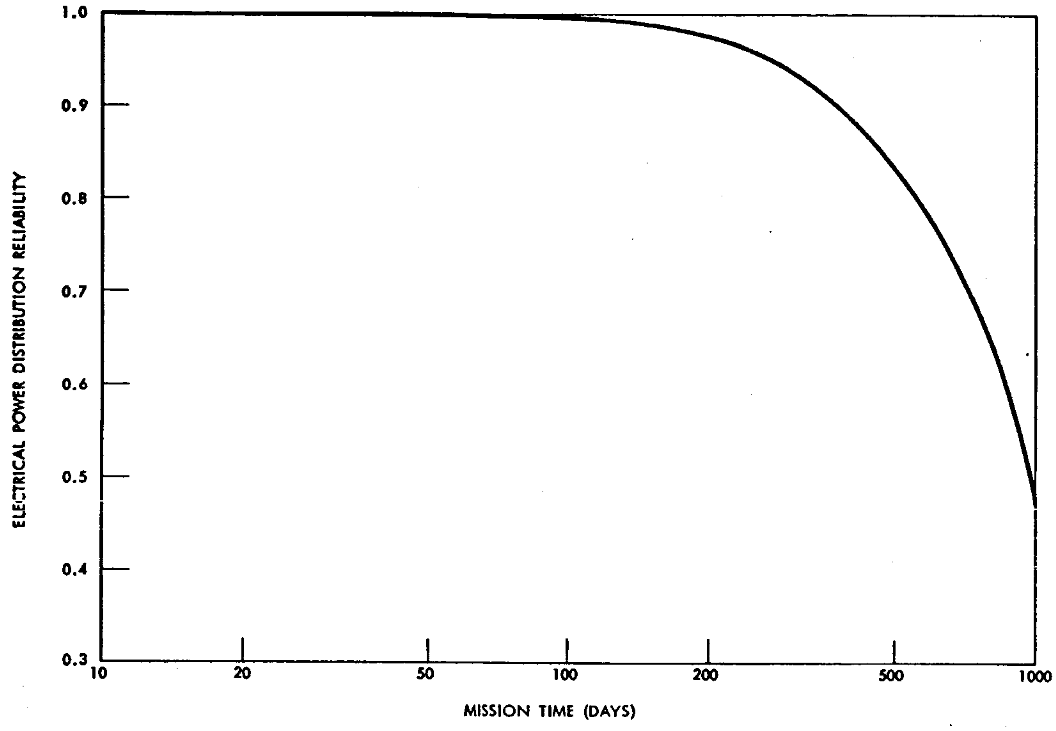

Figure 70. PDS Reliability for Prolonged Mission Apollo

prolonged mission Apollo. Alternatives must be considered, of which an electro-mechanical inverter or a square-wave solid state inverter are likely candidates; the latter appears attractive. Another attractive approach (In-Flight Maintenance) is discussed in Appendix A.

A square wave inverter can be built with a very small number of components; such an inverter will also be lighter in weight and more efficient than a sine wave inverter. It will therefore be more efficient and lighter as well as more reliable. In view of the difficulties associated with providing sine wave AC power for prolonged missions, the necessity of a sine wave inverter must be seriously questioned. A survey of waveform requirements of Apollo subsystems using AC power shows that substantially all subsystems could operate on square-wave power; if sine wave power is indispensable to any subsystem it must be a relatively small amount which may be derived by some less efficient but more reliable means than the present.

D-C SYSTEMS

The categories of subsystems requiring AC electrical power are:

1. Lights; fluorescent or incandescent. These operate as well or more efficiently on a square wave (of 400 cycles) than on a sine wave.

2. Electronic power supplies. These operate more efficiently, more reliably and with less ripple in the output of a square wave source than of a sine wave.

3. Induction motors. These may be made to operate as well on a square wave as on a sine wave--the slightly decreased efficiency of a square wave is offset by the increased efficiency of the square wave inverter: 90 percent versus 80 percent for a sine wave inverter. The fact that an induction motor will be operated on square wave power should be anticipated in its specification and design.

4. Instruments. Certain instruments may require AC power of high sinusoidal purity: these are resolvers and synchros. The amount of power required is not large, however, and may be avoided completely if such instruments are replaced by A/D converters and digital computation.

There is one serious objection to the use of square wave power and that is the greater amount of electrical interference associated with it. It would be advisable to attenuate the higher harmonics by low-pass filters and perhaps to use coaxial cable throughout for AC power distribution.

Electric Motors

The polyphase induction motor, because it is self starting, has no brushes or switches, operates at good efficiency and is reliable, has been selected for most Apollo applications. A review of this motor selection is indicated for prolonged missions since the polyphase inverters do not have sufficient reliability. If sufficiently reliable inverters cannot be developed it may be necessary to select motors which do not require sinusoidal polyphase power.

Brushless DC Motors

Brushless d-c motors are of two types: permanent magnet rotor and a Lundel excited rotor. In either case, either six or twelve switching transistors are required which would adversely affect reliability but not to the same extent as the inverter. (The inverters contain components of marginal reliability, i.e, capacitors, not used in brushless D.C. motors). As regards Apollo, the only characteristic of the DC motor that is desired is the fact that it will run on DC. Brushless D.C. motors that have other characteristics associated with DC motors are not generally desired. Thus the high starting torque of a series motor is accompanied by a high starting current which in larger sizes prevents them from being started on line. Such motors are useful in traction and rolling mills but for Apollo might entail special motor starting equipment to prevent excessive line surges. The work of Lear-Siegler has been directed toward developing brushless DC motors that behave like DC motors. These motors would offer Apollo characteristics of doubtful value at the price of greater weight and lower efficiency. The motors already developed by Sperry-Farragut, on the other hand, seek to maximize the efficiency to weight ratio as well as eliminate brushes. The principal difference is the use of a permanent magnet rotor and saving the weight of the field coils and energy dissipated in their windings. A second generation Sperry-Farragut brushless DC motor has a power output of 1.2 watts at an efficiency of 74 percent and weighs 8 ounces. The reliability is 95 percent for a one year mission. Sperry is also developing a 1/2 horsepower brushless DC pump motor for use on Saturn IB and V. The efficiency is 75 percent and the space envelope is 7 inches by 4 inches in diameter. The motor will run submerged in the pumped fluid. Brushless DC motors are characterized by low acoustic as well as electrical noise, thus providing an advantage in both electrical and acoustic communications. The permanent magnet rotor type motor is well suited for servos. Its linear voltage speed characteristics give it considerable self-damping, and lacking brushes, non-linear stiction effects are reduced. In some cases they could be used without tach feedback.

Square Wave Induction and Hysteresis Motors

The weak point of a brushless DC motor is the reliability of the solid state commutator which typically will employ 12 switching transistors. In a square wave induction or hysteresis motor these transistors can be reduced to four in a 2-phase multivibrator circuit which produces square wave from DC. These square wave inverters operate at efficiencies of 95 percent and have low weight. A schematic of a two phase inverter-motor is shown in Figure 71.

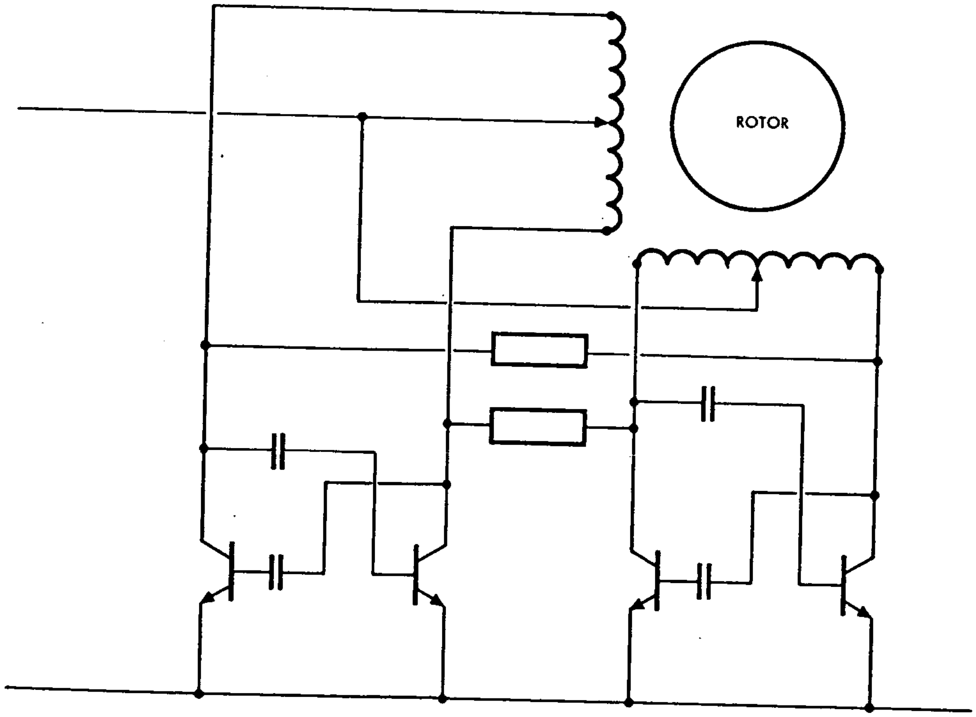

Figure 71. Two Phase Inverter - Motor Schematic

Essentially, there are two independent multivibrators using center-tapped motor field windings as load directly--no transformer required. The multivibrators are kept in proper phase by the networks represented by blocks.

The advantages of this concept are:

1. Any existing two phase motor can be used.
2. On line starting capability, since starting current is limited by winding inductance.
3. Adaptable either to induction type (slip) or hysteresis type (synchronous) rotors.
4. Only four switching transistors.
5. No transformer.
6. Low noise--essentially constant current is drawn from the line.
7. Low weight.

There is the following disadvantage:

A square wave consists of odd harmonics of diminishing intensity. The field of the 3rd and seventh harmonics rotate in a direction opposite to the fundamental and therefore reduce the torque produced by the fundamental--in principle. For induction motors we must distinguish two cases--a high resistance rotor and a low resistance rotor. In a high resistance rotor the current is in phase with the magnetic field and maximum torque is produced. Thus, such induction motors have good starting torque but low running efficiency due to the losses in rotor resistance. Such a motor operated on a square wave would have higher third harmonic losses. As regards the rotor, the induced current from the third harmonic is actually near the fourth harmonic due to relative rotor speed; the high frequency would increase the ratio of inductive reactance to resistance in the rotor and tend to both reduce third (or fourth) harmonic current and to throw it out of phase and eliminate the counter torque.

For a low resistance rotor on start, the current in the rotor is nearly 90 degrees out of phase with the field and low starting torque results. As the rotor picks up speed, the frequency of the induced current is reduced to the slip frequency, the inductive reactance is now smaller than the rotor resistance and good running torque and efficiency is obtained. As regards the third harmonic, the low resistance rotor is in an even more favorable position than the high resistance rotor. Rotor heat losses are proportionately reduced and there is essentially no counter-torque.

In summary, an induction motor operated on a square wave will be less efficient but the loss in efficiency may be negligible. Most induction motors are designed with low resistance rotors for efficiency. AC servo motors are an exception but they are not designed for efficiency in any case. If induction motors are to be operated on a square wave this fact should be taken into account in their specification and design.

A second type of motor operated in a square wave is the hysteresis motor or synchronous motor. Such a motor is usually designed to operate as an induction motor on start. Operated on a square wave, the rotor is subject to eddy current losses but these can be eliminated by a ferrite or laminated rotor.

Summary of DC Motor Characteristics

1. Conventional brush type motors: Low reliability, small weight and size, high efficiency, high RFI.
2. Lear-Siegler brushless DC motor: Medium reliability, greater weight and size, up to 75 percent efficiency, low RFI, quiet, so-called "DC" characteristics.
3. Sperry-Farragut brushless DC motor: As above, but slightly higher efficiency and slightly less weight and size. In a more advanced state of development.
4. Square-wave-inverter-motor combinations: Potentially most reliable, high efficiency, weight and size comparable to induction or hysteresis motors.

DC Communications Systems

The main advantage of using a 400 a-c sinewave power supply in the communications system is the possibility of using the phase of the supplied voltage to synchronize the different parts of the data system. If a-c power is to be replaced with d-c power, a new means of performing the synchronization function must be provided.

At least three different techniques seem feasible. First, the central timer, which is a part of the communication system, receives a 1024-kilocycle sync pulse from the G&N computer and supplies timing pulses to several devices such as the PCM, and PMP, and the data recorder. It would not be difficult to provide additional sync pulses to the other components of the communication system. Secondly, a timing pulse could be added to the dc power in such a way that the pulse be received by the equipment which needs it and filtered out by the equipment that does not need it. Finally, the power could be supplied in square-wave form, which would permit both synchronization and production of high voltage with transformers. The communication equipment manufacturers have indicated that their equipment could easily be redesigned to operate on d-c power instead of d-c and a-c power.

CONCLUSIONS

The Prolonged Missions analyses show that either a solar cell or an isotope power system can be developed in time for this program. The solar cell system can use either flat panels or concentrators and either nickel-cadmium or silver-cadmium batteries. The selection between flat panels and concentrators depends primarily on the cost of solar cells and the meteorite environment, particularly if further satellite programs indicate a high deterioration of mirror surfaces in space. In the absence of such an environment, however, it is recommended that the choice be made not only on the cost basis of this program but also considering future large space stations; if a solar array is contemplated for both programs, it should be the same type of array.

For low altitude earth orbits, silver-cadmium batteries do not exhibit the advantages one would expect from their higher energy density, due to recharge time and depth of discharge. The effects on total system weight from using nickel-cadmium versus silver-cadmium or vice versa are almost insignificant for a one year mission.

The Atomics International study of an isotope power system for Prolonged Missions Apollo indicated that it is entirely feasible to use Po^{210} as a power source in the early 1970 time period, and that a 3 KW Mercury-Rankine power generating system can be installed in Sector IV of the Service Module, using only the surface area of that sector for the radiator-condenser. Based on the operational and experimental flexibility that such a system would provide, it is recommended that the next generation of NASA missions beyond the 45-day Apollo AES use this system. It is further recommended that the system be used in the "Mission Support" mode in that electrical energy would be supplied from a vehicle that is replaced every 90-135 days. In this manner, the first generation dynamic power conversion system would only have to have man-rated reliability for around 120 days rather than its design point of one year. As operational experience with isotopes and the PCS is gained, later spacecraft could convert to longer lived isotopes and undertake missions of a year or longer with much higher confidence in the power system and its operational safety. It is therefore recommended that efforts to develop an isotope power system suitable for installation in the Apollo Service Module be continued.

Prolonged Mission studies indicated that power conversion reliability will be a significant problem and it is recommended that programs in inverter simplification and reliability improvement be initiated.

PROPULSION AND REACTION CONTROL SYSTEMS

CO[redacted]

PROPULSION AND REACTION CONTROL SYSTEMS

The fundamental aim of this study was to generate parametric propulsion and reaction control systems data which would be suitable for prolonged mission applications. The major parameters considered during the study included propulsion system weight, volume, thrust level, specific impulse, minimum impulse, and total impulse. In gross terms these data should enable selection and sizing a propulsion system to satisfy a specific mission cycle and total energy requirements.

The major design factors considered in this study were space environments, mission duty cycles, and durations. The influence of these factors was examined to assess their effect on the operational characteristics and storage life. Limited information indicated that the cumulative effects of mission duration that promote material degradation during exposure to propellants and space environments was of prime importance. Because insufficient data are available from which to accurately predict this cumulative effect of prolonged exposure, additional environmental testing is necessary in critical areas such as propellant valves, positive expulsion bladders, gimbal actuators, and chamber coating.

During this phase of the study technical support was provided by propulsion companies in the areas listed below.

Aerojet	SPS engine
Bell	RCS tanks
Marquardt	SM-RCS engine
Rocketdyne	CM-RCS engine

[redacted]

CONF[redacted]

MAIN PROPULSION SYSTEMS

MAIN PROPULSION ENGINES

The selection of a propulsion system for a space mission is not a straightforward process. Its selection depends to a large extent on a detailed mission and configuration analyses. The design and operation of the propulsion system is very closely inter-related with other spacecraft subsystems such as stabilization and control, guidance and navigation, electrical power, and structure. This complex inter-relationship must be carefully evaluated continuously throughout the design stage to develop an optimized propulsion system. Ideally the selected propulsion system should provide the highest performance and reliability, lowest weight and cost, and flexibility of operations. Since it is practically impossible to achieve all these factors simultaneously, some compromise must be made between mission requirements and state of the art in propulsion system capabilities. In addition, sufficient trade-offs involving the inter-relationship between performance, weight, operation, cost, and schedule must be performed to achieve a satisfactory design.

The engines considered for the main propulsion system of the prolonged mission Apollo vehicle were limited to those currently being developed for the Apollo program. These are the present Service Module engine which develops 21,900 pounds of thrust and the Lunar Excursion Module (LEM) descent engine which develops 10,500 pounds of thrust.

The Service Module engine is currently being developed by the Aerojet-General Corporation and is identified as Model AJ10-137. The AJ10-137 engine uses storable propellants, is pressure fed, provides fixed thrust, and is gimballed for thrust vector control.

The LEM descent engine is a throttlable engine currently under development by Space Technology Laboratory (STL). The STL throttling concept utilizes propellant flow control valves and a variable area injector to stabilize combustion at low propellant flow rates. Otherwise the basic engine design concepts are similar to the Service Module engine.

The performance and design characteristics of these engines are summarized in Tables 19 and 20.

Of primary concern is the capability of the main propulsion system or SPS of the present Apollo Block II to meet the performance and reliability goals specified for the prolonged missions. If these goals cannot be met, consideration would be given to design changes, the use of spares and redundancies and their implementation to improve the life of the critical components, or the use of a solid propellant system to accomplish the retro function.

[redacted]

The most critical reliability problems are reliable restart and satisfactory performance after long quiescent periods. Studies to date indicate the bi-propellant valve to be the most critical of the engine components in meeting the prolonged mission objectives. It is felt that a pneumatic system affords a considerable reliability improvement over the hydraulic actuation system formerly used with the SPS engine. However, the actual effect of the space environments on this and many other components is unknown at this time and tests must be conducted to verify predicted system performance.

Aerojet General Corporation has conducted a study* to determine the critical engine components to meet the prolonged mission reliability goals and how these components might be improved without violating the minimum design change philosophy.

Table 19. Performance and Design Characteristics of Aerojet-General AJ10-137 Apollo S/M Engine

Rated nominal thrust (vac), lb.	21,935
Nominal chamber pressure, psia	100
Rated duration (service life), sec.	730
Nominal specific impulse (vac), sec.	323
Min. specific impulse (vac), sec.	319
Nozzle expansion ratio	60:1
Fuel	0.5 UDMH + 0.5 N_2H_4
Oxidizer	N_2O_4
Ignition	Hypergolic
Nominal mixture ratio	2.0
Engine weight (dry), lb.	692
Type cooling	Ablative chamber/ radiation nozzle extension
Transition (ablative/rad.) at	6:1
Extension material	Columbium-titanium

---

*"Prolonged Missions Final Report - Service Module SPS Engine," Aerojet-General Corp. Report LR 650200, 7 April 1965.

Table 19. Performance and Design Characteristics of Aerojet-General AJ10-137 Apollo S/M Engine (Cont)

Type feed	Pressure
Nominal inlet pressure (valve inlet), psia	160
Nominal propellant inlet temp., °F	70
Oxidizer inlet temp. range, °F	30-135
Fuel inlet temp. range, °F	40-145
Gimbal angle range (nominal), degree	±7
Deflection rate, rad/sec.	0.30-0.35
Deflection acceleration rate, rad/sec.^{2}	2.3-2.8
Nozzle outside exit diameter, in.	100
Overall length (max.), in.	160
Restarts (min.)	50
Throttling range	None

Table 20. LEM Descent Engine Performance and Design Characteristics

Performance	
Thrust (vacuum) lbs., after 5 sec.	10,500
Thrust (vacuum lbs., end of life at maximum thrust setting	11,010
Throttling range	10:1
Chamber pressure, maximum rated thrust, psia	110
Propellants	
Fuel (MIL-P-27402)	Aerozine 50
Oxidizer (MIL-P-26539A)	N_2O_4
Propellant density at 70°F, lb/ft^3	
Fuel	56.3
Oxidizer	96.1

Table 20. LEM Descent Engine Performance and Design Characteristics (Cont)

Mixture ratio, oxidizer to fuel (wt), instantaneous, at maximum rated thrust	1.6
Mixture ratio, oxidizer to fuel (wt), instantaneous, at minimum rated thrust	1.6
Nominal interface pressure, psia	210
Design Characteristics	
Chamber diameter, maximum, in.	14.2
Chamber length, injector face to throat, in.	14.7
Nozzle length, throat to exit plane, in.	62.11
Overall length (including injector), in.	85
Nozzle contour, percent bell	72.3
Characteristic length (L*), in.	40
Gimbal angle, two plane	±6°
Gimbal location	Throat
Shut off valves	Quad, bipropellant
Throttle actuator	Electromechanical redundant
Nozzle extension	Radiation cooled 16:1 to 47.5:1
Weights	
Total engine, dry	350
Throttle actuator	14.5
Shut off valves	15.5
Injector, linkages, flow control valves, etc.	72.5
Thrust chamber	192.0
Nozzle extension	29.5
Harness, instrumentation, miscellaneous	26.0

---

*Standard propellant supply conditions
Inlet pressure = 210 psia
Propellant inlet temperature = 70°F

The space environmental parameters affecting engine design are: (1) vacuum, (2) heat transfer, (3) radiation, and (4) micrometeoroid flux.

The vacuum of space can cause out-gassing of elastomeric parts by being below the vapor pressure of the material at operating temperatures. Cold welding and galling of metal parts in contact can occur. Heat transfer characteristics will be altered by increased heat transfer caused by radiation.

Electromagnetic and particulate radiation could degrade material properties, primarily by lattice displacement of crystalline materials, and severing of long chain molecular bonds in organic compounds.

Damage by micrometeoroid penetration could seriously degrade the performance of the propulsion system and may ultimately cause mission failure. Impact and penetration of the thrust chamber and nozzle extension are the most probable mode of damage.

The operational requirements of the various prolonged missions impose specific duty cycles on the SPS engine. These duty cycles establish the engine operational thermal environment. For the purposes of this study, the engine compartment temperature was specified to be between +30 F and 150 F. Therefore, all engine components within the engine compartment were analyzed assuming this temperature range. The nozzle extension which is outside the engine compartment was thoroughly analyzed, taking into account the heat transfer characteristics of the space environment. This analysis allows determination of the nozzle extension periodic steady-state temperature.

Certain mission duty cycle firing periods were consolidated in order to produce a realistic "most severe case" thermal analysis.

Estimates of component and system life with respect to prolonged missions indicate that the present Apollo Block II SPS engine should meet the mission support and logistics support operational requirements up to 90 days duration. The present SPS engine can also meet the operational requirements for the 360-day earth polar orbit mission support minimum mission profile. For all the other missions, with the exception of the earth polar orbit mission support vehicle maximum 600-day mission profile, the operational requirements can be met by use of selected design modifications. Therefore, the earth polar orbit mission support vehicle maximum 600-day mission is considered beyond the capability of the SPS engine based on the design constraints and assumption used in the study.

The capability of the present Apollo engine and modified engine to meet the prolonged mission requirements is based on engineering estimates of the engine components ability to function properly after exposure to the prolonged mission environment. The actual effect of the space environment on many components, is, however, unknown at this time and tests must be conducted to verify predicted component performance.

The results of this study indicate the bipropellant valve to be the most critical of the engine components in meeting the prolonged mission's reliability goals. The pneumatic system used in Block II Apollo affords a considerable reliability improvement over the hydraulic actuation system formerly used with the SPS engine. However, additional reliability improvement is possible through use of the electrical actuation system. Preliminary analysis of the electrical actuation system presented in this study verifies the engine reliability improvement. Additional studies are required to determine the ultimate capability of the electrical system for extended missions.

Based on preliminary reliability trade-off analysis, the presently designed thrust chamber should provide sufficient margin to achieve prolonged earth orbit missions. The true effect of nozzle meteoroid penetration and erosion is difficult to quantitize; shortening the nozzle or providing shielding should be considered if a problem exists. Additional study should be conducted in this area to define the meteoroid problem.

The propulsion system weight and volume data presented in this report are intended only as a preliminary guide for the selection of propulsion systems. This is because factors other than weight alone must be considered in the design of the propulsion systems for the prolonged mission vehicles. These factors include: (1) controllability of total impulse; (2) controllability of thrust vector angle; (3) engine throttling; (4) engine restart; (5) storability and environmental control; (6) reliability; and (7) cost.

The data do, however, point out the influence of thrust-to-weight ratio on the overall weight of propulsion systems. The thrust-to-weight ratio of liquid propellant systems has a large influence on propulsion system weight, especially for small incremental velocity requirements such as encountered in the operational modes studied here. In systems requiring larger velocity requirements, the propellant quantity increases relative to the module weight, thereby decreasing the quantity (F/W/V), as shown in Figure 72, results in higher propellant fractions.

Figures 72 and 73 present propellant fraction data for solid motors and liquid propellant systems, respectively. Solid motor propellant fractions are representative of values that are presently obtainable in high thrust-to-weight ratio and high performance motors designed for space applications. Propellant fractions for liquid propellant systems were determined from parametric weight data which were generated for the subsystems within the propulsion system. The latter data show clearly the sensitivity of liquid propulsion system weight to thrust level. The large weight increase with increased thrust for liquid systems explains in part why solid motors are often favored over liquid systems for high thrust-to-weight ratio applications. Propellant fractions of solid propellant motors are generally less sensitive to thrust level for a specified combustion pressure.

It should be noted that the propellant fraction and propulsion system weight data presented here for solid motors do not include an allowance for thrust vector control. The effect of a TVC system on propulsion system weight can best be determined in a design study taking into consideration the mission and configuration parameters involved.

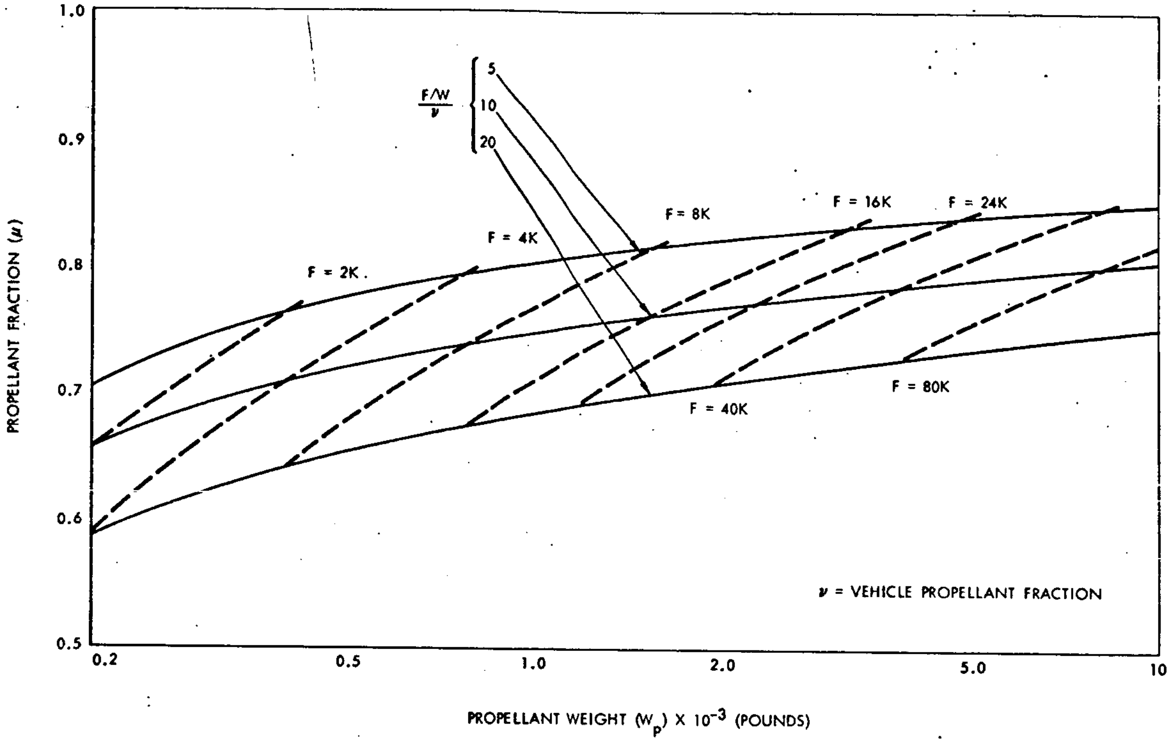

Figure 72. Propellant Fraction - Liquid Propellant Propulsion Systems

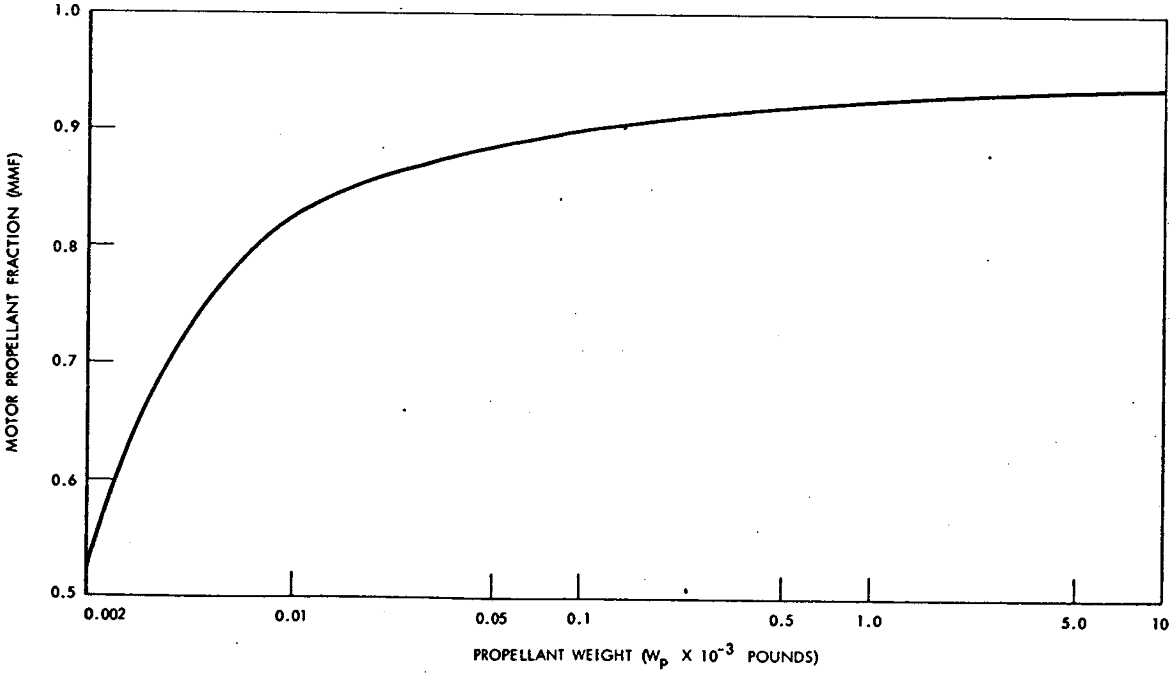

Figure 73. Propellant Fraction - Solid Propellant Motors

The propellant fraction data on liquid propellant propulsion systems is based on the following:

Propellants - N_2O_4/50 N_2H_4 - 50 UDMH at a mixture ratio of 2.0
Chamber pressure (Pc) - 100 to 200 psia
Propellant Tank pressurant - Helium
Engine type - Ablative chamber with radiation cooled nozzle
Pressurant storage pressure - 4500 psia
Propellant tank material - Aluminum 2014 T6
Propellant tank configuration - two tanks per propellant (4 tanks total), each tank having an l/d of 4.0. Tanks are clustered symmetrically around thrust axis.
Residual propellants - no allowance made
Thrust vector control - gimballed engine
Propellant expulsion - settling thrust, no allowance made for bladders, etc.
Inertial loads are not transmitted through the propellant tanks or their supporting structure, except the inertia loads experienced by the propellant and tanks themselves
Propellant tank pressure (P_p) - 300 psia
Pressurant tank material - Titanium 4Al -6V
Engine nozzle area ratio (E_n) - 60
Propellant tank safety factor (S.F.) - 1.5
Pressurant storage tank safety factor (S.F.) - 2.0

The propellant combination N_2O_4/50 N_2H_4-50 UDMH was selected for this study because of the relatively high confidence that can be placed in its storability and high performance. Also, much basic experience has already been gained relative to the use of this combination in throttleable engines and in ablation cooled engines for space application.

PROPELLANT FEED SYSTEMS AND TANKS

The series tank arrangement presently used in Apollo can also be used in the prolonged mission Apollo. However, the use of the parallel tank arrangement offers the following advantages:

1. Reduced y and z plane c.g. excursions which reduce engines gimbal angle requirement

2. Elimination of transfer standpipes which can cause large pressure surges with resultant system problems

3. Potential system weight reduction by allowing lower regulated tank pressure

Care must be taken with the parallel tank arrangement to assure that the two oxidizer and the two fuel tanks deplete simultaneously. This may require that the parallel portion of the oxidizer and fuel feed systems be calibrated to assure equal flow from each oxidizer and each fuel tank. Use of single oxidizer and fuel tanks can eliminate this problem at the expense of lateral C.G. movement. The optimum tank arrangement must be determined by a more detailed design study.

A propellant utilization system is provided to assure that the oxidizer and fuel are depleted simultaneously. The type of system to be used can be similar to the S/M SPS or RCS with modification for the new propellant tank sizes. For some cases; where the vehicle is not weight-limited a propellant utilization system may not be required. Extra propellant can be loaded to provide for the mixture ratio tolerance of the engine. For some missions requiring small quantities of propellant, the propellant utilization system may be heavier than the possible residuals. Table 21 presents the SPS propellant load and tolerances.

Table 21. SPS Propellant Load

	Fuel	Oxidizer
Manufacturing Tolerance	225 lb	450 lb
Ullage	135 lb	420 lb
Loading Tolerance	150 lb	300 lb
O/F Shift	150 lb	300 lb
Trapped	75 lb	150 lb
Usable	15,000 lb	30,000 lb
Prop. Density at 70 F	56.3 $\mathrm{lb/ft^3}$	90.3 $\mathrm{lb/ft^3}$
Tank Volume	279.4 $\mathrm{ft^3}$	350 $\mathrm{ft^3}$

The weight of the propellant tanks were approximated by the following relation:

$$W_t = \frac{1728 \times 2 \times 1.05\, W_p\, P_p\, (S.F.)\, \rho m\, (\ell/d - 1/2)}{\rho_p \times S_u(\ell/d - 1/3)}$$

allowance for 5% ullage space is included

Where

W_t = tank weight (lb)
W_p = Propellant weight (lb)
P_p = propellant tank pressure (psia)
S.F = safety factor
ℓ = tank length (ft)
d = tank diameter (ft)
ℓ_m = tank material density ($\mathrm{lb/in^3}$)
ℓ_p = propellant density ($\mathrm{lb/ft^3}$)
S_u = ultimate material tensile strength (psi)

For the purpose of this study average specific impulses of 315 seconds and 285 seconds were assumed for liquid and solid propellant systems, respectively. The weight of propellants required for the various functions were calculated from the following from the velocity increment equation:

$$W_p = W_i\left(1 - e^{-\Delta V/gI_{sp}}\right)$$

where W_p = propellant weight, lb.
W_i = initial vehicle weight, lb.
ΔV = velocity increment, ft/sec.
I_{sp} = specific impulse, lb_f/lb_m/sec.
$g \doteq$ gravitational constant, 32.174 ft-$lb_m/lb_f sec^2$

Figure 74 presents approximate propulsion system weights for two typical prolonged mission incremental velocity requirements as a function of vehicle weight.

The pressurization system concept is exactly the same as the present Apollo. The helium storage tank is reduced in size because the helium requirement is less than the present Apollo. The pressurization system components located between the helium storage sphere and the propellant tanks have exactly the same configuration and function as the present Apollo. Even though the present Apollo components are designed for a higher flow rate than is required if the LEM descent engine is used, the Apollo components are used where possible to minimize compenent modification or redesign. The regulators and relief valves will require modification to provide higher regulated pressure and relief pressure if the LEM engine is used.

Table 22 summarizes the engine propellant inlet conditions which are reflected in the design of the propellant and pressurization system for the two candidate engines.

The helium pressurizing gas requirement for the two propulsion systems under consideration was determined by

$$W_{sg} = \frac{P_T V_T n}{Z_T R T_{s1}\left(1 - \frac{Z_{s1} P_{s2}}{Z_{s2} P_{s1}}\right)}$$

where W_{sg} = weight of pressurant required
P_T = propellant tank pressure
V_T = propellant tank volume
R = gas constant
T_{s1} = initial pressurant temperature
P_{s2} = final pressurant pressure
P_{s1} = initial pressurant pressure
Z = pressurant compressibility factor

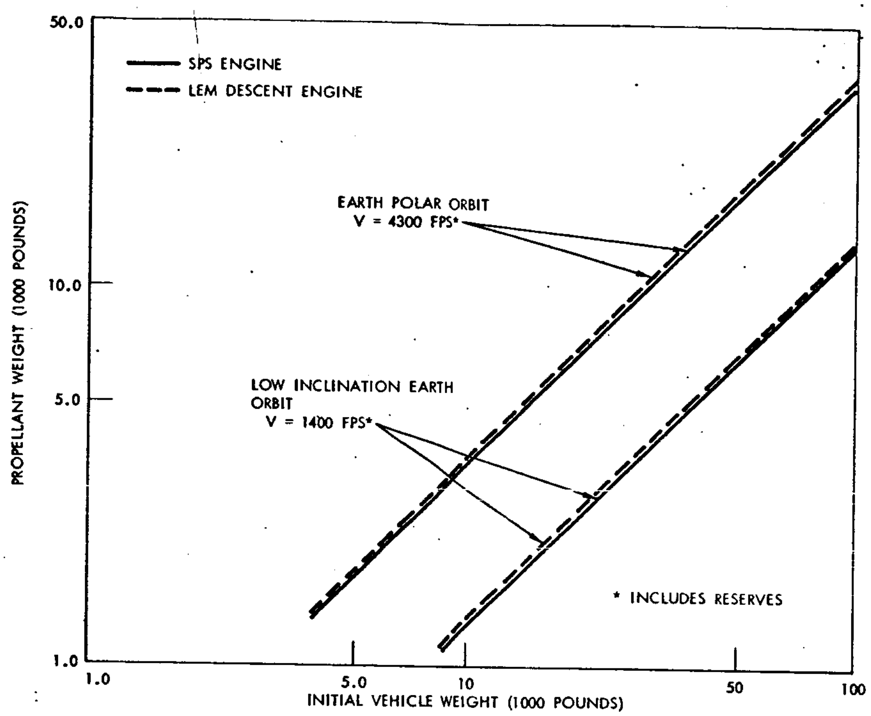

Figure 74. Initial Vehicle Weight

Table 22. Engine Propellant Inlet Requirements

	Apollo SPS Engine	LEM Descent Engine
1. Chamber Pressure, psia	100	110
2. Flow Control Valve Nominal Inlet Pressure, psia		
(a) Oxidizer	160	210
(b) Fuel	163	210
3. Flow Control Valve Nominal Inlet Temperature, F	70	70
4. Oxidizer Flow Rate, lb/sec	45.3	21.2
5. Fuel Flow Rate, lb/sec	22.6	13.2

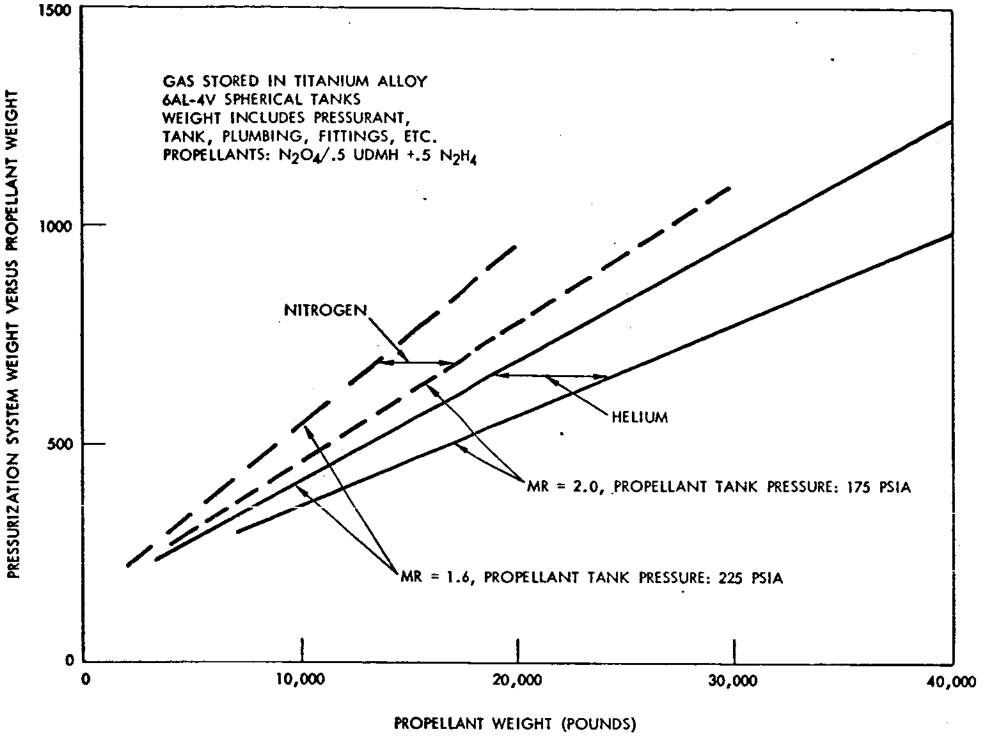

Figure 75. ·Pressurization System Wt. Vs. Propellant Weight

This expression was derived from the conservation of energy, $dQ = dU + dW$, for an isentropic process. Then the expression was modified by replacing the isentropic exponent, $\gamma = C_p/C_v$, by the polytropic exponent n, to approximate the actual process with heat transfer. The value of $n = 1.25$ is being used in the present Apollo for helium.

The weight of pressurization system is shown parametrically in Figure 75. Pressurization system weight is presented as a function of propellant weight for the mixture ratio corresponding to the SPS engine and the LEM descent engine. Pressurization system weight is greater for the LEM engine because of the higher propellant inlet requirement. Pressurization system weight includes the pressurant, pressurant tanks, and components.

REACTION CONTROL SYSTEM

The design of the RCS engine and propellant system are dependent on the requirements established by detailed mission analysis. The control requirements will vary greatly with the various phases of the mission as well as for the different missions. Spacecraft design for complex mission objectives may require a wide range of control capabilities. Therefore, a compromise may be required between the opposite extremes of the control spectrum, i.e., low rotational rates and high precision versus high thrust and fast response.

Vehicle maneuvers requiring low rotational rates and tight attitude may include navigational sightings, extended mapping, and maintenance of proper alignment of solar cells or communication antennas. A high rotational rate would be required to achieve fast vehicle response for main engine propellant settling and terminal rendezvous and docking.

Ideally, it is desired to design RCS that has the maximum possible steady state performance, as well as high pulse performance, and very low highly repeatable minimum impulse capability. However, it is impossible to optimize performance characteristics of the RCS in all these areas.

Since in some particular missions steady state operation may be the dominant mode, whereas in other missions short pulse limit-cycle operation may be dominant, trade-offs will be necessary. If a mission has several duty cycle requirements, then the overall spectrum of these requirements should be evaluated. The importance of these factors becomes increasingly critical as mission durations increase.

RCS ENGINES

The performance capability of the RCS is strongly interrelated with the stabilization and control system. Consequently, the control system logic plays an important role in the optimization of the RCS. Both the RCS and spacecraft must be tailored to match mission requirements with respect to limit cycle operation and the deadband and maneuver rate tolerance specified for such operations. Using a simple box limit cycle as an example, simplified control theory shows that the total propellant required for attitude hold (after acquisition) is dependent on the relationship

$$W_p = \frac{n^2 R \, t_m \, (I_t)^2}{4 \, J \theta_o \, I_{sp}}$$

Where n = number of engine operating simultaneously

R = torque-arm

t_m = elapsed time

I_t = impulse-bit per pulse from each engine

J = moment of inertai about axis considered

θ_o = deadband limit angle

I_{sp} = average specific impulse per pulse

Assuming R, t_m, J, and θ_o to be constant the above expression simplifies to

$$W_p \simeq \frac{K\,(I_t)^2}{I_{sp}}$$

Therefore, extended periods of attitude hold are required for special experiments such as mapping, significant propellant savings can be obtained by utilizing smaller impulse bits as long as they are larger than the disturbing torques. In reality, limit cycle operation is significantly more complex; however, the above discussion shows potential trade-offs that are available.

During limit cycle operation, low minimum impulse bit capability will result in fewer operations of the RCS engines which in turn means increased engine life, increased reliability, and less propellant consumption.

There are several means of extending the minimum impulse capability of a fixed thrust engine such that lower and more repeatable impulse bits are possible. For a design, the impulse bit performance characteristics is a function of electrical pulse width. The tolerance on the impulse bit for a given electrical pulse width is a function of many variables (i.e., solenoid valve characteristics, engine repeatability, system effects, duty cycle, temperature, etc.). However, the dominant factor associated with minimum impulse bit is the solenoid valve operating characteristics as these determine the valve full open time and subsequently the total amount of propellant that will be injected into the combustion chambers during the pulse widths. The solenoid valve characteristics are affected by pressure, temperature, and manufacturing tolerances as well as operating voltage.

For given a thrust size bi-propellant engine, the minimum impulse bit capability can be extended by basically two means:

1. Injecting less total propellant into the combustion chamber

2. Operating the engine less efficiently at the small pulse widths.

At the small pulse widths, the total amount of propellant injected into the combustion chambers is a direct function of the response characteristics of the solenoid valves. By utilizing faster response solenoids or by designing valves which are not sensitive to factors such as voltage, temperature, etc., smaller and more consistent amounts of propellant can be injected into the combustion chamber with subsequently smaller and more consistent impulse bits resulting. For instance, the bi-stable actuator valve developed by the Marquardt Corporation has such characteristics. Changes in response characteristics as a result of variations in voltage, pressure and temperature are significantly smaller with the bi-stable actuator than with the present solenoid valve.

The pulse performance characteristics of a bi-propellant RCS engine is dependent on a very complex inter-relationship of many factors such as injector design, combustion chamber design, valve response characteristics, line dynamic characteristics of the propellant system, duty cycle, etc. However, the major trade-off that is required among this inter-relationship is balancing the desired steady-state performance characteristics versus the desired pulse performance characteristics. Usually desirable design criteria for steady-state operation is undesirable for pulse operation. Engines designed for a short pulse operation should have fast operating valves, small propellant volumes (dribble volume) injector head, and small volume chambers. However, steady-state operating engines can use slower, less power consuming valves, more optimum propellant injection designs, and larger chamber volumes for higher performance. The final engine design, is therefore, a compromise design which is highly dependent on the specified mission duty cycle requirements. However, the utilization of a bi-modal thrust engine concept such as previously discussed holds excellent promise of decoupling many of these adverse relationships between steady-state and pulse operation.

For steady-state operation, increased L* results in increased performance capability. However, when very small pulse width operation is considered, the opposite is true. As L* increases, the thrust chamber time constant increases causing a performance decay in the same manner as increased dribble volume. The net effect is a deterioration of performance resulting when small pulse requirements are imposed on an engine having an L* which permits optimum performance for steady-state combustion.

For low puse widths, the single doublet injector results in more efficient combustion performance. This is because a large dribble volume X (propellant volume in the injector head between the solenoid valves and the combustion chamber) is required for a multiple doublet design as compared to that for a single doublet. After the propellant valves close, the combustion of the dribble volume propellants is inherently inefficient as good mixing no longer occurs. Hence, a fixed dribble volume has an increasingly more detrimental effect on performance as the pulse width is reduced. Conversely, as the pulse width is increased, the better mixing capabilities of multiple doublet injectors obscure the detrimental effect of excessive dribble volume and eventually result in an overall improvement in performance over that obtained with a single doublet injector.

Performance of short pulses is also greatly dependent on the hydraulic line dynamics of the propellant supply system as well as the hydraulic design of the injector head. Optimization of the propellant line dynamics will result in more efficient and more repeatable pulse performance characteristics for a given engine.

One of the most likely methods of increasing the steady-state thrust to minimum impulse ratio is to utilize two or more different thrust level engines on the spacecraft. Some of the concepts that might be utilized are discussed in the following paragraphs. However, these approaches would involve broad interfaces and trade-offs with the mission, vehicle, and other spacecraft subsystems.

An alternative that shows excellent promise for extended ranges of operation is the bi-modal thrust engine. This concept would incorporate high thrust (i.e., 100 lb) as well as a low thrust (i.e., 5 pound) level capability within a single engine. Because of the potential of this concept, the Marquardt Corporation is presently pursuing development of this concept under its own funding.

The Apollo service module RCS is optimized to provide rotational and translational maneuvers of a manned lunar spacecraft. Studies represented in this report indicate that the same system with minor modifications can be used for prolonged manned orbital flight. However, it is possible to further optimize RCS. One area which requires careful consideration is that of using the present system of 100 pound thrust units for vehicle attitude hold during partial or full limit cycle operation.

During the entire 14 day Apollo lunar mission, a small percentage of total RCS propellant allotment is used for attitude hold during limit cycle modes; however, the prolonged mission vehicle RCS main function is to provide vehicle attitude hold for scientific experiments and perhaps for efficient solar cell usage. For this reason a RCS optimized for this type of operation is important. An analysis of propellant consumption for limit cycle operation is discussed below to illustrate thrust chamber size and pulse width effects.

Figure 76 shows a typical thrust-time relation for a single on-off or bang-bang cycle of a short pulse-width type of control engine using a liquid oxidizer and fuel. The inadequacy of using either the 90 percent or 10 percent thrust time interval is readily apparent because of the series of typical pressure spikes resulting from lack of equilibrium between liquid injection and gaseous exhaust flow rates. Accurate integrations of the areas under the thrust-time curve and the corresponding flow-time curve are needed to obtain the total impulse and propellant bits. The ratio $\int F dt / \int \dot{w} \, dt$ is then the pulse average specific performance, $\bar{I}_{sp}$ which must be correlated with the demand on-off signal time to be useful in the limit cycle application.

For on-off times of about 1 second or longer, the average specific impulse performance of such engines is essentially the same as the asymptotic value at steady state. The losses due to initial cold start and to the remaining propellant dribble volume downstream of the valves after closing then become negligible.

Figure 77 illustrates basic concepts involved in the limit-cycle application. Figure 77A shows two similar, but oppositely directed attitude control engines, having equal average thrust $\bar{F}$ during the demand on-off time,

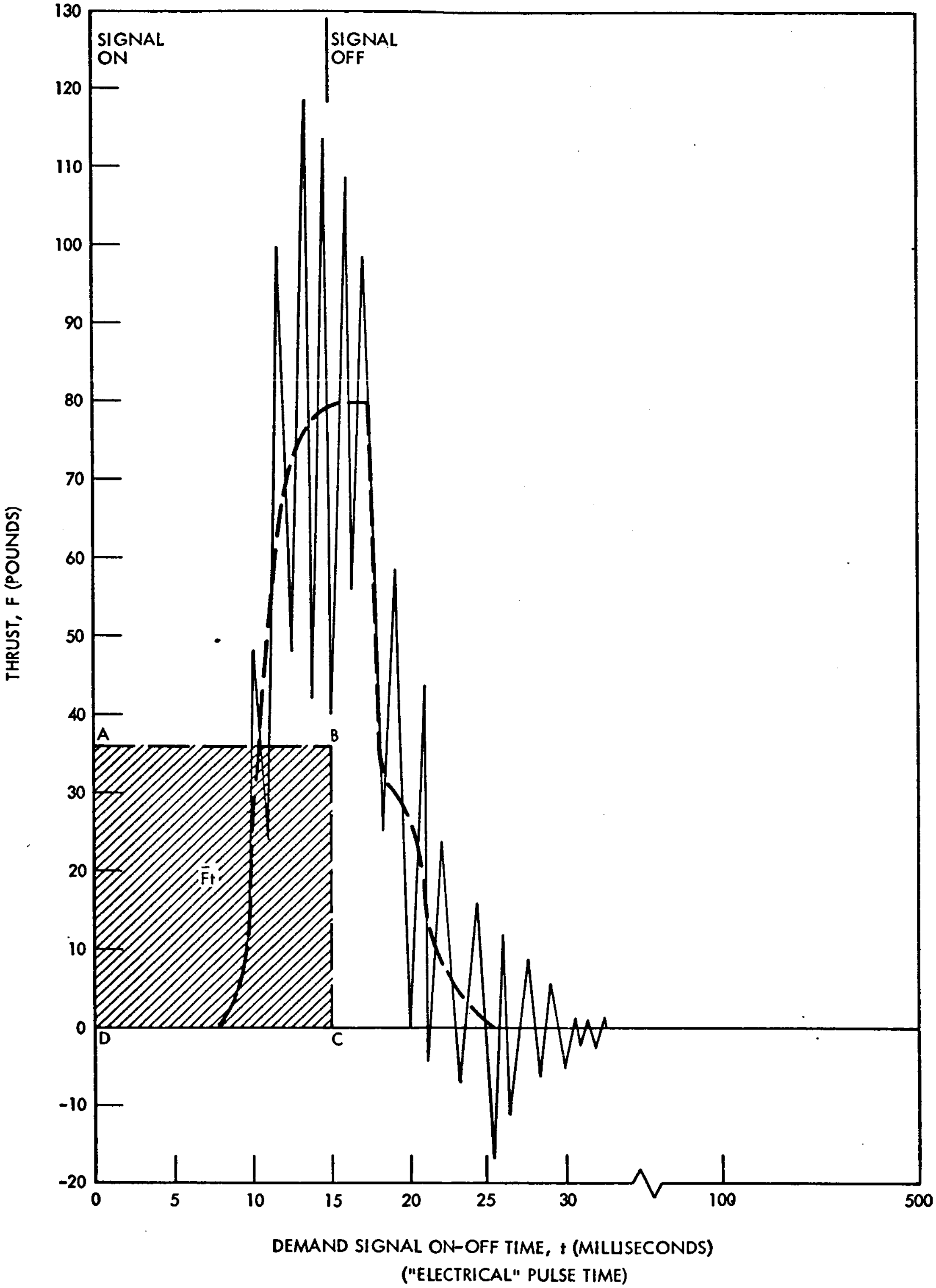

Figure 76. Short-Pulse Reaction-Control-System Engine, Performance Schematic

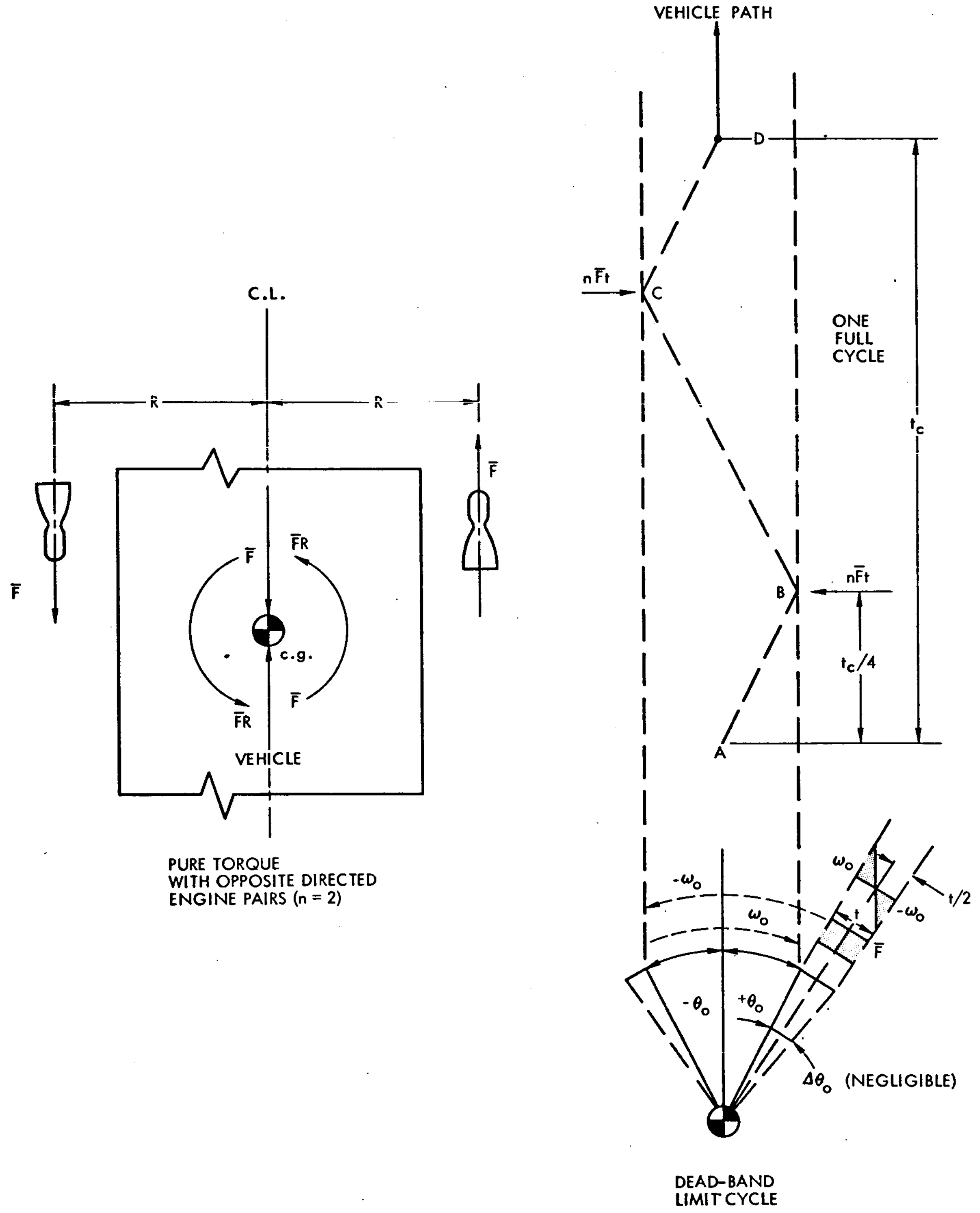
VEHICLE PATH
D
$n\bar{F}t$
C
ONE FULL CYCLE
t_c
B
$n\bar{F}t$
$t_c/4$
A
C.L.
R
R
$\bar{F}$
$\bar{F}$
$\bar{F}$
$\bar{F}R$
$\bar{F}R$
$\bar{F}$
c.g.
VEHICLE
PURE TORQUE WITH OPPOSITE DIRECTED ENGINE PAIRS (n = 2)
$-\omega_o$
ω_o
ω_o
$-\omega_o$
t/2
t
$\bar{F}$
$-\theta_o$
$+\theta_o$
$\Delta\theta_o$ (NEGLIGIBLE)
DEAD-BAND LIMIT CYCLE

Figure 77. Limit-Cycle Theory for Reaction-Control Engines, Schematics

and acting at the same distance R from the center of gravity (or center of mass, in space) to provide pure torque control. Figure 77B is a schematic of one type of deadband limit-cycle concept, as applied to any one of the three axes for pitch, yaw, or roll-control. The angular velocity about the axis under consideration is assumed to be constant at the allowable maximum value in one direction during the quarter-cycle AB, or $t_c/4$. At point B the deadband limit angle θ_o is exceeded and a demand circuit is closed for a reversing angular impulse, n R Ft. Half of this angular impulse bit is required to decelerate ω_o to zero, and the other half to accelerate to $-\omega_o$, in the opposite directions. Thus, from the basic relation between torque and angular acceleration

$$T = J\alpha \tag{1}$$

or

$$\alpha = \frac{d^2\theta}{dt^2} = \frac{-n\,\bar{F}t\,R}{J} \tag{2}$$

the relation between constant deadband velocity and impulse bit is found after integration to half the on-off or nominal pulse time, t/2 to be:

$$\omega = \frac{d\theta}{dt} = \frac{-n\,R\,(\bar{F}t)}{2J} + \omega_o = 0 \tag{3}$$

or

$$\omega_o = \frac{n\,R\,(\bar{F}t)}{2J} \tag{4}$$

where

ω_o = maximum allowable angular velocity in radians/sec within the deadband angle $\pm\,\theta_o$,

n = number of engines operating simultaneously

R = torque-arm, ft

(Ft) = impulse-bit, lb sec

J = moment of inertia about axis considered, slug-ft^2

Neglecting the on-off time (milliseconds) as second-order compared to the quarter-cycle (minutes), the full cycle period becomes:

$$t_c = \frac{4\theta_o}{\omega_o} = \frac{8J\theta_o}{n\,R\,(\bar{F}t)} \tag{5}$$

Since this cycle includes two alternating directions of the angular impulse from n engines, the total number of impulse bits in a mission time, t_m, would be:

$$N = \frac{2\,n\,t_m}{t_c} \qquad (6)$$

or with t_c from Equation (5),

$$N = \frac{n\,\omega_o\,t_m}{2\,\theta_o} = \frac{n^2 R\,t_m\,(\bar{F}t)}{4\,J\,\theta_o} \qquad (7)$$

The total propellant consumed during the mission time for the limit cycle control could be obtained from the total number of bits from Equation (7) for each axis multiplied by the propellant weight per bit, if the latter were available from a characteristic performance curve. The total propellant can also be calculated from the correlated average specific impulse in accordance with the defining relations:

$$\bar{I}_s = \frac{\bar{F}}{\dot{\omega}} = \frac{(\bar{F}t)}{(\dot{\omega}t)} = \frac{N\,(\bar{F}t)}{N\,(\dot{\omega}t)} = \frac{N\,(\bar{F}t)}{W_p} \qquad (8)$$

where W_p = total propellant in lbs for N impulse bits.

From Equations (7) and (8), the total propellant per axis is:

$$W_p = \frac{N\,(\bar{F}t)}{\bar{I}_s} = \frac{n^2\,R\,t_m\,(\bar{F}t)^2}{4J\;\theta_o\,I_s} \qquad (9)$$

The total propellant weight required for pitch, yaw, and roll limit control would be the sum of the three respective weights from Equation (9) for each of the functions, taking into account any differences in the values of the contributing parameters including any changes during the mission life.

Equation (9) indicates that total propellant for the limit cycle will vary directly as the square of the impulse bit and inversely as the average specific impulse performance. Figure 78 shows the resulting relative total propellant consumption for the limit-cycle operation (per axis under control) for two values of the time cycle defined in Equation (5), and varying levels of nominal thrust. The consumption for a time-cycle twice as great as that for the upper solid reference curve is reduced markedly to only 25 percent for nearly all levels of nominal thrust. However, even with this cycle time stipulated by other requirements (not presently clearly established) a reduction in total propellant consumption of about 60 percent is indicated

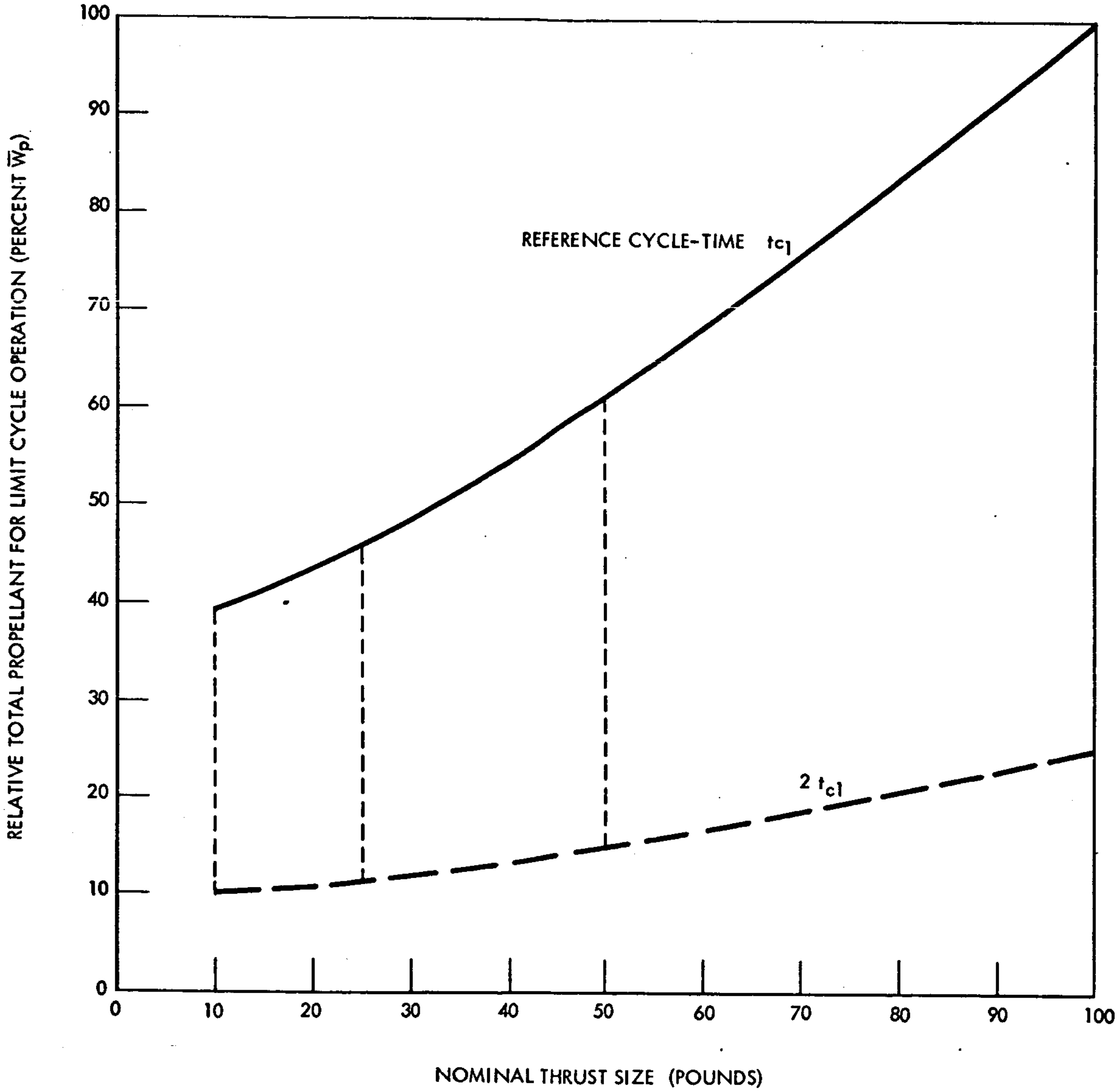

Figure 78. Propellant Requirements a Function of Thrust Level for Reaction-Control-System Limit-Cycle Operation

by use of a 10-pound thrust size. Accurate characteristic operation curves for the various engine sizes will provide the basic data needed for optimization under a variety of required conditions.

RCS TANKS

Results of previous studies indicated that one of the possible problem areas is in the RCS positive propellant expulsion devices. A positive expulsion capability for an RCS propellant tank can be provided by any of several possible mechanisms, some are discussed below. Present day space vehicles are relatively short duration systems which can use the very adaptable bladder system; however, as missions duration increase, the selection of a reliable positive expulsion device becomes more complicated.

In addition to the mission function which must be considered, the environmental conditions encountered during the mission affect the life of the expulsion device; this is especially true when considering Teflon bladders as those used on the Apollo spacecraft. During the study, preliminary analyses were made to determine the possible problems which would be encountered, as well as a survey of applicable expulsion devices. Some of the data presented below is information prepared by Bell Aerosystem Co. The following paragraphs describe various positive expulsion concepts as well as comparisons of each for the desired missions.

The function of a positive displacement liquid storage vessel is to ensure that the system for which it stores liquid will be instantly operative upon demand regardless of the magnitudes and directions of the local accelerations. Under ideal conditions, the dominant ambient acceleration field will be sufficiently intense and properly oriented to ensure positive liquid expulsion. This ideal situation, common to earth-bound operations, can sometimes be established under zero gravity conditions by substituting a centripetal field by rotation of the entire system, or by the firing of rockets to accelerate the system. In the case of the RCS tanks of an Apollo-type vehicle, neither method is applicable, and other means for providing positive expulsion are necessary. Some of these considered for the Prolonged Mission Apollo are discussed below.

Tanks With Plastic Bladders

This concept has been employed in many applications and is presently being used in Apollo. This concept consists of a thin wall titanium tank in which a Teflon bladder is installed which has a surface area equal at least to that of the tank interior and an axially disposed "diffuser" tube (Figure 79). Liquid propellants contained within the Teflon bladder are forced from the tank through the "diffuser" tube by pressurized gas introduced into the space between the outside of the bladder and the tank.

This arrangement is currently capable of executing approximately 20 expulsion cycles. It is relatively light, and is not particularly sensitive to normal vehicular accelerations in any direction.

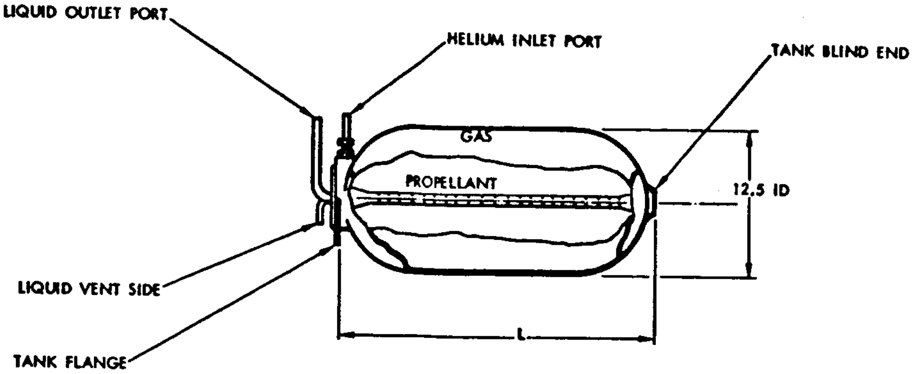

TANK LENGTHS "L" (INCHES)			TANK WEIGHTS (POUNDS)	
PROPELLANT	FUEL	OXID.	FUEL	OXID.
CM	17.3	19.9	7.4	7.9
SM	23.7	28.7	8.2	9.1
LEM	32.2	38.8	10.5	12.5
VOLUMETRIC EFFICIENCY = 95 PERCENT EXPULSION EFFICIENCY = 98 PERCENT				

Figure 79. .Reaction Control System Tank with Plastic Bladder

The ability of both the propellant and the pressurization gas to permeate through the bladder requires that these effects be evaluated for each application. A definite sensitivity of Teflon (which is required for N_2O_4 service) to nuclear radiation also requires evaluation, particularly for long missions. This plastic is also sensitive to temperatures much in excess of 100 F when in the presence of N_2O_4.

Figure 80 is a plot of the effects of nuclear radiation on the physical characteristic of Teflon. It is evident that the definition of what constitutes "significant deterioration" of physical properties can result in a wide range of "threshold values" for the acceptable upper limit of radiation. The selection of a limiting criteria is further confused by the lack of a clear correlation between the physical properties of a bladder material and its useful life in service. However, it is considered reasonable that 2×10^4 rads does not result in a serious deterioration and is therefore considered to be a reasonable limit pending more definitive data.

During the course of the many bladder tank development programs at Bell utilizing Teflon bladders, no degradation of the physical properties of Teflon has been detected. Most storage tests during these programs have not exceeded two months, which makes extrapolation to 600 days imprudent. However, a storage test program was conducted for the Navy, by Bell under contract NOrd 13947, in which Teflon bladders were stored in propellant tanks for

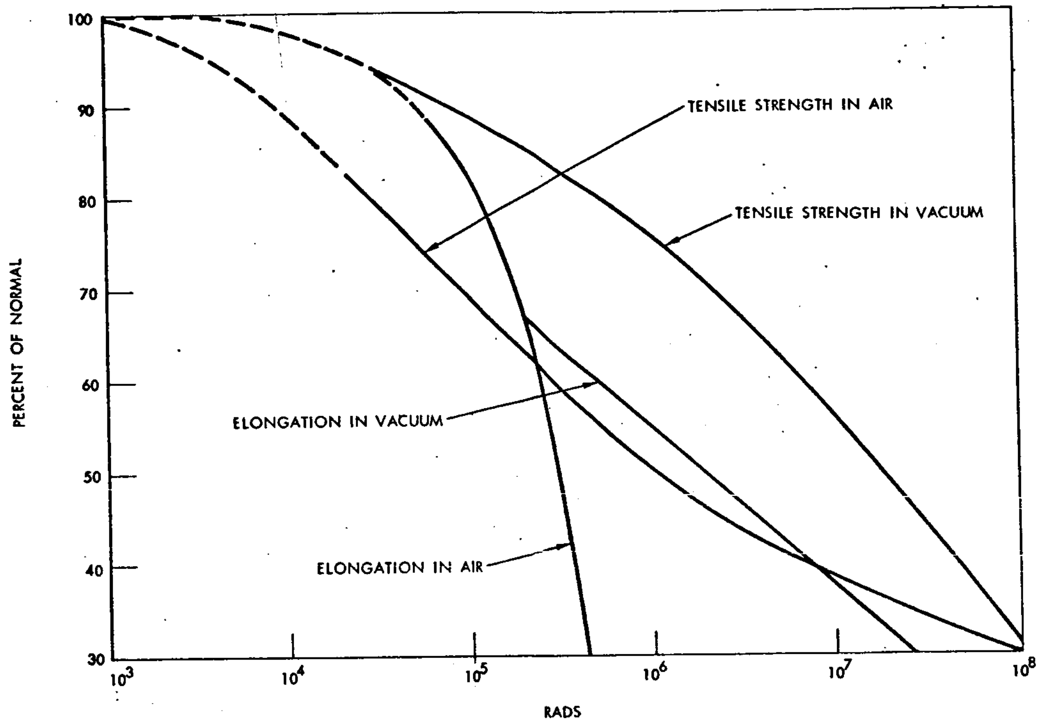

Figure 80. Effect of Nuclear Radiation on Physical Characteristics

one year, at the end of which an expulsion test was conducted on each. In no case was there any evidence of a change in physical properties of the Teflon bladders. The propellants were IRFNA and a hydrazine blend. As a result of this program, it is anticipated that the present LEM and service module Teflon bladders will be virtually unaffected by propellant immersion during a 600-day mission.

It will, however, be necessary to conduct some development tests to determine the capability of the present bladders to withstand the radiation and storage environments.

Tanks With Metal Bellows

The use of a welded metal bellows as a positive expulsion device is attractive where repeated expulsion cycles and zero permeability are required, especially in a nuclear radiation environment. A typical arrangement is shown in Figure 81 with the tank in the fully loaded condition. The volume to the right of the displacement head is pressurized with gas, the pressure being transmitted practically undiminished to the liquid propellant. Upon the initiation of expulsion, the displacement head and secondary bellows translate to the left, collapsing the primary bellows. When the primary

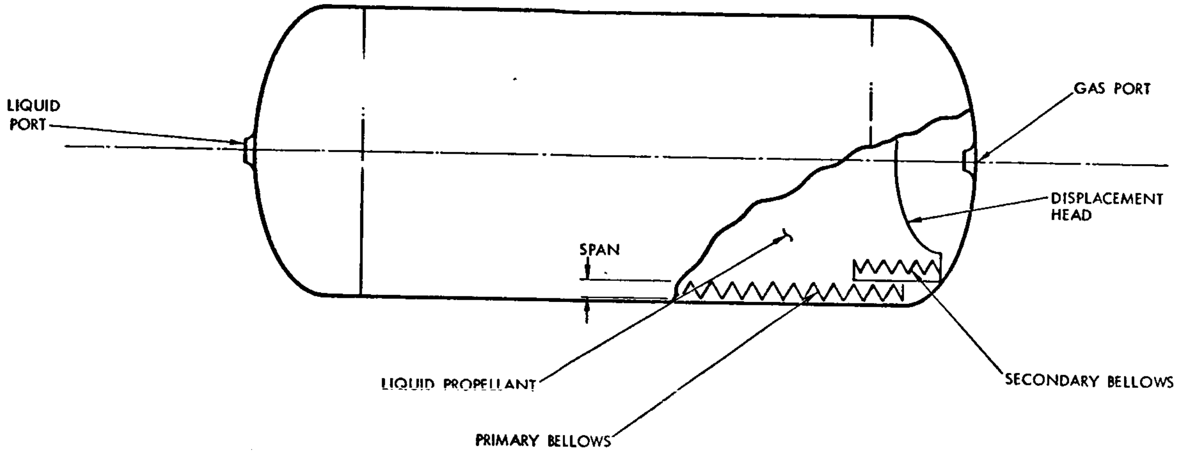

VOLUMETRIC EFFICIENCY ≠ 90 PERCENT
EXPULSION EFFICIENCY ≧ 98 PERCENT

Figure 81. Bellows Tank Configuration

bellows reach the stack height and "bottom" at the left end of the tank, the secondary bellows then collapses to permit the displacement head to approach the tank head and complete the expulsion with a minimum of residual propellant remaining.

Existing designs confirm analytical predictions as to the adequacy of this concept for applicable missions. The all-metallic construction is essentially impervious to the propellants and pressurization gases, and quite insensitive to nuclear radiation. If designed in the inelastic (yield) range of deflection it will endure 200 expulsion cycles. If designed in the elastic range, 10,000 cycles are possible. However, bellows designed in the inelastic range obtain greater displacement per bellows convolution, and are therefore somewhat lighter than those designed in the elastic range. Bellows tanks are relatively heavy and less efficient in terms of volume utilization than the tanks with plastic bladders but they are capable of expulsion efficiencies near 99 percent. Ambient temperature is of no significance since the bellows can endure much higher and lower temperatures than can the propellants.

Using computer solutions for a variety of bellows configurations and selected materials, the maximum elastic deflection per convolution is determined for each case. The deflection per convolution determines its volumetric displacement and with it the number of bellows convolutions required to contain a given volume of propellants. This, then, leads to the weight of the bellows to which must be added the weight of the circumscribing tank. Unfortunately the bellows length, diameter, and span also affect the tank weight in a non-linear manner. Consequently, the tank bellows-combination must be examined for a variety of bellows configurations and materials for a given volume requirement to determine the optimum weight. An example of the results thus obtained for a series of bellows configurations for one material and one volume requirement (7.1 ft^3) is shown in Figure 82. This curve illustrates how the tank weight varies as a function of bellows span and tank radius.

Extension of the bellows convolution into the region of material inelasticity drastically reduces the number of allowable expulsion cycles. As the inelastic strain is increased, the allowable number of cycles determined experimentally will produce very widely scattered values.

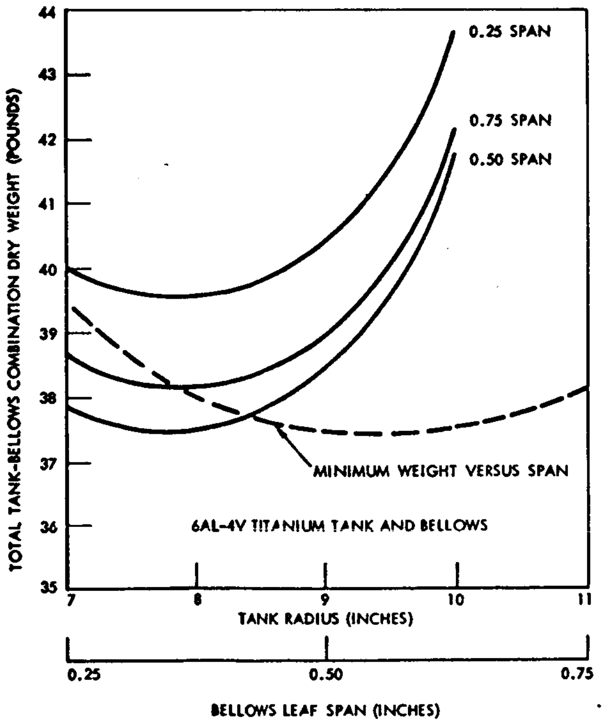

Figure 82. Weight of Bellows Tank Assembly vs. Tank Radius & Bellows Span for Volume of 7.1 ft^3

The design of bellows for an expulsion duty cycle of the order of 200 cycles is in the range of inelastic extension and cannot at present be supported by analytical stress analysis. The applicability of the current elastic computer program is being extended into the inelastic range. However, the availability of such inelastic stress analysis capability remains too far in the future to be of use for current studies. Weight and reliability studies of bellow-tank combinations designed for 200 expulsion cycles in inelastic extension are based upon test results from existing production and experimental hardware. Considerable testing has been conducted on bellows of annealed 347 stainless steel so that weight calculations, based upon this material, are quite accurate.

A very limited amount of testing of commercially pure titanium bellows has been used to obtain reasonable estimates of weights using this material to meet a 200 cycle expulsion requirement. The effect of optimizing tank design on the minimum weight, without regard for shape or L/D ratio is presented in Figure 83. The dry tank weight as a function of loadable tank volume for various materials and duty cycles is indicated in the Figure. This curve indicates that the titanium bellow with a cycle life capability of 200 cycles is the most satisfactory from the standpoint of weight.

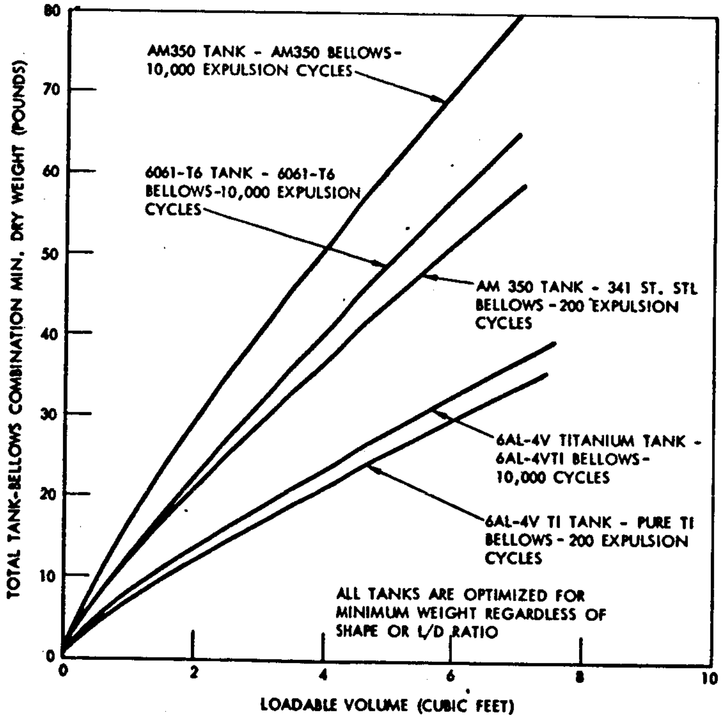

Figure 83. Weight of Bellows Tanks Vs. Loadable Volume

In the absence of gravitation forces and acceleration, a liquid will assume that configuration which minimizes its total surface energy. The surface energy of a liquid is equal to the gas-liquid interfacial tension multiplied by the interface surface area plus the solid-liquid interfacial energy multiplied by its surface area

$$E = LG \times A_{LG} + LS \times A_{LS}$$

This quantity is minimized by the following restraints

1. The two areas (A_{LG}, A_{LS}) are consistent with the volume of the liquid.
2. The liquid-gas interface contacts the solid surface at an angle which is unique for each liquid-solid combination.

The meniscus shape in a weightless environment is primarily dependent on the liquid to solid contact angle. With the contact angle being preserved, it is readily realized that the gometry of a particular tank can grossly affect the liquid gas interface shape. For liquids with a contact angle of zero (e.g., hydrogen), the liquid will entirely wet the walls and leave a spherical vapor bubble in the center of a spherical tank. For liquids that have greater than 0 degree contact angles, but less than 90 degrees, the liquid will contact the tank wall at nearly the same angle as that measured in a 1 g field. For liquids with contact angles approaching 180 degrees, the liquid will assume a spherical mass in the center of the tank away from the walls. In all cases, the liquid surface will attempt to approach a constant curvature configuration.

As a result of these fundamental statements, it appears feasible to design a tank with suitable internal baffling that will properly control the liquid gas interface. The following is a list of several possible approaches:

1. Capillary tubes
2. Screens over the outlet
3. Concentric conical capillaries

Since the surface tension of a particular propellant decreases with temperature, it follows that the holding potential of a surface force orientation device will also decrease. Therefore, it is necessary to know the surface tension of the propellants in question over the expected operational temperature range. The design point for a surface tension type orientation device will, therefore, be determined by the lowest value of surface tension which occurs at the maximum expected operating temperatures.

Conclusions

Of all the concepts considered, the plastic bladder system used on the present Apollo, is recommended as the first choice for a positive expulsion device unless some unforeseen space effect would eliminate its use. The reasons are similar to the philosophy of using existing Apollo hardware for the entire vehicle, that of minimum development time and cost as well as proven state-of-the-art hardware. Figure 84 presents the RCS weight versus system total impulse for an Apollo type of system.

A second recommendation is that the development of a titanium bellows and tank assembly be implemented to take advantage of the very high cycle life and consequent high reliability demonstrated to be characteristic of bellows tank performance. Noting that the materials of which typical bellows tank will be constructed are essentially immune to the effects of radiation, immersion, permeation, and extremes of temperatures, it follows that when fully developed, this concept will implement much longer missions than can be expected with the system with a Teflon bladder. It is significant that the use of titanium for the bellows tank components results in an overall tank weight which approaches closely the weight of the tank with Teflon bladders, and it is deemed possible that with judicious design to reach that low weight with future developments.

The third suggestion is that an experimental program be implemented to evaluate the feasibility of employing capillary type surface force orientation techniques for prolonged mission RCS propellant tanks. This could be a minimum cost program using fixed components which are not vulnerable to environmental hazards known to exist.

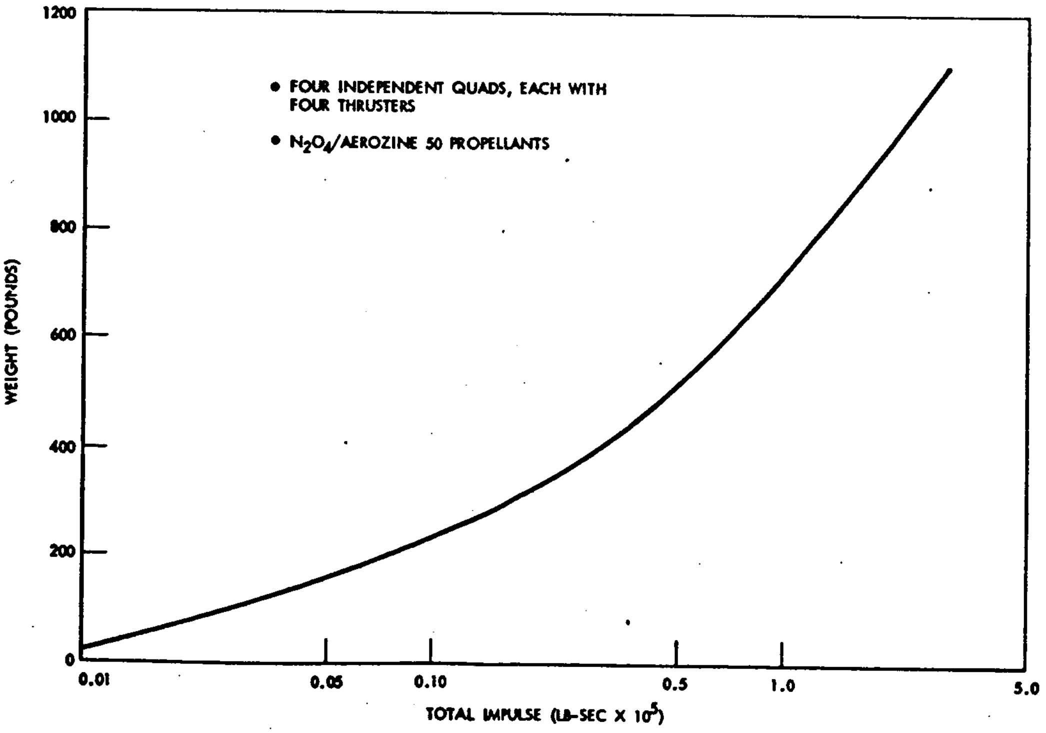

Figure 84. Reaction Control System Total Impulse Vs. Total Weight

STABILIZATION AND CONTROL SYSTEMS

STABILIZATION AND CONTROL SYSTEMS

This section presents the stabilization and control studies which were performed during the Prolonged Missions phase of the Extended Apollo Systems Utilization program. The Block II Apollo system, modified Apollo systems, and alternate system approaches were considered. The control techniques studied include reaction jets, reaction wheels, and twin gyros. A small lab vehicle (Apollo X type) and a large lab vehicle were both studied. The assumed characteristics of these two configurations are shown in Table 23.

Table 23. Assumed Characteristics of Configurations

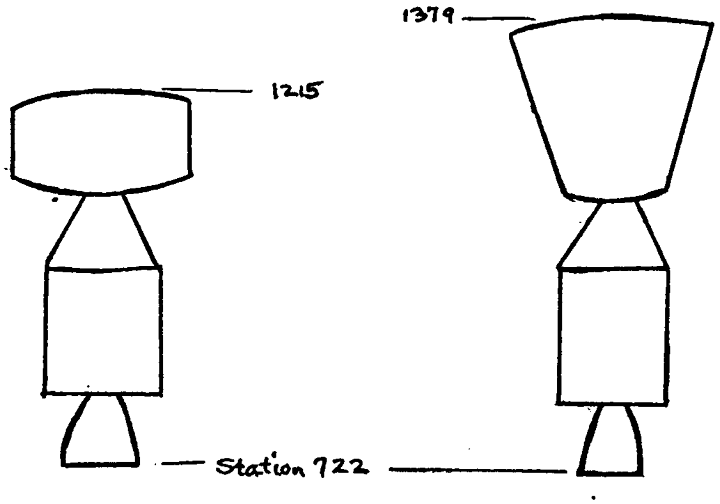

	Configuration 1	Configuration 2
Weight (lb.)	26,000	35,000
Center-of-mass (X_{cm}) (in.)	1,020	1,103
Roll Moment of Inertia (Slug-ft^2)	20,000	25,000
Pitch, Yaw Moments of Inertia (Slug-ft^2)	75,000	225,000
Projected Area (ft^2)	452	642
Center-of-pressure (X_{cp}) (in.)	999	1,163
Point of Solar Panel Attachment (in.)	1,162	1,244

Since the experiment programs for the extended duration missions are not firm, it was not possible to identify specific control requirements. Therefore, material for system evaluation was generated parametrically as a function of mission characteristics. A similar problem existed in the power system area in that the electrical power system is likely to vary depending on mission characteristics. Since the power system influences the stabilization and control problem, various power systems were considered including fuel cells, isotopes and solar panels.

Parametric reliability data were generated by Honeywell for use in evaluation of the current system (Block II) for prolonged missions. Various modes of operation were considered and plots were prepared for reliability versus operating time for the individual modes. Reaction jet reliability is also discussed.

The material presented should permit evaluation of the suitability of the present system to satisfy specified prolonged mission control requirements. In those cases where the present system is not found to be suitable, preliminary parametric data on alternate system approaches should enable the user to perform basic weight comparisons with the present system.

APOLLO BLOCK II SYSTEM

This section concerns stabilization and control systems composed primarily of Block II SCS components. Some system modifications have been considered—addition of horizon scanners for example. Thrust level changes were also investigated. The subjects emphasized are system requirements (reaction control, electronics, and sensors) and reliability.

REACTION JET SIZING

The determination of a thrust level (F) and minimum impulse bit (FΔt) for reaction control jets is based on the requirements associated with the mission profile. In general, the reaction jets will be required to provide angular acceleration for rotational maneuvers, linear acceleration for translational maneuvers and station keeping, and angular impulses for limit cycle attitude hold control. Jet lever arm distances, can be determined from an examination of the vehicle configuration. Using this information, together with the desired angular and linear acceleration characteristics, a parametric evaluation of jet thrust level can be conducted. Rate requirements during the drifting portion of limit cycle operation will allow the determination of jet minimum impulse characteristics (FΔt). Using Figure 85, and the data on thrust level (F) and minimum impulse (FΔt) explained above, a jet size can be selected which will satisfy mission and hardware constraints.

Maneuver Requirements

The theoretical propellant required for a single axis rotational maneuver performed by firing two jets in couple is given by the expression

$$W = \frac{4I\omega}{\ell I_{sp}} \qquad (1)$$

where ℓ is the distance between control jets and ω is the constant slewing rate during maneuvers. The propellant value found using Equation 1 is the total required to accelerate the vehicle to the required rate and then to reduce the rate to zero at the conclusion of the maneuver.

The propellant required for a three axis re-orientation is

$$W_p = \frac{4\omega}{\ell I_{sp}} \sum_{i=1}^{3} I_i \qquad I_{1,2,3} = I_{x,y,z} \qquad (2)$$

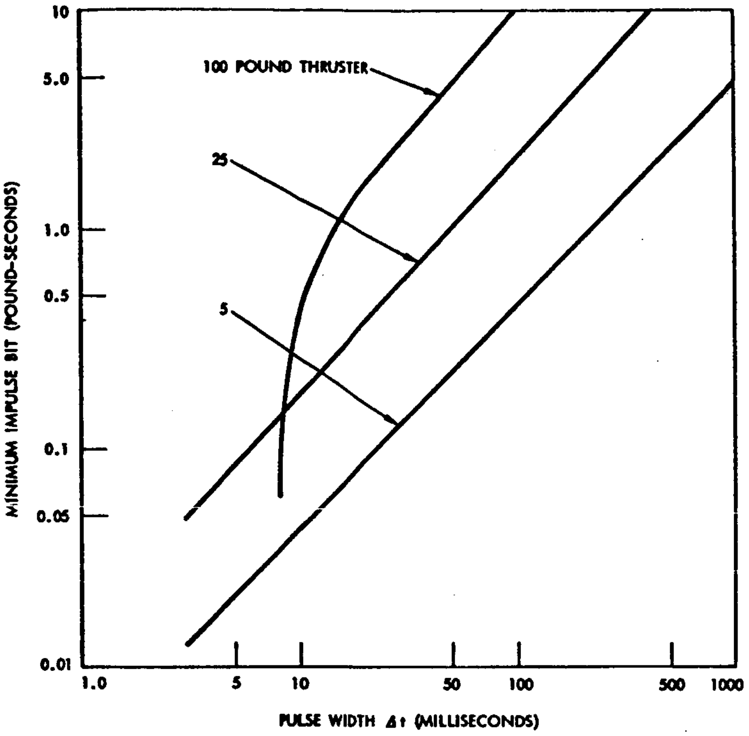

Figure 85. Minimum Impulse Bit vs. Pulse Width

Figure 86 is a plot of the theoretical propellant quantities required, for single axis and three axis maneuvers, as a function of slewing rate. The moment of inertia values used are the quantities for the respective laboratory configurations. Pilot-in-the-loop simulation studies have indicated that actual maneuver propellant quantities are approximately 1.5 times theoretical values.

Actual jet starts during maneuvers are difficult to determine since they are largely dependent on crew technique. Approximate values for jet starts required during maneuver were obtained from the simulation study mentioned above. Table 24 is a summary of the approximate jet starts required for maneuvering.

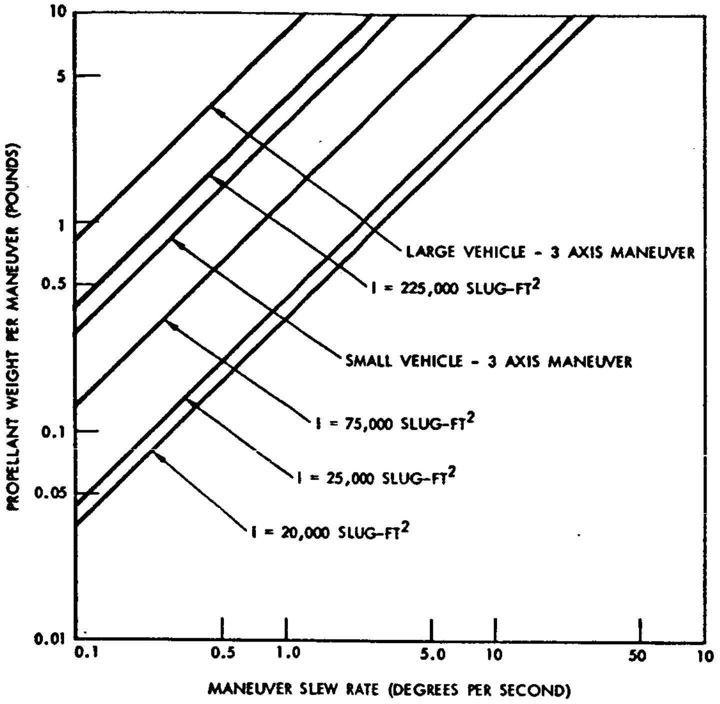

Figure 86. Rotational Maneuver Propellant Requirements

Table 24. Rotational Maneuver Jet Starts (per jet, per maneuver)

Configuration	1	2
Axis		
x	15	18
y	25	25
z	25	25

The method for determining propellant, jet start, and burn time requirements for rotational maneuvers is summarized in Table 25.

CON[redacted]

Table 25. Procedure for Determination of Jet System Maneuver Requirements

		Maneuver Where Found	Pitch	Yaw	Roll	3 Axis
Theoretical Propellant/Maneuver	(W_i)	Figure 86	W_y	W_z	W_x	W_3
Actual Propellant/Maneuver	(W_a)	$W_a = 1.5\ W_i$	$1.5\ W_y$	$1.5\ W_z$	$1.5\ W_x$	$1.5\ W_3$
Actual Starts/jet/maneuver	(N_a)	Table 24	N_{ay}	N_{az}	$\frac{N_{ax}}{2}$	N_{a3}
Number of Maneuvers	n_i		n_y	n_z	n_x	n_3
Total Propellant	W_{it}	$W_{it} = W_{ai}\ (n_i + n_3)$	$W_{ay}(n_y + n_3)$	$W_{az}(n_z + n_3)$	$W_{ax}(n_x + n_3)$	
Total Starts/Jet		$N = n_i\ N_{ai}$	$N_y\ (n_y + n_3)$	$N_z\ (n_z + n_3)$	$\frac{N_x}{2}(n_x + n_3)$	
Total Burn Time/Jet	(t_b)	$\frac{W_{it}\ I_{sp}}{4F}$	$\frac{W_{yt}\ I_{sp}}{4F}$	$\frac{W_{zt}\ I_{sp}}{4F}$	$\frac{W_{xt}\ I_{sp}}{8F}$	

[redacted]

Attitude Hold

The reaction propellant required to provide limit cycle control about each vehicle axis is

$$\dot{W}_i = \frac{3.6 \times 10^3 \ell \, (F \Delta t)^2}{2 \, \text{Isp} \, \theta_{DB} \, I_i} \text{ lb/hr} \qquad (3)$$

where the required Isp value is found using the reaction jet characteristics and Figure 87. Figure 88 is a plot of Equation (3) for the moments-of-inertia of the given vehicles. The total rate for three axis control is given by the expression

$$\dot{W} = \dot{W}_x + \dot{W}_y + \dot{W}_z \qquad (4)$$

In actual operation, however, the limit cycle propellant rate will be influenced by the effects of disturbance torques. These disturbances result from meteoroids, solar pressure, the earth's magnetic field, aerodynamic drag, and gravity gradient. The predominant disturbances at the orbital altitude being considered (260 n.mi.) are due to aerodynamic drag and gravity gradient torques. To assess the effects of these disturbances, consider an orbital axis system with origin fixed at the vehicle's c.g. and having the following orientations: Z_o-axis downward along the local vertical, the X_o-axis in the orbital plane and in the direction of vehicle motion, and the Y_o-axis perpendicular to the orbital plane and completing the right hand system. The orientation of the vehicle's principal axes is obtained by performing successive rotations about the Y_o-axis, the intermediate Z-axis, and the final X-axis. The transformation which expresses the resulting orientation is given by

$$\begin{bmatrix} x \\ y \\ z \end{bmatrix} = (\phi)(\psi)(\theta) \begin{bmatrix} X_o \\ Y_o \\ Z_o \end{bmatrix} \qquad (5)$$

The aerodynamic drag torque on an orbiting vehicle can be expressed as

$$\vec{T}_a = C_D \, q \, A_p \, (X_{cp} - X_{cm}) \begin{bmatrix} 0 \\ C\phi \, S\theta + S\phi \, S\psi \, C\theta \\ -S\phi \, S\theta + S\psi \, C\phi \, C\theta \end{bmatrix} \qquad (6)$$

where q is the dynamic pressure at the orbital altitude, A_p is the projected vehicle cross section area, $(X-X_{cm})$ is the distance between the centroid of the cross section area and the vehicle center of mass, and C_D is the drag coefficient of the vehicle in rarefied flow.

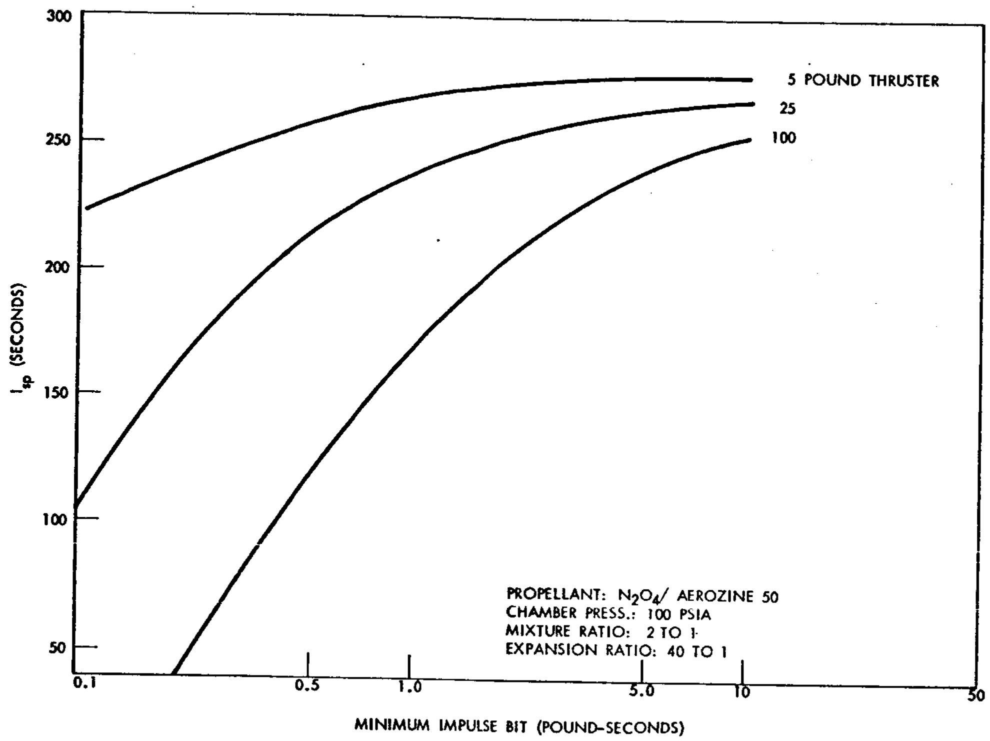

Figure 87. Variation of Effective Specific Impulse

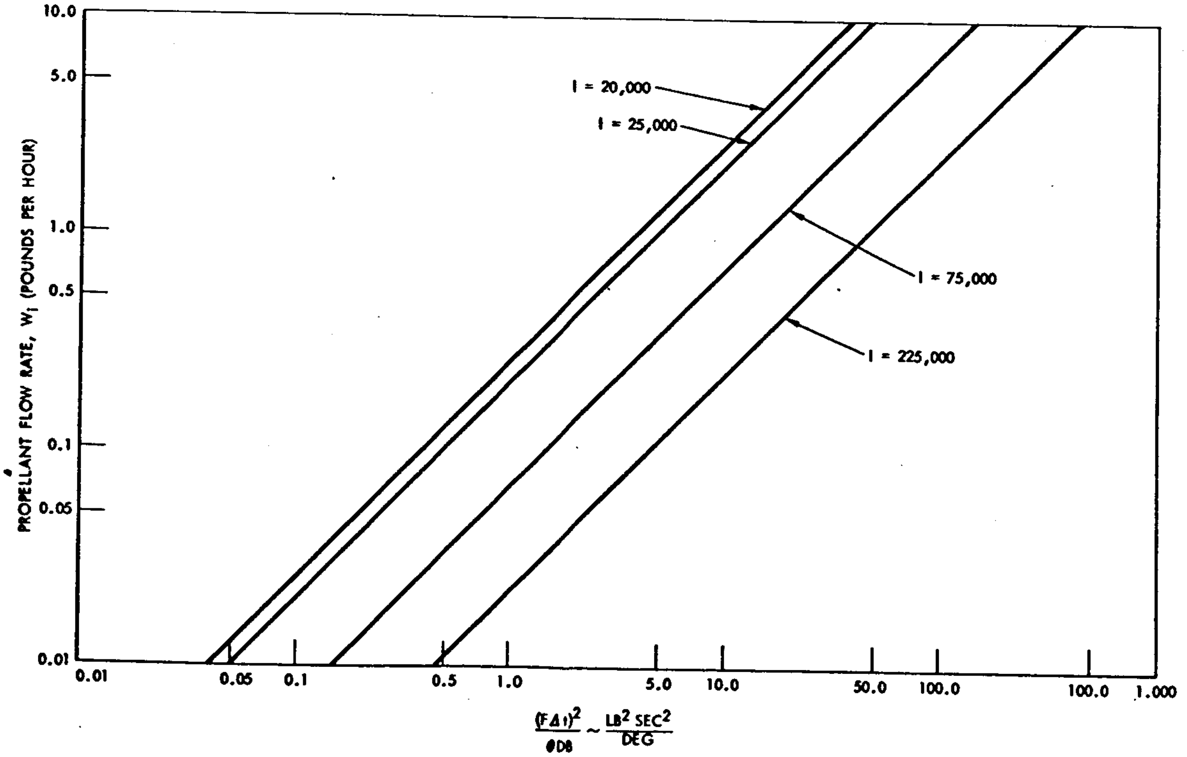

Figure 88. Theoretical Propellant Flow Rate for Limit Cycle Operation

The gravity gradient torque components about the vehicle principal axis are

$$\vec{Tg} = \frac{3GM}{R_o{}^3} (I_x - I_y) \begin{bmatrix} 0 \\ -C\phi \; C\theta \; C\psi \; S\theta + S\psi \; C\psi \; S^2\theta \; S\phi \\ S\phi \; C\theta \; C\psi \; S\theta + S\psi \; C\psi \; S^2\theta \; C\phi \end{bmatrix} \qquad (7)$$

where GM is the universal gravitational constant, R_o is the orbital radius, and I_x and I_y are vehicle moments-of-inertia.

When a vehicle is in limit cycle and an external torque due to gravity gradient and/or aerodynamic drag effects is acting, the torque can alter the characteristics of the limit cycle such that only one set of control jets fires. Depending on the strength of the disturbing torque, the time for the completion of one cycle can be either increased or decreased from the nominal value. If the time between firings is increased, less propellant is required in a given period of time; however, if the time is decreased, the jets fire oftener resulting in increased propellant utilization. The actual propellant consumption of a control axis during the influence of an external torque is

$$\dot{W}a = \mu \dot{W}i \quad \text{lb/hr.} \qquad (8)$$

where the factor μ is

$$\mu = \frac{4\theta_{DB} \, I_i \, T}{(F \, \ell \, \Delta t)^2} \qquad (9)$$

The theoretical number of jet starts for each of the four jets (two provide positive torque, two negative) which controls an axis is given by

$$N_i = \frac{\mathrm{to} \, \ell \;\; F \Delta t}{8\theta_{DB} \, I_i} \; \text{starts} \qquad (10)$$

Equation (10) is plotted in Figure 89 for the moment-of-inertia values of the given vehicles. The starts and burn time for each jet of a control axis are

	Pitch	Yaw	Roll
Starts	N_y	N_z	$N_x/2$
Burn time	$N_y \Delta t$ sec	$N_z \Delta t$ sec	$N_x \Delta t/2$ sec

The number of starts during the influence of an external torque is related to the theoretical value by the factor 2μ where μ is given by Equation 9.

$$N_a = 2\mu N_i \qquad (11)$$

It was previously noted that during a disturbed limit cycle only one set of control jets may fire. Thus the actual jet starts as given by Equation (11)

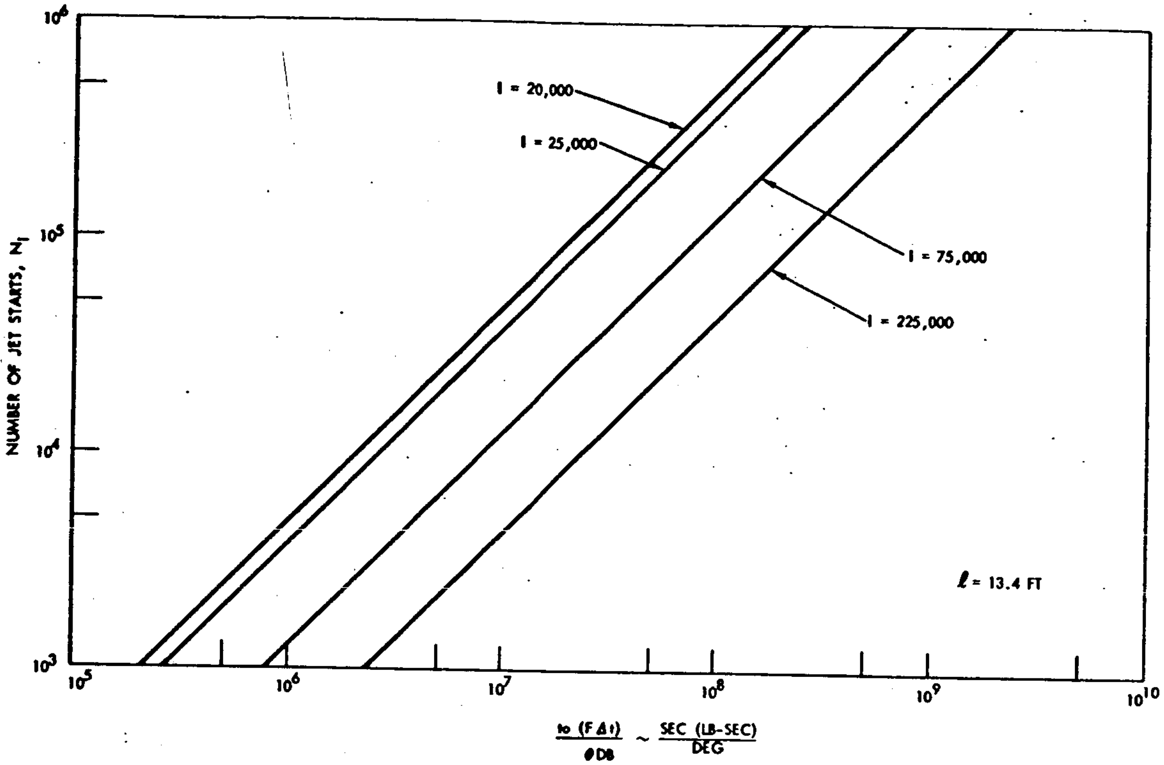

Figure 89. Theoretical Jet Starts for Limit Cycle Operation

are for only two of the jets controlling each axis. For approximation purposes, it will be assumed that the starts are distributed between the two sets of jets with the resulting values shown below.

	Pitch	Yaw	Roll
Starts	$N_{ay}/2$	$N_{az}/2$	$N_{ax}/4$
Burn time	$N_{ay}\Delta t/2$	$N_{az}\Delta t/2$	$N_{ax}\Delta t/4$

Local Vertical Attitude Hold

In the local vertical attitude hold mode, one of the vehicle's principal axes is continuously oriented toward the earth to facilitate mapping or observation experiments. The two orientations usually considered are: longitudinal vehicle axis toward earth ($\theta = 90^\circ$, $\psi = 0^\circ$), and longitudinal axis in the orbital plane and horizontal to the earth's surface ($\theta = 0$, $\psi = 0$). It can be seen from Equation (7), that for both orientations, gravity gradient torque components will be zero. For the case where the longitudinal axis is horizontal to the earth's surface and in the orbital plane, the distance between the center-of-pressure (centroid of the projected area) and the c.g. will be negligibly small for symmetric vehicles. For this case, the aerodynamic disturbance torque will be zero and the actual propellant consumption and jet starts will be equal to the theoretical values.

For the longitudinal vehicle axis toward the earth, the aerodynamic torque will be a maximum and will have components about both the vehicle y and z body axes. For disturbance analyses, it will be assumed that the components are equal and given by

$$T_{ay} = 0.707\ C_{Dq}\ A_p\ (X_{cp} - X_{cm}) \tag{12}$$

$$T_{az} = 0.707\ C_{Dq}\ A_p\ (X_{cp} - X_{cm}) \tag{13}$$

Using these torque values, the values for μ are obtained from Figure 90. The factor μ permits evaluation of the required reaction propellant, and the jet starts and burn time. It should be noted, that since eight jets are utilized for roll control, the jet starts and burn times can be distributed between two essentially redundant roll systems. Table 26 is a detailed description of the analysis of a jet system for local vertical hold.

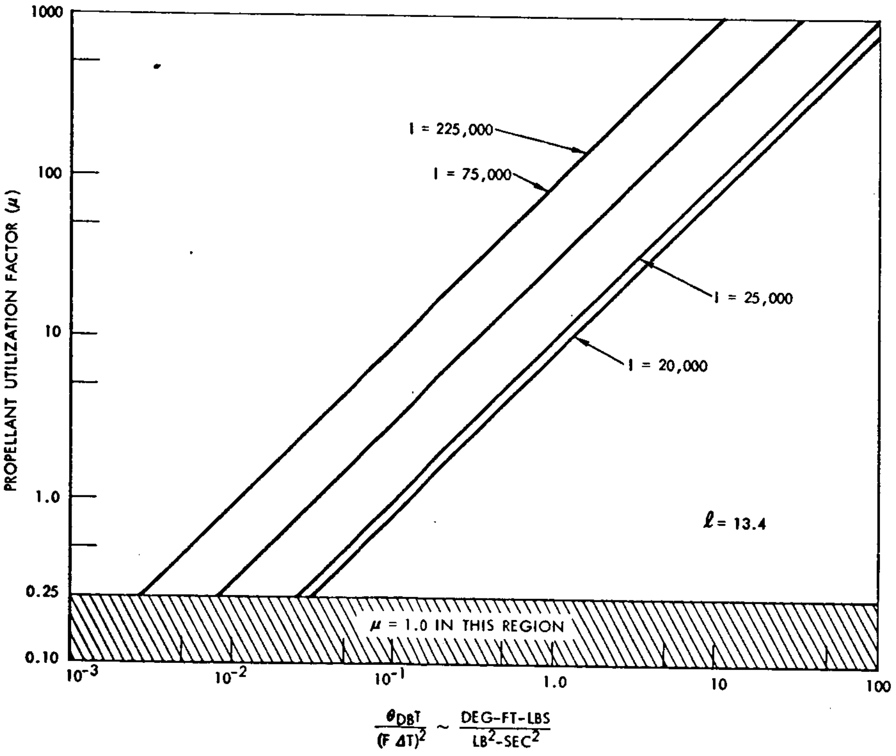

Figure 90. Biased Limit Cycle Propellant Factor

Table 26. Procedure for Determination of Jet Requirements During Local Vertical Hold

		Pitch		Yaw		Roll	
	Config.	1	2	1	2	1	2
Aerodynamic Torque (T_a)		1.68×10^{-3}	5.96×10^{-3}	1.68×10^{-3}	5.96×10^{-3}	0	0
Theoretical Propellant $(\dot{W})$	Fig. 88	$\dot{W}_y$		$\dot{W}_z$		$\dot{W}_x$	
Disturbance Torque Factor (μ)	Fig. 90	μy		μz		1	
Actual Propellant	$\dot{W}_a = \mu_i \dot{W}_i$	$\mu_y \dot{W}_y$		$\mu_z \dot{W}_z$		$\dot{W}_x$	
Theoretical Starts (N)	Fig. 89	N_y		N_z		N_x	
Actual Starts/Jet (N_a)	$N_a = \mu_i N_i$	$\mu_y N_y$		$\mu_z N_z$		$\frac{N_x}{2}$	
Burn Time/Jet (t_b)	$t_b = N_a \Delta t$	$\mu_y N_y \Delta t$		$\mu_z N_z \Delta t$		$\frac{N_x \Delta t}{2}$	

Inertial Attitude Hold

In the inertial attitude hold mode, the vehicle is assumed held in a fixed orientation with respect to inertial space. This orientation is maintained as the vehicle moves in orbit. It can be shown that, to describe an inertial orientation using the previously noted orbital axis system and angular transformations, the angles ϕ and ψ will remain fixed and θ will vary as a function of time (orbital position). During inertial attitude hold at 260 n.mi. altitude, gravity gradient torques will be on the order of 20-30 times larger than the aerodynamic torque. Aerodynamic torques will be neglected during inertial hold periods. The gravity gradient torque components are found using Equation (7). For an arbitrary vehicle orientation of $\phi = 45^o$ and $\psi = 45$ degrees, the resulting torque components are

$$T_{gx} = 0 \tag{14}$$

$$T_{gy} = \frac{3GM}{R_o^3} (I_x - I_y) (-.5\ S\theta\ C\theta + .353\ S^2\theta) \tag{15}$$

$$T_{gz} = \frac{3GM}{R_o^3} (I_x - I_y) (.5\ S\theta\ C\theta + .353\ S^2\theta) \tag{16}$$

The rms values of T_{gy} and T_{gz} over one orbit ($\theta = 0$ to 2π) were evaluated for the given configurations. These rms values are then used together with Figure 90 to determine the disturbance torque factor (μ). Table 27 is a detailed description of the procedure to be utilized in determining propellant utilization, jet starts, and jet burn times during inertial attitude hold periods.

Solar Panel Considerations

The use of solar panels for supplying power to an orbiting vehicle influences vehicle control requirements in two distinct ways. The primary influence is due to the requirement that the vehicle control system provide active control to insure that the panels maintain the correct orientation with respect to the sun. A secondary influence of the panels is the increased area exposed to the free stream causing an increase in aerodynamic torques with a resultant alteration in limit cycle propellant utilization. The control and disturbance effects resulting from solar panels which are fixed to the vehicle, and those which have one degree-of-freedom with respect to the vehicle are examined in the following sections.

Fixed Panels

It is assumed that the panels are attached to the vehicle as shown in Figure 91. To maintain the panels perpendicular to the sun line, thus insuring maximum power, the vehicle is essentially in an inertial attitude hold mode. While this is not true for long periods of time, the effects of nodal regression and earth motion in solar orbit over a daily period are small and for our purposes, it will be assumed that the vehicle is inertially fixed.

Table 27. Procedure for Determination of Jet System Requirements During Inertial Attitude Hold

		Pitch		Yaw		Roll	
	config. / where found	1	2	1	2	1	2
Disturbance Torque (T)		$5.8\text{x}10^{-2}$	$2.08\text{x}10^{-1}$	$5.8\text{x}10^{-2}$	$2.08\text{x}10^{-1}$	0	0
Theoretical Propellant ($\dot{W}_i$)	Fig 88	$\dot{W}_y$		$\dot{W}_z$		$\dot{W}_x$	
Disturbance Torque Factor (μ)	Fig 90	μ_y		μ_z		1	
Actual Propellant	$\dot{W}_a = \mu_i \dot{W}_i$	$\mu_y \dot{W}_y$		$\mu_z \dot{W}_z$		$\dot{W}_x$	
Theoretical Starts (N)	Fig 89	N_y		N_z		N_x	
Actual Starts/Jet (N_a)	$N_a = \mu_i N_i$	$\mu_y N_y$		$\mu_z N_z$		$\frac{N_x}{2}$	
Burn Time/Jet (t_b)	$t_b = N_a \Delta t$	$\mu_y N_y \Delta t$		$\mu_z N_z \Delta t$		$\frac{N_x \Delta t}{2}$	

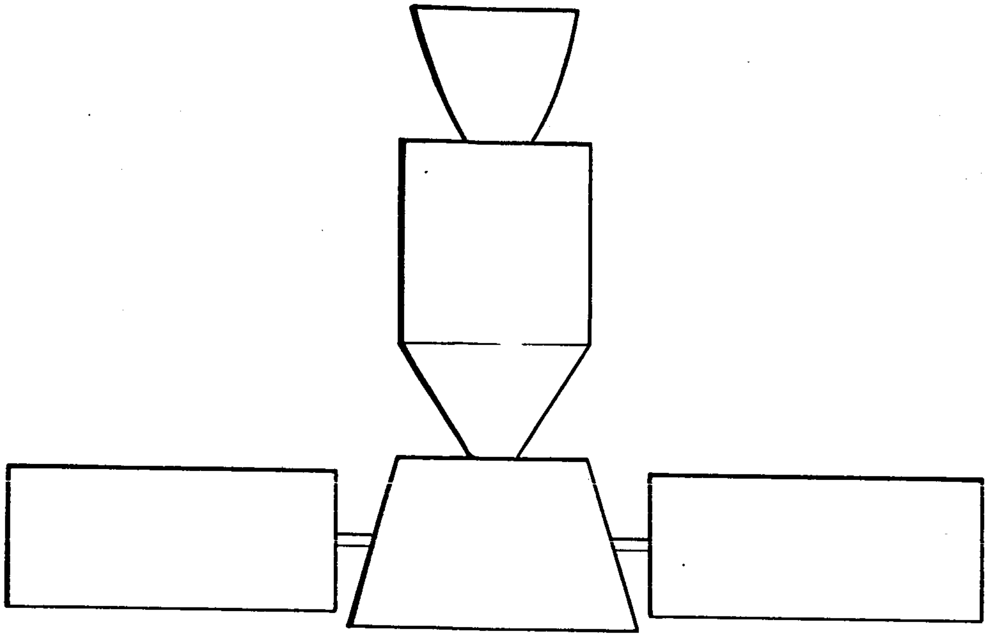

Figure 91. Fixed and Movable Solar Panel Configuration

The proper panel orientation can be maintained if the vehicle longitudinal axis is constrained in the orbital plane and the vehicle roll angle is made equal to the angle between the sun line and the orbit plane (ζ). A computer program was written to evaluate the angle ζ as a function of orbital inclination and earth position in solar orbit. Figure 92 is a plot of the yearly average of ζ as a function of orbital inclination. Knowing the yearly average of ζ, the average roll angle ϕ is known. Using the vehicle and panel geometric characteristics, expressions were determined for the average disturbance torque values resulting from aerodynamic and gravity gradient influences. These values for both vehicle configurations are shown in Table 28 for a 30-degree inclination orbit. The values given are applicable for panel areas up to 1000 square feet since the aerodynamic affects are so much less than those due to gravity gradient.

Table 28. RMS Disturbance Torque Summary for Vehicles With Fixed Solar Panels (ft-lb)

Axis / Config.	Pitch	Yaw	Roll
1	6.16×10^{-2}	2.47×10^{-2}	0
2	2.52×10^{-1}	1.02×10^{-1}	0

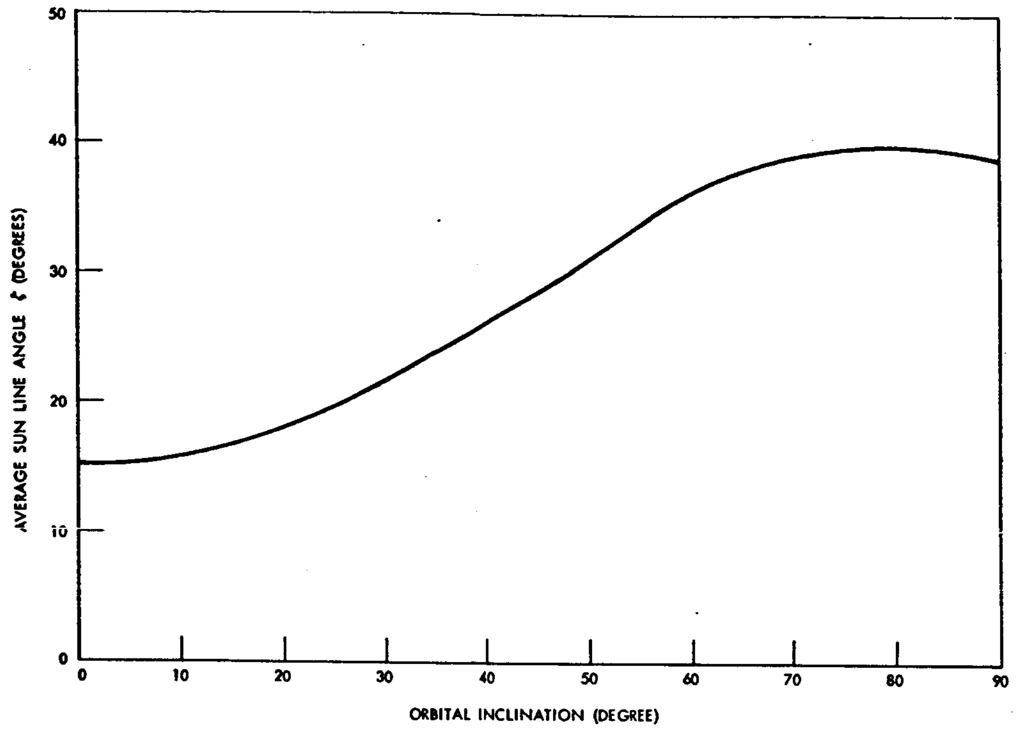

Figure 92. Yearly Average of the Sun Line Angle (ζ)

Movable Panels

The movable panels are assumed to be attached to the vehicle as shown in Figure 91 and have one degree of freedom with respect to the vehicle. The two types of panel orientation control examined are shown in Figure 93. In the first case, the vehicle longitudinal axis is held along the local earth vertical, and the vehicle is rolled and the panels pitched to maintain the desired orientation. The second mode involves holding the vehicle longitudinal axis parallel to the earth's surface and panel control maintained by yawing the vehicle about the local vertical and pitching the panels. The control laws expressing the relationship between the roll angle and sun line inclination in the "local vertical mode," and yaw angle and sun line inclination in the "local horizontal mode" are

$$\phi(\text{rad.}) = \tan^{-1}\left[-\frac{\tan\zeta}{\sin\alpha}\right] \tag{17}$$

$$\psi(\text{rad.}) = \tan^{-1}\left[-\frac{\tan\zeta}{\sin\alpha}\right] \tag{18}$$

where α expresses vehicle position in earth orbit. The above expressions are utilized to evaluate the reaction propellant required for vehicle control during the sun orient modes. A plot of Equations (17) and (18) for various values of ζ is shown in Figure 94. It can be seen that the variation of

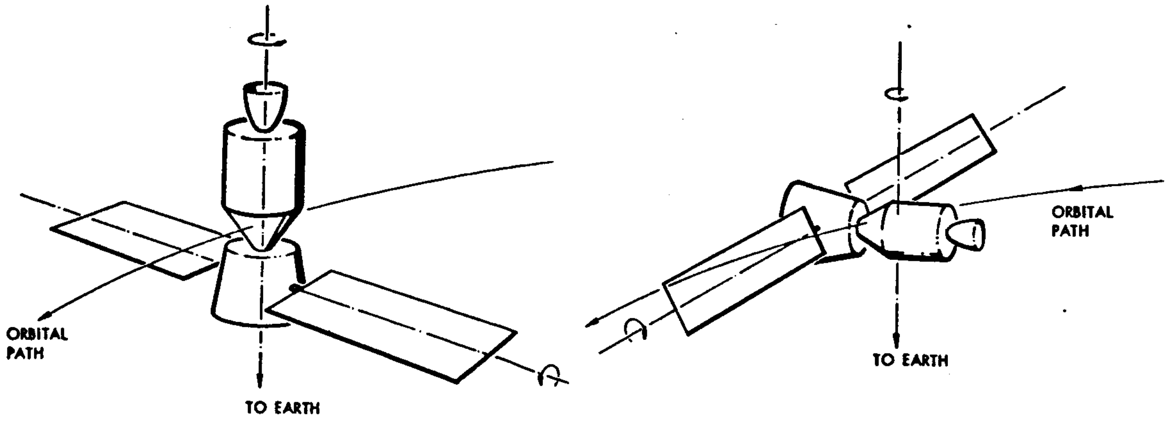
ORBITAL PATH
TO EARTH
ORBITAL PATH
TO EARTH

a. LOCAL VERTICAL MODE

b. LOCAL HORIZONTAL MODE

Figure 93. Vehicle Orientations for Movable Solar Panels

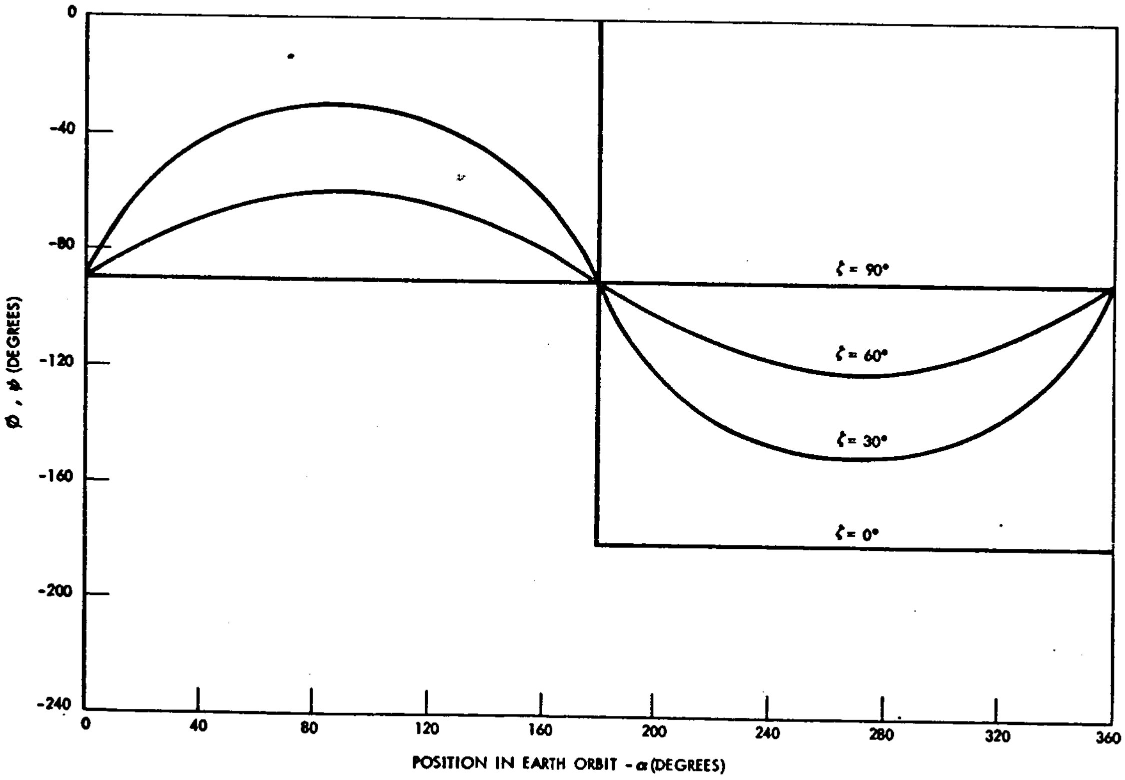

Figure 94. Roll, Yaw Control Law for Local Vertical and Local Horizontal Vehicle Control

CONFID~~ENTIAL~~

ϕ or ψ with orbital position approximates a sinusoid. The roll and yaw rates ($\dot{\phi}$ and $\dot{\psi}$) for the respective orientation modes are found by differentiating Equations (17) and (18).

$$\dot{\phi} = \dot{\psi} = \frac{\tan\zeta \; \cos\alpha \; \dot{\alpha} \; - \sin\alpha \; \sec^2 \zeta \dot{\zeta}}{\sin^2\alpha \; + \tan^2\zeta} \quad \text{rad/sec} \qquad (19)$$

The rate of vehicle motion in earth orbit ($\dot{\alpha}$) is approximately 1.14×10^{-3} rad/sec. while the rate of sun line inclination variation ($\dot{\zeta}$) is on the order of 10^{-7} rad/sec. Neglecting the second term in the numerator of Equation (19) gives

$$\dot{\phi} = \dot{\psi} = \frac{\tan\zeta \; \cos\alpha\,\dot{\alpha}}{\sin^2\alpha \; + \tan^2\zeta} \quad \text{rad/sec} \qquad (20)$$

The maximum rates will occur when $\alpha = 0^\circ, 180^\circ$ and are

$$\dot{\phi}_{max} = \dot{\psi}_{max} \frac{\dot{\alpha}}{\tan\zeta} \quad \text{rad/sec} \qquad (21)$$

Over one orbit (α = 0-360 degrees) the total angular velocity change which must be supplied to the vehicle is $4\dot{\psi}_{max}$ ($4\dot{\phi}_{max}$). The orbital period for a 260 n.mi. orbit is 94 minutes and results in 15.3 orbits per day. Thus, the total $\Delta\omega$ requirement per day is $61.2\,\dot{\psi}_{max}$ ($61.2\,\dot{\phi}_{max}$) rad/sec. Using the data on the frequency of ζ within 10 degree increments, and an average $\dot{\psi}_{max}$ ($\dot{\phi}_{max}$) for each increment determined using Equation (21), a weighted value of $\dot{\psi}_{max}$ is determined. A weighted value of the angular velocity requirement per day is then calculated. Figure 95 is a plot of this curve as a function of orbital inclination. The propellant for vehicle roll control in the local vertical mode, or for vehicle yaw control in the local horizontal mode is found using Figure 95 and the expressions

$$W = \frac{2I_z\,(61.2\;\bar{\dot{\psi}}_{max})}{\ell\,I_{sp}} \quad \text{lb/day} \qquad (22)$$

$$W = \frac{2I_x\,(61.2\bar{\dot{\phi}}_{max})}{\ell\,I_{sp}} \quad \text{lb/day} \qquad (23)$$

Table 29 contains the "per day" propellant requirements for the two vehicle configurations in a 50° inclination orbit.

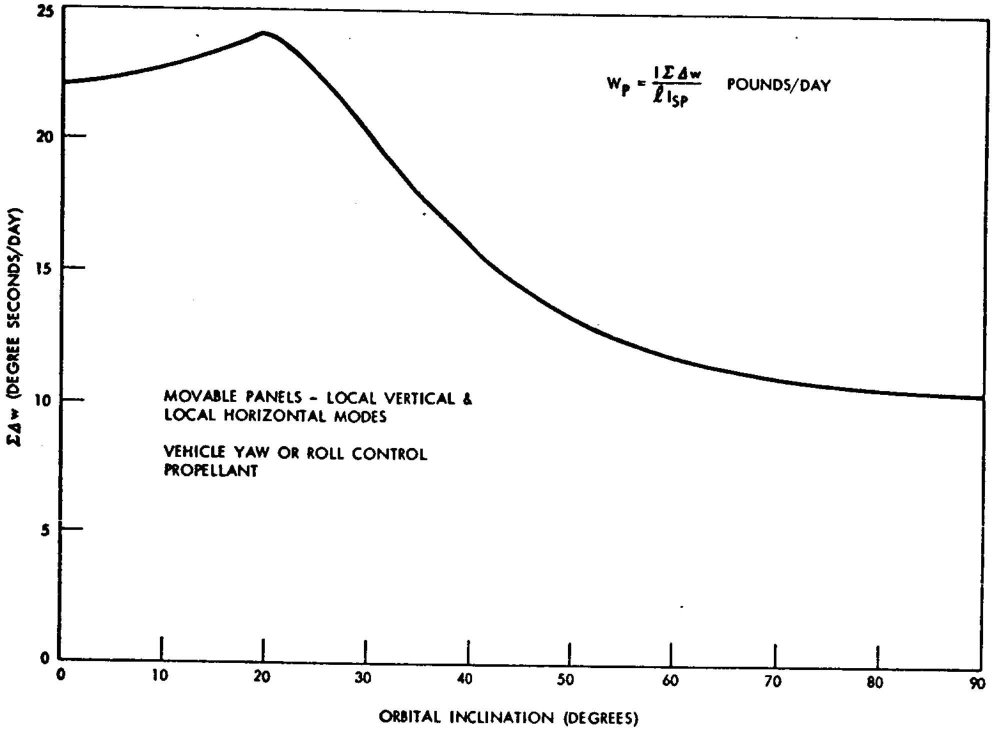

Figure 95. Solar Panel Pointing Requirements

Table 29. Reaction Propellant for Vehicle Pointing (lb/day)
- Movable Solar Panels -

Mode / Config.	Local Vertical	Local Horizontal
1	3.4	12.8
2	4.25	38.3

It can be seen from Equation (7) that in both the local vertical and the local horizontal modes, the disturbance torque components due to gravity gradient are zero (local vertical implies $\theta = -\pi/2$, $\psi = 0$ and in the local horizontal mode, $\theta = 0$, $\phi = 0$). Since gravity gradient torques are zero for the movable panel operational modes, aerodynamic effects will predominate. The exact assessment of the contribution of solar panels to the aerodynamic disturbance torque is extremely difficult. This is caused by the constantly varying area exposed to the free stream flow. The projected areas of the panels and vehicle perpendicular to the free stream flow frequently overlap, creating a complication if a composite projected area is desired. An estimate of the effects has been made using the following procedure. From the vehicle control and solar panel pointing laws, the relationship between vehicle orientation, panel orientation, and solar angle can be made at each point in orbit. Using the weighted value of ζ previously obtained, a representative projected area was obtained. From this area, aerodynamic torque values were obtained which represent average values for a yearly mission. Figures 96 through 98 are plots of the disturbance torque values for the local vertical and local horizontal modes as a function of total solar panel area for the two vehicle configurations.

Table 30 is a summary of the procedure for determining the reaction propellant quantity for a vehicle utilizing solar panels.

"Noon Control"

The so called "noon control" problem occurs for movable panel vehicles during orbits when the sun line angle ζ is equal to 0 degrees, and the vehicle lies on the line from the sun to the earth's center. It can be seen from Equation (21) that for this position in orbit, the vehicle orientation rate "blows-up." The usual procedure during an orbit when $\zeta = 0$ degrees is to begin the required 180 degree turn at some time prior to "noon" and complete it at some time afterward. To insure that panel effectiveness is not severely degraded during this period, it is desirable to start the maneuver when the vehicle is 10 degrees ahead of "noon" and end it when the vehicle is 10 degrees past the "noon" position. In a 260 n.mi. orbit, this maneuver will have to be completed in 5 minutes, requiring a vehicle slewing rate of 0.6 deg/sec.

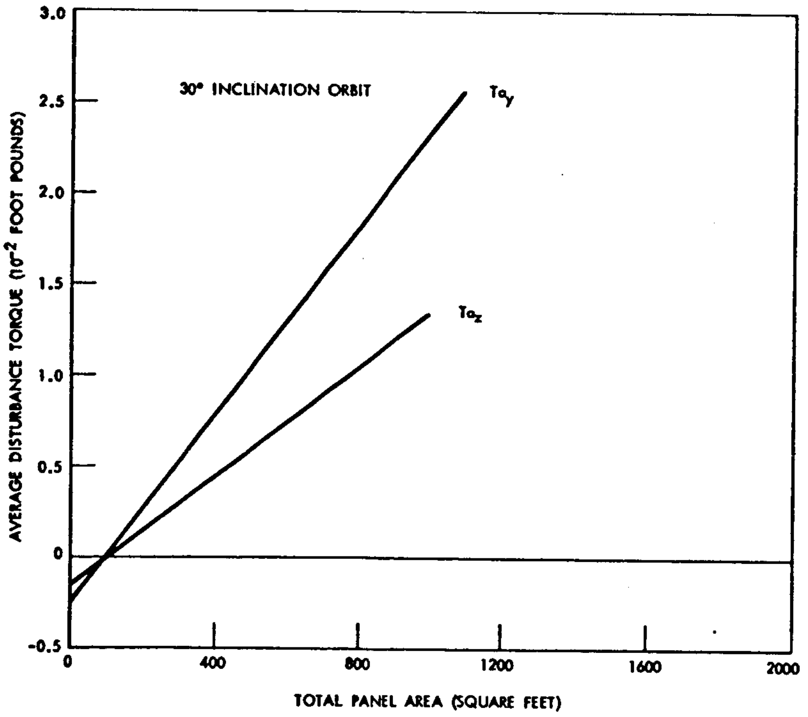

Figure 96. Aerodynamic Disturbance Torques in Local Vertical Mode Configuration #1

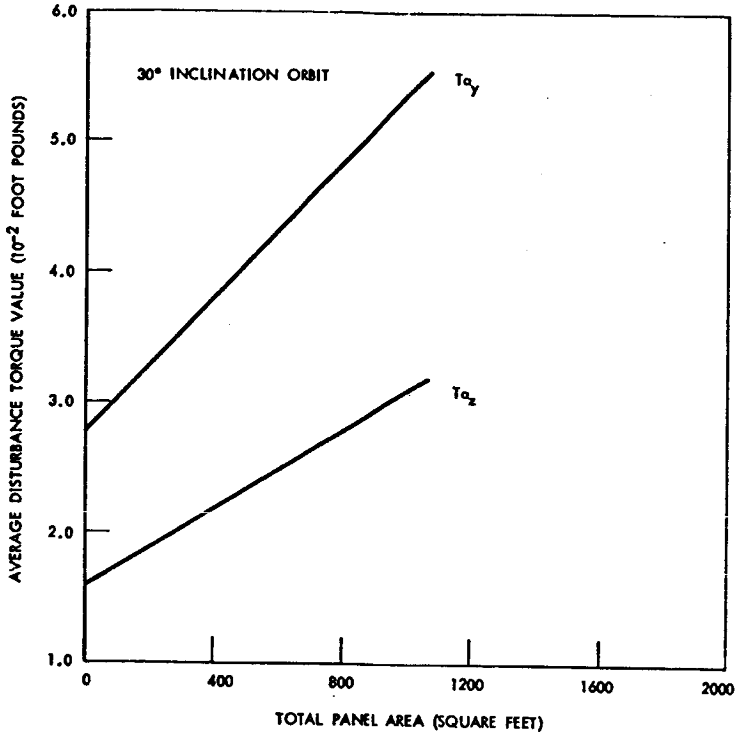

Figure 97. Aerodynamic Disturbance Torques in Local Vertical Mode Configuration #2

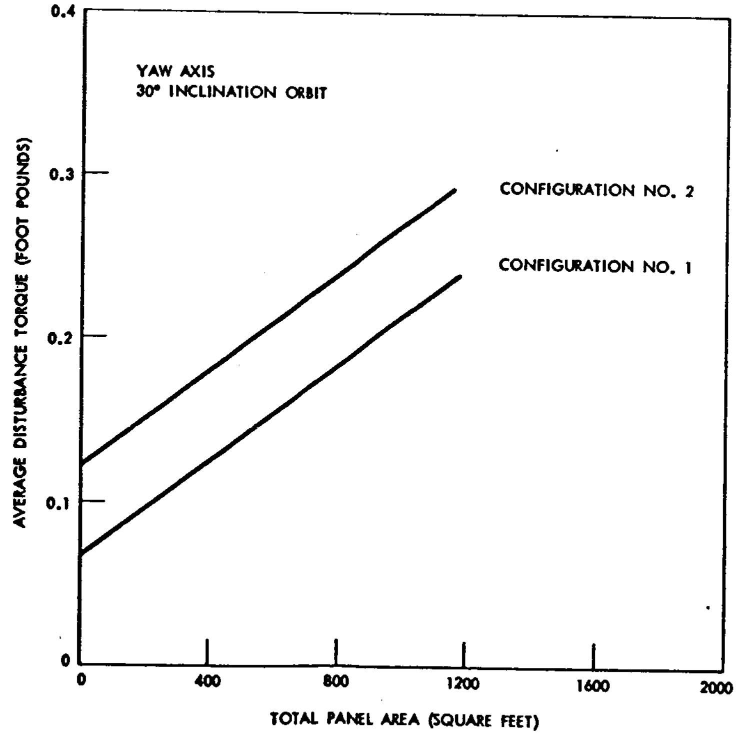

Figure 98. Aerodynamic Disturbance Torques in Local Horizontal Mode

CO[redacted]

Table 30. Procedure for Analysis of Reaction System Requirements on a Vehicle Utilizing Solar Panels

Fixed Panels

	Axis / Where Found	Pitch	Yaw	Roll
RMS Disturbance Torque	Table 28	T_y	T_z	0
Disturbance Torque Factor (μ)	Fig. 90	μy	μz	1
Theoretical Propellant Rate (W_i)	Fig. 88	$\dot{W}_y$	$\dot{W}_z$	$\dot{W}_x$
Actual Propellant Rate	$\dot{W}_a = \mu \dot{W}_i$	$\mu y\ \dot{W}_y$	$\mu_z\ \dot{W}_z$	$\dot{W}_x$
Theoretical Jet Starts (N)	Fig. 89	N_y	N_z	N_x
Actual Jet Start (N_a)	$N_a = \mu_i N_i$	$\mu y\ N_y$	$\mu z\ N_z$	$\frac{N_x}{4}$
Burn Time/Jet (t_b)	$t_b = N_a \Delta t$	$\mu y\ N_y \Delta t$	$\mu z\ N_z \Delta t$	$\frac{N_x \Delta t}{4}$
	Movable Panels			
Attitude Hold	Axis / Where Found	Pitch	Yaw	Roll
Disturbance Torque	Figs. 96, 97, 98	T_y [1]	T_z	0
Disturbance Torque Factor (μ)	Fig. 90	μy [1]	μz	1
Theoretical Propellant Rate (W_i)	Fig. 88	$\dot{W}_y$	$\dot{W}_z$	$\dot{W}_x$
Actual Propellant Rate	$\dot{W}_a = \mu_i \dot{W}_i$	$\mu_y\ \dot{W}_y$	$\mu_z\ \dot{W}_z$	$\dot{W}_x$
Theoretical Jet Start (N_i)	Fig. 89	N_y	N_z	N_x
Actual Starts/Jet	$N_a = \mu_i N_i$	$\mu y\ N_y$	$\mu z\ N_y$	$\frac{N_x}{4}$
Burn Time/Jet	$t_b = N_a \Delta t$	$\mu y\ N_y \Delta t$	$\mu z\ N_z \Delta t$	$\frac{N_x \Delta t}{4}$

[redacted]

CON[redacted]

Table 30. Procedure for Analysis of Reaction System Requirements on a Vehicle Utilizing Solar Panels (Cont)

Vehicle Pointing	Axis / Where Found	Pitch	Yaw	Roll
Propellant for Vehicle Yaw, Roll Control	Table 29	0	W_z [2]	W_x [1]
Burn Time/Jet	$t_b = \frac{Wi\, I_{sp}}{4F}$	0	$\frac{I_{sp}\, W_z}{4F}$ [2]	$\frac{I_{sp}\, W_x}{8F}$ [1]

1 For local horizontal mode $T_y = 0, \mu_y = 1, W_x = 0$

2 For local vertical mode $W_z = 0$

System Requirements Summary

From the analyses of maneuver and attitude hold requirements, total mission requirements can be derived. The reaction propellant weights, jet starts, and burn times for each mission phase are totaled. The total weight for the reaction control system consists of reaction propellant weight, the required tankage, thrusters, and plumbing. Using the total propellant determined above, the additional system weight can be evaluated using Figure 99. The approximate volume required for the propellant can be estimated by assuming a reaction propellant density of 70 lb/ft^3.

Reaction jet reliability can be evaluated using Figure 100 and the mission start and burn time totals.

The basic components of the Block II SCS are listed in Table 31 together with weight and volume data. This information when used with propellant weight, tankage, plumbing, and sparing data can be used to estimate total system weight and volume.

[redacted]

CON[redacted]

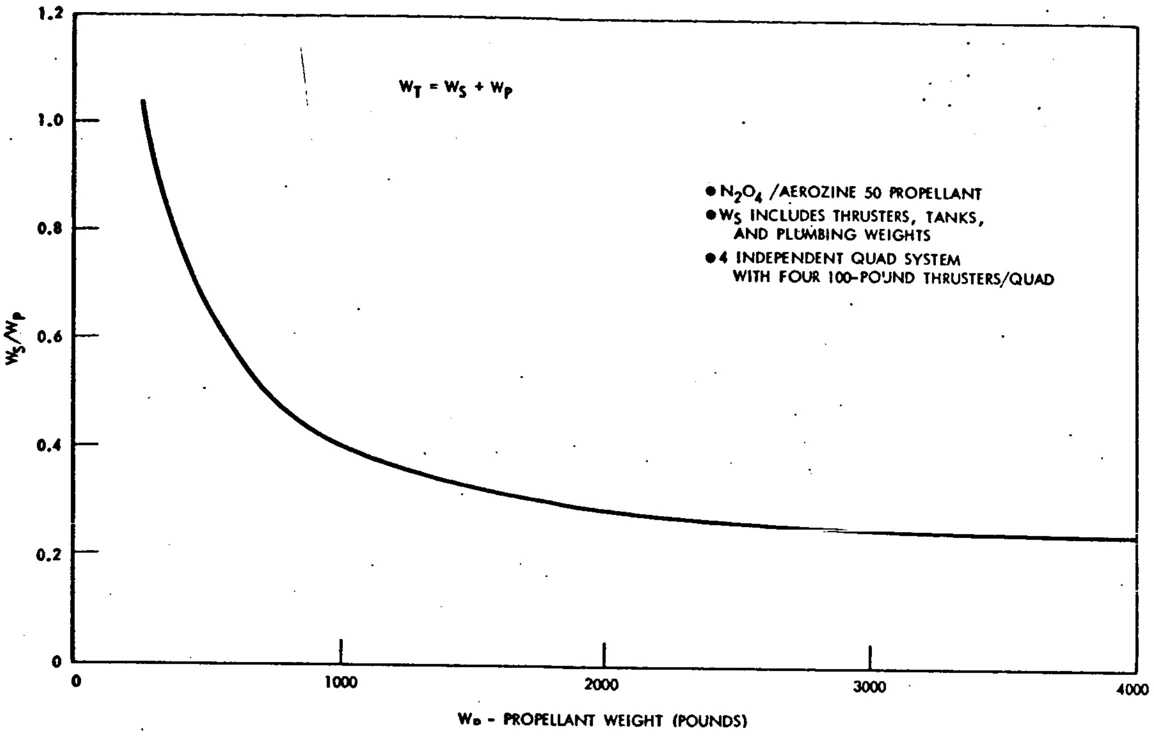

Figure 99. Reaction Control System Total Weight

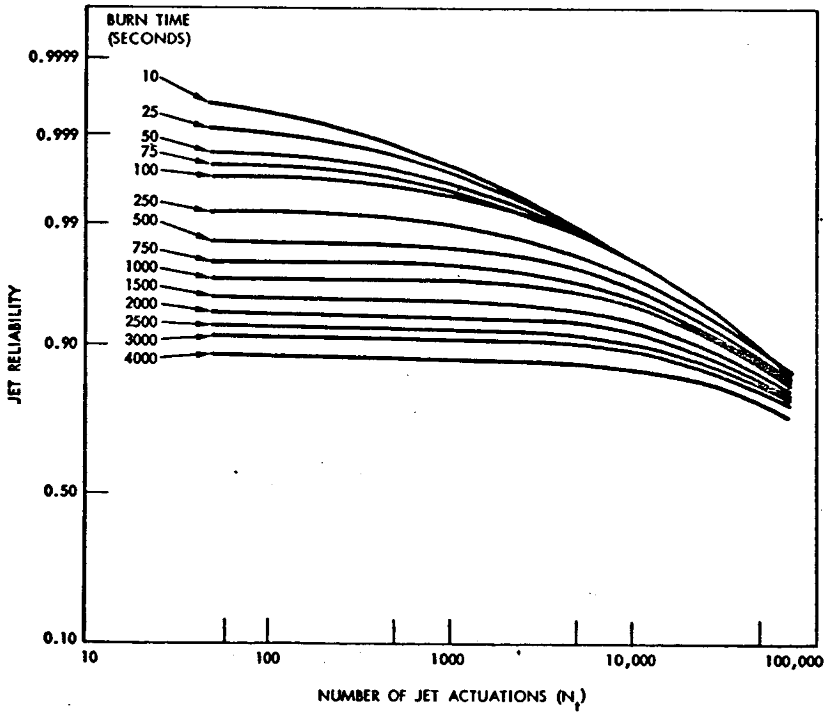

Figure 100. Reaction Jet Reliability as a Function of Actuations and Operating Time

[redacted]

Table 31. System Component Summary (Block II SCS)

Component	Weight/Unit (lbs)	Volume/Unit (inches3)	No. for Basic Sys.
Solenoid Driver Assembly	12.2	476	1
Control Electronics Assembly	16.1	495	1
Display Electronics Assembly	19.6	615	1
Gyro Display Coupler	15.7	430	1
Servo Amplifier (TVC)	14.6	430	1
Gyro Assembly	17.5	525	2
Flight Director Attitude Indicator	7.9	428	2
Gimbal Position & Fuel Pressure Indicator	3.7	150	1
Attitude Set Control Panel	3.7	115	1
Translation Control	4.3	70	1
Rotation Control	6.2	94	2
Entry Monitor System	5.0	112	1

CO[redacted]

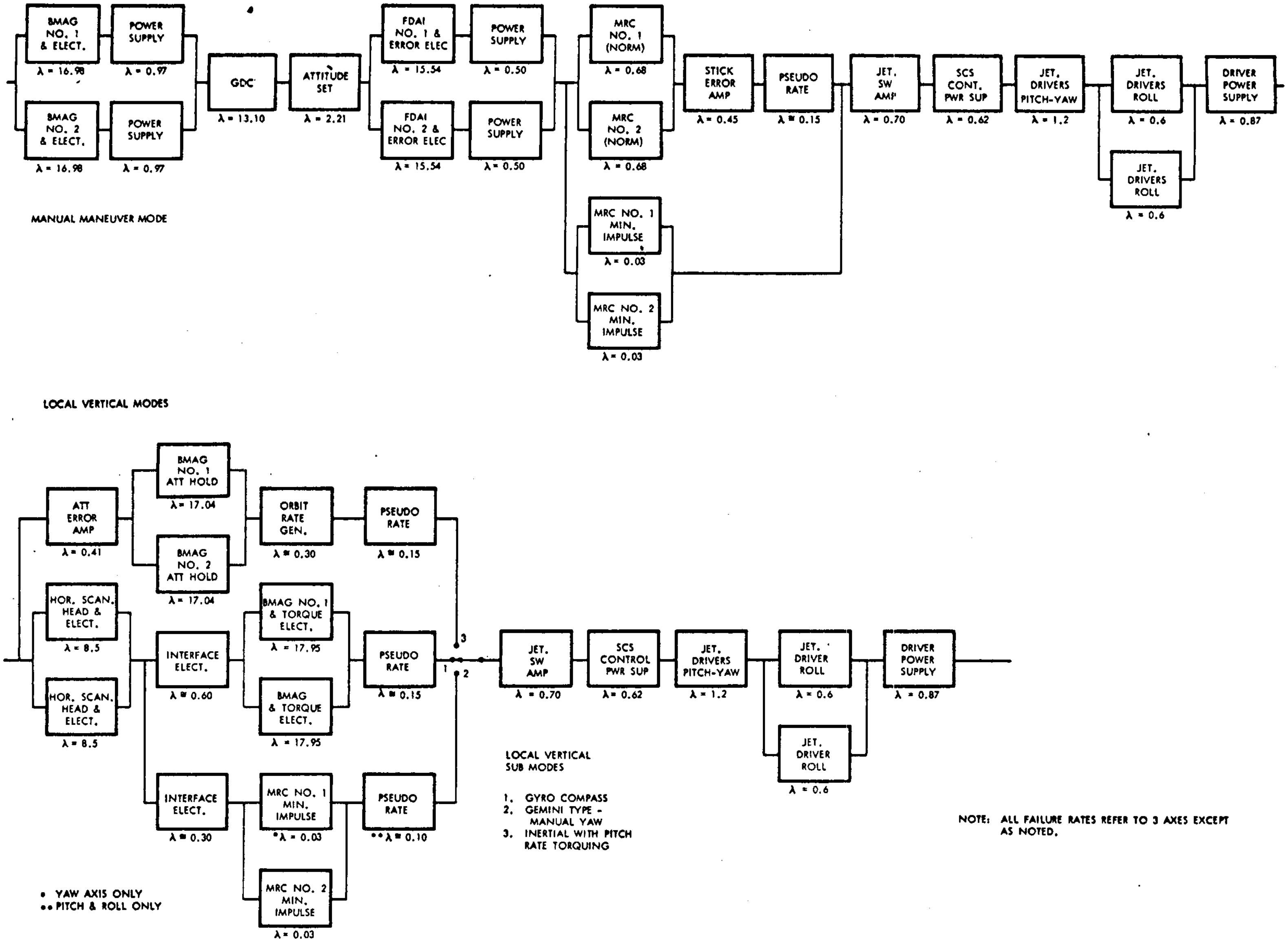
BMAG NO. 1 & ELECT. λ = 16.98
POWER SUPPLY λ = 0.97
BMAG NO. 2 & ELECT. λ = 16.98
POWER SUPPLY λ = 0.97
GDC λ = 13.10
ATTITUDE SET λ = 2.21
FDAI NO. 1 & ERROR ELEC λ = 15.54
POWER SUPPLY λ = 0.50
FDAI NO. 2 & ERROR ELEC λ = 15.54
POWER SUPPLY λ = 0.50
MRC NO. 1 (NORM) λ = 0.68
MRC NO. 2 (NORM) λ = 0.68
MRC NO. 1 MIN. IMPULSE λ = 0.03
MRC NO. 2 MIN. IMPULSE λ = 0.03
STICK ERROR AMP λ = 0.45
PSEUDO RATE λ = 0.15
JET. SW AMP λ = 0.70
SCS CONT. PWR SUP λ = 0.62
JET. DRIVERS PITCH-YAW λ = 1.2
JET. DRIVERS ROLL λ = 0.6
JET. DRIVERS ROLL λ = 0.6
DRIVER POWER SUPPLY λ = 0.87
MANUAL MANEUVER MODE
LOCAL VERTICAL MODES
ATT ERROR AMP λ = 0.41
BMAG NO. 1 ATT HOLD λ = 17.04
BMAG NO. 2 ATT HOLD λ = 17.04
ORBIT RATE GEN. λ = 0.30
PSEUDO RATE λ = 0.15
HOR. SCAN. HEAD & ELECT. λ = 8.5
HOR. SCAN. HEAD & ELECT. λ = 8.5
INTERFACE ELECT. λ = 0.60
BMAG NO. 1 & TORQUE ELECT. λ = 17.95
BMAG & TORQUE ELECT. λ = 17.95
PSEUDO RATE λ = 0.15
INTERFACE ELECT. λ = 0.30
MRC NO. 1 MIN. IMPULSE *λ = 0.03
MRC NO. 2 MIN. IMPULSE λ = 0.03
PSEUDO RATE **λ = 0.10
3
1
2
JET. SW AMP λ = 0.70
SCS CONTROL PWR SUP λ = 0.62
JET. DRIVERS PITCH-YAW λ = 1.2
JET. DRIVER ROLL λ = 0.6
JET. DRIVER ROLL λ = 0.6
DRIVER POWER SUPPLY λ = 0.87
LOCAL VERTICAL SUB MODES
1. GYRO COMPASS
2. GEMINI TYPE - MANUAL YAW
3. INERTIAL WITH PITCH RATE TORQUING
NOTE: ALL FAILURE RATES REFER TO 3 AXES EXCEPT AS NOTED.
* YAW AXIS ONLY
** PITCH & ROLL ONLY

Figure 101. Orbit Mode Success Diagrams (Sheet 1 of 3)

[redacted]

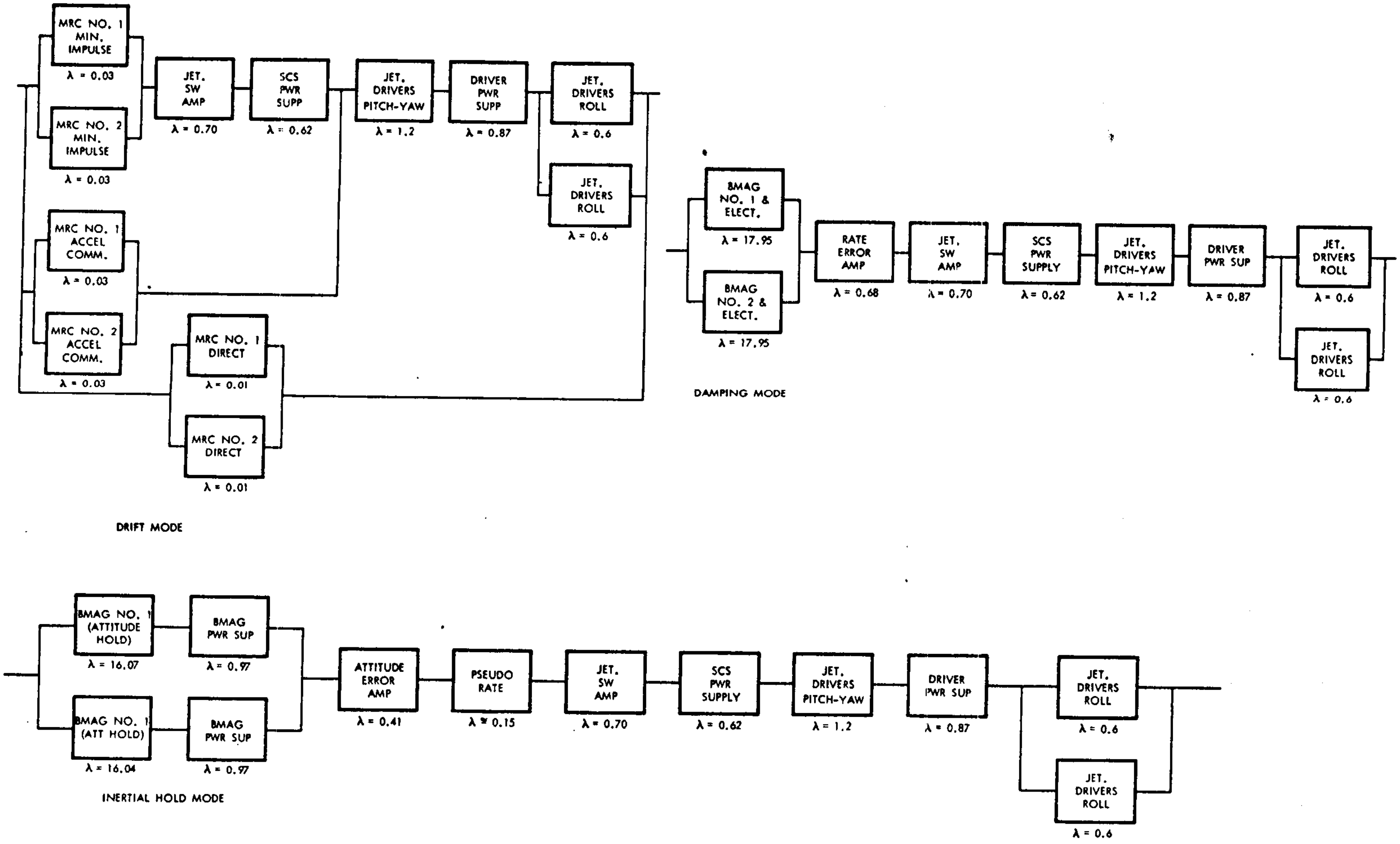
MRC NO. 1 MIN. IMPULSE
λ = 0.03
MRC NO. 2 MIN. IMPULSE
λ = 0.03
MRC NO. 1 ACCEL COMM.
λ = 0.03
MRC NO. 2 ACCEL COMM.
λ = 0.03
JET. SW AMP
λ = 0.70
SCS PWR SUPP
λ = 0.62
JET. DRIVERS PITCH-YAW
λ = 1.2
DRIVER PWR SUPP
λ = 0.87
JET. DRIVERS ROLL
λ = 0.6
JET. DRIVERS ROLL
λ = 0.6
MRC NO. 1 DIRECT
λ = 0.01
MRC NO. 2 DIRECT
λ = 0.01
DRIFT MODE
BMAG NO. 1 & ELECT.
λ = 17.95
BMAG NO. 2 & ELECT.
λ = 17.95
RATE ERROR AMP
λ = 0.68
JET. SW AMP
λ = 0.70
SCS PWR SUPPLY
λ = 0.62
JET. DRIVERS PITCH-YAW
λ = 1.2
DRIVER PWR SUP
λ = 0.87
JET. DRIVERS ROLL
λ = 0.6
JET. DRIVERS ROLL
λ = 0.6
DAMPING MODE
BMAG NO. 1 (ATTITUDE HOLD)
λ = 16.07
BMAG PWR SUP
λ = 0.97
BMAG NO. 1 (ATT HOLD)
λ = 16.04
BMAG PWR SUP
λ = 0.97
ATTITUDE ERROR AMP
λ = 0.41
PSEUDO RATE
λ ≈ 0.15
JET. SW AMP
λ = 0.70
SCS PWR SUPPLY
λ = 0.62
JET. DRIVERS PITCH-YAW
λ = 1.2
DRIVER PWR SUP
λ = 0.87
JET. DRIVERS ROLL
λ = 0.6
JET. DRIVERS ROLL
λ = 0.6
INERTIAL HOLD MODE

Figure 101. Orbit Mode Success Diagrams (Sheet 2 of 3)

CO[redacted]

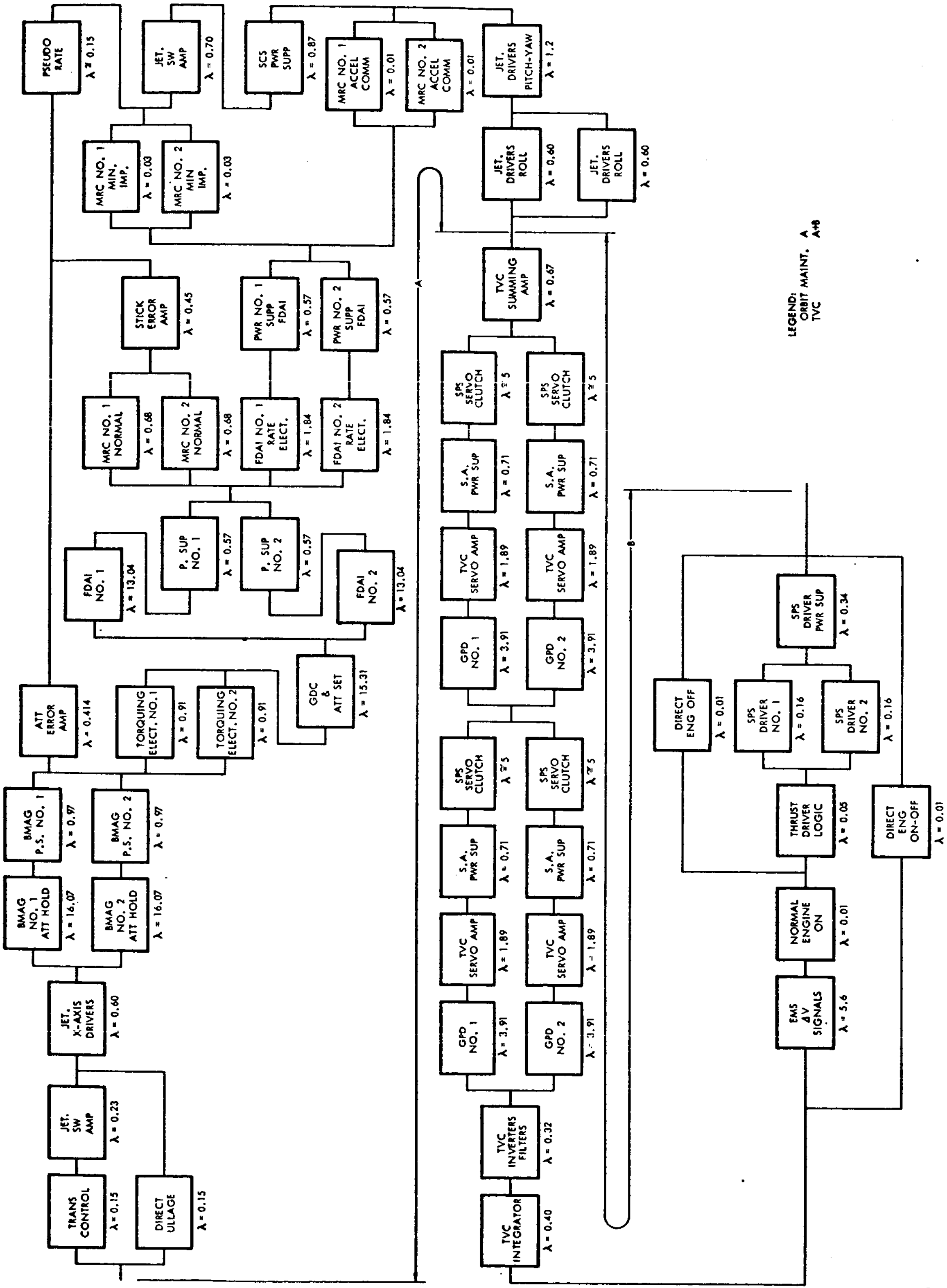
PSEUDO RATE
λ = 0.15
JET. SW AMP
λ = 0.70
SCS PWR SUPP
λ = 0.87
MRC NO. 1 ACCEL COMM
λ = 0.01
MRC NO. 2 ACCEL COMM
λ = 0.01
JET. DRIVERS PITCH-YAW
λ = 1.2
MRC NO. 1 MIN. IMP.
λ = 0.03
MRC NO. 2 MIN IMP.
λ = 0.03
JET. DRIVERS ROLL
λ = 0.60
JET. DRIVERS ROLL
λ = 0.60
STICK ERROR AMP
λ = 0.45
PWR NO. 1 SUPP FDAI
λ = 0.57
PWR NO. 2 SUPP FDAI
λ = 0.57
TVC SUMMING AMP
λ = 0.67
LEGEND:
ORBIT MAINT. A
TVC A+B
MRC NO. 1 NORMAL
λ = 0.68
MRC NO. 2 NORMAL
λ = 0.68
FDAI NO. 1 RATE ELECT.
λ = 1.84
FDAI NO. 2 RATE ELECT.
λ = 1.84
SPS SERVO CLUTCH
λ = 5
S.A. PWR SUP
λ = 0.71
FDAI NO. 1
λ = 13.04
P. SUP NO. 1
λ = 0.57
P. SUP NO. 2
λ = 0.57
FDAI NO. 2
λ = 13.04
TVC SERVO AMP
λ = 1.89
GPD NO. 1
λ = 3.91
GPD NO. 2
λ = 3.91
B
SPS DRIVER PWR SUP
λ = 0.34
GDC & ATT SET
λ = 15.31
ATT ERROR AMP
λ = 0.414
TORQUING ELECT. NO. 1
λ = 0.91
TORQUING ELECT. NO. 2
λ = 0.91
DIRECT ENG OFF
λ = 0.01
SPS DRIVER NO. 1
λ = 0.16
SPS DRIVER NO. 2
λ = 0.16
BMAG P.S. NO. 1
λ = 0.97
BMAG P.S. NO. 2
λ = 0.97
THRUST DRIVER LOGIC
λ = 0.05
DIRECT ENG ON-OFF
λ = 0.01
BMAG NO. 1 ATT HOLD
λ = 16.07
BMAG NO. 2 ATT HOLD
λ = 16.07
NORMAL ENGINE ON
λ = 0.01
JET. X-AXIS DRIVERS
λ = 0.60
EMS ΔV SIGNALS
λ = 5.6
JET. SW AMP
λ = 0.23
TVC INVERTERS FILTERS
λ = 0.32
TRANS CONTROL
λ = 0.15
DIRECT ULLAGE
λ = 0.15
TVC INTEGRATOR
λ = 0.40
A

Figure 101. Orbit Mode Success Diagrams (Sheet 3 of 3)

[redacted]

RELIABILITY ANALYSIS

A parametric reliability analysis was conducted using the Block II SCS as the basic system. Some system modifications were considered including addition of various local vertical modes. Seven modes of operation, typical of prolonged mission functional requirements, were formulated. The reliability of each mode was determined as a function of time. Thus, total system reliability for a specified mission may be estimated by first determining the mission time in each mode and then using the parametric data presented graphically in this section. The effect of adding redundancy has been investigated in some cases and the results are illustrated.

The seven modes of operation are shown in success diagram form in Figure 101. Minor changes are required in the functional switching to accommodate some of these modes as follows:

1. Manual Maneuver: It is assumed that functional switching in Block II will provide the mechanization required.
2. Local Vertical
    a. Gyro compass mode
        (1) Add interface electronics for the horizon scanners
    b. Gemini type using manual yaw control
        (1) Add switching for pseudo rate in pitch and roll
        (2) Add switching for scanner interface electronics
        (3) Change pseudo rate to special charge and discharge time constants
    c. Attitude hold with orbit rate torquing in pitch axis
        (1) Add orbit rate generator
        (2) Add switching to allow both sets of BMAGs to become attitude-hold units
3. Drift Mode

    For power saving, some circuits in the SCS could be de-energized.

    a. Error amplifiers
    b. Deadband and limits
    c. Any shaping filters
    d. Relays

4. Damping Mode

   This mode is essentially similar to proportional manual maneuver with the GDC not energized and the rotation controller centered.

5. Inertial Hold

   It is recommended that both sets of BMAG's be capable of attitude reference.

6. Orbit Maintenance with X Reaction Jets

   This mode is essentially a combination of attitude hold and manual maneuver for redundancy.

   a. Each set of BMAG's should be capable of providing attitude reference.

7. TVC

   The mode is composed of the orbit maintenance mechanization and the TVC gimbal control and thrust logic.

In the reliability analyses it was assumed that all parallel paths are operating during the times designated for each mode. A check of reliability with standby redundancy (de-energized hard wired spares) where applicable, for the local vertical gyro compass mode showed little change. This would probably be true in most modes because of the limit established by the SCS switching electronics.

It is recommended as a result of this study that redundant switching amplifiers, pitch jet drivers, and yaw jet drivers be considered for prolonged missions.

Manual Maneuver Mode

Assumptions

(1) Mode is used for maneuvers that require precise rate or rotations to known orientations.

(2) Pseudo rate stabilization is used with normal manual rotation control.

Results

The analytical results are tabulated below and plotted on Figure 102.

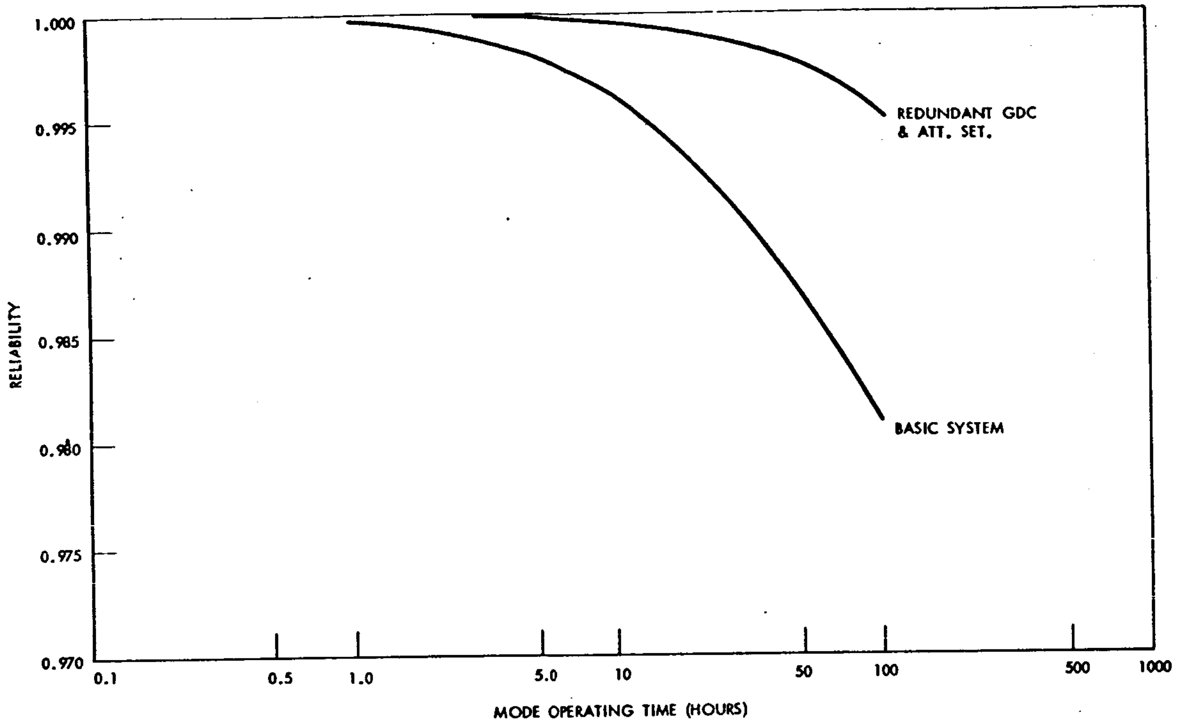

Figure 102. Manual Manuever Mode Reliability

Configuration	Reliability t = 10 hours	Reliability t = 100 hours
(1) As diagrammed Figure 101	0.99632	0.9809
(2) With redundant GDC and Attitude Set	0.999619	0.9953

Local Vertical Modes

Assumptions

(1) Local vertical mode is shown with three paths for attitude error signal generation.

(2) Gyro compassing (Mode 1) requires horizon scanner and a gyro in each axis. Pilot workload is zero and accuracy is about ±0.5 degree for each axis.

(3) Mode 2 assumes no gyros operating and the scanner coupled directly to the switching amplifier. Manual control of yaw is required. Accuracy in pitch and roll may be as good as ±0.5 degrees if scanner noise is favorable. Yaw accuracy depends on skill of the pilot and may be limited to 1 degree.

(4) Mode 3 assumes no scanner. It uses inertial hold with gyros in the roll and yaw axes after initial alignment. The pitch gyro is torqued at orbit rate. Accuracy of this mode is a function of initial alignment and gyro drift. Best average accuracy is 1 to 2 degrees.

Results

The analytical results are tabulated below and plotted on Figure 103.

	Configuration	Reliability			
		t = 1 hr.	t = 10 hrs	t = 100 hrs	t = 1000 hrs
(a)	Gyro-compassing only	0.99993	0.99956	0.99556	0.92751
(b)	Gyro-compass and Gemini type				0.95998
(c)	Gyro-compass and Gemini type and orbit torquing				0.96630
(d)	Gemini type alone				0.95723
(e)	Gyro-compassing with standby redundancy on scanner, gyros, and roll jet drivers	0.999955	0.999586	0.995711	0.93968

Drift Mode

Assumptions

(1) Visual reference for attitude corrections

(2) Failure in any axis negates use of that path

(3) Mode used for coarse attitude or rate control

Results

The analytical results are tabulated below and plotted on Figure 104.

[redacted]

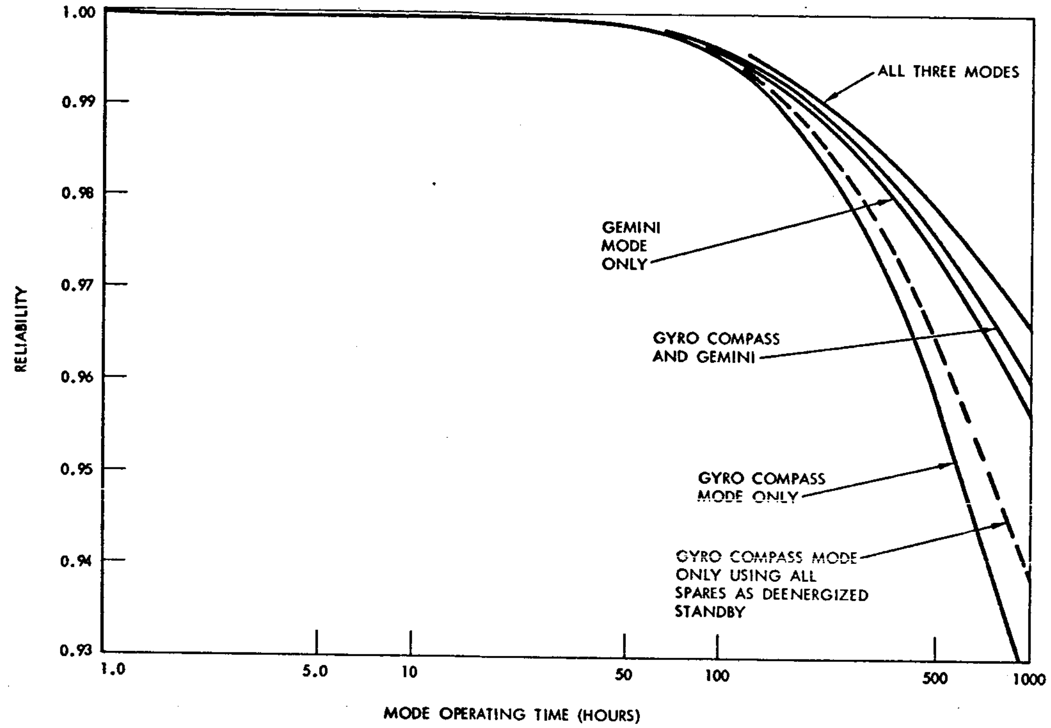

Figure 103. Local Vertical Mode Reliability

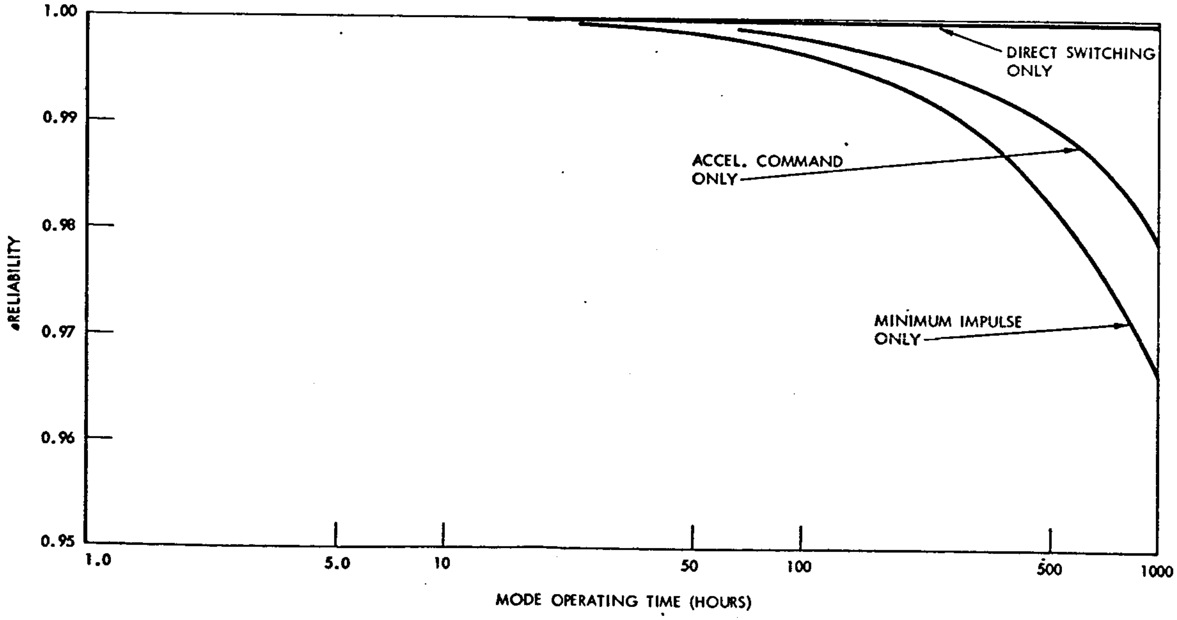

Figure 104. Drift Mode Reliability

[redacted]

[redacted]

Configuration	Reliability t = 100 hrs	 t = 1000 hrs	 t = 10,000 hrs
(a) Accel. Command Path		0.97915	
(b) Accel. Command Path and Direct Path		0.99999	
(c) Direct Path Only			0.99999
(d) Minimum impulse path only	0.99658	0.96653	

Damping Mode

Assumptions

(1) No need for attitude control

(2) Used to control angular rate in presence of disturbance torques

Results

The analytical results are tabulated below and plotted on Figure 105.

Configuration	Reliability t = 100 hr	 t = 1000 hrs
(1) As shown on Figure 101.	0.99568	0.93465
(2) With redundancy*	0.99966	0.97132

*Redundancy includes

(a) Rate error amplifier

(b) Jet switching amplifier

(c) SCS power supply

(d) Jet drivers - (pitch and yaw)

(e) Driver power supply

Inertial Hold Mode

Assumptions

(1) Pseudo rate used for stabilization

(2) No manual control

(3) FDAI not used

[redacted]

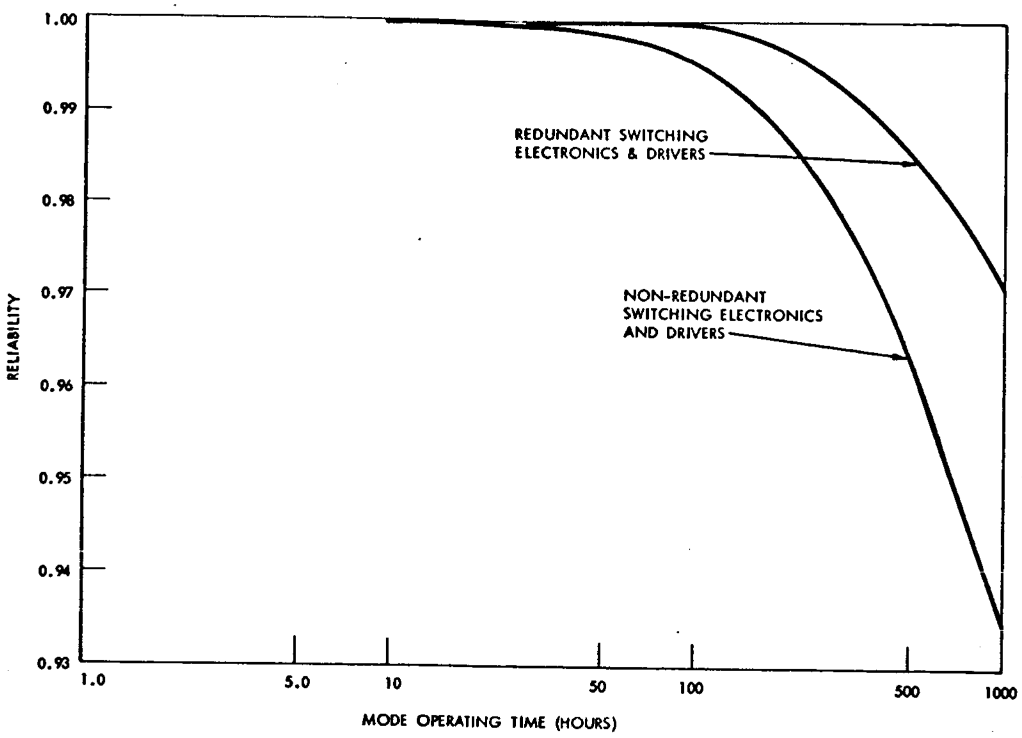

Figure 105. Damping Mode Reliability

Results

The analytical results are tabulated below and plotted on Figure 106.

Configuration	Reliability t = 1 hr.	 t = 10 hrs	 t = 100 hrs	 t = 1000 hrs
(a) Present system			0.98920	0.81050
(b) Both BMAG sets can be used for attitude data (as per Figure 101)	0.99994	0.99958	0.99571	0.9372
(c) Case (b) plus additional redundancy*			0.99969	0.97400

* Jet switching amplifier
SCS power supply
Jet drivers (pitch and yaw)
Driver power supply
Pseudo rate
Attitude error amplifier

[redacted]

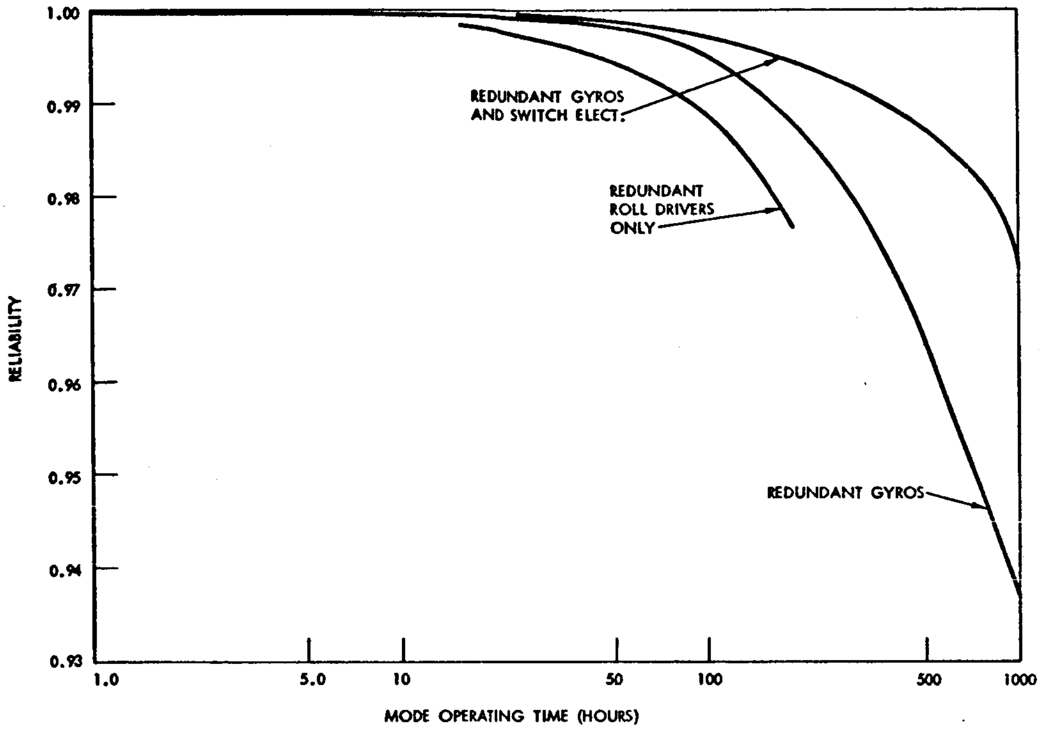

Figure 106. Inertial Hold Mode Reliability

Orbit Maintenance Mode

Assumptions

(1) Both sets of BMAG's can be used in the attitude hold mode.

(2) The normal mode is inertial hold using the attitude control amplifiers.

(3) Backup modes include the use of the GDC and manual control through the normal, minimum impulse and acceleration options.

(4) All equipment remains energized.

Results

The analytical results are tabulated below and plotted on Figure 107.

Configuration	Reliability		
	t = 1 hr	t = 10 hrs	t = 100 hrs
(1) Attitude error path only		0.99958	0.99576
(2) All paths	0.999978	0.99981	0.99786.

[redacted]

[redacted]

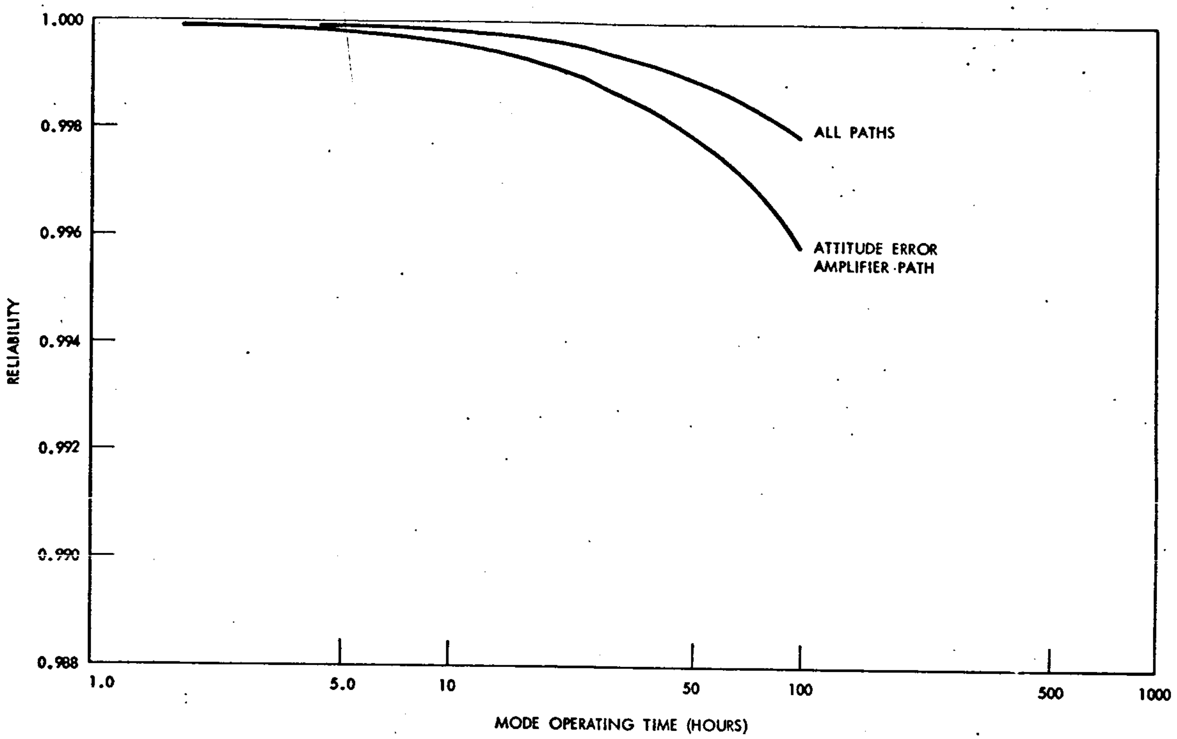

Figure .107. Orbit Maintenance Mode Reliability

TVC Mode

Assumptions

(1) Attitude is maintained through any of the three channels shown.

(2) Two parallel paths are available for the engine On and Off signals.

(3) The roll jet drivers are redundant.

(4) Ullage can be controlled through the direct command or the translation control.

(5) SPS clutch has failure rate of 5 percent per 1000 hrs.

Results

The analytical results are tabulated below and plotted on Figure 108.

Configuration	Reliability	
	t = 1 hr	t = 10 hrs
Total System	.0999963	0.999672

[redacted]

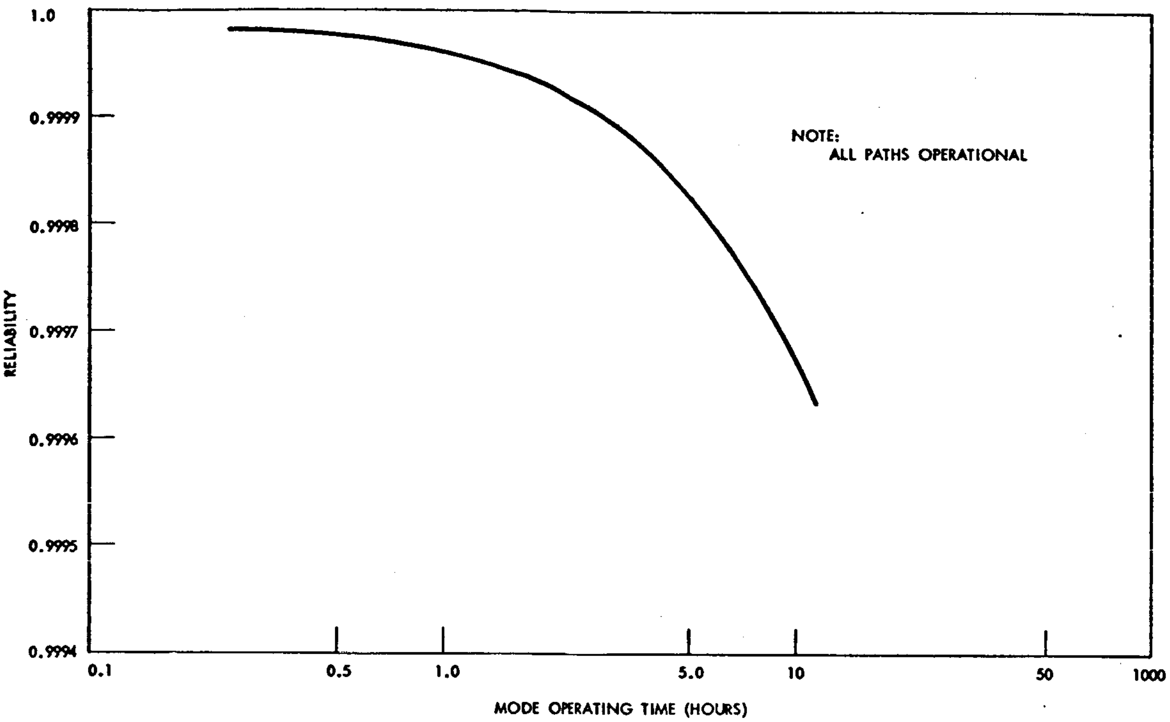

Figure 108. TVC Mode Reliability

De-energized Failures

The problem of de-energized failures cannot be treated in detail until failure rates are available. However, a parametric analysis provides some insight into the problem. The formula for reliability of an element including a de-energized failure rate is

$$R = e^{-\lambda e^{t}} \left[1 + \frac{\lambda e}{\lambda d} \left(1 - e^{-\lambda d^{t}} \right) \right] \qquad (24)$$

where

λe = energized failure rate

λd = de-energized failure rate

As an example, consider horizon scanner reliability. This parameter has been plotted versus the ratio $\lambda d/\lambda_e$ on Figure 109 for two missions.

[redacted]

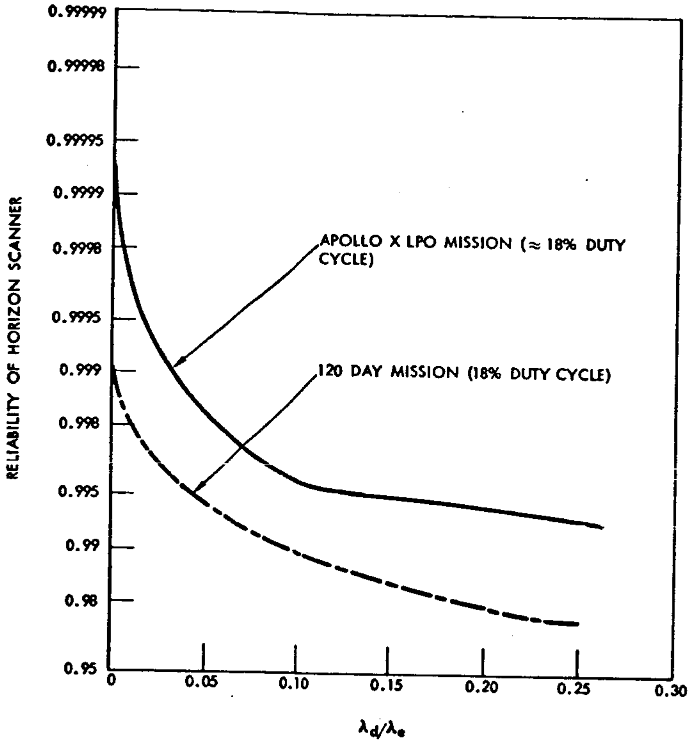

Figure 109. Typical Effect of De-Energized Failures

[redacted]

ALTERNATE CONTROL SYSTEMS

The alternate control systems considered were momentum storage systems, composed of reaction wheels and twin gyros systems. The attractive feature of momentum storage devices is the ability to control cyclic disturbances without the increased weight encountered using reaction jet systems. A disadvantage of most momentum storage devices is the large power requirements for vehicle maneuvering. The following section will discuss techniques for estimating the weight, power, and volume of momentum storage control systems based on vehicle and mission control requirements.

Momentum storage system weight and volume will be determined primarily from the momentum requirements due to maneuvering and those due to integrated disturbance torques. An analysis was conducted of the momentum requirements imposed by slewing rate, attitude hold mode, and the use of solar panels for the vehicle power supply. This portion of the analysis is independent of the system being considered. The effect of these requirements on the various systems will then be considered.

ROTATIONAL MANEUVERS - REACTION WHEEL

System torque and momentum requirements for vehicle maneuvering can be determined for both acceleration and rate mode maneuvers. In an acceleration mode, the system torques the vehicle in one direction for a time $t_m/2$ and then reverses the torque until vehicle motion ceases at time t_m. In a rate mode maneuver, the vehicle is torqued until the desired rate is achieved and then coasts until near the intended orientation where an opposing torque stops motion.

The equation describing an acceleration mode maneuver is

$$T = \frac{4\theta I}{t_m{}^2} \quad \text{ft-lb} \tag{25}$$

where T is the torque required to rotate the vehicle through θ radians in time t_m. Figure 110 is a plot of Equation (25) for the two laboratory configurations being considered. The maximum momentum occurs at $t_m/2$ and the rate at the point is twice the average rate (θ/t_m). The maximum momentum requirement is found using Figure 111 with a rate of $(2\theta/t_m)$ and the vehicle inertia value.

For maneuvers where the vehicle is accelerated from rest to a given rate and slews at that rate until application of an opposing torque, the required

[redacted]

torque is given by

$$T = \frac{I\dot{\theta}^2}{(\dot{\theta}t_m - \theta)} \quad \text{ft-lb} \qquad (26)$$

where $\dot{\theta}$ is the desired slewing rate and θ the total rotation from rest to rest. Figure 112 is a plot of the torque requirements for 180 degree maneuvers and given maneuver times. The maximum momentum occurs during slewing and is given by

$$H = I\dot{\theta} \quad \text{ft-lb-sec} \qquad (27)$$

Figure 111 is a plot of the momentum requirements for the two vehicle configurations during maneuver.

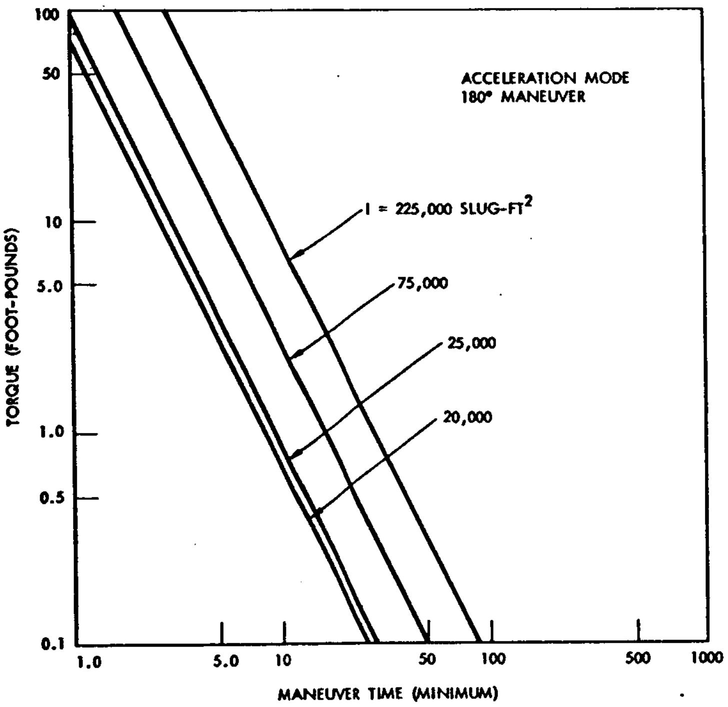

Figure 110. Maneuver-Torque Requirements for Reaction Wheels

[redacted]

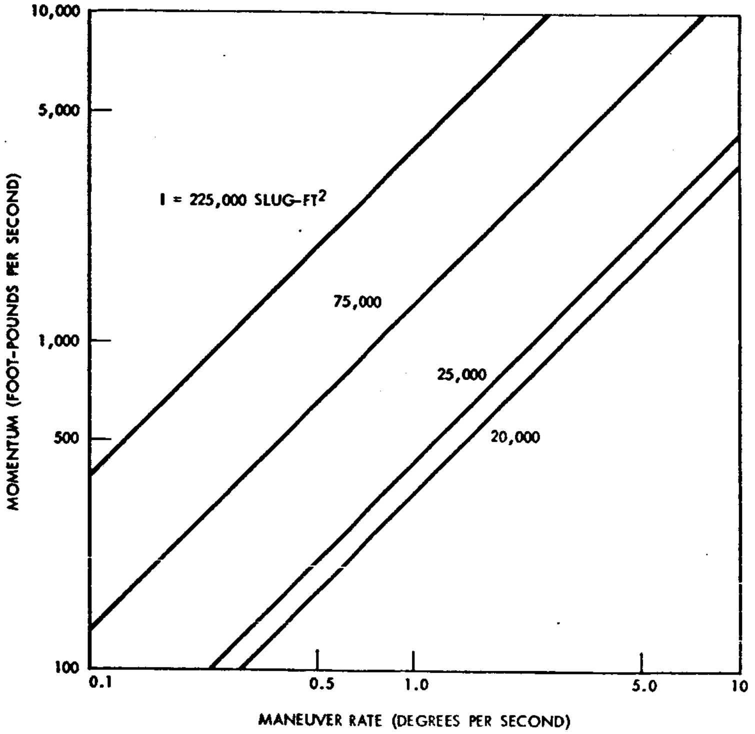

Figure 111. Vehicle Maneuver-Momentum Requirements

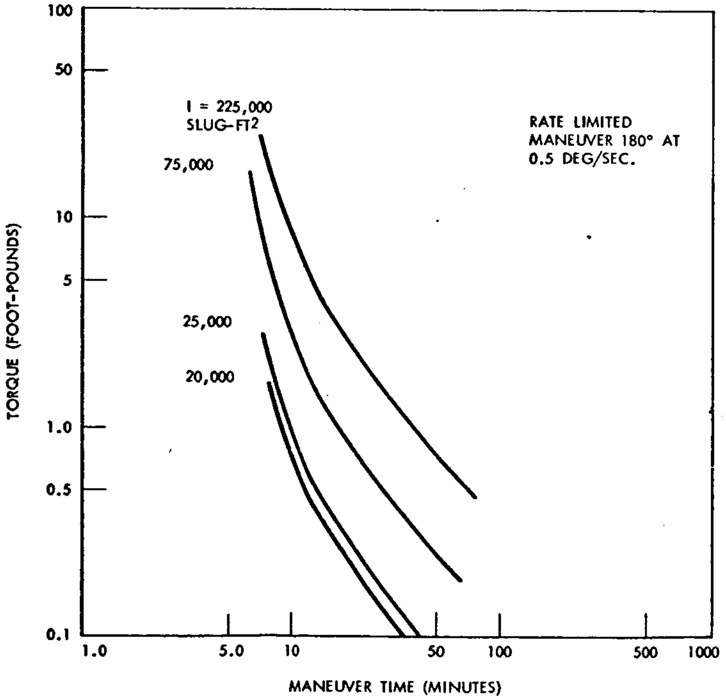

Figure 112. Maneuver-Torque Requirements for Reaction Wheels

[redacted]

Attitude Hold

The primary requirement during attitude hold is that the system be capable of holding the vehicle in the desired orientation by counteracting the effects of disturbance torques. As previously mentioned, these will result mainly from aerodynamic and gravity gradient influences on the vehicle.

Inertial Attitude Hold

It was noted in a preceding section that in general, gravity gradient torques will be much greater than aerodynamic torques. The torque components about each vehicle axis, assuming the inertial orientation previously discussed ($\theta = 45^\circ$, $\psi = 45^\circ$, θ varying), are

$$T_{gx} = 0 \tag{28}$$

$$T_{gy} = \frac{3GM}{R_o{}^3} (I_x - I_y) \left| -.5 \sin\theta \cos\theta + .353 \sin^2\theta \right| \tag{29}$$

$$T_{gz} = \frac{3GM}{R_o{}^3} (I_x - I_y) \left| .5 \sin\theta \cos\theta + .353 \sin^2\theta \right| \tag{30}$$

The angle θ which varies with orbital position, can be represented as θt where

$$\dot{\theta} = \frac{2\pi}{t_o} \quad \text{rad/sec} \tag{31}$$

and t_o is the orbital period. The angular momentum per orbit required to counter the disturbance torques is

$$H_x = \int_0^{t_o} T_{gx}\, dt = 0 \tag{32}$$

$$H_y = \int_0^{t_o} T_{gy}\, dt \tag{33}$$

$$H_z = \int_0^{t_o} T_{gz}\, dt \tag{34}$$

The above equations were evaluated for the selected vehicle configurations and the values are presented in Table 32.

[redacted]

Table 32. Inertial Attitude Hold Momentum Requirements (ft-lb-sec/orbit)

Configuration / Axis	1	2
H_x	0	0
H_y	2.59×10^2	1.03×10^3
H_z	2.59×10^2	1.03×10^3

Local Vertical Hold

For the local vertical hold mode ($\theta = -\pi/2$, $\psi = 0$) Equation (7) indicates that gravity gradient torque components are zero. However, aerodynamic torque effects are a maximum. The integrated torque values per orbit are 16.3 ft-lb-sec for the small laboratory vehicle (Configuration 1) and 176 ft-lb-sec for the large laboratory (Configuration 2), and can occur about either the pitch or yaw axis. In addition, the system must supply constant momentum orbital rate requirements of 83.5 ft-lb-sec for Configuration 1 and 223 ft-lb-sec for Configuration 2.

Solar Panel Considerations

The analysis of momentum exchange devices on vehicles utilizing solar panels was not conducted in the same manner as the analysis of the effects of solar panels on an all-jet system. For extended missions where reaction jets are used on vehicles with solar panels, it is only necessary to determine the average disturbance torque value over the required period to assess the effects on reaction propellant consumption and hence system weight. However, for momentum storage systems, where an advantage is gained by the ability to counter cyclic torques with no weight increase, it is desirable to size the system to counter integrated torque values.

For vehicles utilizing solar panels, the torques will not always be cyclic, and momentum build-up will occur. The effects of fixed and movable solar panels are investigated in the following sections. Much of the analysis is based on the explanation in the corresponding section under "Current System."

Fixed Panels

For vehicles utilizing fixed solar panels, the aerodynamic torques do not become significant until the total panel area exceeds 1000 square feet. The gravity gradient torque effects for fixed panel vehicles are cyclic over an orbit because of the selected orientation. A determination was made of the maximum integrated torque values which could occur during one orbit. For a 30-degree inclination orbit, the maximum momentum which occurs during a given orbit about the z-axis occurs when the sun-line angle is at the maximum value of 50 degrees. The maximum value about the y-axis occurs when the sun line angle is 0 degrees. Table 33 summarizes these values.

Table 33. Maximum Integrated Torque Value per Orbit for Vehicle with Fixed Panels (ft-lb-sec)

Axis / Configuration	Pitch	Yaw	Roll
1	8.24×10^2	6.3×10^2	0
2	3.24×10^2	2.51×10^3	0

For vehicles using movable panels, only the local vertical vehicle orientation was considered. In this mode, the vehicle's longitudinal axis is directed toward the earth and panel control is effected by rolling the vehicle and pitching the panels. Using the solar panel control laws which give panel and vehicle orientation at each point in orbit, expressions were determined for vehicle area exposed to the free stream at each position in orbit. From this information, the aerodynamic torque values were calculated. From momentum storage considerations, it is desirable to make the capability of each axis at least as great as the maximum value to be encountered on any orbit. This permits the storage device to counter those cyclic torques which are periodic over one orbit.

The maximum integrated torque value (ft-lb-sec) for the pitch (y) axis occurs during orbits when the sun line inclination ζ is zero degrees. Figure 113 is a plot of this maximum integrated torque value for configurations 1 and 2 as a function of solar panel area. The maximum value about the yaw (z) axis occurs when the sun line angle is at a maximum for 30° inclination orbits (i.e., $\zeta = 50^{\circ}$). The maximum integrated torque values for Configurations 1 and 2 as a function of solar panel area are shown in Figure 114.

In addition to the disturbance torque requirements, the orbit rate momentum requirements previously noted must be provided.

Momentum Storage Requirements

The accurate determination of momentun storage requirements on a "per axis" basis is extremely difficult. This is a result of mission profile variation and the lack of an exact time line history. At best, an estimate of the requirements for the three control axes can be obtained from the previous analyses.

As a basic ground rule, no axis should require desaturation more than once per orbit. This permits momentum storage devices to effectively counter the cyclic disturbance torques with periods of one orbit. The integrated

[redacted]

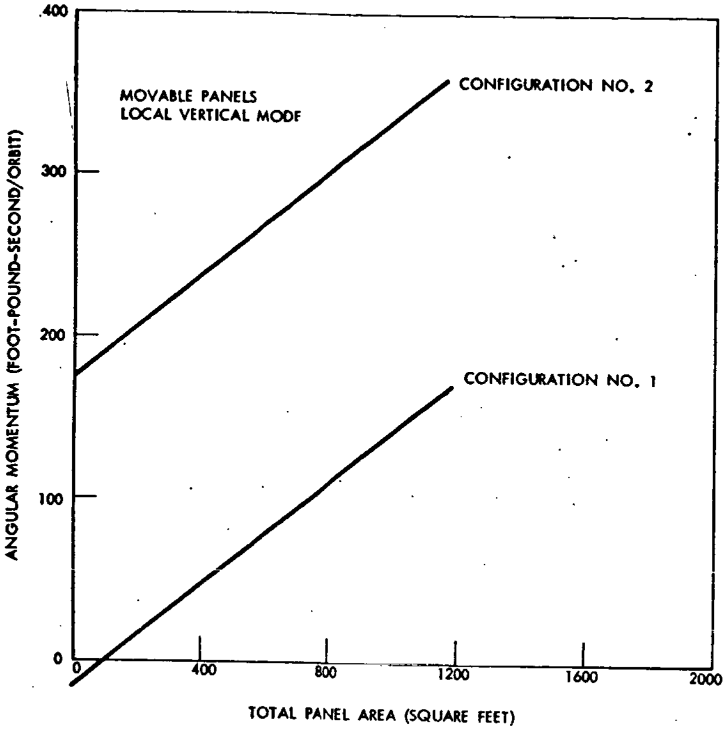

Figure 113. Maximum Stored Momentum to Counter Disturbance Torques - Y Axis

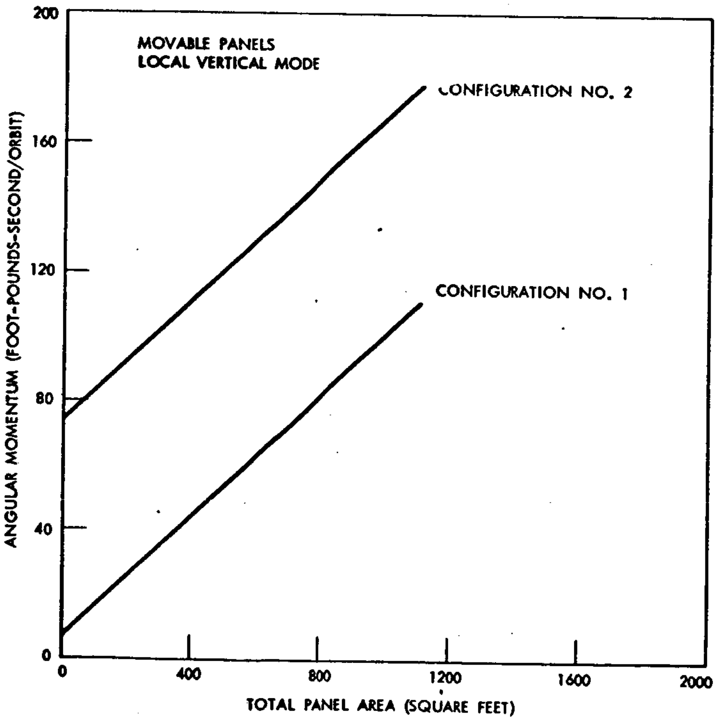

Figure 114. Maximum Stored Momentum to Counter Disturbance Torques - Z Axis

[redacted]

torque value for each axis as a function of operational mode is discussed in the preceding sections. This value is the basepoint for momentum storage sizing. To this value must be added the expected maneuver requirements per orbit; and for earth oriented vehicles, the orbit rate requirements.

Vehicles utilizing solar panels are treated in an analogous manner. The "per axis" requirements are discussed in the Solar Panel Considerations section. In addition to the disturbance torque effects, vehicle roll control requirements and orbit rate requirements must be considered.

Sizing Reaction Wheels

With the momentum and torque requirements known for each axis, it is possible to size a reaction wheel system to provide the desired quantities. It will be assumed that one wheel will be utilized for each vehicle control axis.

From conservation of momentum considerations

$$H = I_W \omega \tag{35}$$

which states that the angular momentum of the reaction wheel is equal to the required angular momentum of the vehicle about the given axis.

A hollow disc with an inside to outside radius ratio of 0.7 will be utilized. The moment-of-inertia of the disc is

$$I = \frac{W}{2g} (r_o^2 + r_i^2) \text{ slug-ft}^2 \tag{36}$$

where the weight (W) can be represented as

$$W = \pi h (r_o^2 - r_i^2) \gamma \text{ lb} \tag{37}$$

For the selected radius ratio of 0.7, and a wheel thickness to radius ratio of 0.2, the angular momentum of a steel wheel can be determined from Equations (35), (36), and (37) as

$$H = 3.56 \, r_o^5 \omega \quad \text{ft-lb-sec}^2 \tag{38}$$

Reaction wheels require peak power during vehicle maneuvering. The maximum power required can be determined from the following expression:

$$P = \frac{1.87 \times 10^{-2} H \cdot \omega_{max}}{\tau_m} \text{ watts} \tag{39}$$

where τ_m is the time constant of the motor (assumed equal to 50) and ω_{max} is the maximum speed of the wheel. Equations (38) and (39) are plotted in Figure 115 to indicate design constraints and suitable operating regions as a function of maximum required momentum capability. From Figure 115, it is

[redacted]

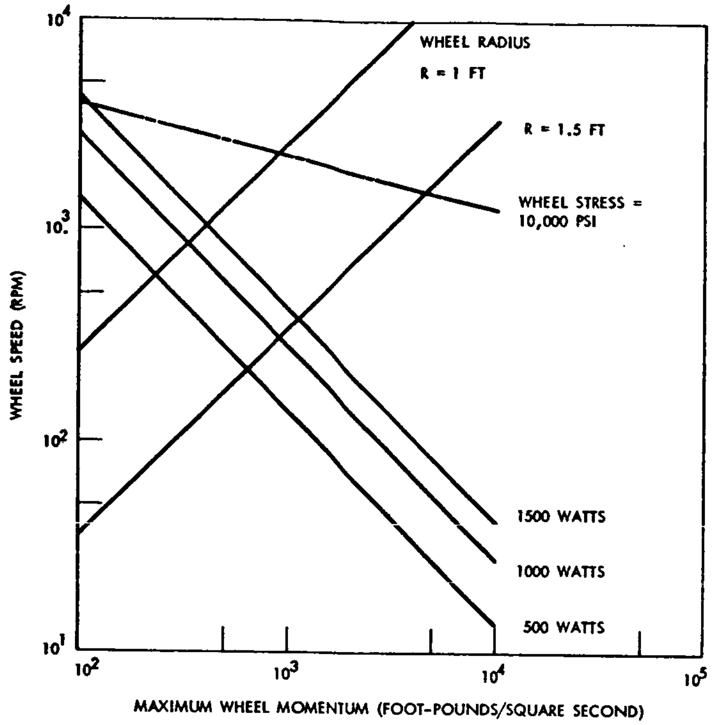

Figure 115. Reaction Wheel Design Criteria

possible to select a wheel radius and spin rate for a given momentun requirement (H) and amount of peak power available (P). It should be noted that the power required is mechanical output power and the actual power requirement considering motor efficiency will be somewhat larger.

From the selected angular momentum and spin rate values, the wheel moment-of-inertia can be selected, and using Equation (37) the wheel weight can be evaluated.

In general, reaction wheels will be placed in the service module due to volume limitations in the command module. The wheels will then have to be sealed to allow proper functioning. An empirical expression for the weight of the wheel case and integral motor in terms of wheel radius is

$$W_c = \frac{r_o^2}{7.4} \text{ lb} \tag{40}$$

where the radius r_o is in inches. The total weight per axis is the sum of Equations (37) and (40).

Windage Losses

Associated with a reaction wheel or gyro rotation in a pressurized environment, are the power requirements necessary to overcome the losses

[redacted]

[redacted]

due to aerodynamic drag on the disc. Drag effects on a solid rotating disc not enclosed in a housing have been analyzed.* Since it has been assumed that hollow discs will be used for the momentum devices, the expression for the moment coefficient due to drag was doubled to account for the effects of spokes. It was further assumed that turbulent flow would be encountered.

The expression for the power required to overcome windage losses on a rotating disc in an environment of air at 1 atmosphere is

$$P = 9.7 \times 10^{-5} \omega^{2.8} r_o^{4.6} \text{ watts} \tag{41}$$

where ω is the rotational rate in rad/sec. and r_o is the disc radius in feet. The power required is directly proportional to the air pressure. Thus for a reduction in air pressure to 1/2 atmosphere power would be reduced to 1/2 the above value. The power requirements can be reduced even further if helium is used as the pressurization evnironment rather than air. The corresponding power expression for maintaining wheel speed in a medium of helium at 1 atmosphere is

$$P = 2.02 \times 10^{-5} \omega^{2.8} r_o^{4.6} \text{ watts} \tag{42}$$

Equations (41) and (42) are used to evaluate the power requirements during steady wheel spin.

MOMENTUM REQUIREMENT FOR TWIN GYROS

It is assumed that the twin gyro unit would be used for vehicle maneuvering as well as attitude control and rate stabilization. To determine the total momentum requirement for a unit, it is necessary to establish the momentum requirements associated with each control function and combine them properly.

Attitude control and rate stabilization includes countering disturbance torques and satisfying vehicle orientation profiles associated with the power system and/or the mission experiment program. These problems were discussed previously in this section and the angular momentum requirements for the various functions were indicated. By using this information together with specified mission requirements and a definition of the power system, the momentum requirements can be determined and tabulated. To be conservative, these individual requirements are then summed. At this point in the analysis, a momentum requirement for all functions except maneuvers is available.

Consider next the problem of maneuvering with a twin gyro system. It is assumed that rate limited maneuvers would be used. An analytical expression was derived which relates the characteristics of such a mechanization to the maneuver parameters.

---

*Schlichting, "Boundary Layer Theory," 4th Edition, McGraw-Hill, 1960

[redacted]

This expression is

$$\theta_T = \frac{2H}{I}\left\{\frac{1}{\dot{\psi}}\left[\cos\psi_1 - 2\cos\psi_2 - (\psi_2 - \psi_1)\sin\psi_1 + \cos(\psi_2 - \psi_1)\right] + \left[\sin\psi_2 - \sin\psi_1\right]\left[t_m - \frac{2(\psi_2 - \psi_1)}{\dot{\psi}}\right]\right\} \tag{43}$$

where

θ_T = the maneuver magnitude

t_m = the time per maneuver

I = the vehicle inertia about the maneuver axis

H = the angular momentum of one of the gyros

$\dot{\psi}$ = the rate at which the gyros are torqued

ψ_2 = the maximum allowable gimbal deflection

ψ_1 = the gimbal deflection when the maneuver is initiated.

Since control effectiveness is reduced for large gimbal angles, the term ψ_2 was limited to 60 degrees for the purposes of this study. The gyro torquing rate was assumed to be 1 degree per second which represents a compromise between time response and torquing power. The remaining unknowns, H and ψ_1 as θ_T and t_m, represent the maneuver requirements to be satisfied and I is a vehicle characteristic.

The total gimbal deflection must be sufficient to satisfy the maneuver requirement as well as the combined requirement of all other functions. To be conservative the gimbal deflection components are summed as indicated in the following expression.

$$(\psi_2 - \psi_1) + (\psi_2 - \psi_D) = \psi_2 \tag{44}$$

where

ψ_D is the gimbal deflection at the start of a non-maneuver control task

This forces each of the deflection components to be sufficient for operation in the least effective portion of the available deflection range. One other equation can be written to relate the non-maneuver deflection to the required momentum and the total momentum of one gyro.

$$H = \frac{H_D}{2\sin(\psi_2 - \psi_D)} \tag{45}$$

[redacted]

The term H_D is the momentum requirement associated with all functions except maneuvers which were discussed previously.

With the above three equations, it is possible to determine the gyro momentun required to satisfy both the maneuver and non-maneuver functional requirements. This procedure was used to obtain the parametric data shown on Figure 116. The data assumes a requirement to perform a 180-degree reorientation in 6 minutes.

Twin Gyro Sizing

A preliminary study was conducted to investigate sizing of twin gyro units. Wheel radius was optimized to minimize total system weight. Wheel designs similar to those discussed for reaction wheels were assumed, i.e., thin, hollow, circular, steel disks with an inner to outer radius ratio of 0.7 and a thickness to outer radius ratio of 0.2.

The individual items which contribute to the total system weight include the rotors and spin motors, the cases which enclose the rotors and spin motors, the gimbal torque motors, the frame, and a power system weight penalty. Each of the above items were considered except the frame and gimbal torque motors which were neglected.

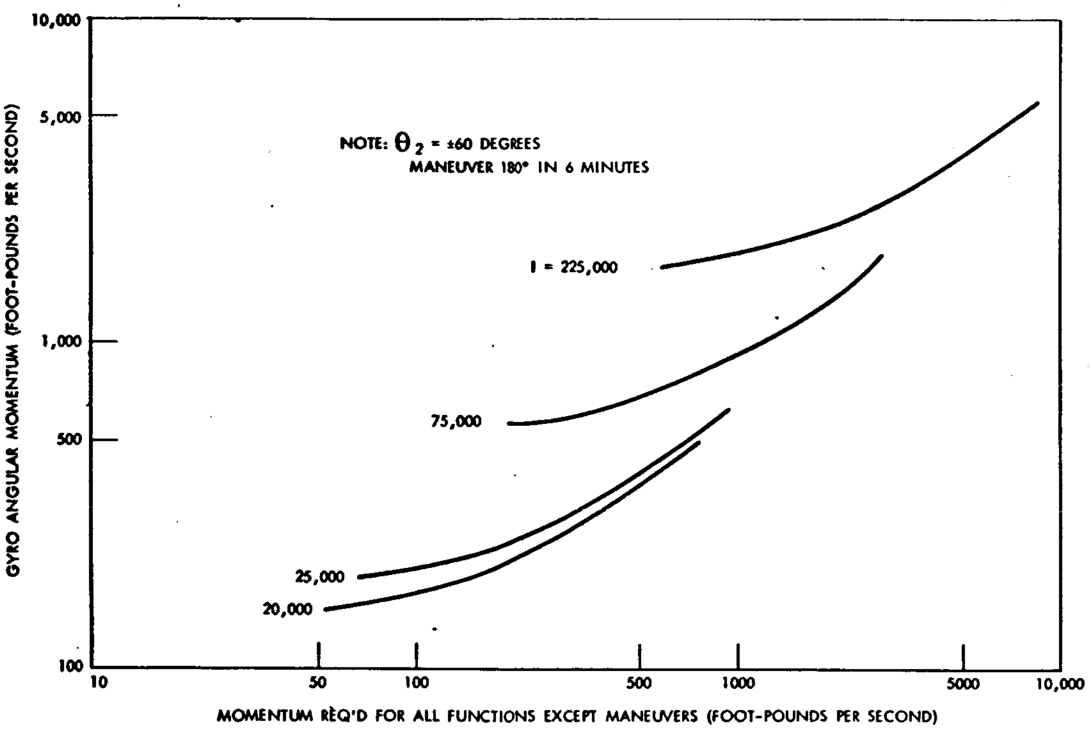

Figure 116. Gyro Angular Momentum Requirements

[redacted]

[redacted]

The expression used to define case weight in terms of radius is the same as that discussed in the reaction wheel section (Equation 40). The only power requirements considered were those necessary to counter rotor drag. A helium environment was assumed at a pressure of 0.1 atmosphere with the power required specified by Equation (42). A weight penalty of 630 pounds per kilowatt was used which corresponds to a solar panel power system. The equivalent penalty for an isotope system would be approximately 500 pounds per kilowatt.

The parametric data shown on Figure 117 were obtained using the above considerations. It is apparent that there is a unique wheel radius for a specified momentum value which will minimize system weight. At the right side of Figure 116 (large radii) system weight is shown to be independent of momentum. This is due to the fact that the power penalty becomes negligible. At the left side of the figure (small radii) the power penalty predominates.

Figure 118 was obtained by plotting the minimum points of the curves on Figure 117. It should be noted that the weights quoted pertain to one gyro of a twin gyro system and include a power system weight penalty. To obtain total system weight, the data from the figure should be doubled and frame weight together with gimbal torquer weight should be added to that number.

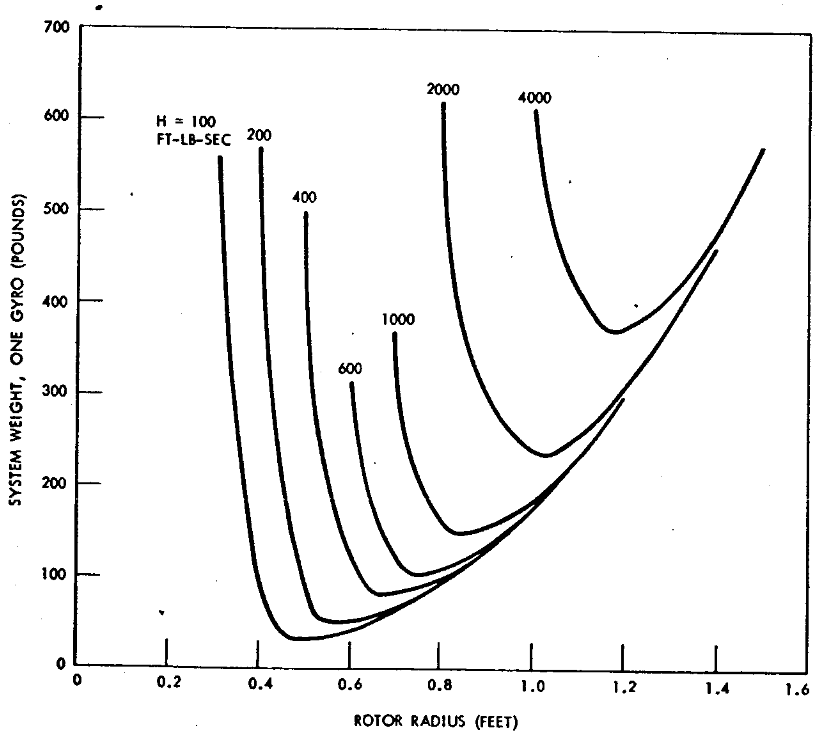

Figure 117. Effect of Rotor Radius on System Weight

[redacted]

[redacted]

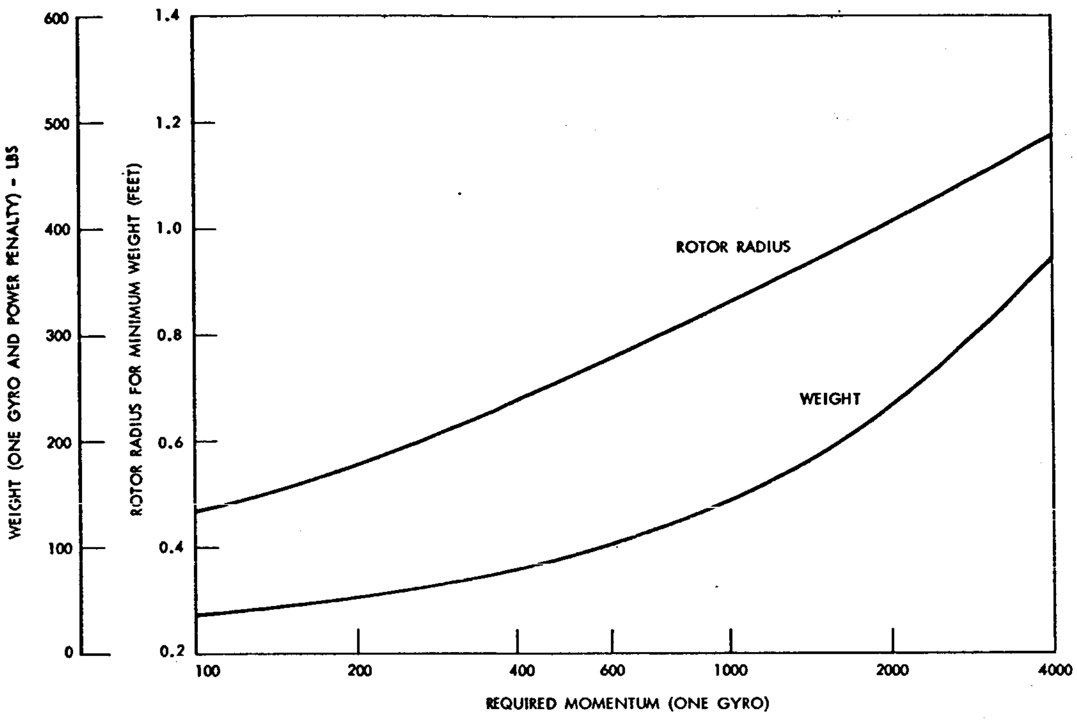

Figure 118. Rotor Radius for Minimum Weight

DESATURATION CONSIDERATIONS

The nature of momentum storage devices is such that only a finite amount of angular momentum can be absorbed by the system. Once this level has been reached, it is necessary to remove the stored momentum to permit further vehicle control capability. This removal is accomplished in a reaction wheel system by reducing the wheel spin rate; and in a twin gyro system, by reducing the gimbal angle. Reaction jets are fired intermittently during wheel de-spin to prevent the stored momentum from being transferred to the vehicle. The desaturation propellant can be evaluated by considering that the angular momentum supplied by the jets must be equal to the angular momentum being removed from the system. The propellant required for desaturation is

$$W = \frac{2\ H_{V_{max}} \quad \text{lb}}{\ell\, Isp} \qquad (46)$$

where $H_{V_{max}}$ is the stored momentum in the system. The desaturation frequency is determined by dividing the system capability in each axis by the average momentum requirement. This value is determined by multiplying the average torque values from the Current System section by the time for one orbit (5.52×10^3 sec). The desaturation frequency is thus based on the yearly average of disturbance torque on the vehicle. Knowing the desaturation

[redacted]

frequency, the propellant weight for a given mission can be determined. This value will indicate tankage and plumbing weight which must be included in the total system weight.

It should be noted that the desaturation propellant requirements are independent of desaturation frequency, and dependent only on the momentum capacity of the system.

POWER SYSTEM CONSTRAINTS

Associated with the selection of a control system is the necessity of assessing the constraints imposed by power considerations. The three power systems considered for prolonged mission application are fuel cells, isotope, and solar panels. Once a control system is selected, it is important to evaluate the penalties associated with using the given control system and the selected power system.

For vehicle control using reaction jets, power requirements are relatively small and no penalties are incurred.

Control devices utilizing momentum exchange are typified by periodic increases in power loads during spin-up, maneuvering, and de-saturation. The following discussion presents the relationships between average and peak power requirements and resultant penalties for the three power systems.

FUEL CELLS

No particular vehicle orientation is required. There is a weight penalty of 1.3 lb/kwh associated with the average power consumption over the mission duration. Penalties associated with power peaks using fuel cells are difficult to readily assess. If all peaks are less than 500 watts there is no penalty. If peaks of greater than 500 watts occur but fall within the power profile shown in Figure 119, there is no penalty if the peak is scheduled. For peaks of greater than 500 watts which are either unscheduled or exceed the profile in Figure 119, special consideration must be given. The nature of fuel cell power characteristics is such that unscheduled peaks may exceed system capability and necessitate system redesign. Peaks of this type should be avoided if possible. If they cannot, factors such as mission duration and other vehicle power requirements at that time are important and the situation will require analysis by the power system engineer.

ISOTOPE

No particular vehicle orientation is necessary. There is a weight penalty of 500 lb/kw associated with the continuous power requirements and any power required on a random basis. There is no peak penalty if all peaks are below 500 watts. For peaks greater than 500 watts which can be scheduled and which lie below the power profile in Figure 119, there is no penalty. For peaks in excess of the profile, or those which cannot be scheduled, there is a penalty of 500 lb/kw.

SOLAR PANELS

It is necessary to orient the vehicle and panels such that incident solar radiation is perpendicular to the solar panels at all times. A weight

[redacted]

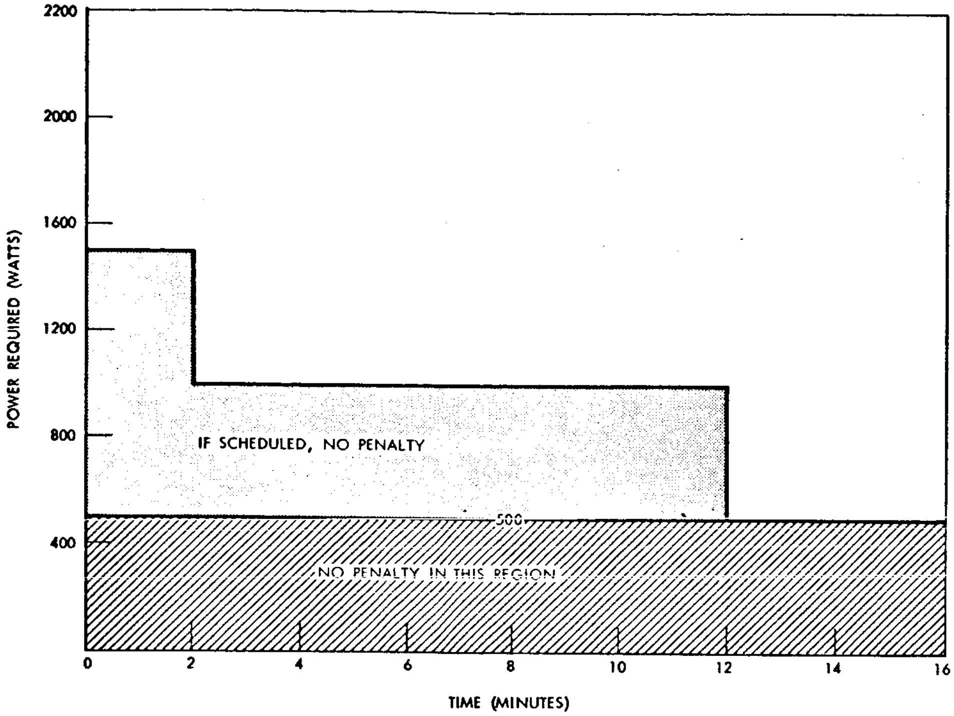

Figure 119. Isotope or Fuel Cell Peak Power Penalties

penalty of 630 lb/kw is associated with the average power requirements. For any loads exceeding 36 minutes duration which occur more than twice a day, apply a penalty of 630 lb/kw. Peaks which lie below the profile shown in Figure 120 incur no penalties. Those peaks in excess of the allowable profiles require special consideration.

Table 34 contains a summary of the penalties associated with the three power systems.

[redacted]

[redacted]

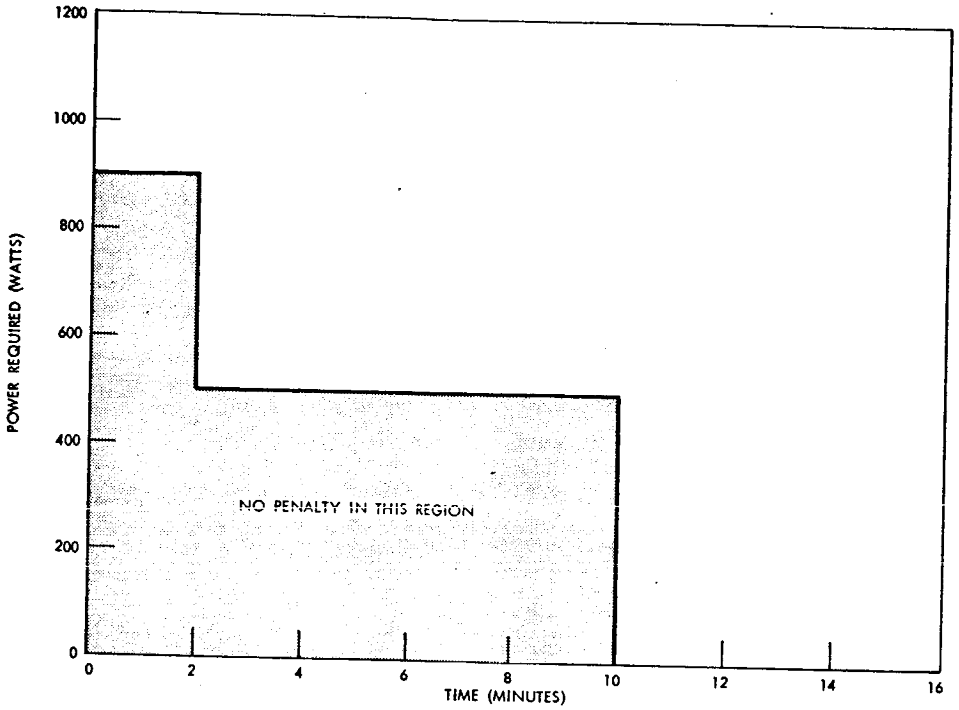

Figure 120. Solar Panel Peak Power Penalties

[redacted]

Table 34. Summary of Power System Penalties

	Fuel Cells	Isotope	Solar Panels
Orientation Constraints	None	None	Vehicle attitude hold required
Average Power Penalty	1.3 lb/kwh		630 lb/kw
Continuous Power Penalty		500 lb/kw	Loads exceeding 36 min. more than twice a day - 630 lb/kw
Peak Power Penalty	< 500 watts - no penalty > 500 watts but scheduled and within profile in Figure 119 - no penalty not scheduled and/or greater than profile - special considerations	< 500 watts - no penalty > 500 watts but scheduled and within profile in Figure 119 - no penalty not scheduled and/or greater than profile - 500 lb/kw	Less than profile in Figure 120 - no penalty Greater than profile - special considerations

APPENDIX A. INVERTERS

APPENDIX A. INVERTERS

The power rating of the inverter is assumed to be the same, that is, 1250 VA output from a 25-30 volt d-c input, although the advantages of a 3-wire ± 28-volt d-c input are to be considered. The ideal power rating suited to the available 30-ampere and 65-ampere transistors from either 28-volt or 56-volt input is 1500 VA where 16 silicon power transistors are used.

In order to provide qualified equipment for space missions no later than 1970, the circuit components must come from sources which are apparent now. The most advanced power switch to be considered is a 100-ampere transistor from the Westinghouse Semiconductor Division. This switch has reached a stage of development permitting inverters to be built using it in 1966. Using 16 of these 100-ampere transistors in the ideal configuration to be discussed, yields a power rating of 3000 VA from a 25-30 volt d-c input. These power ratings are based upon the ability of the inverter to deliver a 300 percent output current under short-circuit conditions. Also, the overload capabilities of the present APOLLO inverter, such as 200 percent for 5 seconds and 150 percent for one minute, are to be accepted as typical.

Reliability, efficiency and weight are to assume this order of preference in this discussion because the weight-efficiency trade-off will tend to favor increased efficiency due to fuel-weight importance in an extended-time-period space mission.

Since 81 percent efficiency at full-load 0.9 power factor, with 28-volt d-c input, is the practical maximum attainable using the buck-boost voltage regulation approach of the present APOLLO inverter, a counterbalanced phase-shift method of voltage regulation is preferred to achieve higher efficiencies. An efficiency of 87 percent is possible by this approach.

A MTBF of approximately 18,000 hours is all that can be expected from an extensive reliability improvement program applied to a unitized inverter. The probability of successful operation for 600 days of a single unitized inverter is only 45 percent when the MTBF is 18,000 hours, while the present APOLLO inverter, which has a calculated MTBF of 7600 hours, would offer but a 17 percent chance of success.

Some method of redundancy is required to decrease appreciably the risk of losing all the inverters in the space vehicle. The method suggested is the use of three full-system-rated inverters, as in the present APOLLO, but there is to be, in addition, the capability to make in-flight manual replacement of a power module whose failure indicator has tripped. There would be four such identical and interchangeable power modules per inverter.

As in the present APOLLO inverter, all cooling is done by conduction. Front access would permit power-stage replacement without removing the inverter base-plate from the vehicle cold-plate.

The following sections will provide more detail of the possible approaches suggested.

PARAMETER RELATIONSHIPS FOR AN EXTENDED-TIME-PERIOD MISSION

For extended-time-period space missions, the weight-efficiency trade-off of static inverters tends to make increased efficiency the most important parameter. For such cases the following generalizations may be stated concerning the design of an inverter:

1. With a 28-volt d-c input, either germanium or silicon power transistors should be used as the inversion elements. Germanium is preferred, if the ambient temperature is not too high, because of its gain, low saturation resistance, and low emitter-base diode drop. Maintaining the power-transistor junction temperature below 71 degrees centigrade for reliable operation may not be practical for the space-craft designers and probably precludes the use of germanium, especially when power-stage modules separable from the inverter base plate are to be considered.

   Controlled rectifiers are not considered a good choice despite high power gain because of the fixed 1.0 - 1.2 volt drop of the device. This drop alone represents an immediate 4% loss in efficiency for a nominal 28 volt input. Controlled rectifiers also require auxiliary commutating devices to return them to the high impedance state. These commutating devices generally circulate high currents which increase losses and further degrade efficiency.

2. The power switches should operate at the fundamental frequency. Some inverter circuits generate a high-frequency square wave which is then either rectified and inverted again or synthesized into the desired output waveshape with a cycloconverter. These schemes are employed to eliminate a fundamental-frequency transformer thereby saving weight. With that approach, efficiency is sacrificed due to the multiple conversions and due to the high-frequency inverter

employed in these schemes. One of the loss components in a power transistor is switching loss. The switching loss may be calculated from the following formula:

$$W_S = .625\, E_C\, I_C\, f\, (t_r + t_f)\ *$$

where E_C = collector to emitter voltage when transistor is off

I_C = collector current when transistor initiates turn-off

f = switching frequency

t_r = voltage rise time

t_f = voltage fall time

The switching loss is directly proportional to the switching frequency so that switching should be as low as possible.

3. The regulation and inversion functions should be accomplished simultaneously. The inverter should be of the type which regulates the output voltage with the same transistors that invert the d-c power. This bars the use of a d-c chopper-inverter or a d-c buck-boost regulator inverter combination.

---

* "Formulas for Transistor Dissipation During High Frequency Switching", Concurrence and Wheeler, Westinghouse Control Engineering, August 1960

4. A center-tapped power stage should be used with a 28-volt d-c input. The other choice is that of a bridge circuit. The bridge circuit requires four power switches instead of the two required by the center-tap circuit and therefore the losses of the bridge circuit are approximately twice as high.

Based upon these generalizations and the desirability of high efficiency, a circuit configuration can be determined which represents an advanced inverter. Figure 1 is a block diagram of an inverter which satisfies all the previous criteria. It is a phase-shift regulated inverter which controls output voltage by generating two sine waves that are counter-shifted by θ degrees (See Figure 122). The sum of these counter-shifted waves is then equal to the sum of the individual wave magnitudes times cosine θ. The output can thus be controlled by varying θ.

Input power is filtered by a low-pass L-C network which attenuates voltage transients from the d-c source and filters current ripple from the inverter power stages. Four center-tapped power stages are mutually phase displaced by 45 electrical degrees and have their outputs summed in a special way called a "harmonic neutralization interconnection". The resultant waveform is devoid of third and fifth harmonics which simplifies the output filtering of the waveshape. A 3-phase set of voltages is generated from the four square waves and the whole set is phase shifted by plus θ degrees which is represented on the block diagram by $V_{01}e^{+j\theta}$. Another 3-phase set is generated in the same manner escept that it is phase shifted by minus θ degrees and it is represented by $V_{02}\, e^{-j\theta}$. The sum of these two outputs is then $(V_{01} + V_{02})$ cosine θ. Since the two output sets counterbalance, the resultant phase displacement of the 3-phase set is not a function of θ, although magnitude varies as cosine θ. The independence of the absolute phase-displacement angle of the output from the action of the regulator may or may not be of importance depending upon the inverter load. If the load can stand a variable phase angle, the control circuit of Figure 121 could be simplified. Instead of phase-shifting V_{01} by plus θ degrees, it could be maintained at a fixed phase displacement and V_{02} could be given a minus $2\,\theta$ degree phase shift which would produce an output equal to $(V_{01} + V_{02})\cos\theta\, e^{-j\theta}$.

A type of load that would be sensitive to phase angle would be a heavily-loaded synchronous motor. A sudden change in output voltage phase angle could cause the motor to slip a pair of poles which would cause serious system transients.

The output voltage of Figure 121 is compared to a reference and an error signal is generated which in turn controls the contra-shift angle θ to keep the average 3-phase output voltage nearly constant. A signal proportional to output current dominates the voltage regulator circuit when output current exceeds 200% to ultimately limit fault current to 300%.

The harmonic neutralization approach is documented in AIEE Transactions Paper: "Static Inverter with Neutralization of Harmonics", by Kernick, Roof, and Heinrich. It has been used successfully by Westinghouse Aerospace Electrical Division in the APOLLO Static Inverter to provide light-weight power conditioning equipment.

The base-drive losses incurred from driving the power transistors are minimized by controlled current feedback transformers. Base drive is supplied by positive feedback of the collector current via current transformers. Because of this feedback technique, base drive is always instantaneously proportional to collector current and efficiency remains high even at half-load. The APOLLO inverter incorporates controlled current feedback and has an efficiency of 76% at half-load unity power factor, and an efficiency of 77% at full-load unity power factor. The combination of controlled current feedback and phase-shift regulation in conjunction with silicon power switches should allow an efficiency objective of 87% to be realized with 28-volt d-c input.

Some disadvantages of the phase-shift regulation approach are the following:

1. Slightly higher relative weight results because of the necessity of designing the power transformer so as not to saturate when the input voltage assumes its highest values. The magnitude of this weight penalty depends upon the percentage difference between

the highest input voltage and the lowest input voltage. However, this is compatible with the high efficiency objective since at nominal input voltages the flux density is low and therefore, iron loss is also low.

2. A phase-shift-regulated inverter would not be able to demodulate input voltage ripple in the 100 to 1000 cps range as would an inverter with a chopper or a buck-boost regulator.

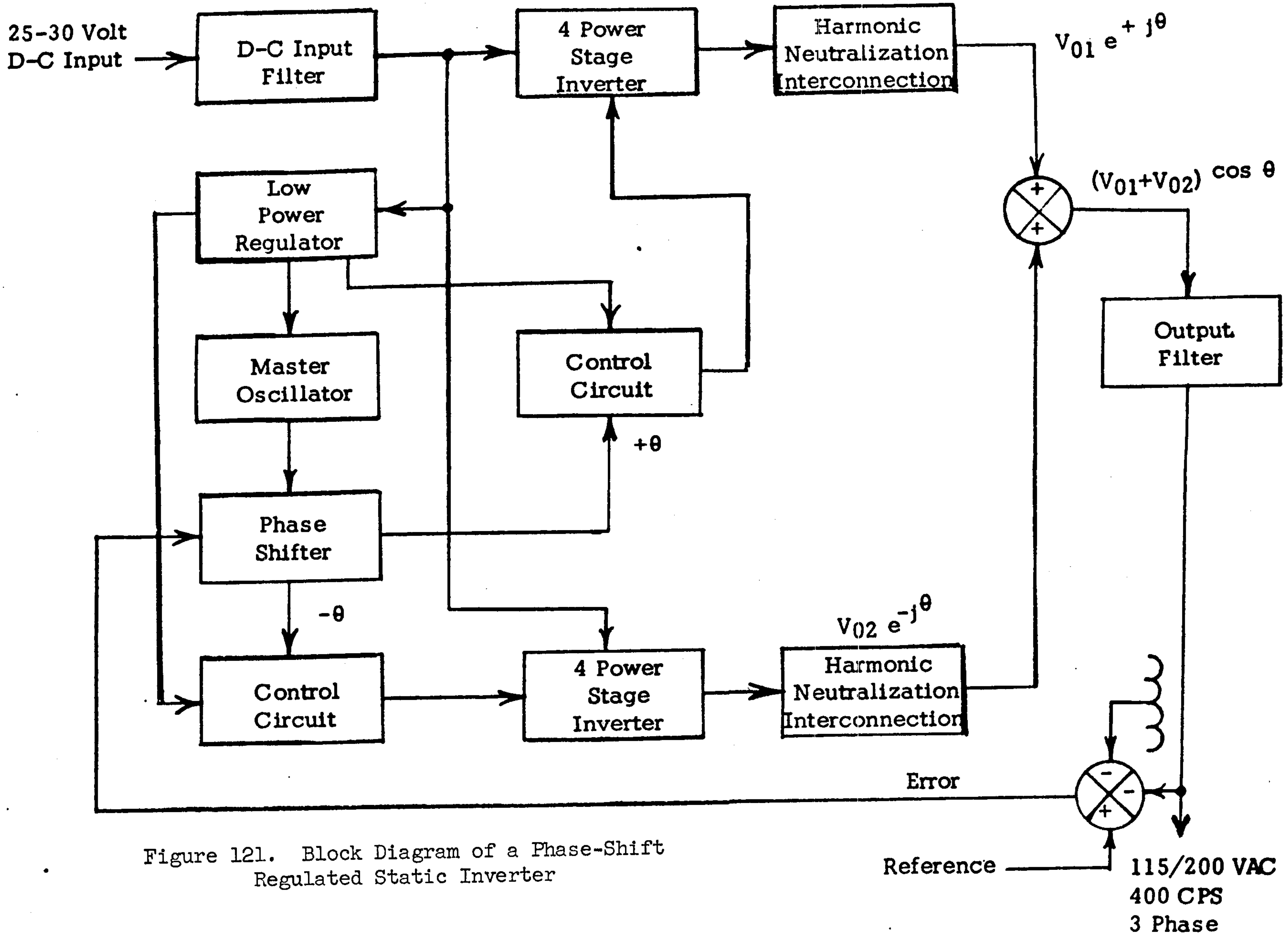
25-30 Volt
D-C Input
D-C Input Filter
4 Power Stage Inverter
Harmonic Neutralization Interconnection
$V_{01}\, e^{+j\theta}$
Low Power Regulator
Master Oscillator
Control Circuit
+θ
Phase Shifter
-θ
Control Circuit
4 Power Stage Inverter
$V_{02}\, e^{-j\theta}$
Harmonic Neutralization Interconnection
+
+
$(V_{01}+V_{02}) \cos\theta$
Output Filter
Error
-
-
+
Reference
115/200 VAC
400 CPS
3 Phase

Figure 121. Block Diagram of a Phase-Shift Regulated Static Inverter

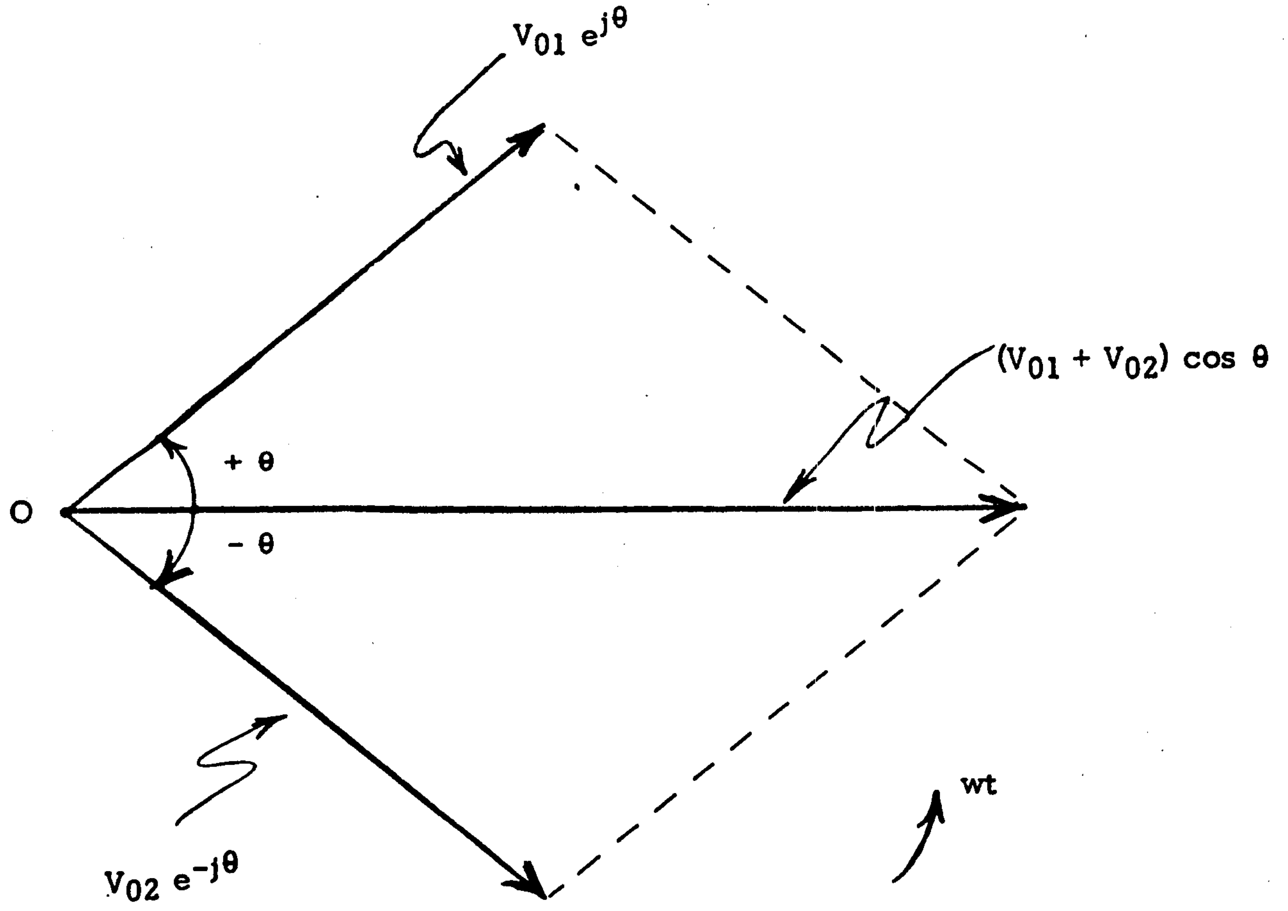
$V_{01}\ e^{j\theta}$
$(V_{01} + V_{02}) \cos \theta$
$+ \theta$
O
$- \theta$
wt
$V_{02}\ e^{-j\theta}$

Figure 122. Output Voltage Vector Diagram for Phase-Shift Regulated Inverter

SELECTION OF 1, 2, OR 3 PHASES

Serious consideration must be given to the selection of the number of phases in the a-c output over and above the obvious methods of redundancy, derating and high-reliability parts in order to achieve reliable circuitry. The use of a single-phase inverter in lieu of a polyphase inverter can possibly overcome the following disadvantages because it is somewhat less complex:

1. A single-phase or a 2-phase inverter has the disadvantage of having to overcome power utilization device inertia. Even though 3-phase 3-wire systems have obvious advantages realized on shipboard and under the seas, the 3-phase 4-wire system has been firmly established in aircraft as a heritage to space power systems.

2. The weight of a single-phase inverter will exceed that of an equivalent 2 or 3-phase 400 cps inverter because of greater input filter requirements. The flow of single-phase reactive power back to the d-c source results in an 800 cps ripple current. This current is neutralized inherently in poly-phase inverters because there is staggering of instantaneous real and reactive power demands between or among the phases.

3. Since it is not practical to provide an inverter input filter that is sufficiently large to make the 800 cps ripple negligible, an 800 cps ripple voltage is impressed upon the d-c source thereby appearing at the inputs of the other d-c power utilization and conversion equipment.

4. Single-phase motors do not have inherent starting capability.

5. When multiple power stages are staggered in order to form a stepped-wave approximation to a sine wave, there is a wide spread in power factor from power stage to power stage. In some of the power stages the unfavorable power factor requires the static switches to interrupt sine-wave

peak current continuously under normal output conditions. In poly-phase inverters that use harmonic neutralization from a set of multiple, staggered power stages, the power factor in each power stage of the set is the same under balanced poly-phase load conditions.

6. Poly-phase transformer-rectifier units do not require such large output filters as do their single-phase counterparts.

The use of harmonic neutralization can still be important in a single-phase inverter design so that the weight and losses in the output filter can be diminished. The single-phase inverter, using the harmonic neutralization technique has nearly the same block diagram as that shown in Figure 1 with two major differences. The obvious difference is a single phase output. The other variation concerns the power-stage transformers used in the 3-phase inverter versus those used in the single-phase inverter. The phase-shift-regulated 3-phase inverter employs a pair of "quadratic" transformers while the phase-shift regulated single-phase inverter uses four transformers consisting of a pair of 3-phase E-cores and a pair of single-phase C-cores.

The "quadratic" transformer uses a flux cancellation principle discussed in the IEEE Transaction Paper on Aerospace: "Controlled Feedback in an Inverter With Neutralization of Harmonics," by Heinrich and Kernick. Figure 123 shows the flux distribution and core dimensions as they apply to a "quadratic" transformer (as opposed to the "octadic" transformer that is used in the present APOLLO inverter). Figure 124 is included to clarify the operation further. Figures 125 and 126 give dimensions of a special set of laminations that are used to stack the transformer cores. Figure 127 shows the E-core and C-core plan used in the single-phase inverter.

There is simplification of the power circuit in the single-phase inverter as established originally since two arrays of three power stages each are used instead of two four-power-stage arrays as required in the poly-phase inverter.

When the other approach is taken to simplify inverter design by using brute-force filtering, there are the combined deficiencies of more weight and less efficiency. In order to minimize heating in the various motors in the electrical system virtual elimination of the third harmonic is essential. Eliminating the harmonic is a severe penalty upon a brute-force design. A harmonic-neutralization approach eliminates the third harmonic completely. Also the fifth harmonic is neutralized so that effects of fifth-harmonic counter-torque in motors are neither present to degrade motor efficiency while running nor to cause a particularly adverse condition when starting.

Figure 128 shows the 2-phase array with the a-c output phase vectors lying half-way between the power-stage segment vectors. A variation in the stepped output waveform occurs, but the harmonic content is identical. The objective of this choice in the array will take on some significance when the modular concept is discussed, because the power transformers all become identical if separate transformers in each module are used rather than a common "quadratic" power transformer.

Having identical power modules complete with power transformers may influence the choice of power system because of the repair or replace in flight option. If the failure-rate of the power transformer is considered sufficiently low, the power modules need not be complete with power transformer. This latter choice does seem preferable because of the size and weight advantages to be obtained in the "quadratic" transformers.

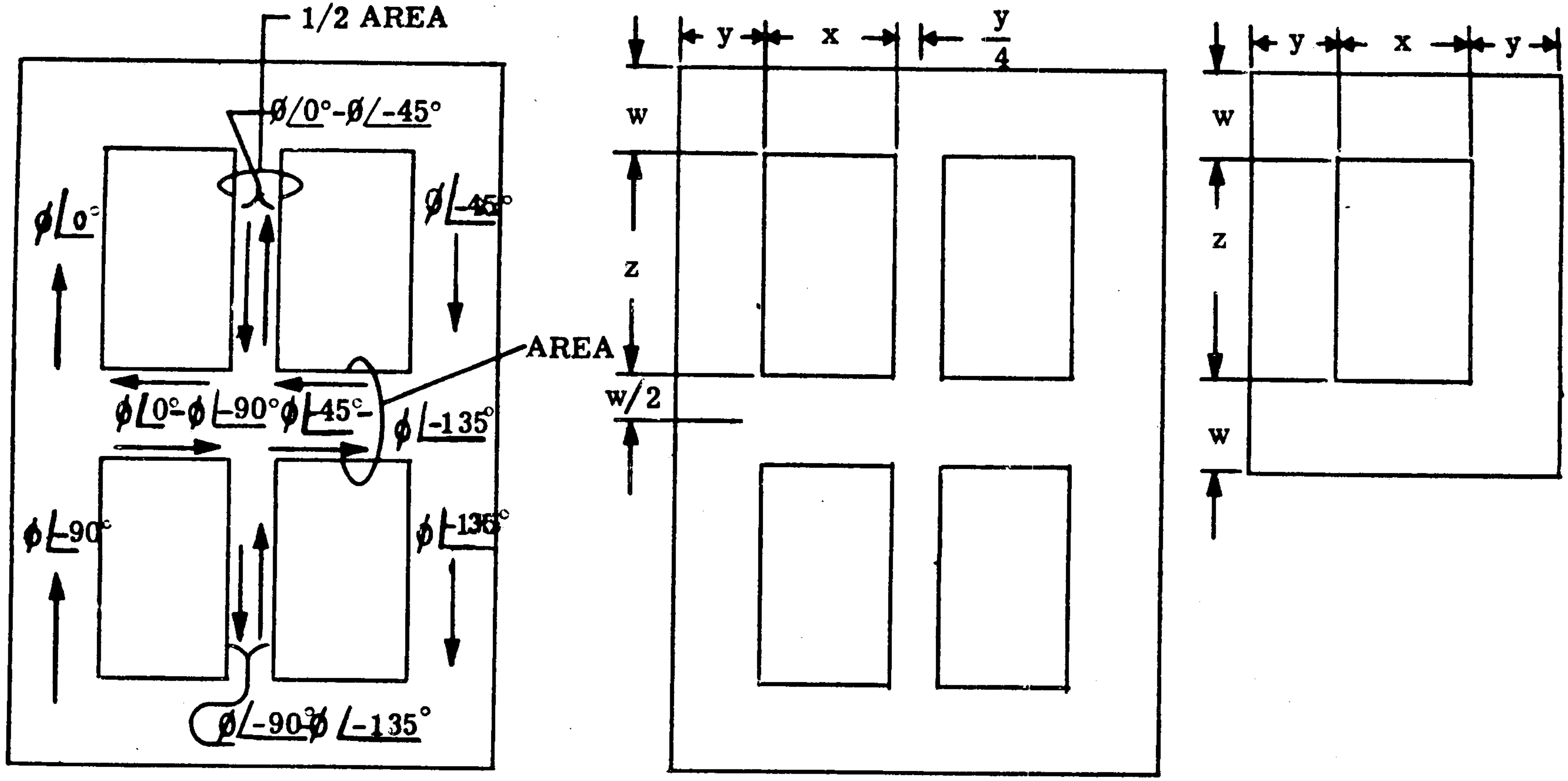
1/2 AREA
ϕ/0°-ϕ/-45°
ϕ/0°
ϕ/-45°
AREA
ϕ/0°-ϕ/-90°
ϕ/-45°-ϕ/-135°
ϕ/-90°
ϕ/-135°
ϕ/-90°-ϕ/-135°
y
x
y/4
w
z
w/2
y
x
y
w
z
w

3a. Flux distribution (fluxes are defined in Figure 4)

3b. Dimensions of quadratic transformer core.

3c. Dimensions of single-phase core.

Figure 123. Definitions of Flux Distribution and Core Dimensions of Output Transformer

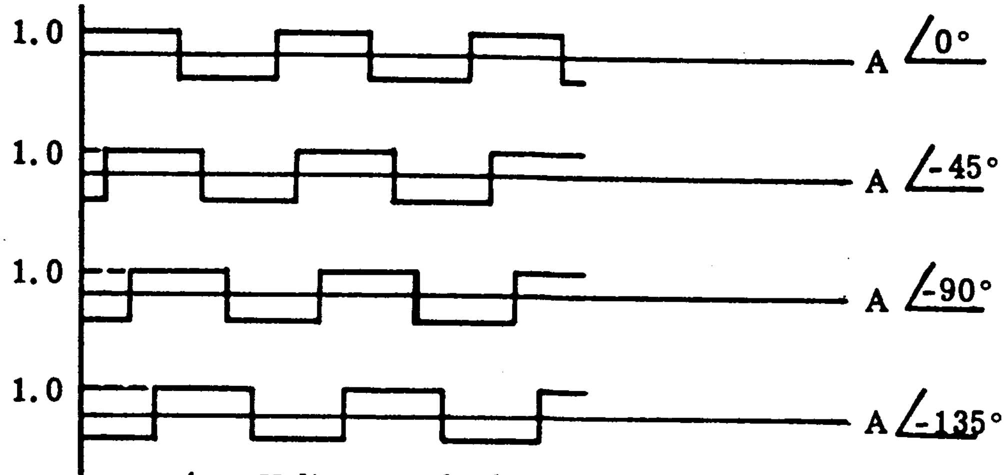

4a. Voltage applied to the transformer primaries

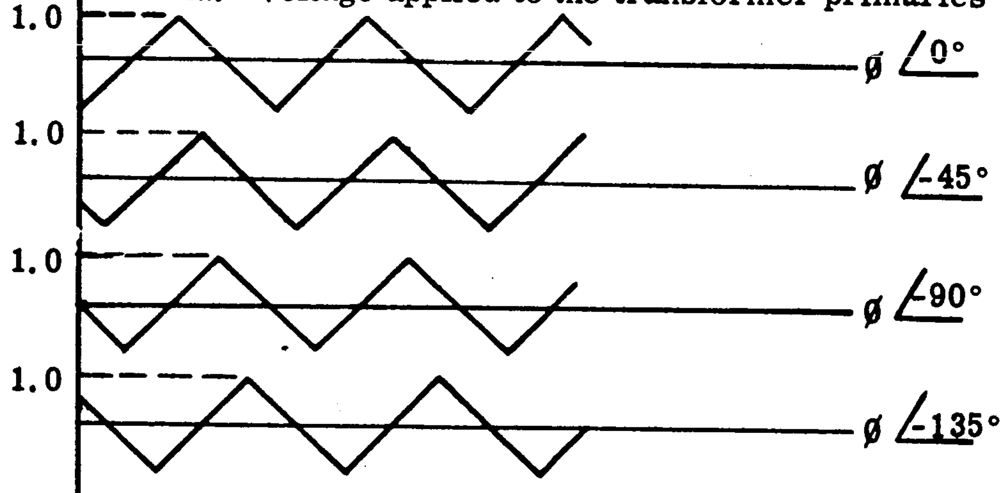

4b. Flux in the primary legs

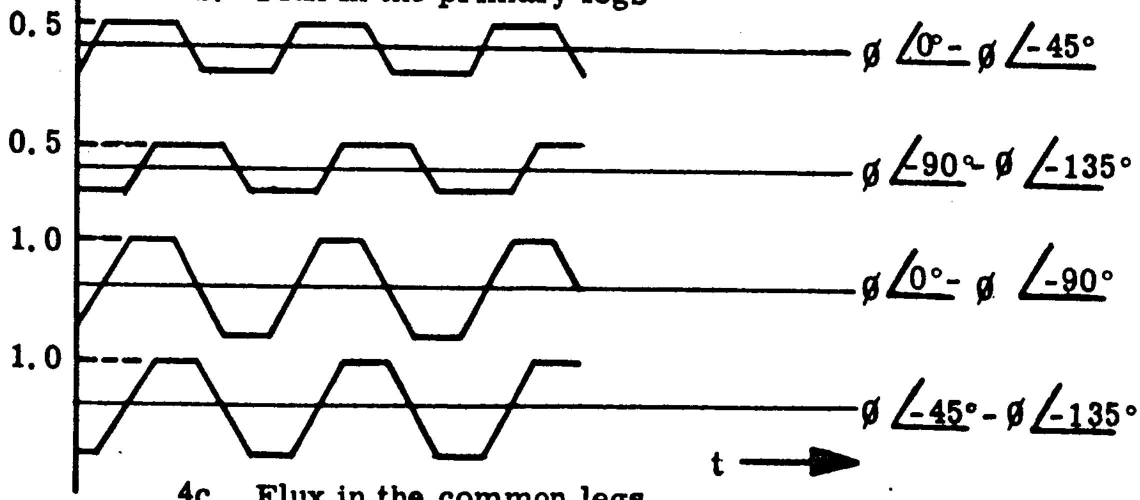

4c. Flux in the common legs

Figure 124. Voltage Applied to the Primary Coils and the Flux Distribution in Each Core Leg

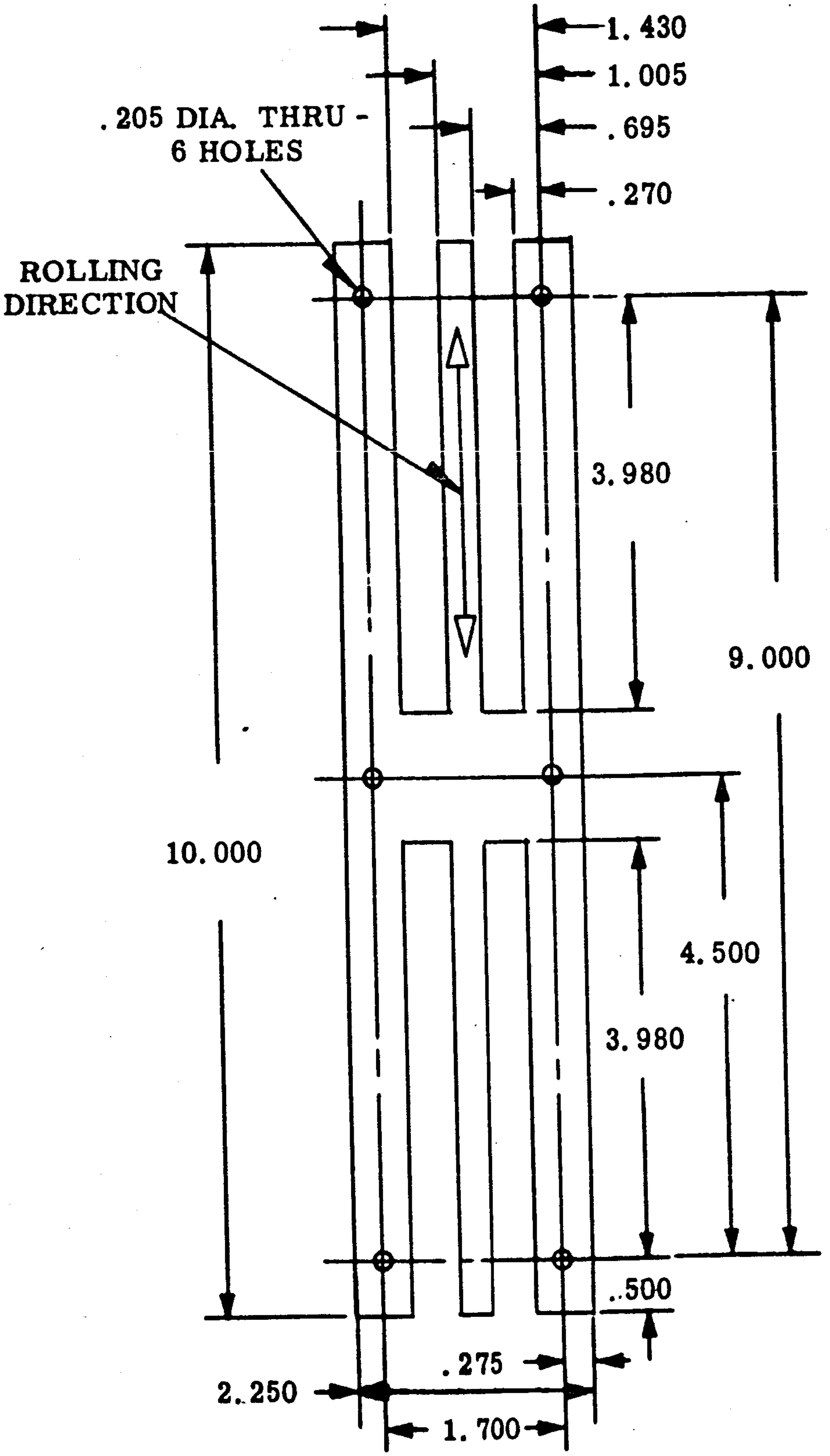
1.430
1.005
.695
.270
.205 DIA. THRU - 6 HOLES
ROLLING DIRECTION
3.980
9.000
10.000
4.500
3.980
..500
.275
2.,250
1.700

Figure 125. Actual Output Transformer Long Lamination Dimensions

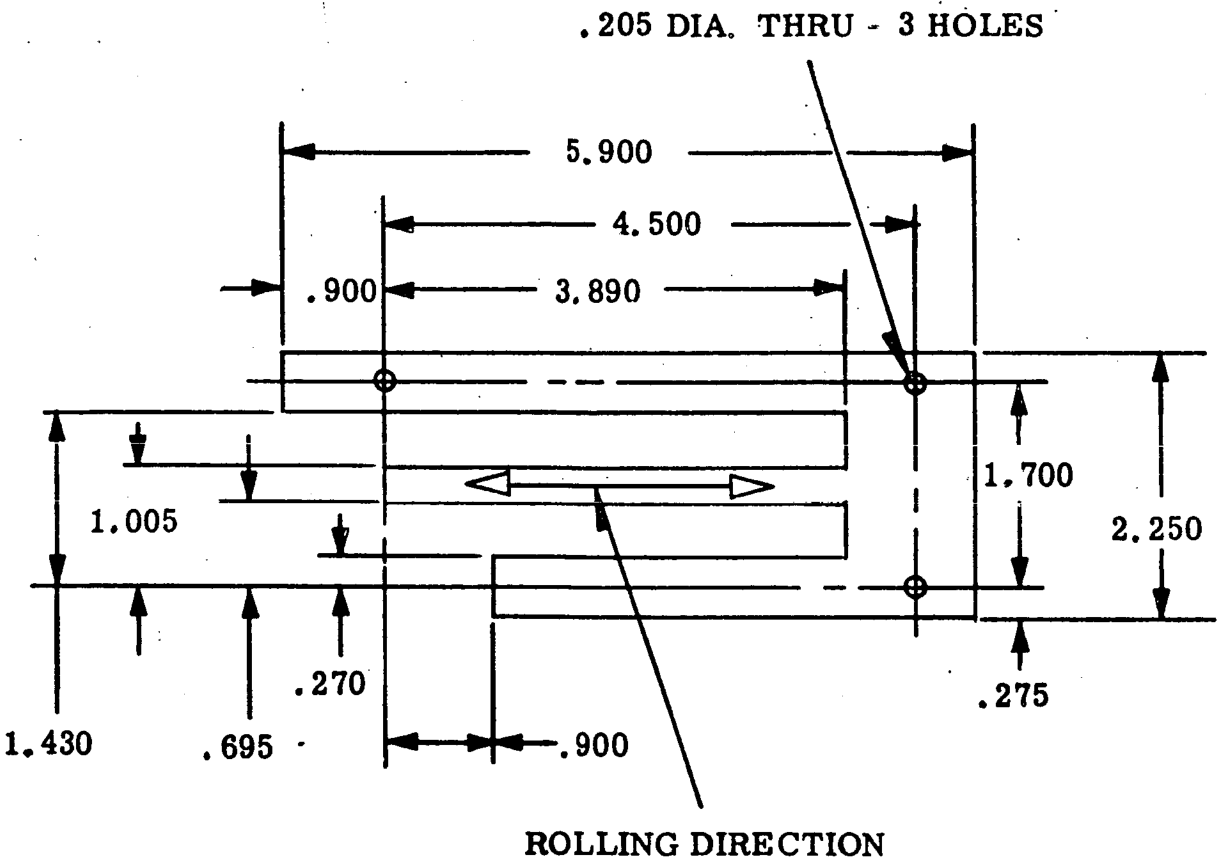
.205 DIA. THRU - 3 HOLES
5.900
4.500
.900
3.890
1.005
1.700
2.250
.270
.275
1.430
.695
.900
ROLLING DIRECTION

Figure 126. Actual Output Transformer Short Lamination Dimensions

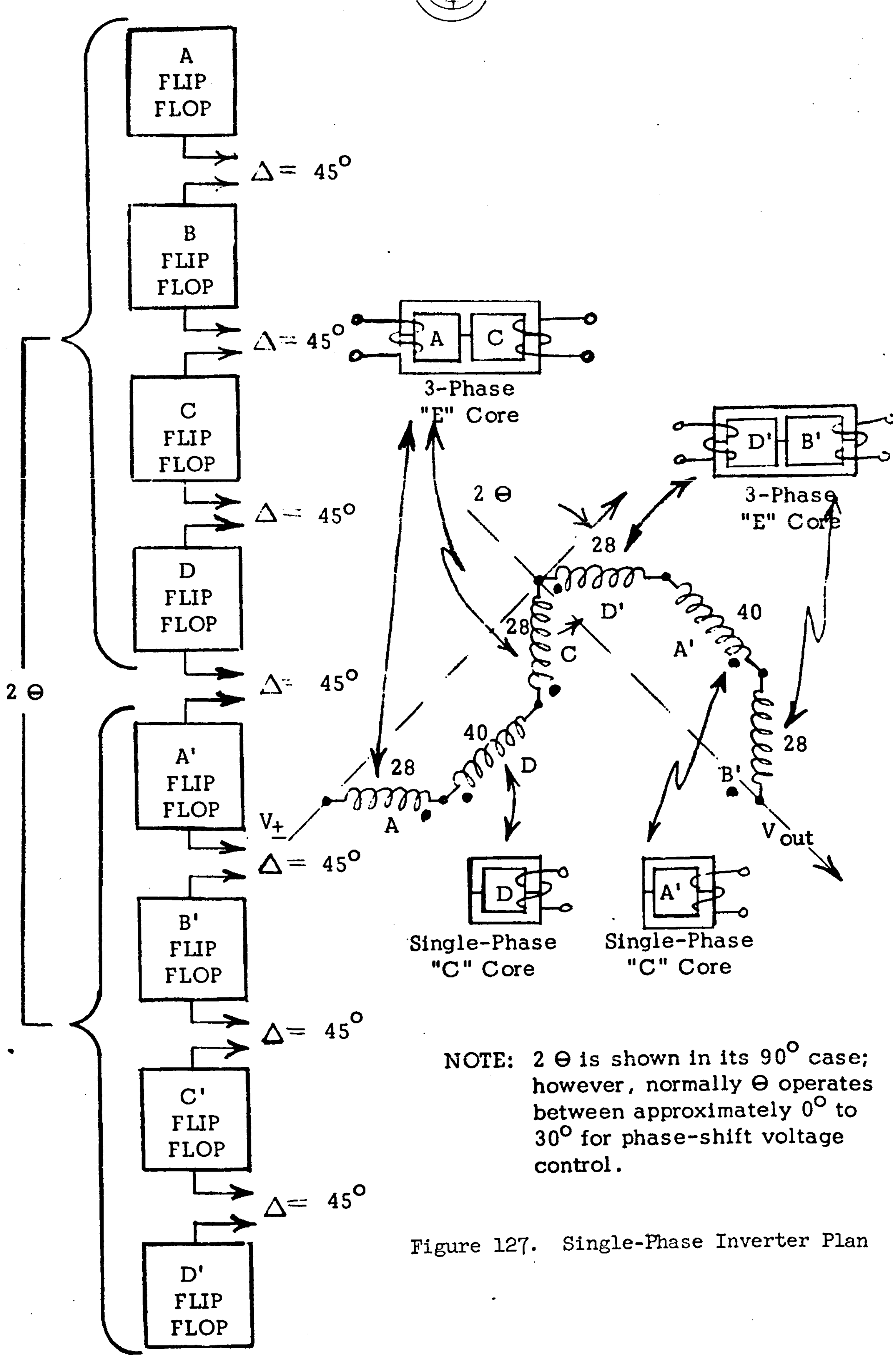
A FLIP FLOP
Δ = 45°
B FLIP FLOP
Δ = 45°
C FLIP FLOP
Δ = 45°
D FLIP FLOP
Δ = 45°
A' FLIP FLOP
Δ = 45°
B' FLIP FLOP
Δ = 45°
C' FLIP FLOP
Δ = 45°
D' FLIP FLOP
2 Θ
A
C
3-Phase "E" Core
D'
B'
3-Phase "E" Core
2 Θ
28
28
D'
40
C
A'
40
28
28
D
B'
V+
A
V out
D
Single-Phase "C" Core
A'
Single-Phase "C" Core

NOTE: 2 Θ is shown in its 90° case; however, normally Θ operates between approximately 0° to 30° for phase-shift voltage control.

Figure 127. Single-Phase Inverter Plan

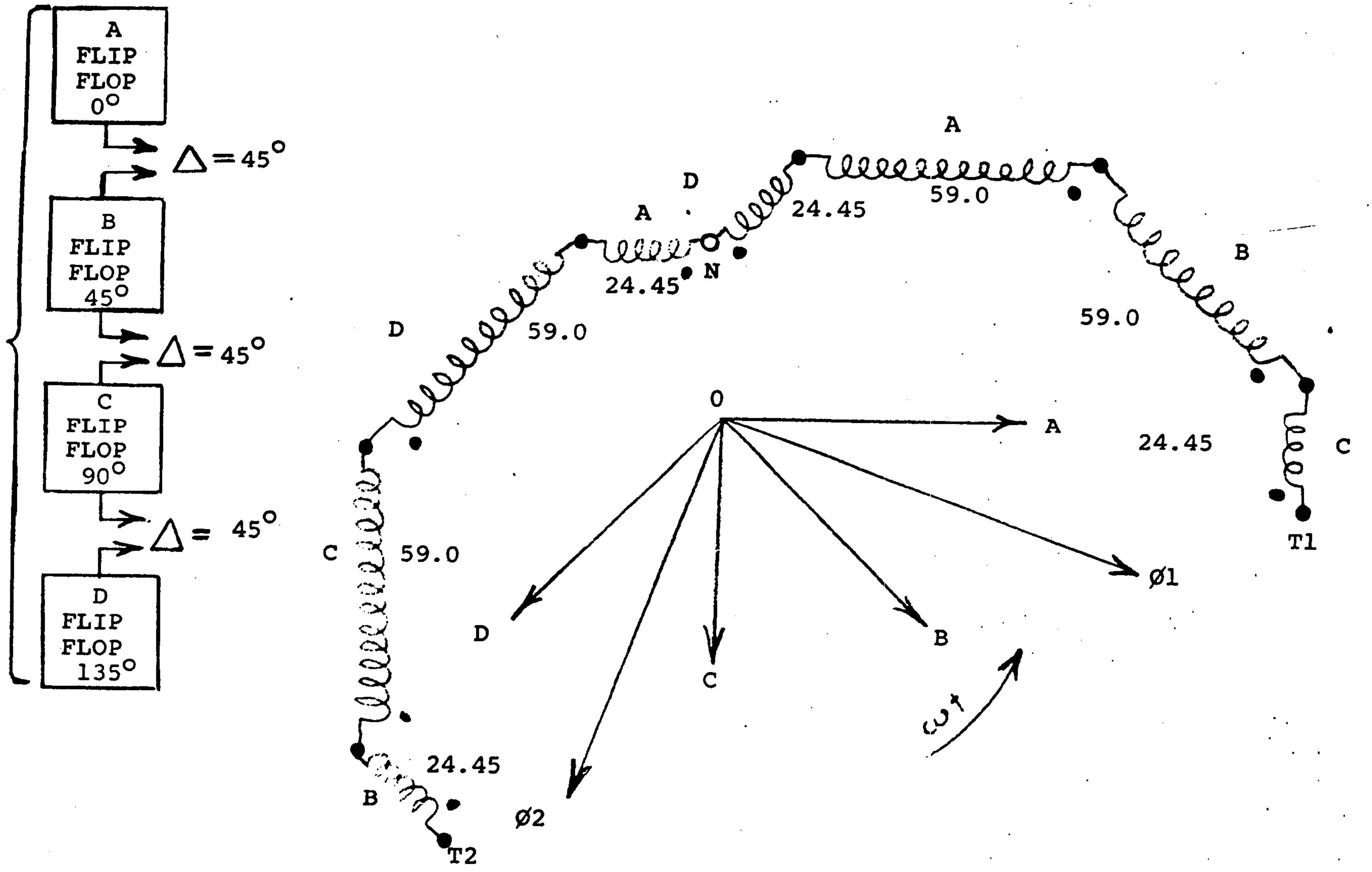
A
FLIP
FLOP
0°
Δ = 45°
B
FLIP
FLOP
45°
Δ = 45°
C
FLIP
FLOP
90°
Δ = 45°
D
FLIP
FLOP
135°
A
59.0
D
24.45
A
24.45
N
D
59.0
B
59.0
24.45
C
T1
C
59.0
24.45
B
T2
O
A
Ø1
B
C
D
Ø2
ωt

Figure 128. Identical Power-Stage-Transformer 2-Phase Inverter Plan

LIMITATIONS OF 28-VOLT D-C SUPPLY

The full power capability of alloy-junction silicon power transistors can be realized if the 3-wire 28-volt power system were adopted. Many advantages found in the old Edison 3-wire system (125-volt system) could be revived in this new 28-volt system. Obviously, at 125-volts a power system would be operating at too high a voltage level because of corona considerations at very high altitude; however, the inertia for 28-volt power utilization devices could still be met, even offering a reliability factor for consideration since two 28-volt buses exist for possible redundancy.

Two big advantages to semiconductor circuits are:

1. Both plus and minus voltage potentials present the designer with natural means for bias power of the opposite polarity.
2. The 56-volt level reduces power losses in circuits that prefer bridge configurations.
3. Saturation voltage drop and base-drive loss in the full utilization of alloy-junction power transistors (V_{ceo} to 250 volts) affords an inverter design with 90 plus percent efficiency capability in a center-tap type of circuit approach.

Use of the alloy-junction power transistor in a center-tap configuration at 56-volts is a safe approach because this switching device is not vulnerable to secondary breakdown in good designs. Because of its lower switching speeds, the alloy-junction power transistor would be limited to use in 400 cps power stages lest the efficiency achieved by 56-volt application be lost due to increased switching losses that may over-shadow the savings in saturated voltage drop and in base-drive losses.

The ideal configuration for 1500 VA at 56-volt input would use 16 silicon power transistors such as the 2N2754 or the 2N2772. Since a 65-ampere transistor is a diffused junction type, the 250-volt rating is not available, and its use is not feasible because of the danger of secondary breakdown in the center-tap configuration. With the advent of the 200-volt, 65-ampere transistor that is immune from secondary breakdown, a 3000 VA power rating is feasible from the 56-volt input to the inverter. Efficiency of such an inverter would be approximately 90 percent at unity power factor.

MODULAR-REPLACEMENT CONCEPT OF REDUNDANCY

In a manned space mission there can be a human link to implement the redundnacy where five power-stage modules of an original thirteen (one spare) can fail while still leaving two of the three inverters operable. No practical method is known to automatically perform the cannibalism which follows in the event of a second or succeeding power-stage-module failure. The plan works as follows:

1. The first module to fail will blow its fuse-relay which indicates the failed module and which provides the trip signal to the d-c input circuit breaker.

2. An automatic start-up and load transfer follows a failure within 250 milliseconds to a manually pre-selected reserve inverter. Each inverter of the original three has full-system-power capability, so that the whole system load is taken by the reserve inverter.

3. The spare power-stage module is installed in place of the failed one. Since a rapid trip-off is made in the event of a power module failure, other modules should not be affected; therefore, three operable inverters can be obtained.

4. The second module failure, if it occurs, determines the inverter that will have its power modules cannibalized to maintain the other two inverters as one main and the other reserve.

5. In the event of a sixth power-module failure, two inverters must be cannibalized in order to keep one operable. This last-resort maintenance is to no avail unless the power system can tolerate at least 10 - 15 seconds of a-c power black-out. During this time it is possible to provide a quick manual replacement means so that restart can be accomplished within seconds. This level of redundancy would provide the chance of survival in which one inverter can be maintained in operation if only four of the original thirteen power modules are still good.

6. Inverter portions other than the power-stage modules can fail, and when three such inverter portions are failed there is no survival, fortunately the chance of such an event is remote. The first inverter to lose its portion other than power-stage modules will become the cannibalized unit. One method of determining a failure not originating in a power-stage module depends upon the astronaut and a fuse coordination within the inverter. The assumption is that a large overcurrent to all the power stages simultaneously is caused by a failure outside the power modules; therefore, the main feeder fuse within the inverter will blow before any power-stage fuse-relay trips. Other malfunctions will be detected by the astronaut such as:

   1) Off frequency

   2) High-or-low phase voltages

   3) Over-temperature

   4) Excessive ripple or voltage modulation

   5) Any other evidence of improper operation

Assuming an MTBF of 7600 hours (present APOLLO inverter calculated MTBF) for the new inverter, and assuming that the portions of the new inverter other than power-stage modules have an MTBF of 50,000, the MTBF of one of the four power-stage modules per inverter becomes 35,800 hours.

The chances for survival will be calculated for the options of redundancy presented above assuming that the contributions made by the astronaut are without error. A survival to the first level of redundancy will assume that at least eight of the original power-stage modules are still good and that no more than one set of inverter components other than power-stage modules has failed without degrading any power-stage modules. The second level of redundancy assumes that at least four power-stage modules of the original thirteen remain good while at least one set of inverter components other than power-stage modules remains good. Also it is assumed that any failure outside the power-stage modules does not cause any power-stage module degradation. Because of the assumptions of perfect astronaut function and of only independent power-stage module failure, survival probability will be calculated assuming that the failure rate is the same for a stand-by unit as it is for an operating unit.

The reliability of a power-stage module for a 600 day mission will be represented by R_p and is given by:

$$R_p = e^{-(2.7856)\,10^{-5}\,(14,400)} = 0.66956542$$

$$Q_p = 1 - R_p = 0.33043458$$

The reliability of the rest of the inverter for a 600 day mission will be represented by R_x and is given by:

$$R_x = e^{-(2)\,10^{-5}\,(14,400)} = 0.7497616$$

$$Q_x = 1 - R_x = 0.2502384$$

The probability of two "X" modules surviving for 600 days is given by:

$$\begin{aligned} R'_{x-2} &= R_x^{\,3} + 3\,R_x^{\,2}\,Q_x \\ &= 0.42147283 + 3(0.56214246)\,(0.2502384) \\ &= 0.42147283 + 0.42200889 \\ &= 0.84348172 \end{aligned}$$

The probability of 8 power-stage modules out of thirteen surviving for 600 days is given by:

$$R'_{p-8} = R_p^{13} + R_p^{12} Q_p + \frac{13\cdot 12}{2} R_p^{11} Q_p^{2} + \frac{13\cdot 12\cdot 11}{3\cdot 2} R_p^{10} Q_p^{3}$$

$$+ \frac{13\cdot 12\cdot 11\cdot 10}{4\cdot 3\cdot 2} R_p^{9} Q_p^{4} + \frac{13\cdot 12\cdot 11\cdot 10\cdot 9}{5\cdot 4\cdot 3\cdot 2} R_p^{8} Q_p^{5}$$

$$= 0.0054363733 + 13(0.0081192562)(0.33043458)$$

$$+ 78(0.012126158)(0.10918701)$$

$$+ 286(0.018110491)(0.036079164)$$

$$+ 715(0.040396539)(0.0039393760)$$

$$= 0.0054363733 + 0.0348774792 + 0.1032734769$$

$$+ 0.1868756532 + 0.2305606372 + 0.2048095200$$

$$= 0.76583314$$

The probability of two (2) inverters surviving for a 600 day mission is represented by R'_{I-2} and is given by:

$$R'_{I-2} = R'_{x-2} \cdot R'_{p-8} = (0.84348172)\ (0.76583314)$$

$$= 0.64596625$$

The probability of one (1) "X" module surviving for 600 days is given by:

$$\begin{aligned}
R'_{x-1} &= R_x^{3} + 3\,R_x^{2}Q_x + 3\,R_xQ_x^{2} \\
&= 0.42147283 + 0.42200889 + 3(0.7497616)\,(0.06261926) \\
&= 0.42147283 + 0.42200889 + 0.1408485497 \\
&= 0.98433027
\end{aligned}$$

The probability of four (4) power-stage modules out of thirteen (13) surviving for 600 days is given by:

$$\begin{aligned}
R'_{p-4} &= R_p^{13} + 13R_p^{12}Q_p + 78\,R_p^{11}Q_p^{2} + 286\,R_p^{10}Q_p^{3} + 715R_p^{9}Q_p^{4} \\
&\quad + 1287\,R_p^{8}Q_p^{5} + 1716R_p^{7}Q_p^{6} + 1716\,R_p^{6}Q_p^{7} + 1287R_p^{5}Q_p^{8} \\
&\quad + 715\,R_p^{4}Q_p^{9} \\
&= 0.0054363733 + 0.0348774792 + 0.1032734769 \\
&\quad + 0.1868756532 + 0.2305606372 + 0.2048095200 \\
&\quad + 1716\,(0.060332476)\,(0.001301706) \\
&\quad + 1716\,(0.090106916)\,(0.00043012868) \\
&\quad + 1287\,(0.13457523)\,(0.00014212939) \\
&\quad + 715\,(0.20098890)\,(0.000046964466) \\
&= 0.0054363733 + 0.0348774792 + 0.1032734769 \\
&\quad + 0.1868756532 + 0.2305606372 + 0.2048095200 \\
&\quad + 0.1347663105 + 0.0665079881 + 0.0246165717 \\
&\quad + 0.0067491255 \\
&= 0.99847314
\end{aligned}$$

The probability of one inverter surviving for 600 days is represented by R'_{I-1} and is given by:

$$R'_{I-1} = R'_{x-1} \cdot R_{p-4} = (0.98433027)(0.99847314)$$

$$= 0.98282733$$

The above figures are pessimistic because they are based on the assumption that the failure rate during standby operation is the same as during normal operation which is not realistic. No data is available to calculate the true failure rate during standby.

However, by assuming a failure rate of zero during standby, an optimistic figure can be obtained. The calculations below for R'_{I-2} and R'_{I-1} assume that the modules cannot fail when in the standby condition.

The reliability of the "X" modules for standby operation can be calculated by the exponential expansion:

$$R_x = e^{-\lambda t} + \lambda t e^{-\lambda t} + \frac{(\lambda t)^2}{2!} e^{-\lambda t} + \frac{(\lambda t)^3}{3!} e^{-\lambda t}$$

In this expansion the terms give the probability of exactly zero, one, two, or three failures respectively from left to right. The probability of one (1) "X" module surviving is the probability of two or less failures and will be represented by R''_{x-1} and is given by:

$$R''_{x-1} = e^{-\lambda t} + \lambda t e^{-\lambda t} + \frac{(\lambda t)^2}{2!} e^{-\lambda t}$$

since λ = 2%/1000 hours and t = 14,400 hours

$$\lambda t = 0.288$$

$$R''_{x-1} = e^{-0.288} + 0.288\, e^{-0.288} + \frac{(0.288)^2}{2} e^{-0.288}$$

$$= 0.74976160 + 0.21593134 + 0.03109411$$

$$= 0.99678705$$

The probability of two "X" modules surviving which will be represented by R''_{x-2} is the probability of one or less failures and is given by:

$$
\begin{aligned}
R''_{x-2} &= e^{-\lambda t} + \lambda t\, e^{-\lambda t} \\
&= e^{-0.288} + 0.288\, e^{-0.288} \\
&= 0.74976160 + 0.21593134 \\
&= 0.96569294
\end{aligned}
$$

The reliability of the power-stage modules for standby can be calculated from the exponential expansion:

$$
\begin{aligned}
R_p = {} & e^{-4\lambda t} + 4\lambda t e^{-4\lambda t} + \frac{(4\lambda t)^2}{2!} e^{-4\lambda t} + \frac{(4\lambda t)^3}{3!} e^{-4\lambda t} + \frac{(4\lambda t)^4}{4} e^{-4\lambda t} \\
& + \frac{(4\lambda t)^5}{5!} e^{-4\lambda t} + \frac{(4\lambda t)^6}{6!} e^{-4\lambda t} + \frac{(4\lambda t)^7}{7!} e^{-4\lambda t} \\
& + \frac{(4\lambda t)^8}{8!} e^{-4\lambda t} + \frac{(4\lambda t)^9}{9!} e^{-4\lambda t}
\end{aligned}
$$

In this expansion the terms give the probability of exactly zero, one, two, three, four, five, six, seven, eight, and nine failures respectively from left to right.

The probability of four power-stage modules surviving which will be represented by R_{p-4} is the probability of nine or less of the thirteen available modules failing.

λ = 2.7856%/1000 hours, t = 14,400 hours

$\therefore$ $4\lambda t$ = 1.60450560

$$
\begin{aligned}
R''_{p-4} = {} & e^{(x)} + 1.60450560\, e^{-(x)} + \frac{(1.60450560)^2}{2} e^{-(x)} \\
& + \frac{(1.60450560)^3}{6} e^{-(x)} + \frac{(1.60450560)^4}{24} e^{-(x)} + \frac{(1.60450560)^5}{120} e^{-(x)} \\
& + \frac{(1.60450560)^6}{720} e^{-(x)} + \frac{(1.60450560)^7}{5040} e^{-(x)} + \frac{(1.60450560)^8}{40320} e^{-(x)} \\
& + \frac{(1.60450560)^9}{362880} e^{-(x)}
\end{aligned}
$$

NOTE: Where $e^{-(x)}$ appears substitute 1.60450560 for (x).

$$
\begin{aligned}
= {} & 0.20098890 + (1.60450560)(0.20098890) + (1.28721910)(0.20098890) \\
& + (0.68845008)(0.20098890) + (0.27615550)(0.20098890) \\
& + (0.00542404)(0.20098890) + (0.00108946)(0.20098890) \\
& + (0.00019423)\,(0.20098890) \\
= {} & 0.20098890 + 0.32248782 + 0.25871675 + 0.13837082 \\
& + 0.05550419 + 0.01781136 + 0.00476307 + 0.00109017 \\
& + 0.00021897 + 0.00003904 \\
= {} & 0.99999109
\end{aligned}
$$

The probability of eight power-stage modules surviving which will be represented by R''_{p-8} is the probability of 5 or less of the 13 available modules failing.

$$
\begin{aligned}
R''_{p-8} = {} & 0.20098890 + 0.32248782 + 0.25871675 + 0.13837082 \\
& + 0.05550419 + 0.01781136 \\
= {} & 0.99387984
\end{aligned}
$$

If the true reliability of the three inverters are represented by R_{I-2} and R_{I-1} for the probability of two surviving and one surviving respectively:

0.64596625 R_{I-2} 0.99387984

0.98282733 R_{I-1} 0.99999109

THREE LEVELS OF RELIABILITY IMPROVEMENT

The 7600 hour estimate of MTBF is valid for 1965 using the best choices of high-reliability parts that are available without expenditure on component reliability improvement programs. This group of parts are represented by the bill of material of the present APOLLO Inverter.

In 1969 the best choice of high-reliability parts that will be available for the new APOLLO inverter should increase the MTBF from natural forces. In addition, circuit improvements will be known. An MTBF of 12,000 hours can be expected without the APOLLO inverter program making expenditures on component reliability improvement programs.

With component reliability improvement programs aimed at selected higher-failure-rate parts required by the new APOLLO inverter, it is reasonable that an MTBF in 1969 of approximately 20,000 hours can be generated.